NUMERICAL MODELLING OF THE ANTARCTIC ICE SHEET

Zheng Wang

Doctor of Philosophy

The University of Edinburgh

2001

To Stella

Acknowledgements

This thesis is accomplished under the constant encouragement and inspiration from my supervisor, Prof David E Sugden. I am also deeply indebted to my supervisor, Dr Nick R J Hulton, for his comprehensive input. Without their help, I can't even imagine the achievement today.

Dr Ross S Purves's seminars benefited me a lot. Dr Andy Kerr, Dr Mike J Mineter, Dr Mike J Bentley and Dr Jens-Ove Näslund provided me useful data and material. I also thank Keith W. Morrison and Steve Dowers for their warm-hearted help in computing. Thank Dr Robert L. Hodgart for his warm-hearted help.

My colleagues, Sara, Jez, Tom, Kate, Steve, Darcey, Lorrain, Hannah, Rafael, Javier, Nick, Keith and Sarah *etc.*, made my study life in Edinburgh so enjoyable. I shall cherish this friendship forever.

The entire work is dedicated to my Stella, whom I happily married here in Edinburgh. Stella supports my work with her full-hearted love.

I am particularly grateful to the Sino-British Fellowship Trust who sponsored my research and the Overseas Research Students Awards Scheme.

Declaration

I, Zheng Wang, hereby declare that the thesis has been composed by myself, the work is my own and any cited materials have been acknowledged.

Zheng Wang

Abstract

This thesis develops a three-dimensional time-dependent numerical model that dynamically simulates the evolution of the flow and thermal regime of the Antarctic Ice Sheet in response to climatic changes. As one of the most important heat sinks and water reservoirs in the Earth's energy and water systems, the behaviour of the Antarctic Ice Sheet strongly influences the natural environment on Earth. This thesis first reviews the factors that affect the thermal and dynamical processes in the Antarctic Ice Sheet system and quantifies their function. The universal conservation equations of mass and energy serve as the governing equations of the ice sheet model. Different boundary and initial conditions for solving the governing equation set are used to explore different scenarios of ice sheet behaviour. They are crucial components of the ice sheet model and are analysed at every interface between the Antarctic Ice Sheet system and the outside environment. An Alternating Direction Implicit (ADI) scheme is used to compute the ice sheet model in one-dimensional, two-dimensional, and finally three-dimensional systems in order to highlight the role of the various factors affecting the behaviour the ice sheet. The sensitivities of the various factors are tested in these idealised ice sheet systems. The parameters employed to model the Antarctic Ice Sheet in the three-dimensional system are then calibrated against field data. By reconstructing the thermal and dynamical regimes of the Antarctic Ice Sheet under present-day and glacial maximum climatic conditions, the ice sheet model simulates the behaviour of the Antarctic Ice Sheet under changing climates. The modelling results support the idea of a stable East Antarctic Ice Sheet and a comparatively dynamic West Antarctic Ice Sheet. The modelling results also corroborate the hypotheses about landscape evolution in the Dry Valleys area, East Antarctica, suggested by field research. Based on the good match between the modelled basal pressure melting areas and the subglacial lake clusters identified by RES research, the ice sheet model predicts that the volume of meltwater locked in subglacial lakes in Antarctica could be greater than previous predictions.

Symbols and Notations

a	surface accumulation rate, m/yr
$A(T)$	$mA_0 \exp\left(-\frac{E}{RT}\right)$, flow law coefficient, $Pa^{-n}yr^{-1}$
A_0	heuristically adjusting coefficient independent of temperature
$\overline{A}$	vertically averaged flow law coefficient, $Pa^{-n}yr^{-1}$
c_p	specific heat capacity, $Jkg^{-1}K^{-1}$
d	diameter of the meltwater channel, m
D	non-linear diffusion coefficient depending strongly on ice thickness and surface slope
E	activation energy of ice flow, kJ/mol
f_s	sliding parameter
F	mass flux, kg/m^2
g	acceleration of gravity, 9.81 m/s^2
G	geothermal heat flux, -1.32×10^{-6} $Jm^{-2}a^{-1}$
$h(x,y)$	bedrock elevation, m
$h^0(x,y)$	unloaded bedrock topography, m
$H(x,y)$	ice thickness, m
k	thermal conductivity, $Jm^{-1}K^{-1}yr^{-1}$
L_{ice}	specific latent heat of fusion of ice, 3.35×10^5 J/kg
m	tuning parameter to slightly adjust the height-width ratio
M	melting rate, m/yr (ice thickness equivalence)
M_d	meltwater discharge
M_p	meltwater potential
n	flow law exponent (Paterson suggests a mean value of 3)
N	mesh grid number
p	balance of pressure gradient that drives ice flow
P	Peclet number, relative efficiency of heat conduction to advection
$\dot{q}$	internal heating, $Jm^{-3}yr^{-1}$
$\dot{q}_{geoth}$	geothermal heat flux, $Jm^{-3}yr^{-1}$

q_x''	heat flux, W/m²
Q	potential energy released by a column of ice
r	iceberg calving rate
R	gas constant, 8.314 $Jmol^{-1}K^{-1}$
R_{el}	radius of the equilibrium line where surface ablation equals the accumulation
s	distance along the water channel in the direction of flow, m
s_a	empirical gradient of surface mass balance change with latitude
s_T	empirical gradient of surface temperature change with latitude
t	time, yr
t^*	characteristic evaporation time
T	absolute temperature, K
T^0	273.16 K, triple-point temperature of water
T_0	annual mean ice surface temperature
T^*	$T+T_{cc}(H+h-z)$, absolute temperature corrected for the dependence of the melting point on pressure
T_{cc}	Clausius-Clapeyron gradient, designating the change of ice melting point with pressure under an ice sheet, 8.7×10^{-4} K/m
T_s	annual surface temperature distribution
T_m	half the annual temperature range
T_{pmp}	local pressure melting point
u-v-w	x-y-z components of the three-dimensional velocity vector $\vec{V}$, m/yr with the assumption that $\partial w/\partial x << \partial u/\partial z$, $\partial w/\partial y << \partial v/\partial z$
$\vec{V}$	ice flow velocity vector, m/yr
W	atmospheric precipitable water equivalence
x-y-z	Cartsian co-ordinates, with x the flow direction and z the vertical direction
$(\hat{x}, \hat{y})$	coordinates of the two-dimensional idealised ice sheet centre
α-β-γ-δ	ADI coefficients
α_{ice}	thermal diffusivity of ice, m²/s
α_x	surface slope
β_x	basal slope

$\dot{\varepsilon}_{ij}$	strain rate component related to velocity gradients by definition
γ_g	G/k, prescribed geothermal gradient
φ	embayment factor
κ	$\rho_{water} c_{p\_water} T_{cc}$
μ	coefficient to adjust precipitation exponent
Θ	a given point in the annual cycle
θ	radian facing the coast line
ρ	density, kg/m^3
τ_{ij}	stress tensor, N/m^2, with $i,j = x,y,z$
	subscript ij means on the plane of i = constant, along the direction of j
τ'_{ij}	diviatoric stress tensor, N/m^2
τ_*	effective stress defined in terms of all the stress deviator components so that it is independent of the co-ordinate system, N/m^2
$\vec{\tau}_b$	basal shear stress vector, N/m^2
ω	deflection of the lithosphere, m
ζ	normalised dimensionless ice thickness

Index

Chapter 1 Introduction

The Antarctic Ice Sheet is the largest ice sheet on the Earth (Figure 1.1). Because of its enormous scale and special location, it plays a crucial role in the climatic system on a global scale. The behaviour of the Antarctic Ice Sheet in response to the local and global climatic changes has attracted the attention of scientists from various disciplines for decades.

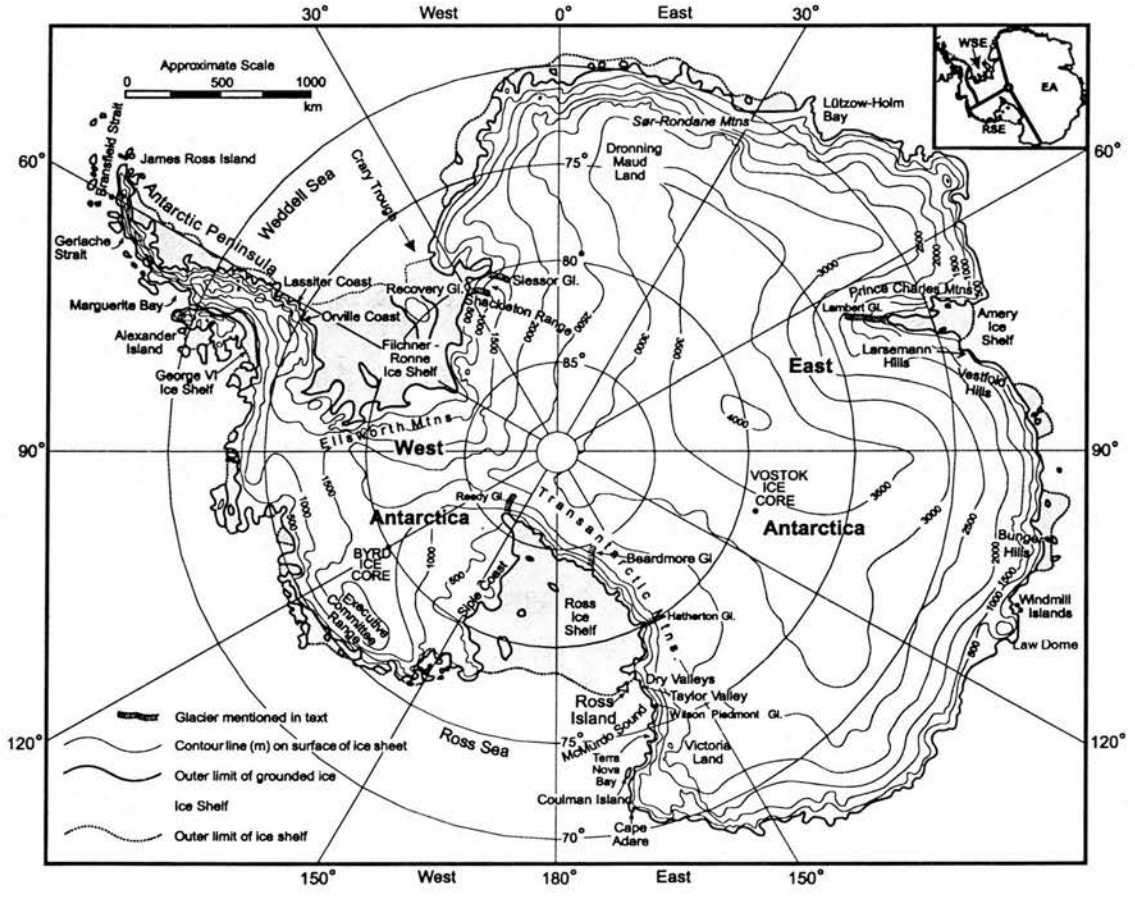

Figure 1.1 Present-day Antarctic Ice Sheet. Adapted from Bentley [1999].

1.1 The Aim of this Research

This research is concerned with the modelling of the thermodynamics of the Antarctic Ice Sheet. It aims to develop a numerical model that dynamically simulates the mass and energy flow of the Antarctic Ice Sheet system and the response of the ice sheet to climatic changes. Thermal and dynamical regimes determine the behaviour of an ice sheet. By modelling and analysing the thermal and dynamical regimes under different scenarios of surface mass balance, ice surface temperatures and sea level, this research helps to understand the response of the Antarctic Ice Sheet to climatic changes. This knowledge helps to predict the stability of the Antarctic Ice Sheet, which crucially relates to the living environment of human beings. It also helps to interpret the landscapes that are a result of Antarctic glaciation processes.

1.2 Mass and Energy

The flow of mass and energy underpins the Earth's climatic system. The imbalance of heat on different regions on the Earth's surface drives the air and water flow. The Antarctic region, due to its currently low temperatures, is a key player in the global climatic system.

1.2.1 The Antarctic Ice Sheet in the global water mass system

The balance of the proportions of the three phases of water on the Earth – ice, liquid and vapour – is a key factor that keeps the harmonious and stable environment suitable for life. Viewed from outer space, the Earth can with some justification be described as a glacial planet. During the northern hemisphere winter, over half of the world's land surface area and up to 30 percent of its ocean area may be covered by a blanket of snow and ice [Sugden and John, 1976]. Glacier ice currently covers more than 15.8 million km^2, some 10 percent of the Earth's surface, and contains 75 percent of the world's freshwater resources [UNEP, 1992]. More than 85 percent of

the ice, or some 30 million km^3 of ice in volume, is found in present-day Antarctica [Drewry, 1991] (Figure 1.1). The Antarctic Ice Sheet presently covers an area about 13.6 million km^2, some 98 percent of the Antarctic continent. It represents the largest mass of glacier ice on the Earth. The Antarctic Ice Sheet currently has an average thickness of 2300 metres with the thickest point of more than 4700 metres in East Antarctica [NERC, 1989].

The above physical figures suggest that the Antarctic Ice Sheet is the main reservoir of the global water mass system. It is a crucial link in the water mass balance on the Earth. It is pivotal in the atmospheric circulation of the Southern Hemisphere. It provides cold bottom water to the world's oceans and thus influences ocean circulation over the world. It influences world sea level and an equivalent of 60 metres of sea level of water is currently locked up on land [Sugden *et al.*, 1993]. So any suspicion that it might melt in the future has profound implications [Sugden, 1996]. Fluctuations of the ice volume of the Antarctic Ice Sheet and the extent of the ice shelves provide crucially important modulating effects on the global environmental system in term of sea level, ocean circulation, radiation budget, and oceanic and atmospheric circulation at a variety of timescales. Better knowledge of the mechanisms and dynamics of the Antarctic Ice Sheet will help us understand global climatic changes. By simulating the evolution of the modelled ice sheet under different scenarios of mass balance and sea level, this research helps to understand the relationship between the Antarctic Ice Sheet and climate. For example, what kind of climatic conditions could lead the Antarctic Ice Sheet to grow to its present-day scale? Will the Antarctic Ice Sheet keep stable under the present-day climatic conditions? Is the Antarctic Ice Sheet currently losing mass or, on the contrary, gaining mass?

1.2.2 The Antarctic Ice Sheet in the global energy system

The present-day environment on the Earth depends on two delicately balanced equilibria [Petrenko and Whitworth, 1999]. The first is the energy equilibrium between the radiation received from the Sun and that reflected and re-radiated from

the Earth. Due to the high albedo of snow and ice, more solar radiation will be reflected back into the outer space if ice sheets on the Earth expand. The resulting global average temperature is therefore highly sensitive to the area of the Earth's surface covered by snow and ice. The second is the mass equilibrium concerning the evaporation of water from the oceans, leading to snowfall over the Polar Regions and subsequent flow of the ice sheets back into the oceans. Ice sheets play an important role in both energy and mass flows, so their behaviour is critical to the Earth's natural environment that supports life.

Incoming radiative energy from the Sun is not evenly distributed around the surface of the Earth. Tropical regions receive most solar energy, whilst polar regions receive about 40 percent less solar radiation than tropical regions due to the angle of the Earth's surface in relation to solar rays [Barry and Chorley, 1992]. Moreover, the albedo of snow and ice material covering polar regions is so high that about 80 to 90 percent of the solar radiation reaching the polar regions is reflected back into the outer space [Oke, 1978]. This unevenness of solar heating not only causes polar regions to have the lowest surface temperatures on the Earth, but also acts as the driving force of the Earth's climatic system [Oerlemans and van der Veen, 1984]. On average, the radiation budget is positive at lower latitudes and negative at higher latitudes, so a poleward flux of energy is thus required to create a state of balance. This flux is accomplished by large-scale atmospheric circulation and ocean currents, because temperature gradients cause density and salinity gradients in the oceans and pressure gradients in the atmosphere.

On the present-day Antarctic plateau, the annual mean temperature is –50°C [Rubin and Weyant, 1965] and the lowest natural temperature on Earth, –89.5°C, was recorded in July 1983 at Vostok [Hansom and Gordon, 1998]. Antarctica is currently one of the world's greatest heat sinks of the global energy system. In other words, the Antarctic Ice Sheet helps regulate temperatures on the Earth. It affects the climate not only in the Southern Hemisphere but the whole global climatic system [Phillpot, 1985; Yuan *et al.*, 1996]. Spatial and temporal variations in the Antarctic Ice Sheet

system are crucially important not only to human understanding of how our Earth currently functions but also in the prediction of its changing trend in the future.

The behaviour of the Antarctic Ice Sheet is, in turn, a good indicator of global climatic change. The mass balance of an ice sheet is sensitive to small but persistent variations in surface temperatures, precipitation and other meteorological factors [Hubbard, 1996; Purves and Hulton, 2000b]. It directly determines the advance or retreat of the ice sheet. Ice flow velocities, hence the energy budgets, tend to reflect medium and long-term changes of these factors. The extent of ice shelves can reflect shorter-term climatic changes. Medium and long-term global climatic changes also manifest themselves as variations in the mass balance of the Antarctic Ice Sheet, resulting in advance or retreat of the ice sheet and the concomitant storage or release of water into the sea.

1.3 Rationale to the Study of the Thermal and Dynamical Regimes of the Antarctic Ice Sheet

The Antarctic Ice Sheet is a dynamic system: cold ice accumulates on the surface of the continental ice sheet, and warm ice evolves with depth. The ice flows towards the Southern Ocean where floating ice shelves lose mass mainly by iceberg calving from the edges and ice melting at the ice-water interface. These mass and energy flows are driven by the thermodynamic regime. This thesis develops a thoroughly tested model of the basal temperature distributions beneath the Antarctic Ice Sheet during its evolution and also in the past when the ice sheet was more extensive and extended to the outer continental shelf. The predicted basal temperatures are important because they can be related to the dynamics of ice flow, patterns of erosion and deposition and also to the routes of subglacial meltwater. One implication is that it is possible that the subglacial Lake Vostok has drained periodically beneath the ice sheet and thus is younger than some estimates underpinning NASA's plans to probe the lake.

1.3.1 Ice sheet dynamics

The dynamics of the Antarctic Ice Sheet is one of the main concerns of this research since it directly determines the behaviour of the ice sheet. The stability of the East Antarctic Ice Sheet relates directly to global environmental and sea level changes. There are controversial debates surrounding the issue of ice sheet stability [Sugden *et al.*, 1993; Sugden, 1996]. The focus of these debates is on the response of the Antarctic Ice Sheet to warmer-than-present polar climates. This controversy is important because the East Antarctic Ice Sheet plays a vital role in moderating the global environment and any suspicion that it is liable to melt in future has profound implications [Sugden, 1996].

Based crucially on the inferred age and origin of reworked marine diatoms found in Sirius Group outcrops along the Ross Sea sector at high altitudes in the Transantarctic Mountains, dynamists (so called by van der Wateren and Hindmarsh [1995]) Webb *et al.* [1984] and Harwood [1986] argue that the East Antarctic Ice Sheet collapsed during the Pliocene warm interval. The deposits at that time reflect the former presence of glaciers advancing into a temperate forest akin to that in Patagonia today with climatic conditions about 40°C warmer than occurs at some of the same sites today. This scenario implies that collapse of the East Antarctic Ice Sheet can be triggered by relatively modest global warming. If this hypothesis is the case, the Antarctic Ice Sheet may again be under threat if global temperature warms a few degrees more than present [Barrett *et al.*, 1992].

A contrary view, based on geomorphologic evidence from the Dry Valleys, Victoria Land, concludes that the East Antarctic Ice Sheet remains robust throughout Pliocene-Pleistocene time [Denton *et al.*, 1993]. This view, championed by the stabilists, suggests that the Dry Valleys' landscape is largely inherited from a climatic regime that existed prior to the imposition of the present cold, hyper-arid desert environment [Sugden, 1992; Marchant *et al.*, 1993]. Sugden *et al.* [1999] interpret landscape development in the Royal Society Range, southern Victoria Land, and suggest that the East Antarctic Ice Sheet has remained at its present magnitude

for at least 14 million years [Denton *et al.*, 1993; Sugden, 1996], which strongly supports the stable hypothesis. Besides geomorphologic and geologic evidence, a stable East Antarctic Ice Sheet is also supported by the interpretation of the marine sediment record of the Southern Ocean and oxygen isotope ratios of planktonic foraminifera [Kennett, 1982]. Further, the only plausible mechanism to cause deglaciation is to melt the ice sheet surface [Denton *et al.*, 1993], but the present-day polar climate is far too cold to form a surface melting ablation zone over the Antarctic Ice Sheet.

Huybrechts [1993] tested the sensitivity of ice volume of the Antarctic Ice Sheet to surface temperature perturbations by a three-dimensional time-dependent thermodynamic-coupled ice-sheet model. Modelling results show that the Antarctic Ice Sheet will become even bigger for a climate warming of up to 5°C. For the ice sheet to recede from the continental platform, the climate would first have to warm enough to produce a peripheral ablation zone of sufficient width. Under the current cold climate, where little melting occurs and precipitation amounts are limited by the low air temperatures, the Antarctic Ice Sheet is still located in a region where mass balance will increase with temperature because of increased precipitation [Huybrechts and Oerlemans, 1990].

Applying numerical modelling, Huybrechts [1993] further points out an interesting, mutually contradictory scenario. If a massive ice sheet once overrode the present Transantarctic Mountains, polar conditions were required for ice to expand across the Ross Sea floor, yet warmer-than-present conditions were required for the greatly increased accumulation needed for interior thickening. His modelling results show that high accumulation rates due to higher polar temperatures would not significantly increase the interior ice surface elevations. This is because higher temperatures of the ice sheet, coupled with greater ice flow velocities, would compensate for the extra accumulation. This modelling result is consistent with some field studies by different approaches. Based on geomorphologic analysis, Denton *et al.* [1993] conclude that any Pliocene thickening of sectors of the East Antarctic Ice Sheet adjacent to the Dry Valleys was minimal. Based on volcanic ash analysis, Marchant *et al.* [1993a,b]

conclude that wide tracts of the western Dry Valleys adjacent to the inland ice sheet remained free of glacier ice throughout the Pliocene Epoch.

The majority of recent research seems in favour of a stable East Antarctic Ice Sheet. If the ice sheet could survive the warm climate during the Pliocene Epoch, it should again survive future global warming. The key issue here is how sensitive the Antarctic Ice Sheet is to warmer surface temperatures and higher surface accumulation. The modelling research in this thesis will investigate the ice sheet's response to a warmer climate in respect to its thermal and dynamical regimes.

1.3.2 Glacial erosion by ice sheets

The linkages between the Antarctic and other global systems have changed through time, particularly as the Antarctic Ice Sheet has fluctuated in size. Marine sediments conclusively suggest that the Antarctic Ice Sheet has deeply eroded the continent and continental shelf. Glacial erosion is most pronounced along geologic boundaries, such as fault zones, resulting in the creation of glacial troughs on the continental shelf [Anderson, 1999].

The Transantarctic Mountains lie across Antarctica from the northern Victoria Land on the Pacific coast to the Thiel Mountains at the junction of the East and West Antarctic Ice Sheets. The mountains continue as a coherent topographic feature in a series of ranges as far as the Theron Mountains which terminate near the South Atlantic Ocean (Figure 1.1). Throughout its length, the plateau forming the Transantarctic Mountains is divided into discrete blocks by outlet glaciers that drain from the East Antarctic Ice Sheet and flow into adjacent ice shelves or the ocean. Rising to elevations in excess of 4000 metres and extending for more than 3000 km, the Transantarctic Mountains provide a valuable case study for the assessment of the relative role of tectonic and surface processes in landscape development.

Controversial debates about the surface processes responsible for shaping the Transantarctic Mountains have existed since the early 20th Century [Ferrar, 1907;

Priestley, 1909; David and Priestley, 1914; Taylor, 1922]. In the mid 20th Century, research carried out after the International Geophysical Year in 1959. Bull *et al.* [1962], Denton *et al.* [1971], Nichols [1971], Selby and Wilson [1971] and Calkin [1974] suggest that valley benches in the Dry Valleys area were attributed to earlier phases of trough excavation. It implies a conclusion that it was the outlet glaciers and cirque glaciers that created the main erosional features of the Transantarctic Mountains. These debates continue today. Van der Wateren and Verbers [1990] and Verbers and van der Wateren [1992] suggest that the present landscape in northern Victoria Land is the result of glacial dissection of an original low-relief planation surface. On the contrary, Webb [1994] argues that the valleys now occupied by glaciers such as the Beardmore in northern Victoria Land were eroded down to near sea level by rivers as well as being overdeepened by glaciers. Sugden *et al.* [1995] also conclude that the landscape in the Dry Valleys area is essentially fluvial in origin, with diagnostic features such as sinuous valleys, major long profiles graded to near sea level, fluvial valley benches and dendritic valley patterns all still apparent (Figure 1.2). The latter view argues that the landscape of the main valleys along the Transantarctic Mountains is primarily fluvial in origin, and the subsequent glacial modification, even over the long term, has been selective and limited to straightening of certain troughs and partial scouring of pre-existing surfaces. Many landscapes with no sign of glacial modification are thought to have survived intact beneath cold-based ice.

Based on the interpretation of some channel systems at the Dry Valleys area, Sugden *et al.* [1991] postulate the former existence of large-scale subglacial meltwater streams. Typical examples include the Labyrinth system at the head of Wright Valley (Figure 1.2) and Miller Glacier Valley and pothole system cut along the western flank of a sandstone butte in the western Asgard Range (Figure 1.3). Denton *et al.* [1984] relate the glacial modification of the above area, involving areal scouring and the formation of striations and meltwater channels, to overriding by a thicker warm-based ice sheet.

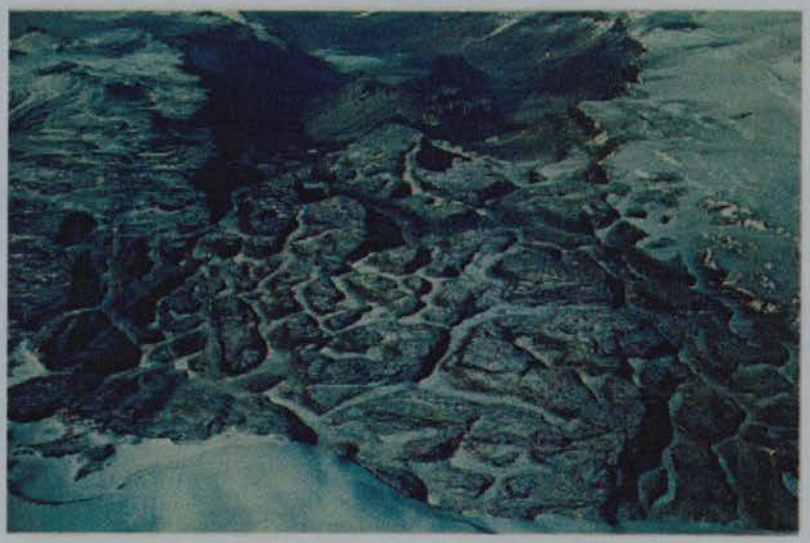

Figure 1.2 The Labyrinth in upper Wright Valley, the Dry Valleys, southern Victoria Land, East Antarctica. Viewed eastward down Wright Valley. It is postulated that the Labyrinth was cut by subglacial meltwater streams (from Denton *et al.*, 1993).

Glacial unconformities also provide conclusive evidence that the Antarctic Ice Sheet has, on several occasions, eroded and modified the Antarctic continental shelf. Direct evidence of deep glacial erosion on the Antarctic continental shelf is seen in virtually every seismic profile that crosses the shelf [Anderson, 1999]. Seismic profiles from the central Ross Sea and the northern Antarctic Peninsula continental shelves illustrate the manner in which repeated advance of ice sheets across these continental shelves has resulted in their great depth, rugged bathymetry, and landward-sloping profiles.

Ice has no doubt been present as a geomorphic agent in Antarctica since at least the Oligocene [Robert and Chamley, 1992]. The above debates imply that ice can both be erosive if it is warm-based and conservative if it is cold-based. There are three key questions [Kerr *et al.*, 2000]: Does the present landscape reflect the actions of current glacial processes? If it does, at what rate is the landscape being changed? If it does not, then how and when was it formed? To answer these questions, we must first understand the thermal regime, especially the basal temperature distribution, of the Antarctic Ice Sheet.

Figure 1.3 Meltwater channel and potholes system cut along the western flank of a sandstone butte in the western Asgard Range, Dry Valleys, southern Victoria Land. Cliffs alongside tributary channels in foreground are about 30 to 40 metres high. It is postulated that these channels were cut by subglacial meltwater streams beneath northward-flowing ice that overrode the western Asgard Range (from Denton *et al.*, 1993).

Numerical modelling has unique advantages in testing different hypotheses underpinning the above questions. The ice sheet model developed in this research is to study the mechanism of heat and mass flow in the Antarctic Ice Sheet system. It helps to understand the behaviour of the Antarctic Ice Sheet under different climatic and geothermal conditions, *i.e.* boundary conditions in the language of numerical modelling. It can be applied to calculate the temperature distribution under the Antarctic Ice Sheet. In particular, it helps to estimate whether sufficient basal ice could be melted to form such large-scale meltwater flows capable of shaping the landscapes like those in Figures 1.2 and 1.3.

1.3.3 Subglacial lakes

Oswald and Robin [1973] reported 17 subglacial lakes on the Antarctic continent from airborne radio echo sounding (RES) records at 60 MHz. This figure went up to 68 when further studies covered more than half of the Antarctic continent [Robin *et al.*, 1977; Siegert and Ridley, 1998]. Together with seismic evidence, a total area of 54,000 km^2 or a total volume of 4,000 ~ 12,000 km^3 of subglacial water has been inferred [Dowdeswell and Siegert, 1999]. The biggest subglacial lake, Lake Vostok in East Antarctica, alone occupies an estimated area of 14,000 km^2 and involves about 2,000 km^3 of water [Kapitsa *et al.*, 1996]. Potential release of such huge volumes of subglacial water would cause massive floods with ability to mould the landscape [Shaw, 1996] and raise sea level [Blachon and Shaw, 1995].

The majority of these subglacial lakes are located in the interior of the ice sheet [Siegert *et al.*, 1996]. Ice thickness over most lake locations are over 3000 metres and ice surface slope, ice flow velocity and surface accumulation rate are all small [Oswald and Robin, 1973; Drewry, 1983; Giovinetto and Bentley, 1985]. Antarctic subglacial lakes provide an important boundary condition for the thermal analysis of ice sheets, in that the basal temperature of an ice sheet over subglacial lakes may be assumed to be at pressure melting point [Siegert and Dowdeswell, 1996]. Pressure melting takes place in two main regions of the Antarctic Ice Sheets. One is beneath the centre of the ice sheet, and the other is closer to the ice margin than to the ice divide. In the former locations, the ice thickness is normally greater than 3000 metres. In the latter locations, heat derived from internal ice deformation and sliding, added to geothermal energy, produces melting [Siegert and Dowdeswell, 1996; Dowdeswell and Siegert, 1999]. The presence of these subglacial lakes strongly influences the heat flow at the base of the Antarctic Ice Sheet. Meltwater drainage systems could be associated with the periodic drainage of subglacial lakes and thus explain meltwater channel systems such as those illustrated in Figures 1.2 and 1.3.

1.3.4 Antarctic Ice Sheet and sea level

The thermal regime in the Antarctic Ice Sheet is a key factor in estimating the source and amount of water contributing to the suspected global sea level rise in the 20th Century. The ice mass locked in the Antarctic Ice Sheet counts for about 60 metres of water equivalent in sea level rise [Drewry, 1982]. Although the Antarctic Ice Sheet cannot collapse overnight, coral records show two periods of particularly rapid meltwater influx into the oceans during deglaciation, which are termed MWP(MeltWater Pulse)-1A and MWP-1B by Fairbanks [1989]. MWP-1A corresponded to a 13.5±2.5 metres of sea level rise in less than 290±50 years and MWP-1B 7.5±2.5 metres in less than 160±50 years [Blanchon and Shaw, 1995; Bard *et al.*, 1996]. Sea level rise on such a scale would significantly threaten global environments in a few decades. It is thus important to assess the likely rates of meltwater production beneath the Antarctic Ice Sheet.

1.3.5 Global warming?

Since the industrial revolution in the mid 19th Century, human impact on the environment has been increasing at an unprecedented rate. During the past century especially, mainly due to fossil fuel combustion and industrialised agriculture, concentrations of carbon dioxide (CO_2), methane (CH_4), nitrous oxide (N_2O), and chlorofluorocarbons CFC-11 (CCl_3F) and CFC-12 (CCl_2F_2) in the Earth's atmosphere have been increasing dramatically [Schimel, *et al.*, 1996; Hansen *et al.*, 1998]. Figure 1.4 shows their concentrations in the industrial era [Ledley *et al.*, 1999]. The observed concentration of CO_2 in the atmosphere increased from about 280 ppmv in the pre-industrial era to about 364 ppmv in 1997 [Keeling and Whort, 1998] (Figure 1.4a). The atmospheric concentration of CH_4 increased from about 700 ppbv in pre-industrial times to about 1721 ppbv in 1994 [Prather *et al.*, 1996] (Figure 1.4b). The atmospheric concentration of N_2O increased from about 275 ppbv in pre-industrial times to about 312 ppbv in 1994 [Prather *et al.*, 1996] (Figure 1.4c). Chlorofluorocarbons CFC-12 and CFC-11, mainly used as refrigerants, are human-made compounds that catalyse decomposition of stratospheric ozone and were not

appreciably present in the atmosphere before 1950 (Figure 1.4d). Many researches suggest that the increase of the concentration of these so-called greenhouse gases in the atmosphere has led to global climatic changes [Jones and Briffa, 1992; Overpeck *et al.*, 1997; Briffa *et al.*, 1998; Jones *et al.*, 1998; Mann *et al.*, 1998, 1999].

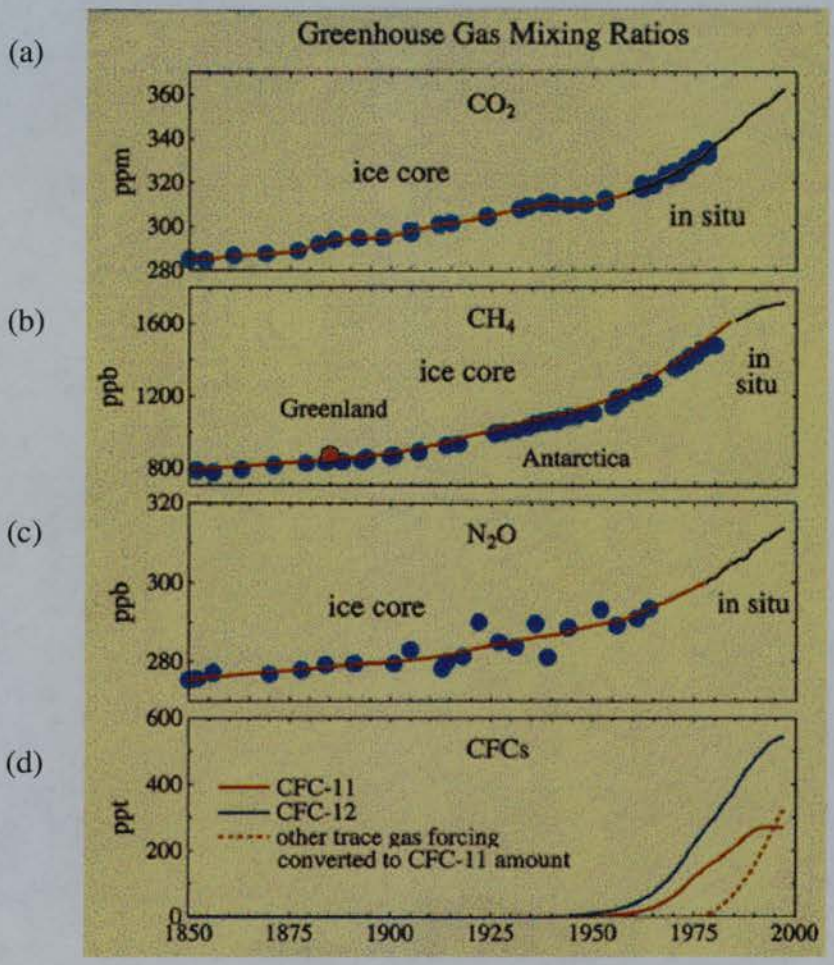

Figure 1.4 Concentrations of principal anthropogenic greenhouse gases in the industrial era. Black curves denote measurements of in situ atmospheric samples collected in recent years. Points denote concentrations determined from air bubbles trapped in polar ice sheets using ice cores obtained in Antarctica or Greenland; red curves denote fits to these points. Data for CFCs are from in situ samples since 1977. Mixing ratios of CFC-11 and CFC-12 prior to the first in situ atmospheric measurements were estimated from industrial production data and assumed atmospheric lifetimes of 50 and 100 years, respectively (from Ledley *et al.*, 1999).

The most commonly considered indicator of climatic changes is the surface air temperature. The reconstruction of the Northern Hemisphere temperature anomaly trend from 1000 A.D. to present shows that the mean annual temperatures of the Northern Hemisphere have warmed up dramatically since the beginning of the 20th Century (Figure 1.5). The analyses of ice cores from Vostok, Antarctica, also indicate a positive correlation between surface air temperature and the carbon dioxide and methane concentrations [Jouzel *et al.*, 1993] (Figure 1.6). Hansen and Lebedeff [1987], Nicholls *et al.* [1996] and Jones *et al.* [1997] estimate that the annual mean temperatures of the Earth's surface have increased between 0.3°C and 0.6°C during the last 150 years.

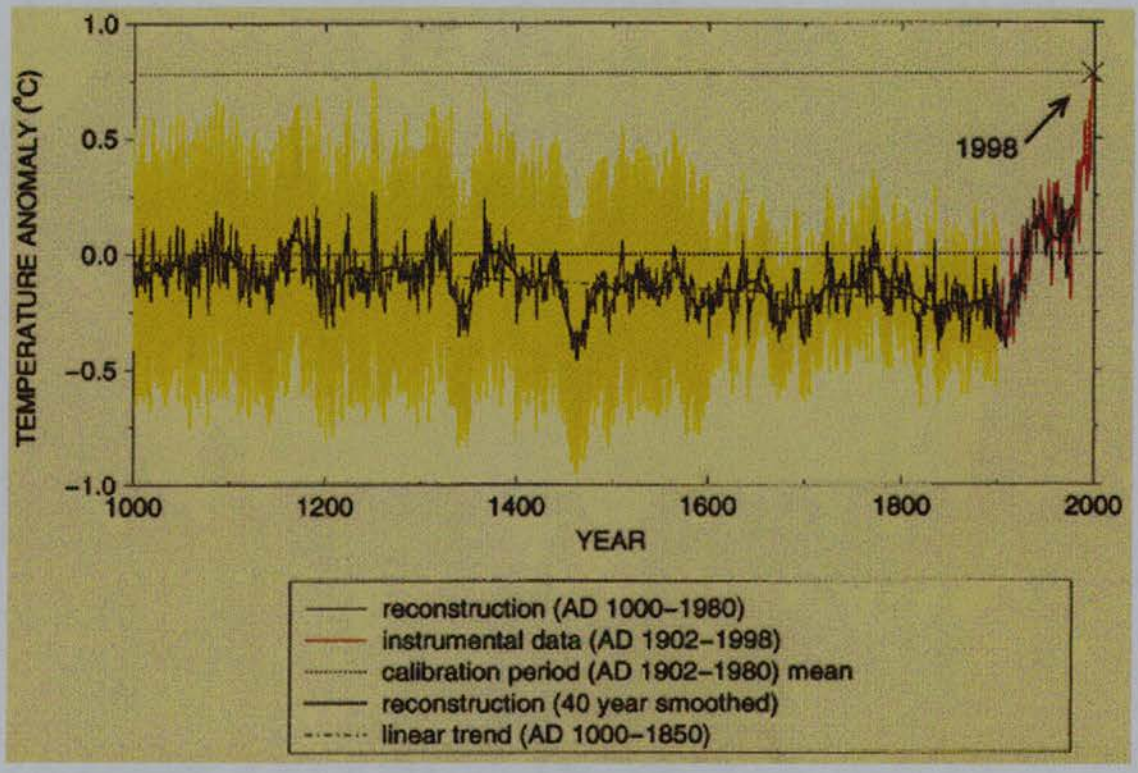

Figure 1.5 Reconstruction of Northern Hemisphere temperature anomaly trend from 1000 A.D. to present from dendroclimatic, coral, and ice-core proxy records as calibrated by instrumental measurements. Thin curves give reconstruction and raw data from 1000 to 1998 A.D. Smoothed version (thick solid), linear trend from 1000 to 1850 A.D. (long dashed), and two standard error limits (shaded) are also shown (from Ledley *et al.*, 1999).

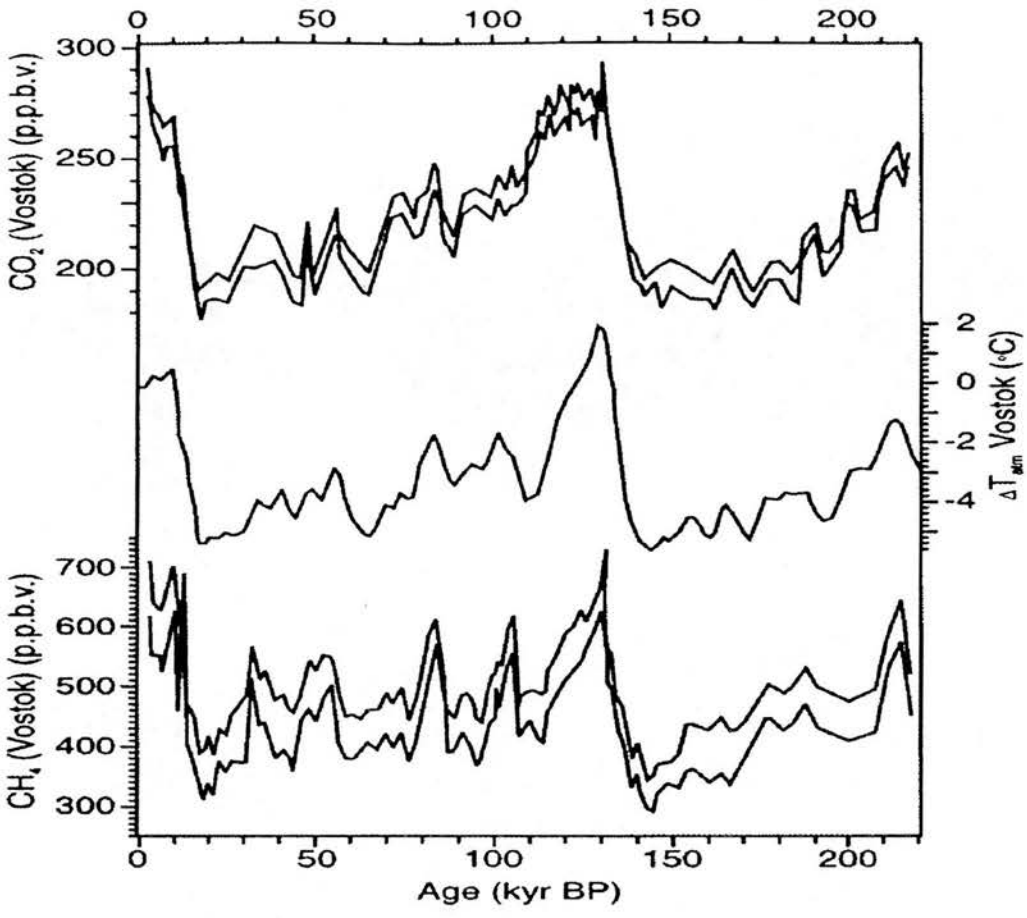

Figure 1.6 Carbon dioxide concentration (top), proxy temperature (middle), and methane concentration from analyses of ice cores from Vostok, East Antarctica (from Jouzel *et al.*, 1993).

This small but persistent global temperature rise is no doubt influencing the behaviour of the Antarctic Ice Sheet. Will the Antarctic Ice Sheet or part of it collapse? How long can the Antarctic Ice Sheet sustain the present climatic change? Or on the contrary, will the present climatic change make the Antarctic Ice Sheet even bigger due to higher precipitation? In that case, how many degrees of temperature rise will trigger the collapse of the Antarctic Ice Sheet? More basically, has the present-day Antarctic Ice Sheet reached equilibrium? To answer these questions, we must have a clear understanding of the thermal regime of the Antarctic Ice Sheet.

A considerable body of evidence suggests that the current temperate interglacial period could be simply the latest of a number of warm episodes forming part of a long-term climatic cycle. In some parts of the world, temperatures may have fluctuated through more than 15°C between warm and cold episodes, temperature change was frequently rapid, and the last 800,000 years alone have witnessed as many as ten full glacial-interglacial cycles [Lowe and Walker, 1997]. So is it possible that the estimated 0.3°C to 0.6°C of global warming during the last 150 years is simply a part of a natural warming episode following a cooling phase in the present interglacial period (Figure 1.5)? Since ice sheets in high latitudes advance and retreat with such climatic oscillations, the modelled time scale of changes in the thermal regime of the Antarctic Ice Sheet may help to answer this question.

Global warming seriously affects the natural environment on the Earth. By testing the behaviour of the Antarctic Ice Sheet under different climatic conditions, the modelling research in this thesis will help in understanding the role of the ice sheet in a warming climate and estimate the degree of response and the time scales involved.

1.4 Ice Sheet Numerical Modelling

There are two main research approaches to the study of the behaviour of ice sheets: field research and numerical modelling. With the rapid development of powerful computers and the increased supply of more detailed and accurate field data, numerical modelling has become more and more popular in ice sheet research. Traditional field studies and numerical modelling are complementary to each other. The former supplies the latter with data of initial and boundary conditions and data for calibrating and justifying the latter. Similarly, the latter can help interpret the field data and help develop ideas for the former.

In the real world, an ice sheet is a complex dynamic system; all its natural phenomena appear as results of intricate factors. These factors interact with each other such that it is extremely difficult for field studies to draw a clear picture of the

role of each one. Besides, the terrestrial stratigraphic record is often highly fragmented; evidence is absent from many areas, while detailed sequences are only locally preserved. Moreover the cyclical nature of climatic change has produced similar environmental conditions at different times and, because many records cannot be dated precisely, the process of correlation is frequently beset with difficulties.

Compared with traditional field research, numerical modelling has its own advantages in simulating the physical characteristics and dynamics of an ice sheet. A theoretically-based numerical model can highlight the intrinsic properties of such a system and make them apparent. This helps researchers understand the system as a whole. By switching on and off certain parameters, a numerical model can also easily highlight the function of an individual factor in ice sheet evolution at a variety of spatial and temporal scales, depending on the focus of investigation. More significantly, by changing input variables, researchers can easily aim to predict the behaviour of the ice sheet under different environmental conditions. Field studies are a "snap-shot" of hundreds of thousand years of history and it is only possible to collect data covering discrete amounts of time. With numerical modelling by contrast, researchers can run the model without a time restriction. This can give a panorama of the whole history of ice sheet evolution that helps us to understand its recent and developing trends. The modelling results can be evaluated by comparisons with field data. This in turn helps modellers to adjust their initial hypotheses. Only after having satisfactorily reconstructed the evolution of an ice sheet can the researchers apply the numerical model to predict the future behaviour of the ice sheet with credibility.

Modelling approaches seek to simplify the complexity of the real world by selectively exaggerating the fundamental aspects of a system at the expense of incidental detail. In presenting an approximate view of reality, a model must remain simple enough to understand and use, yet complex enough to be representative of the system being studied [Anderson and Burt, 1985]. The basic idea of the ice sheet model developed in this research is simple: by isolating the Antarctic Ice Sheet as an open system, the model exams the mass and energy exchange between the ice sheet

system and its outside. The theory of the ice sheet model is based on the Navier-Stokes equation set that governs the mass and energy flow in the natural world. The initial and boundary conditions applied to constrain each model run are based on field studies. These ensure the ice sheet model adequately represents the physical world.

Since Robin [1955] set up the first successful numerical model for steady state ice flow and temperature distribution in ice sheets, an increasing number of researchers have been choosing numerical modelling to study the evolution and behaviour of glaciers and ice sheets. Especially in recent decades, with rapid development of computing facilities and dramatic increases of computing speed, numerical modelling has affected many fields in earth science.

Due to the great differences in geomorphologic and climatic conditions experienced by each glacier or ice sheet, almost all the existing glacier and ice sheet models are site-specific and contain simplifications and assumptions that preclude their use universally. The development of physically based theoretical models reflects a general desire to provide more widely applicable models. Due to the strong couplings of natural factors and high non-linearity of the mathematical relations involved, these physical models have to be computed numerically. Hindmarsh [1993] analysed some theoretical techniques employed in some ice sheet models. His work is of great help to ice sheet modellers in choosing modelling methods for their own work. Bentley [1999] reviewed and compared different methodologies in estimating the volume of the Antarctic Ice Sheet at the Last Glacial Maximum and global sea level change. It is helpful in justifying the performance of an ice sheet model.

The reliability of a numerical ice sheet model depends to a large extent on the credibility of the theories relative to physical factors of the ice sheet, especially ice shelves, geology, climatology and oceanography. The inaccuracy in ice thickness, geothermal heat flux and surface ice accumulation rates, for example, caused the numerical results of Budd *et al.* [1971] to estimate the basal temperatures to be −20°C to −30°C under the central part of the Antarctic Ice Sheet where the existence

of the main group of subglacial lakes indicates the ice is at the pressure melting point. With more abundant and accurate field data, results from this numerical research match the RES analysis well. Another uncertainty of numerical calculation arises in assuming that the true temperature distribution can be approximated by a steady state system, which, although can never be reached in the real world, is adopted in most models. To increase the reliability of a numerical model, the results should be compared with field data whenever possible and the model itself should be corrected according to the comparison.

1.5 Modelling Strategy

To make sure the ice sheet model developed in this thesis addresses the questions raised earlier, we should have a big picture of the overall research in mind, which is summarised in Figure 1.7.

The first and most important step of modelling is to isolate the system of study, the Antarctic Ice Sheet, and clearly define the problem. We can then identify important relationships among the factors involved and choose appropriate mathematical equations that govern the natural processes. To keep the model easy to understand, the simplest mathematics that provides acceptable accuracy should be adopted. Simple mathematics makes the model easy to follow and also helps minimise computing time. Every term in the equations should bear clear physical meaning. Model complexity must not be confused with accuracy. The model should be appropriate to the problem. The assumptions and limitations of the model structure should always be remembered, and the degree of uncertainty associated with model predictions should always be known.

The spatial extent and time scale of the modelled system reflect both the modelling objectives and the degree of realism sought in the model. No natural systems exist in isolation. All systems undergo mass and energy exchanges with the outside. These mass and energy exchanges are the boundary conditions of the model. The system

evolution period starts from a certain status. This status is the initial condition of the model. Both boundary and initial conditions can be derived from data from field studies, idealised conditions to highlight the principal factors, or even modelling results from the previous system evolution. Like the modelled processes of the natural system, boundary and initial conditions should also be expressed mathematically in as simple a way as possible.

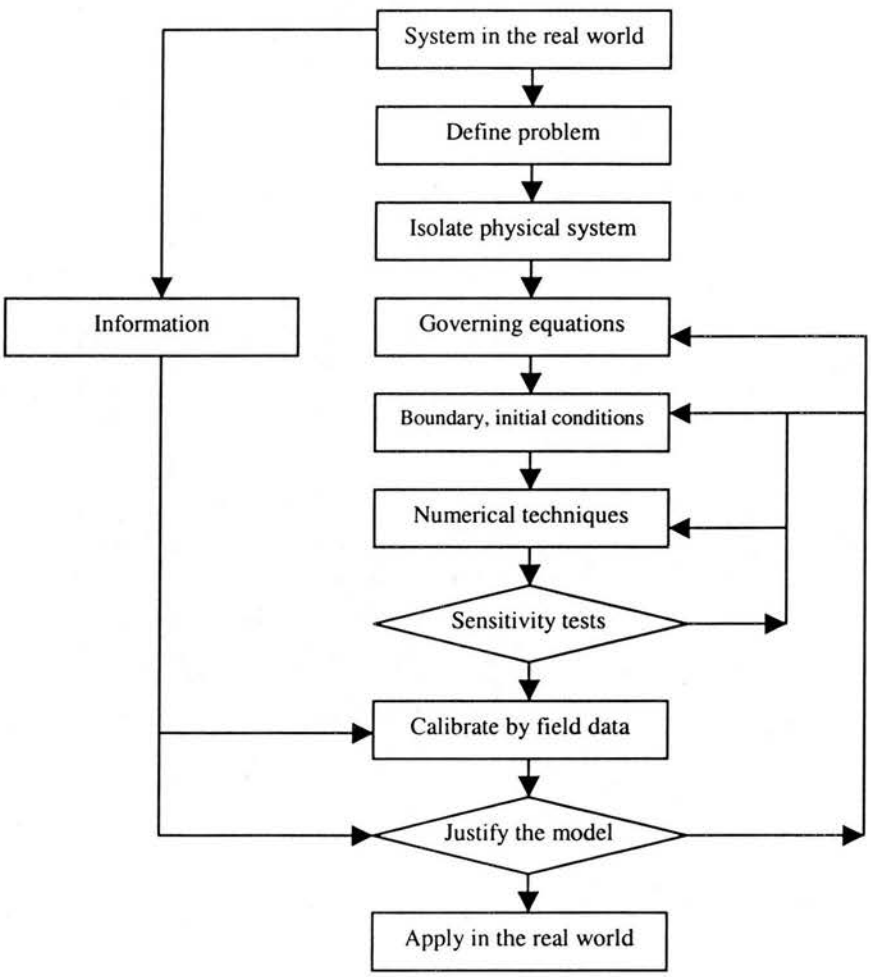

Figure 1.7 Modelling flow chart adopted in this research. From the real world to the real world, the modelling strategy isolates the research objective from its surrounding environment, employs proper modelling techniques, and finally, reinterprets the natural phenomena.

Most natural processes in the real world are non-linear processes. In most cases, no analytical solutions for the governing equations exist. Modellers have to choose an accurate, stable and time-efficient numerical technique to solve the equations. With the increase in the speed and memory of computers, modellers now have more and more freedom to choose numerical algorithms with more accuracy and more stability. The numerical technique applied in this research is the Alternating Direction Implicit (ADI) scheme.

Before a numerical model can be applied to reconstruct the evolution of an ice sheet or to predict the development of the modelled system, it is essential to evaluate, or calibrate, the performance of the model. Evaluation of model performance involves consideration of several components of the modelling procedure. In all cases, there is scope for a greater understanding of the role of each procedure within the overall scheme. In calibration, parameter interdependence can be a problem in numerical models. When examining the performance of one parameter in the numerical model, we should try to keep other parameters unchanged. Sensitivity analysis applied to each parameter can identify the importance of individual variables within the numerical model as a whole. It is also crucial in testing the stability of the numerical technique applied in the model.

The reliability of input data also affects model calibration and verification. The errors introduced into the model by the input data could be amplified by the numerical scheme and thus increase the uncertainty of the modelling results. In this research, for instance, great uncertainty concerns the input value of geothermal heat flux, which is inferred from indirect geological data. Iceberg calving rates from the edge of ice shelves also change from place to place and even year by year, so the modelling of iceberg calving rate is a big challenge. Comparison of model output to field data may say more about the quality of input data, rather than the model mechanisms themselves. Before considering changing the model mechanisms, it is worthwhile trying a range of values that make sense in the real world.

1.6 Research Procedure and Thesis Structure

Before any attempt at modelling, the first and most important step is to define the system that is going to be modelled. This step is the cornerstone for the entire modelling work and the focus of Chapter 2. Mass and energy flow on the Earth is a global-scale intricate dynamic system, within which every subsystem and all factors are related to one another. The Antarctic Ice Sheet system is a subsystem that plays a central role in the global super system. The process of isolating a subsystem out of its super system is to define closed artificial boundaries that totally separate the subsystem from its super system. One key criterion for setting the artificial boundaries is that the mass and energy fluxes across these boundaries are clear and easily quantified. After having clearly defined the modelling system, the chapter analyses each factor that takes a direct role in the Antarctic Ice Sheet system. Both system definition and the analysis of individual factors are prerequisites for numerical modelling. Chapter 2 briefly reviews some approaches to modelling these factors and introduces the approaches employed in this research.

Chapter 3 discusses the numerical tasks of this modelling research. The Antarctic Ice Sheet system is abstracted into a three-dimensional Cartesian system. Under such an idealised system, the mass and energy flow in the Antarctic Ice Sheet system can be depicted by mass continuity and energy conservation equations. This Navier-Stokes equation set universally governs thermodynamic processes. The mass and energy transports across the artificial boundaries are correspondingly abstracted as the boundary conditions for the governing equation set. Likewise, the situation at the time from which the numerically analysis starts is abstracted as the initial condition of the governing equation set. After accomplishing the mathematical depiction of the modelled system, we then explore numerical algorithms to solve the equations efficiently.

Chapter 4 takes the next step and focuses on calibrating the numerical model and its assumptions. This is achieved by producing model predictions that can be compared against independent data such as the present-day subglacial lake distribution and ice

thicknesses derived from airborne Radio-Echo Sounding (RES). Different factors affect the Antarctic Ice Sheet system on different scales. Geothermal heating, for example, is overwhelmingly important at the ice/bedrock boundary. In an ice sheet of a continental scale, thermal conduction in the vertical direction is much stronger than in the horizontal direction. In order to highlight the function of an individual parameter in a simplest possible numerical system, we set up one-dimensional, two-dimensional and three-dimensional idealised ice sheet systems step by step. This approach also benefits model users in understanding the progressive complexity of the numerical system.

Chapter 5 discusses the experiments designed to investigate the evolution and stability of the thermal and dynamical regime of the Antarctic Ice Sheet under different climatic conditions. The ice sheet model is run under two sets of climate forcing conditions: the present-day conditions and those at the glacial maximum. The glacial maximum climate forcing conditions are simulated by artificially dropping the sea level by 120 metres and ice surface temperatures by 6°C from their present-day values. Contrasts in the development of the modelled thermal and dynamical regimes between the East Antarctic Ice Sheet and West Antarctic Ice Sheet suggest the two components of the Antarctic Ice Sheet may respond differently to climatic changes. Based on these analyses, the Dry Valleys in Victoria Land, East Antarctica, is chosen as a case study to demonstrate the model applications.

Chapter 6 summarises the achievements of this research and the conclusions drawn from the modelling results. Under the present-day and glacial maximum climatic conditions, the ice sheet model developed in this research successfully builds up the Antarctic Ice Sheet. The modelling results from this numerical research correspond with the field studies and theoretical analyses.

Chapter 2 Modelling Factors Affecting the Mass and Energy Flow in the Antarctic Ice Sheet

As mentioned in Chapter 1, the Antarctic Ice Sheet acts as a major heat sink in the global climate system. The temperature gradients it causes drive the mass and energy flow at a global scale. The quantities of mass and energy involved in its thermophysical processes are a significant proportion of the global mass and energy flow. Since the Antarctic Ice Sheet is of continental scale, the thermophysical processes of the ice sheet system are also of a continental scale. The mass and energy flows in these thermophysical processes are therefore characterised by very high quantities and very low densities due to the large spatial scale and long time scale. Climatic changes at the global scale are reflected by small but persistent variations in temperature, precipitation and other meteorological quantities. For some short-term records, the signal-noise ratio may be too high to analyse accurately. However, the dynamical and thermal regimes in the Antarctic Ice Sheet system, especially the mass balance and basal temperatures, are sensitive to these small but persistent variations. Thus, the long-term evolutionary trend of the Antarctic Ice Sheet is a good indicator of global climatic changes.

This chapter aims to abstract the individual factors that affect the thermophysical processes in the Antarctic Ice Sheet system. The purpose of these abstractions is to sift out the unimportant details of the factors so that only the appropriate characteristics that portray the functions of these factors remain. The role of this chapter is to show the techniques and approaches inherited from past work and explain the new approaches to deal with some factors and why we need them. In the following text, we are going to review the important ice sheet parameters, including physical properties, thermodynamical processes at the basal and upper boundaries and in the body of the ice sheet and isostasy. These parameters determine the

behaviour of the ice sheet. The precision of these parameters is the cornerstone in understanding the mechanisms of ice sheet evolution.

2.1 Thermophysical properties of ice

The thermophysical properties of the material in the Antarctic Ice Sheet system, ice, determine the thermophysical processes in the system. Those thermophysical properties of ice normally involved in ice sheet modelling are thermal conductivity, thermal diffusivity, specific heat capacity, specific latent heat of fusion, density and the Arrhenius factor. Given the depth of an ice sheet, the high pressure makes the ice behave in a way similar to the pure material. Therefore, the values of the thermophysical properties of pure ice are normally applied in ice sheet modelling [Huybrechts, 1992; Paterson, 1994]. The ice sheet model developed in this research will follow this convention. Except for the Arrhenius factor for ice, other thermophysical properties of ice are conventional and well established.

Laboratory experiments suggest that ice behaves as a viscous fluid under high pressure and its viscosity depends on the stress and temperature fields [Jacka, 1984; Jacka and Maccagnan, 1984; Jacka and Budd, 1991]. Field measurements confirm that these laboratory conclusions apply to ice sheets over appropriate time scales [Budd and Jacka, 1989]. Plastic flow of ice can occur at any stress at a strain rate which, ignoring the small additional effect of primary transient creep, increases as the nth power of the stress [Petrenko and Whitworth, 1999]. Glen [1955] gives the relation between the strain rate $\dot{\varepsilon}$ (deformation rate) and the stress τ,

$$\dot{\varepsilon} = A(T, \cdots)\tau^n \tag{2.1}$$

where $n \approx 3$ for the polycrystalline ice in ice sheets. Equation (2.1) is often referred to as Glen's flow law. It forms the basis for the theoretical understanding of ice flow.

$A(T,\cdots)$ in equation (2.1) is the Arrhenius factor for ice. It directly influences the behaviour of ice flow, so it is also referred to as the flow-law coefficient. The Arrhenius factor depicts the sensitivity of the strain-stress relationship of ice. It is normally modelled as a function of temperature, either as discrete values for a series of temperatures [Paterson, 1994] or as an empirical temperature-flow coupling formula [Paterson, 1994; Huybrechts, 1992]. The ice sheet model developed in this research applies the former for quick experimental runs and the latter for calibration and specific experiments.

In practice, Paterson [1994] proposes that the Arrhenius relationship according to laboratory experiments is

$$A(T^*) = A_0 \exp\left(-\frac{E}{RT^*}\right) \tag{2.2}$$

where T^* is the absolute ice temperature (in K) corrected for the dependence of the melting point on pressure; R = 8.314 $\mathrm{Jmol^{-1}K^{-1}}$, the gas constant; A_0 a heuristically adjusting coefficient which is independent of temperature; E the activation energy of ice flow.

Huybrechts [1992] suggests the values of A_0 and E as

$$\left\{\begin{array}{ll} A_0 = 1.14\times10^{-5}\,Pa^{-3}yr^{-1}; E = 60kJmol^{-1} & T^* < 263.15K \\ A_0 = 5.47\times10^{10}\,Pa^{-3}yr^{-1}; E = 139kJmol^{-1} & T^* \geq 263.15K \end{array}\right\}. \tag{2.3}$$

The higher value of E for $T^* \geq -10°C$ may be related to enhanced creep due to the presence of meltwater at grain boundaries.

Huybrechts [1992] adds a tuning coefficient m into the standard expression for the Arrhenius constant, equation (2.2), in order to map the modelling results closer to the results from field survey,

$$A(T^*) = mA_0 \exp\left(-\frac{E}{RT^*}\right). \tag{2.4}$$

Huybrechts [1992] suggests a value of 20 for this tuning parameter. Although the choice of this figure is rather arbitrary, this tuning coefficient may reflect the height-width ratio of a real ice sheet that is difficult to model in a laboratory.

The temperature distribution in an ice sheet is not uniform; hence the flow law coefficient is not uniform either. When dealing with vertically integrated quantities, such as the flow velocities of the ice sheet, a proper vertically averaged flow law coefficient should be applied. The vertical profile of ice flow velocity is characterised by the relative depth, *i.e.* layers, in the ice sheet body rather than the absolute depth. For this reason, a dimensionless vertical coordinate for ice depth, ζ defined by the absolute depth over the thickness of an ice sheet, is adopted with $\zeta = 0$ denoting the ice surface and $\zeta = 1$ the ice bottom. $\overline{A}$ is heavily weighted to the bottom of an ice sheet where the temperatures are highest because heating processes are strongest [Paterson, 1994]. Based on the normalised vertical community-ordinate, Hindmarsh [1993] models the vertically averaged flow law coefficient for ice sheets as

$$\overline{A} = (n+2)\int_0^1 A\zeta^{n+1} d\zeta \tag{2.5}$$

where n is the exponent in Glen's flow law and normally adopts the value 3 in ice sheet calculations.

Equation (2.2) or (2.4) couples the dynamical regime of an ice sheet with its thermal regime during the running of an ice sheet model. Paterson [1994] suggested a series of values for the flow law coefficient of ice at different temperatures when the exponent in Glen's flow law is treated as 3 (Table 2.1). A thermo-dynamical de-coupled ice sheet model can employ these segmented linear values of the Arrhenius factor for ice. The thermo-dynamical de-coupled ice sheet modelling is a coarser

approximation than the corresponding coupled modelling. The Arrhenius values suggested in Table 2.1 will be applied in the sensitivity tests presented later.

Table 2.1 Recommended values of the Arrhenius constant for ice at different temperatures when the exponent in Glen's flow law is treated as 3 (from Paterson, 1994).

T (°C)	A ($s^{-1}kPa^{-3}$)
0	6.8×10^{-15}
–2	2.4
–5	1.6
–10	4.9×10^{-16}
–15	2.9
–20	1.7
–25	9.4×10^{-17}
–30	5.1
–35	2.7
–40	1.4
–45	7.3×10^{-18}
–50	3.6

Table 2.1 gives us an idea how the Arrhenius factor for ice changes with temperature. Its value will further drop to less then a thousandth of that at melting point if the ice temperature drops below –60°C [Hindmarsh, 1993]. Besides temperature, the Arrhenius factor and other thermophysical properties also depend on some other factors like moisture content [Duval, 1977], dirt content [Fisher and Koerner, 1986], isotopic contents and ice crystal structure [Budd and Jacka, 1989]. To what extent the impurities in ice sheets affect the thermophysical properties of ice is a big uncertainty, if not the biggest, in ice-flow studies. Paterson and Budd [1982] studied the parameters for ice sheet flow. Budd and Jacka [1989] reviewed the rheological properties of ice required for modelling the flow of ice sheets. They conclude that the Arrhenius factor for ice can effectively serve as a combined tuning parameter: adjusting its value could implicitly incorporate the effects of crystal structure, impurity content and basal sliding, *etc.*

2.2 Ice-bedrock Interface

The ice-bedrock interface is the most thermoactive part in the ice sheet energy system. This interface is not necessarily above sea level. Most of the West Antarctic Ice Sheet, for example, is grounded at over 1 km below sea level and at more than 2 km below sea level in the Byrd Subglacial Basin [Anderson, 1999]. The majority of the East Antarctic Ice Sheet is grounded above sea level.

Thermal processes at the ice-bedrock interface to a large extent control ice sheet behaviour. Due to the difficulties of access, our knowledge is mostly inferred from indirect means of study, such as radio echo sounding (RES) for the phase status and seismics for ice thickness. Heat sources involved in thermophysical processes at the ice-bedrock interface are: geothermal heat flux from the interior of the Earth, basal sliding, ice deformation and viscous dissipation due to the flow of meltwater through passages in the ice sheet [Nye and Frank, 1969; Shreve, 1972]. The effect of long-term climate changes can also affect temperatures at the base of the ice sheet.

2.2.1 Geothermal heat flux

The geothermal heat flux contributes a considerable proportion of energy consumed in basal melting processes and normally serves as the basal boundary condition for calculations of temperature distribution in an ice sheet. Because 98 percent of the Antarctic continent is currently covered by a huge ice sheet, direct measurement of the values of geothermal heat flux is extremely difficult. Values often used in most Antarctic ice sheet models are normally estimated from the correlation between heat flux and major geological features [Lee and Uyeda, 1965]. Huybrechts and Payne [1996] applied a value of 42.0 mW/m^2 for the geothermal heat flux when calculating basal temperature distribution under the Antarctic Ice Sheet. This value is believed to be applicable to the East Antarctic Ice Sheet [Näslund, 1998] since it is valid for precambrian shields in general [Lee and Uyeda, 1965]. Based on geophysical studies to the heat flow through oceanic and continental crust, Sclater *et al.* [1980] suggest a higher geothermal heat flux value of 54.6 mW/m^2 for the average value for the entire

Antarctic continent. Huybrechts [1990a] and Näslund [1998] apply this higher geothermal heat flux value in their modelling experiments for the Antarctic Ice Sheet because they believe this value better reflects the geological character of the Antarctic continent. Hansen and Greve [1996] test a range of geothermal heat flux values between 42 and 105 mW/m² in their polythermal Antarctic ice sheet model. They conclude that a value of 50 ~ 60 mW/m² gives the best coincidence of model results and measurements with regard to properties such as total ice volume and maximum ice thickness.

Since all values for geothermal heat flux come from estimation rather than direct field measurement, a range of values are tested in this research in order to evaluate the effect of geothermal heat flux on basal temperatures. Näslund's [1998] experiments conclude that a 25 percent reduction in geothermal heat flux corresponds to a decrease of about 3.5 K in the basal temperatures of the Antarctic Ice Sheet under present-day climatic conditions. For easy comparison with previous modelling exercises, the experiments in this thesis apply 42.0 mW/m² as the reference value for the geothermal heat flux of the Antarctic continent. Our testing results indicate that basal temperatures could be more sensitive to geothermal heat flux than Näslund's estimation (Chapter 4).

2.2.2 Ice/bedrock frictional heating

Ice sheets tend to slide over bedrock where a shear stress gradient exists at the boundary layer above the ice/bedrock interface. The meltwater layer between ice and bedrock acts as lubricant, so basal sliding is expected under warm-based ice sheets where the basal ice is at the pressure melting point. Friction between the sliding ice and bedrock dissipates mechanical energy of the ice into heat. In the present Antarctic Ice Sheet system, basal meltwater is not thought to exist in extensive or wide enough layers to enhance the flow of the ice sheet by basal sliding [Anderson, 1999].

Frictional heating, which is concentrated within the boundary layer of a grounded ice sheet, can exceed geothermal heating by a factor of 10 in areas where ice flows fast [Paterson, 1994]. Hindmarsh [1990] suggests that along the x direction, frictional heating $\dot{q}_{bf}$ can be calculated as the product of the x component of the vertically averaged ice velocity $\bar{u}$ and the basal shear stress τ_{xz},

$$\dot{q}_{bf}\Big|_x = \bar{u}|\tau_{xz}|, \tag{2.6}$$

where the subscript *bf* denotes *b*asal *f*riction. Equation (2.6) implies that frictional heating will increase from the ice sheet divide to the ice sheet margin due to the increase of ice flow velocity. In grounded ice sheets where basal friction is high but ice flow velocity and velocity gradient are not, basal shear stress is essentially controlled by the surface slope and ice thickness. In other words, under such conditions shear stress in an ice sheet can be obtained from the surface slope of the ice sheet [Morland, 1984], such that:

$$\tau_{xz} = -\rho_{ice} g(H + h - z)\frac{\partial(H + h)}{\partial x} \tag{2.7}$$

where ρ_{ice} is ice density; g = 9.81 m/s², the acceleration of gravity. Equation (2.6) therefore becomes

$$\dot{q}_{bf}\Big|_x = \bar{u}\rho_{ice} g(H + h - z)\frac{\partial(H + h)}{\partial x}. \tag{2.8}$$

Equation (2.8) indicates that frictional heat at the boundary layer above the ice/bedrock interface is directly proportional to ice flow velocity, ice thickness and ice surface slope. Similarly, along the y direction,

$$\dot{q}_{bf}\Big|_y = \bar{v}\rho_{ice} g(H + h - z)\frac{\partial(H + h)}{\partial y}, \tag{2.9}$$

where $\bar{v}$ is the y component of the vertically averaged ice velocity.

Numerical calculations show that frictional heating alone is sufficiently strong for the base of the seaward marginal zone of a grounded ice sheet to reach the melting point [Hutter *et al.*, 1986; Herterich, 1988; Huybrechts and Oerlemans, 1988; Hindmarsh *et al.*, 1989; Huybrechts, 1990b]. The magnitude of this marginal zone can extend upstream as far as a tenth or more of the span of the ice sheet.

2.2.3 Ice deformation – Internal strain/frictional heating

Like all materials, ice deforms under pressure. In a deep ice sheet, the stress is so strong that the ice can no longer be treated as a rigid material. The elastic ice crystals undergo non-Newtonian strain under strong internal stress and sliding between ice crystals also occurs. These dissipation processes transform mechanical energy into heat through friction between ice crystals. This internal strain heating is an important heat source in an ice sheet system. The internal frictional heating rate per unit volume of ice can be expressed as

$$\dot{q}_{if} = \dot{\varepsilon}\tau \tag{2.10}$$

subscript *if* denotes *i*nternal *f*riction.

Near the base of an ice sheet where heating processes are strongest, ice-deformational heating due to longitudinal strain rates $\dot{\varepsilon}_x$ and $\dot{\varepsilon}_y$ is small compared to that due to the horizontal shear strain rates $\dot{\varepsilon}_{xz}$ and $\dot{\varepsilon}_{yz}$ [Paterson, 1994]. Using this assumption, Huybrechts [1986] estimated the internal frictional heating as

$$\dot{q}_{if} = 2\dot{\varepsilon}_{xz}\tau_{xz} + 2\dot{\varepsilon}_{yz}\tau_{yz} = -\rho_{ice}g(H+h-z)\frac{\partial \vec{V}}{\partial z}\cdot\nabla(H+h) \tag{2.11}$$

where $\vec{V}$ is the three-dimensional ice flow velocity. The ice sheet model developed in this research follows this estimate.

2.2.4 Viscous dissipation

Observations have proved the existence of a network of water-filled channels under ice sheets [Nye and Frank, 1969]. When water flows through these channels, viscous dissipation due to the friction between the channel walls and flowing water tends to melt the channel walls. The heat generated by viscous dissipation can be strong enough to change the network of the subglacial meltwater channels. Shreve [1972] gave a formula for calculating the melting rate, M, of the channel walls:

$$M = -\frac{M_d\left[(1-\kappa)\frac{\partial M_p}{\partial s} + \kappa\rho_{water} g \frac{\partial z}{\partial s}\right]}{\pi d \rho_{ice} L_{ice}} \tag{2.12}$$

where M_d is the meltwater discharge; M_p the meltwater potential; s the distance along the water channel in the direction of flow; ρ_{water} and ρ_{ice} the densities of water and ice respectively; g the acceleration of gravity; d the radius of the meltwater channel; L_{ice} the specific latent heat of fusion of ice, 3.35×10^5 J/kg; and

$$\kappa = \rho_{water} c_{p\_water} T_{cc} \tag{2.13}$$

where c_{p_water} is the specific heat capacity of water and T_{cc} the decrease rate of ice melting temperature under pressure. The size of a water channel is determined primarily by the gradient of the meltwater potential along the channel and the amount of discharge through it, and secondly by the roughness of its walls.

The above melting rate is calculated under the assumption of steady state. In the real world, however, a steady state is never quite attained. In non-steady states, the response at any one point depends in part on conditions in the whole system of the water channels rather than those in their immediate vicinity. What is more, the

disparity in response time of the meltwater and the ice is significant. In a non-steady state, meltwater almost instantaneously reflects any disturbance by changing the pressure, and hence the melting rate, throughout the system. The response of ice is propagated through the system much less rapidly as kinematic waves [Shreve, 1972]. In the Antarctic Ice Sheet, because almost all the meltwater is trapped under the ice sheet, the system of water channels tends to ignore the short-term fluctuations in climate.

In this research, however, we are interested in the response of the Antarctic Ice Sheet to long-term climatic changes. In this case, we can safely ignore the details about how exactly the subglacial meltwater is produced and drained, and merge them into a relationship on a continental scale linking climatic change and meltwater quantity.

2.2.5 Subglacial meltwater drainage

The nature of meltwater at the base of the Antarctic Ice Sheet has long attracted the interests of scientists, especially in West Antarctica where most of the ice sheet is grounded below sea level. Does the meltwater occur as a thin film that spreads under the immense hydrostatic pressure at the base of the ice sheet [Weertman, 1972] or do channelised meltwater systems exist beneath the ice sheet [Hughes, 1981]? Alternatively, the meltwater may be incorporated into the sedimentary bed upon which the ice sheet rests. These are important issues, because they bear on the mechanism of ice sheet sliding and ultimately on the stability of the Antarctic Ice Sheet.

Hindmarsh [1993] summarised the drainage of subglacial meltwater as four types. They are normal Darcian flow through underground aquifers, flow in channels at the glacier base incised into either ice or bedrock, sheet flow between ice and base, and linked-cavity flow where water is stored in large cavities in the ice which are linked by small channels. The temperatures around all of these subglacial meltwater systems must be at their local pressure melting points, including situations where a subglacial lake can form. Analysis of the RES frequency distributions of the bedrock

heights and slopes bordering each identified subglacial lake implies that most of these Antarctic subglacial lakes are located in the areas of relatively low bed relief and large lakes tend to occur where bed topography is subdued [Dowdeswell and Siegert, 1999]. In other subglacial areas where the topography does not favour the presence of subglacial lakes, basal ice may still be melting and some forms of subglacial meltwater systems exist. The modelled basal temperature distributions of the Antarctic Ice Sheet in this research support this point. In Chapter 5 we see that there are greater areas at the pressure melting point than suggested by the subglacial lakes identified by the RES research.

The flow of subglacial meltwater is controlled mainly by two factors: the ice thickness gradient and the basal slope. The resultant pressure gradient beneath an ice sheet normally serves to drive the meltwater outwards. The balance of the pressure gradient, p, guides the direction of water flow [Oswald and Robin, 1973]:

$$p \propto -\rho_{water} g \beta_x - \rho_{ice} g \frac{\partial H}{\partial x} \tag{2.14}$$

where β_x is the basal slope. Since

$$\frac{\partial H}{\partial x} = \alpha_x - \beta_x \tag{2.15}$$

where α_x is ice surface slope,

$$p \propto -\left(\frac{\rho_{water}}{\rho_{ice}} - 1 \right) \beta_x - \alpha_x . \tag{2.16}$$

Thus flow in the positive sense due to a negative surface slope can be prevented by a basal slope in the opposite sense and greater by a factor of at least $\frac{\rho_{wate}}{\rho_{ice}} - 1$, in which

case, where the meltwater potential is low, a subglacial lake will be formed. Such conditions are most likely to be found in localities where surface slopes are small.

Röthlisberger [1972] gives a detailed analysis of the volume of ice melt in subglacial channels. He assumes the steady flow of meltwater together with the equilibrium of closure and melting rate as the principles on which to compute pressure. Röthlisberger's ice-melting model is based on the analysis of the energy loss in hydraulics of the meltwater. His model applies to subglacial channels at least 50 metres below the ice surface. Röthlisberger's modelling results show that pressure decreases with increasing discharge and the pressure change involves a temperature change as well.

The ice sheet model developed in this research does not take these factors into account because we assume the meltwater under the Antarctic Ice Sheet is in a closed system. The mass loss of the Antarctic Ice Sheet system is through iceberg calving and ice shelf melting rather than by subglacial meltwater discharge. So the pressure under the Antarctic Ice Sheet is overwhelmingly determined by the thickness of ice. Understanding the mechanisms of subglacial meltwater drainage helps justify the assumptions employed in this research.

2.3 Ice-Atmosphere Interface

The ice-atmosphere interface is the upper boundary of the system for a grounded ice sheet. Energy and mass exchange across this interface is directly related to climatic changes.

2.3.1 Mass balance on the ice surface

One of the most important problems in modelling the Antarctic Ice Sheet concerns the precise estimate of the present-day mass balance over the ice surface. Snow falls onto the surface of ice sheets and compacts itself into ice. The expansion of the

Antarctic Ice Sheet increases both the albedo and the altitude of the surface of the Antarctic continent, thus introducing a powerful feedback loop reinforcing the glacial climate and promoting further glacial growth [Payne, 1988; Sugden, 1996]. Climatic changes are directly mirrored by the rate of snowfall over the surface of the Antarctic Ice Sheet. Higher air temperature increases the moisture capacity, and hence increases the rate of snowfall. Today about $2.2\sim2.7\times10^{12}$ tons of ice accumulates over the Antarctic Ice Sheet each year [Doake, 1985; Giovinetto and Bentley, 1985]. To a large extent, this net mass accumulation determines the stability of the Antarctic Ice Sheet. For a polar ice sheet, even a small disturbance in ice accumulation will produce a considerable effect on the temperature gradient in the ice sheet [Robin, 1955]. Since the present-day air temperatures over the Antarctic continent are so low that surface melting and runoff are virtually absent, the ice surface mass balance is positive almost everywhere on the continent [Huybrechts, 1993]. As a consequence, the modelling of the ice surface mass balance can be satisfactorily simplified to the modelling of the ice equivalent of snowfall capacity. The ice sheet model developed in this research therefore employs an empirical formula that estimates the snowfall capacities over Antarctica dependent on geographical location represented by the surface temperature (See §3.3.2 – Surface mass balance).

Since ice flow will transport a mass balance change downstream, an ice sheet model sometimes may have to correct this effect in order to simulate a realistic mass-balance/temperature relationship [Jóhannesson *et al.*, 1989; Nye, 1960]. This correction can be achieved by subtracting the mass loss at the downstream ice sheet margin from the ice surface accumulation. The Antarctic Ice Sheet loses its mass primarily by iceberg calving at the marine margins of the ice shelves and some basal melting beneath the ice shelves. The mass balance of the entire Antarctic Ice Sheet system is estimated by obtaining the difference between the accumulation over the ice sheet and ablation by iceberg calving and ice shelf melting. The influence of the changes on surface mass balance can reach as far as the bottom of the ice sheet since the stress field of an ice sheet is determined by its local geometry. The ability of an ice sheet model to simulate a real ice sheet therefore depends primarily on a good specification of mass balance on the ice surface in time and space.

Hulton and Sugden [1995] link ice sheet models to the surface mass balance by focussing on the role of changing atmospheric patterns and their influence on precipitation. They develop a mass balance model that accurately reflects the present-day distribution of precipitation and seasonal snow mass balance in Patagonia and is forced by a fairly simple set of regional climatic variables that can be adapted to adjust the importance of precipitation and evaporation. The precipitation model is defined by a revised vertically integrated moisture-balance equation for describing atmospheric precipitable water. Boundary conditions of this precipitation model are moisture gradients and wind. Moisture gradients are prescribed as zero at the boundaries. The inputs to the model are sea-surface temperatures and the geostrophic wind at 700 mbar. This precipitation model employs a sinusoidal function to simulate temperature variation throughout the year for each location. Hulton and Sugden's model works satisfactorily in reconstructing the evolution of the ice sheet in Patagonia. Their work is a good reference for modelling alpine ice sheets that are under strong marine influence. For the Antarctic Ice Sheet, however, marine influence is significant only at the ice sheet margin.

2.3.2 Ice surface temperature

The Antarctic continent is located at the South Pole region. It has the coldest surface temperatures on the Earth. The surface temperatures in the interior of the Antarctic Ice Sheet are about 35°C lower than near its marine margin (See Figure 5.2). The annual mean temperature on the whole continent is about -50°C [Rubin and Weyant, 1965]. Under such low temperatures, surface melting on the Antarctic Ice Sheet is virtually negligible. Air temperature changes are therefore reflected by the surface ice the whole year round. In Antarctica, ice accumulates at the cold surface and sinks towards the warmer bottom. However, field studies found that the annual temperature fluctuation over the Antarctic Ice Sheet fades out at about 10 metres below the ice surface [Loewe, 1970], meaning that the annual temperature fluctuation cannot affect the temperature distribution down into the ice sheet. This phenomenon is essential to the analyses of thermal processes in the Antarctic Ice

Sheet in this modelling research. Since this 10-metre-deep layer can be treated as an iso-thermal layer, it is justifiable to set the ice surface temperature as equivalent to the annual mean ice surface temperature. More significantly, the surface of the ice sheet can be treated as infinitely far from the bottom to simplify the numerical scheme. A detailed analysis is given in §4.1.1.

In inland Antarctica, air temperature alone explains over 85 percent of the variation of the accumulation rate [Fortuin and Oerlemans, 1990]. As analysed in the previous section, it is actually a controlling factor for precipitation, *i.e.* mass balance, of the Antarctic Ice Sheet system. A rise of 10°C of the annual mean surface temperature over the Antarctic Ice Sheet would correspond roughly to a 60 percent increase of the surface accumulation rate, which would then be analogous to present-day Greenland [Huybrechts, 1993]. In the ice sheet model developed in this research, ice surface temperature directly determines the mass input into the modelled Antarctic Ice Sheet system.

2.4 Thermal Processes in an Ice Sheet

Energy and mass flows in the ice body, although not as active as at the interfaces, drive the ice sheet as a dynamical system. Cold ice accumulated at the surface flows down towards the bottom and margin of the ice sheet. The heat flux driven by the temperature gradients and by mass displacement determines the thermal regime of the entire ice sheet system.

2.4.1 Thermal conduction

Wherever temperature gradients exist in a continuous medium, thermal conduction occurs. Fourier's law of thermal conduction depicts the relation between heat flux and temperature gradient. In an isotropic uniform continuous material, heat flux, q_x'', is directly proportional to the thermal conductivity of the medium, k, and the

temperature gradient, $\frac{dT}{dx}$, and of the opposite direction with the temperature gradient [Incropera and Dewitt, 1996],

$$q_x'' = -k\frac{dT}{dx}. \tag{2.17}$$

As analysed in §2.1, following modelling convention, the ice sheet model developed in this research employs the thermal conductivity of pure ice.

According to the measurement of temperature profiles in some accumulation areas of the Antarctic Ice Sheet, the temperature difference between the bottom and surface of the ice sheet is 10°C ~ 25°C [Paterson, 1994]. Since the average thickness of the Antarctic Ice Sheet is about 2300 metres and ice is a bad thermal conductor, according to the Fourier's law, the actual thermal flux due to thermal conduction is very low. Thermal conduction is therefore not a dominant thermal process in the Antarctic Ice Sheet system. In §4.1 and §4.2, we will exam the functionality of thermal conduction in comparison with thermal advection, which dominates the mass and heat transfer in the Antarctic Ice Sheet system.

2.4.2 Thermal advection

Ice flow displaces not only mass but also heat. Thermal advection in an ice sheet refers to the heat transfer due to the motion of ice. In the ice sheet model developed in this research, mass transfer along vertical and horizontal directions due to ice flow in the Antarctic Ice Sheet system is represented by the vertical and horizontal components of ice flow velocity respectively in the governing thermodynamical equation.

Field observations find that heat flux due to advection in an ice sheet can be estimated against that due to conduction by the Peclet number [Hindmarsh, 1993],

$$P = \frac{aH}{36} \tag{2.18}$$

where a is the surface accumulation rate in m/yr; H ice sheet thickness in m. The ice sheet model uses the Peclet number to evaluate the functionality of thermal advection against that of thermal conduction. Equation (2.18) suggests that in an ice sheet whose annual accumulation is of the order of 10^{-1} m and ice thickness is of the order of 10^3 m, thermal advection in the ice sheet is stronger than thermal conduction by an order of 10. The Peclet number is typically of this order for the Antarctic Ice Sheet, and means that thermal advection is the dominate means of heat transfer. If the magnitude of annual accumulation drops to the order of 10^{-2} m, the Peclet number will be of the order of 1; hence the effects of heat conduction and advection are compatible.

The temperature gradient is directly proportional to the temperature difference and inversely proportional to the distance. Only under large temperature gradients is thermal conduction significant. Heat is therefore transported principally by advection in the upper part of an ice sheet. In the lower part of the ice sheet, however, especially within the boundary layer formed immediately above the bedrock, thermal conduction is comparable with, or even more important than, thermal advection. Here, we assume that horizontal thermal conduction is negligible. The relative functionality of thermal conduction and thermal advection in an ice sheet system is investigated in §4.2.5.

2.5 Dynamic Characteristics of an Ice Sheet

The stability of the Antarctic Ice Sheet is explicitly indicated by its dynamic characteristics. The oscillation of the area of the sea ice influences not only the thermal radiation, but also the global air and water circulation. The volume of the Antarctic Ice Sheet directly influences global sea level. Bentley [1999] reviewed research on the volume of the Antarctic Ice Sheet. This section briefly analyses ice

thickness, ice flow velocity and iceberg calving from the marine margin of the ice sheet. These dynamic characteristics are crucial parameters in the ice sheet model developed in this research.

2.5.1 Ice thickness

The ice in ice sheets is generally treated as incompressible material. Consequently, the change in ice thickness at a given point is the net result of ice flux, surface accumulation, ablation, basal melting and re-freezing. Ice thickness plays a key role in the thermodynamic regime of the Antarctic Ice Sheet system. The weight of the overlying ice imposes extraordinarily high pressures near the bottom of an ice sheet. The melting temperature of crystal materials is a function of pressure; higher hydrostatic pressure results in higher melting temperature [Hutter, 1983]. Higher melting in turn provides more "lubricant" between ice and bedrock; ice slides more easily over bedrock. Ice deforms under high pressure, which reinforces ice flow and more frictional heat will be generated. Ice thickness also strongly influences the temperature distribution in the ice sheet system. Airborne radio-echo sounding (RES) research provides evidence that the mean thickness of ice above the subglacial lakes in Antarctica is about 3000 metres [Dowdeswell and Martin, 1999]. Increased basal temperatures soften basal ice by increasing its Arrhenius parameter, which in turn makes the ice flow more easily.

Surface mass balance is essentially used as a tuning parameter in modelling ice thickness. Oerlemans and van der Veen [1984] model ice thickness as a function of geographical position and time following the spatial and temporal changes of ice surface mass balance. Analytical solutions [Weertman, 1961] suggested that small changes in the ratio of accumulation to ablation and in the spatial gradient of the equilibrium line elevation give rise to far larger changes in the span and maximum elevation of the ice sheet, which is reflected by the ice thickness. Numerical research reinforces the concept of ice thickness sensitive to surface mass balance distribution [Budd and Jenssen, 1975; Mahaffy, 1976; Birchfield, 1977; Birchfield *et al.*, 1981; Oerlemans, 1981]. In particular, Hindmarsh [1990] and Johannesson *et al.* [1989]

find that the maximum ice thickness H_{max} in Antarctica can be estimated as proportional to $(a/A)^{1/8}$, where a is accumulation rate and A the Arrhenius factor for ice. The ice sheet model developed in this research calculates the ice thickness from the mass continuity equation (3.1). This is a dynamic relation that links ice thickness with ice flow. Surface mass balance, together with the basal melting rate, is employed as a tuning term in the mass continuity equation.

2.5.2 Ice flow

As analysed in §2.1, ice in an ice sheet system is no longer a rigid body. From the view of microstructure, ice crystals deform under high pressure. From the view of macrostructure, cold ice accumulated on the ice sheet surface sinks towards the bottom, and warmer, hence softer, ice near the bottom creeps towards the edge of the ice sheet. Ice over a warm base, where a layer of meltwater exists as lubricant, may also slide along the base. These different forms of ice flow can be classified as vertical and horizontal movements and treated separately with the three components of ice flow velocity.

Ice flow is one of the most dynamic aspects of an ice sheet system. The patterns and velocities of ice flow are crucial issues in ice sheet modelling. However, because it is strongly related to the topography on-site, a general model to satisfy diverse situations is very difficult. Previous research generates some general guidelines when modelling ice flow. For example, ice flow velocity, especially at the upper layers of an ice sheet, is primarily determined by ice surface slope, which is also regulated by the basal topography [Paterson, 1994]. Basal sliding can contribute a significant proportion of the total ice flow velocity if the ice sheet is warm-based, whereas we can ignore basal sliding and only consider plastic flow for a cold-based ice sheet. However, under the present-day East Antarctic Ice Sheet, where a majority of areas are warm-based, ice flow is mainly plastic with little basal sliding [Anderson, 1999]. Glen's flow law, equation (2.1) [Glen, 1955], is normally employed when modelling the plastic component of ice flow by a strain-stress relationship, in which the

expression of the flow law coefficient (equation (2.2) [Paterson, 1994]) can be adjusted accordingly, *e.g.* equation (2.4) [Huybrechts, 1992].

2.5.3 Mass loss — Iceberg calving

As analysed in §2.3.2, the present-day surface temperatures of the Antarctic Ice Sheet are far too low to form surface run-off. Mass loss of the Antarctic Ice Sheet system is dominantly through iceberg calving from the marine margin of the ice sheet into the sea. Modelling iceberg calving is therefore vital to the success of an ice sheet model.

Huybrechts [1990a, 1993] explicitly calculates ice-shelf flow and grounding-line dynamics. He takes the present grounding-line position as a constraint. It is assumed that all ice is lost to the ocean beyond this constraint. The expansion of grounded ice over terrain below sea level is still possible, but this is entirely controlled by the surface mass balance and the ability of the ice sheet to extend down to sea level. This approach to modelling iceberg calving, although simple to implement from the numerical point of view because the grounding line is relatively stable, tends to over-estimate the mass loss. In effect all ice is treated as grounded ice irrespective of the bed elevation, with the limitation that it cannot expand beyond its present limits. This approach to modelling the marine boundary is not considered a serious problem when modelling a retreating scenario, because the ice sheet will retreat onto the East Antarctic continent in a warmer climate and will no longer interact with the ocean directly. It can however cause unrealistic results when modelling an expanding ice sheet under a glacial maximum climatic condition, the experiment we are going to carry out in Chapter 5.

A segmental linear calving is designed in the ice sheet model developed in this research. At the edge of a marine margin, if the ice is thicker than a threshold, a certain percentage of ice is lost in every computing time step; if the ice is thinner than the threshold, a linear calving rate that is inversely proportional to the ice thickness is applied. If the calving rate is larger than the ice thickness at the marine

margin, this means that all the ice at the margin will be lost; in addition, the surplus calving will reduce the ice thickness on the landward side. This approach fundamentally improves the precision of iceberg calving modelling. It not only more closely reflects the behaviour of iceberg calving in the real world, but also provides the numerical scheme with a mechanism that allows the modelled Antarctic Ice Sheet to expand and retreat. A detailed mathematical depiction will be presented in the next chapter.

Ice melting under the bottom of ice shelves is also significant near the ice shelf front. It contributes to the mass loss of the Antarctic Ice Sheet system. At the ice front of the Ross Ice Shelf and the Ronne-Filchner Ice Shelf, for example, the melt rates can reach as high as 10 m/yr [Robin, 1979; Doake, 1985]. The ice sheet model developed in this research uses ice shelf melting as a tuning parameter to adjust the mass loss.

2.6 Ice Flow Velocity

In a dynamic ice sheet system, two factors contribute to ice flow — basal sliding and ice deformation; both are driven by the gravitational gradient. As discussed earlier, basal sliding is significant when the ice sheet is warm-based and the basal topography is steep. The main driving mechanism for ice deformation is ice surface slope. Compared with the horizontal scale of an ice sheet, its vertical scale is hundreds, even thousands, of times smaller. Under such circumstances, it is reasonable and practical to assume that ice deformation is caused solely by horizontal shear stresses τ_{xz} and τ_{yz}, where the subscripts describe the planes normal to the horizontal directions of x and y and in the vertical direction of z,

$$\begin{cases} \tau_{xz}(z) = -\rho_{ice} g (H + h - z) \dfrac{\partial (H + h)}{\partial x} \\ \tau_{yz}(z) = -\rho_{ice} g (H + h - z) \dfrac{\partial (H + h)}{\partial y} \end{cases} \tag{2.19}$$

where g is gravitational acceleration. This approach to modelling the strain in an ice sheet is often referred to as the shallow ice approximation.

Glen [1955] modelled the creep of polycrystalline ice by an expression relating ice deformation $\dot{\varepsilon}$ to stress τ:

$$\dot{\varepsilon}_{ij} = A(T^*)\tau_*^{n-1}\tau'_{ij} \tag{2.20}$$

where $A(T^*)$ is the flow law coefficient analysed in §2.1; τ'_{ij} is the stress deviator tensor; τ_* the effective stress and n the flow law exponent, normally treated as 3 by most modellers. The subscript ij means on the plane of i = *constant* and in the j direction, with i and j both applying to x, y and z axes. Equation (2.20) is normally referred to as Glen's flow law. It is fundamental to the whole model theory.

The stress deviator in equation (2.20) is defined as the difference of the full stress and the hydrostatic component,

$$\tau'_{ij} = \tau_{ij} - \frac{\tau_{xx} + \tau_{yy} + \tau_{zz}}{3}. \tag{2.21}$$

Since the ice sheet deforms by shear under its own weight in planes parallel to the geoid, the ice does not experience shear at its side, which results in

$$\tau_{xy} = 0. \tag{2.22}$$

The effective stress is thus defined in terms of all the non-zero stress deviator components so that it is independent of the coordinate system, namely

$$\tau_* = \sqrt{\tau_{xz}^2 + \tau_{yz}^2}. \tag{2.23}$$

With the further assumption that the vertical gradients of the horizontal components of ice flow velocity are far greater than the horizontal gradients of its vertical component,

$$\begin{cases} \dfrac{\partial u}{\partial z} >> \dfrac{\partial w}{\partial x} \\ \dfrac{\partial v}{\partial z} >> \dfrac{\partial w}{\partial y} \end{cases}, \tag{2.24}$$

the two-dimensional horizontal velocity vector $\vec{v}(z)$ ($\vec{v} = u\vec{i} + v\vec{j}$) can thus be expressed as

$$\vec{v}(z) = -2(\rho_{ice} g)^n \left[\nabla(H+h)\cdot\nabla(H+h)\right]^{\frac{n-1}{2}} \nabla(H+h) \int_b^z A(T^*)(H+h-z)^n dz + \vec{v}(h). \tag{2.25}$$

2.7 Isostasy

Isostasy refers to the equilibrium that exists between the rigid lithosphere and the viscous asthenosphere, which behaves as if it consists of blocks floating on the underlying mantle, rising if material (such as an ice cap) is removed and sinking if material is added. The thickness of an ice sheet can easily reach several thousand metres. The Antarctic Ice Sheet is more than 4700 metres thick in some places and the average ice thickness is about 2300 metres. Under the great weight of such a massive ice sheet, the Antarctic continent is depressed in such a manner that the continental surface is bowl shaped [Anderson, 1999]. The elevation of the bedrock will affect the altitude of the ice sheet surface, hence the surface mass balance. The isostatic effect will also influence the interaction between the ice sheet and the sea, such as the grounding line. A comprehensive ice sheet model should take isostasy into account.

The Earth, from the centre to the surface, consists of three major layers: the very high-temperature high-density core, the middle high-temperature high-density mantle and the cool solid crust. The mantle can further be divided into a lower viscous asthenosphere and an elastic upper mantle. The boundary between these two layers is normally defined as the 1600 K isotherm [Oerlemans and van der Veen, 1984]. When modelling the behaviour of an ice sheet, modellers are interested in the bedrock depression caused by the overlying ice load, rather then the mechanism of isostasy itself. Since the physical properties of the upper mantle and the crust needed in this research are similar [Oerlemans and van der Veen, 1984], we simply treat them as one layer, the lithosphere. The density of this combined lithosphere is used to calculate the isostatic effect related to changing volumes of ice and seawater.

Hindmarsh [1993] points out that the properties of the earth's interior have not been well justified in contemporary ice sheet modelling. There is a time lag for the more viscous lithosphere to respond to the load change of the above ice sheet. However, the change of ice load concerned in this modelling research is not abrupt (See §4.3.3 – Quasi-equilibrium state); it is a long-term process itself. It is thus reasonable to assume that isostatic effects occur within the time scale of the evolution of the modelled Antarctic Ice Sheet.

Chapter 3 The Ice Sheet Model

All natural processes, including ice sheet evolution, follow the universal principles of mass continuity, momentum conservation and energy conservation. This chapter aims to abstract the mathematical depictions from the corresponding thermophysical processes in the Antarctic Ice Sheet system. These mathematical depictions, *i.e.* the governing equation set and the boundary and initial conditions, and the numerical techniques employed to solve the mathematical equation set form the kernel of the numerical ice sheet model.

Ice sheet evolution reflects the accumulative effect of small but persistent climatic changes over the long term [Näslund, 1998]. In terms of numerical modelling, this process can be regarded as quasi-stationary. Changes in momentum are therefore normally ignored when we model ice sheet flow. Together with boundary and initial conditions, the mass continuity equation and the energy conservation equation, which is often called the Navier-Stokes equation set, govern the thermodynamic processes of the ice sheet evolution. Huybrechts [1990a, 1992], Hindmarsh [1993] and Payne and Dongelmans [1997] provide detailed discussions of the principles of the ice sheet models derived from these fundamental numerical relations. Because the Navier-Stokes equation set and the binding conditions are highly non-linear and generate some fairly complex partial differential equations (PDEs), this equation set has to be simplified according to proper assumptions before being solved numerically.

Forcing conditions for ice sheet evolution can be introduced into the ice sheet system through the ice/bedrock interface, marine margin and ice/atmosphere interface. The interactions among factors such as ice temperature, ice flow, mass balance and isostasy, *etc.* are extremely complicated. Different modellers simplify these relations in different ways; hence different approaches to ice sheet modelling exist. It is during

the processes of simplification that uncertainties are likely to be generated in various ice sheet models.

One of the difficulties of ice sheet modelling is to ensure correct model coding and behaviour in terms of the defining equations, given that a number of numerical approaches can be taken to the same equation set. To this end, the EISMINT (European Ice Sheet Modelling INiTiative) group establishes a set of benchmark model scenarios specifically to evaluate model inter-compatibility for a standard set of ice sheet defining equations and forcing parameters [Huybrechts *et al.*, 1996]. The work described in this thesis builds on an ice sheet model developed by Dr Nick Hulton and Dr Mike Mineter at the University of Edinburgh [Hulton and Mineter, 2000; Mineter and Hulton, 2001]. The model has been successfully evaluated against the EISMINT scenarios as a means of ensuring internal consistency and model behaviour. It has also successfully reconstructed the ice sheet evolution in Europe and Patagonia, South America [Hulton *et al.*, 1994, 1995]. The ice sheet model developed in this research improves the Edinburgh model in aspects of the treatments to the potential energy, isostasy and marine margin.

3.1 System Definition

The first step of setting up a numerical ice sheet model is to reach a clear definition of the ice sheet system we are going to work with. All the mathematical expressions in the ice sheet model developed in this research are based on the right-handed Cartesian coordinate system, Figure 3.1.

The x-y plane is parallel to the horizontal geoid and the axis z points vertically upwards. The plane $z = 0$ is set at sea level. H denotes ice thickness and h bedrock surface altitude. As a consequence, $H+h$ designates the vertical coordinate of the ice surface in relation to sea level and $H+h-z$ denotes depth from the ice surface.

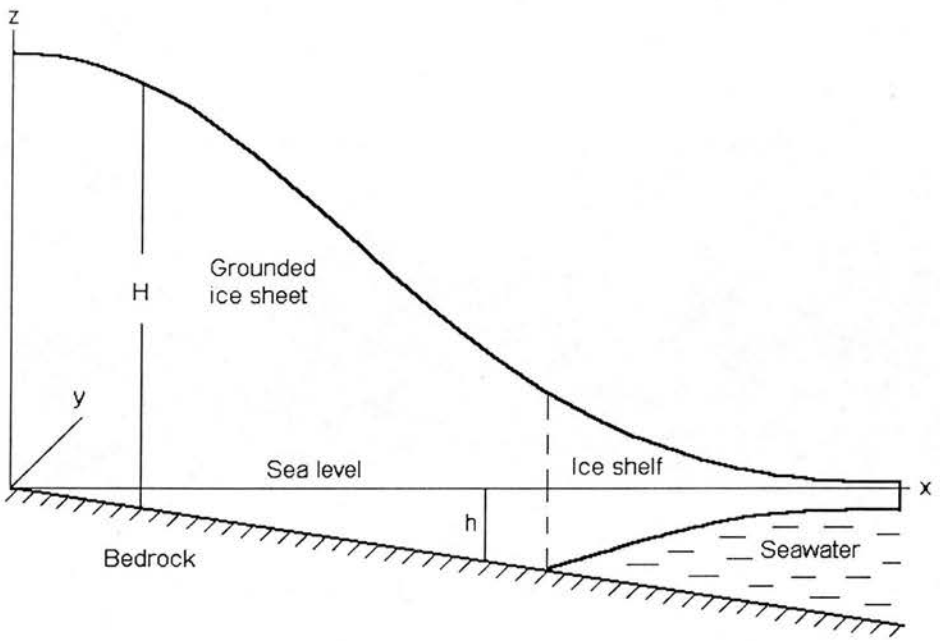

Figure 3.1 Right-handed Cartesian coordinate system for the ice sheet system studied in this research. The zero-altitude line is set at sea level.

Figure 3.1 defines a three-dimensional ice sheet system. When testing and calibrating the numerical ice sheet model, we also need an idealised one-dimensional ice sheet system and an idealised two-dimensional ice sheet system depending on the parameters we are highlighting. These two idealised systems will be fully discussed in Chapter 4.

3.2 Ice Sheet Evolution - the Governing Equation Set

The Antarctic Ice Sheet is a dynamic system. Positive mass balance accumulates ice in the interior of the continent. Driven by gravity, ice flows along the gravitational gradient; thus the ice sheet grows. At lower altitudes near the margin of the ice sheet, mass balance may become negative due to stronger ablation. When the ice sheet reaches the sea, since ice density is less than water density, grounded ice floats and eventually contributes to the formation of ice shelves. For ice shelves, ice mass

comes from surface precipitation and mass input from the inland ice sheet. Iceberg calving from the ice front, together with ice melting from the bottom, dominates mass losses from the ice shelf. Eventually, the ice front of the ice shelf stabilises at the line where ice loss balances ice gain. Numerical ice sheet modelling aims to simulate these dynamic processes by mathematical equations that depict the relationship of all factors involved.

The thermodynamic behaviours of an ice sheet, *i.e.* temporal and spatial distributions of ice thickness, ice flow velocities and ice temperatures *etc.*, are governed by the coupling of the ice mass continuity equation

$$\frac{\partial H}{\partial t} = -\nabla \cdot \left(\overline{u\vec{i} + v\vec{j} + w\vec{k}}\right) H + a - M_b, \tag{3.1}$$

the isostatic equation [Oerlemans and van der Veen, 1984]

$$\frac{\partial h}{\partial t} = D_a \nabla^2 \left(h - h^0 + h_{bed}\right), \tag{3.2}$$

and the energy conservation equation [Incropera and Dewitt, 1996]

$$\frac{\partial T}{\partial t} = \frac{k_{ice}}{\rho_{ice} c_{p\_ice}} \nabla^2 T - \left(u\vec{i} + v\vec{j} + w\vec{k}\right) \cdot \nabla T + \frac{\dot{q}}{\rho_{ice} c_{p\_ice}} \tag{3.3}$$

where H is ice thickness in m; h, basal topography in m, with h^0 the unloaded bedrock topography; T, absolute ice temperature in K; t, time in year; $u\vec{i} + v\vec{j} + w\vec{k}$, three-dimensional vector of ice flow velocity in m/yr, with $\overline{u\vec{i} + v\vec{j} + w\vec{k}}$ its modulus mean and u, v and w the components of the ice flow velocity vector in x, y and z directions respectively; a, surface mass balance in m/yr; M_b, basal melting rate in m/yr; D_a, the diffusion coefficient of asthenosphere in m²/yr; h_{bed}, deflection of asthenosphere in m; k_{ice}, thermal conductivity of ice in J/m·K·yr; ρ_{ice}, ice density in

kg/m^3; c_{p_ice}, specific heat capacity of ice in J/kg·K; and $\dot{q}$, internal strain heating in J/m^3·yr.

Equation (3.1) depicts the fundamental natural principle of mass conservation. It governs mass flow in the ice sheet system. It is a non-linear time-dependent parabolic differential equation. Equation (3.2) depicts the isostatic response of the viscous asthenosphere to the changes of the above ice load. It implies that the characteristic time scale for bedrock sinking or rebounding depends on the size of the ice load. Equation (3.3) depicts another fundamental natural principle of energy conservation. It governs the energy flow in the ice sheet system. Assuming lateral thermal conduction is negligible, equation (3.3) accounts for vertical thermal conduction, three-dimensional thermal advection and the heat generation by internal deformation. The coupling of the above equation set governs the spatial and temporal flow of mass and energy in an ice sheet system, hence the overall behaviour of ice sheet evolution. The solution of this governing equation set depends on the boundary and initial conditions of the modelled ice sheet system. Before choosing a suitable mathematical algorithm to find the solutions of the coupled governing equations, we must first analyse and quantify these controlling relations at the boundaries of the ice sheet system.

3.3 Boundary Conditions

An ice sheet system consists of two sub-systems: a grounded continental ice sheet and a floating marine ice shelf. For the grounded ice sheet, the basal boundary is at the ice-bedrock interface and the upper boundary is at the ice-atmosphere interface. For the floating ice shelf, the basal boundary is at the ice-water interface.

3.3.1 Ice-bedrock interface

Energy from the Earth's core causes temperature differences between the ice and the bedrock. There are three specific heat sources at the base. Geothermal heat flows

across the ice-bedrock interface and enters the ice sheet system. Frictional heat from horizontal shear strain is greatest within the basal layers of an ice sheet where ice deformation is concentrated [Paterson, 1994]. Ice sliding over the bedrock also generates heat by friction. These heat sources compose the energy input to the ice sheet system:

$$-k_{ice}\left.\frac{\partial T}{\partial z}\right|_{z=h} = \dot{q}_{geoth} + \vec{\tau}_b \cdot \vec{v}_b \tag{3.4}$$

where $\dot{q}_{geoth}$ is geothermal heat flux in J/m²·yr; $\vec{\tau}_b$ and $\vec{v}_b$ are the two-dimensional basal shear stress vector and basal sliding velocity vector respectively. Equation (3.4) is the basal boundary condition of the ice sheet system adopted in this research. It assumes pure ice with isotropy.

- **Geothermal heat flux**

Most Antarctic ice sheet models so far apply a constant geothermal heat flux over the entire Antarctic continent due to the lack of field data [Huybrechts, 1986, 1990; Huybrechts *et al.*, 1996; Näslund, 1998]. From the geological point of view, however, geothermal heat flux should be a function of the thickness of the Earth's crust; a thicker crust corresponds to lower geothermal heat flux and vice versa. This research makes an attempt to model this relationship,

$$\dot{q}_{geoth} = \frac{c_1}{c_2 + h}\overline{\dot{q}_{geoth}} \tag{3.5}$$

where $\overline{\dot{q}_{geoth}}$ is the mean geothermal heat flux over the entire Antarctic continent; c_1 and c_2 are constants so that

$$\frac{\iint_{x,y}\frac{c_1}{c_2 + h}dxdy}{x \cdot y} = 1. \tag{3.6}$$

Equation (3.6) ensures that the total amount of geothermal heat entering the modelled Antarctic Ice Sheet system is equivalent to an average value, but that it is partitioned according to crustal thickness. When analysing isostasy in §2.6, we assumed that the lithosphere floats on the underlying mantle. It is hence reasonable as a first approximation to use bedrock elevation h to represent the thickness of the crust. The values of c_1 and c_2 in equation (3.6) are rather arbitrary. In practice, the general guide is that c_1 should be larger than the average bedrock elevation $\overline{h}$ by an order of 1 and c_2 can be derived by the difference of c_1 and $\overline{h}$.

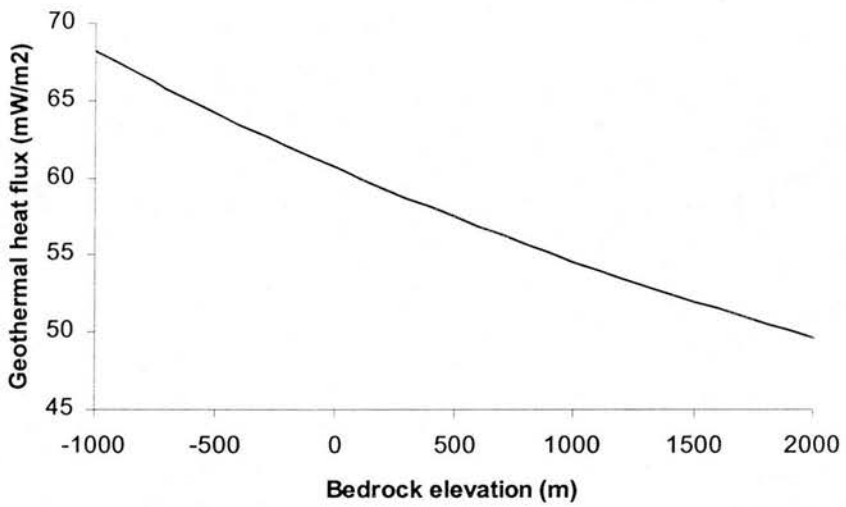

Figure 3.2 Geothermal heat flux from different bedrock elevations of the Antarctic continent modelled by equation (3.12), where c_1 and c_2 are set to 10000 m and 9000 m respectively. Here the bedrock elevation is assumed to represent the thickness of the Earth's crust.

In the idealised one-dimensional and two-dimensional ice sheet models, we simply set $\dot{q}_{geoth} = \overline{\dot{q}_{geoth}}$ and use a value of 42.0 mW/m² as the reference value for geothermal heat flux. In the three-dimensional Antarctic Ice Sheet system, $\overline{\dot{q}_{geoth}}$ is set as 54.6 mW/m² as recommended by Hansen and Greve [1996] and Näslund [1998]. In this latter case, we assume the average bedrock elevation is 1000 m, and c_1 and c_2 are set to 10000 m and 9000 m respectively in equation (3.5). The change of

geothermal heat flux with bedrock elevation is shown in Figure 3.2. The sensitivity of geothermal heat flux to bedrock elevation in Antarctica can be adjusted by tuning the values of constants c_1 and c_2. This approach to modelling geothermal heat fluxes makes better sense than simply applying one value to the entire Antarctic continent; nevertheless it needs to be justified by more comprehensive geophysical studies. As we have mentioned in §2.2.1, even the average geothermal heat flux in the Antarctic continent itself is derived from a theoretical estimate rather than from field evidence.

- **Potential energy release**

Heat from basal sliding reflects the energy dissipation caused by the friction between the ice and bedrock. Due to complex factors such as basal topography, the purity of ice, meltwater, till and bedrock permeability *etc.*, this heating is very difficult to quantify at a large scale. Fundamentally however, all heat generated within the ice sheet system comes from the system's internal energy. Since ice sheet flow can be regarded as a quasi-static movement, the kinetic energy change for one ice column is negligible. Therefore, the internal energy source for slide and strain heating can only be the release of potential energy of the ice mass. This energy will be used to heat up or melt the ice at the basal boundary layer.

Figure 3.3 shows a cross section of an ice sheet sliding downhill over the bedrock. Let us first analyse the component of the potential energy release in the x direction. A column of ice is originally at position i-1 at a point in time. During a time step Δt, it slides with a vertically averaged velocity u downhill in the x direction. According to the geometry shown in Figure 3.3, the vertical displacement of this column of ice in the x direction is

$$\Delta h_x = \frac{(h_{i-1} - h_{i+1})u\Delta t}{2\Delta x}. \tag{3.7}$$

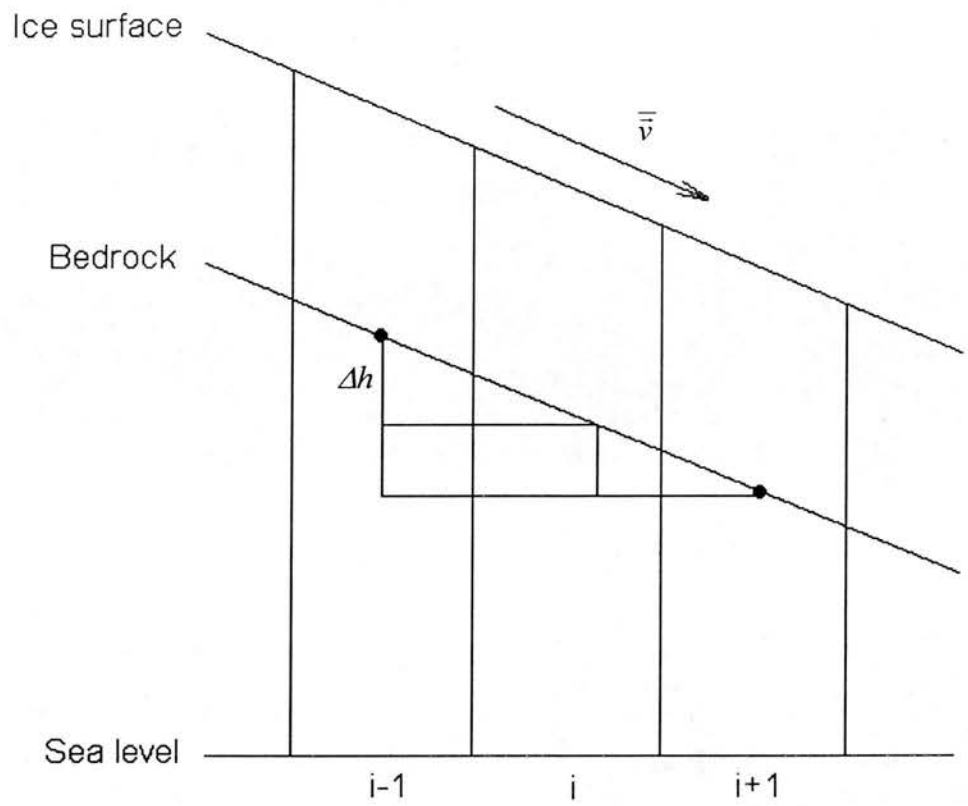

Figure 3.3 When a unit column of ice flows downhill over the bedrock from column i–1 to column i+1 with a constant velocity of $\bar{\bar{v}}$, the amount of potential energy that column of ice releases is $\rho_{ice} g \Delta h$, where Δh is the vertical displacement.

By the same analysis, the vertical displacement of this column of ice in the y direction is

$$\Delta h_y = \frac{(h_{j-1} - h_{j+1}) v \Delta t}{2 \Delta y}, \tag{3.8}$$

where u and v are ice flow velocity components along x and y axes respectively; Δx and Δy are the resolutions of the computing grid cells. Because energy is a scalar quantity, the total amount of potential energy released by this column of ice, Q, is simply the sum of the potential energy released in both x and y directions,

$$Q = \rho_{ice}\Delta x\Delta y(H-h)g(\Delta h_x + \Delta h_y). \tag{3.9}$$

This amount of heat must serve either as the specific heat to warm up the ice at the basal boundary layer or as the latent heat of fusion to melt the ice.

If the basal temperature is below the local pressure melting point, the temperature rise caused by the release of potential energy (subscript *pe*) is

$$\Delta T_{pe} = \frac{(H-h)g(\Delta h_x + \Delta h_y)}{(H_{bottom\_layer} - h)c_{p\_ice}}. \tag{3.10}$$

If the basal temperature has already reached the local pressure melting point, the thickness of ice melted by the released potential energy is

$$\Delta h_{pe} = \frac{(H-h)g(\Delta h_x + \Delta h_y)}{L_{ice}}, \tag{3.11}$$

where $L_{ice} = 3.35\times10^5$ J/kg, is the latent heat of fusion of ice.

- **Strain heating**

In regions of compressing flow, friction between ice crystals due to ice deformation generates heat within the ice sheet. This strain-heating rate per unit volume is the product of the stress and its corresponding strain rate,

$$\dot{q} = \sum_{ij} \dot{\varepsilon}_{ij}\tau_{ij} \qquad i,j = x,y,z. \tag{3.12}$$

Equation (3.12) is generally applicable throughout the ice mass. However, at the ice-bedrock boundary layer, deformational heating due to longitudinal strain is far smaller than that due to horizontal shear strain [Paterson, 1994]. Hence, the rate of strain heating, equation (3.12), can thus be simplified as

$$\dot{q} = 2\dot{\varepsilon}_{xz}\tau_{xz} + 2\dot{\varepsilon}_{yz}\tau_{yz} = -\rho_{ice}g(H+h-z)\frac{\partial \vec{v}}{\partial z}\cdot\nabla(H+h)\,. \qquad (3.13)$$

In most areas of the Antarctic Ice Sheet, strain heating is greatest toward the bottom of the ice sheet where stress is greatest. Therefore, the rate of strain heating at the ice-bedrock boundary layer, equation (3.13), is a reasonable approximation of the internal heating in the entire Antarctic Ice Sheet system.

- **Basal melting rate**

In areas where the basal ice temperature reaches its local pressure melting point, ice begins to melt and its temperature remains at the pressure melting point. The local pressure melting point (subscript *pmp*) of an ice sheet is a function of ice thickness [Huybrechts, 1986; Paterson, 1996; Näslund, 1998],

$$T_{pmp} = T^0 - T_{cc}(H+h-z) \qquad (3.14)$$

where $T^0 = 273.16$ K is the triple-point temperature of water; and $T_{cc} = 8.7\times10^{-4}$ K/m is the Clausius-Clapeyron gradient, designating the change of ice melting point with pressure.

As long as the basal ice is at its local pressure melting point, the latent heat of fusion of ice will absorb all the heat flowing into and generated inside the ice sheet system and the ice temperature will remain at the pressure melting point. If the phase-change were not to happen, equation (3.4) could result in a basal temperature of ice higher than the pressure melting point. Since ice temperature cannot be higher than the pressure melting point, the heat used to "raise the temperature of ice" above the pressure melting point is obviously used to melt the ice. The basal melting rate, M_b in m/yr, can thus be calculated as

$$M_b = \frac{1}{\rho_{ice} L_{ice}} \left[k_{ice} \left(\left. \frac{\partial T}{\partial z} \right|_{pmp} - \left. \frac{\partial T}{\partial z} \right|_{z=h} \right) + \int_h^{z_{pmp}} \dot{q} dz \right]. \quad (3.15)$$

In Antarctica, meltwater is mostly trapped under the ice sheet to form subglacial lakes, which regulate the thermal regime of the Antarctic Ice Sheet significantly. In this research, we focus on subglacial meltwater production and are not going to investigate the drainage systems of the meltwater.

- **Basal sliding**

At the warm-based ice-bedrock interface, meltwater acts as a lubricant between ice and bedrock. This phenomenon makes it possible for ice to slide on the bedrock in the direction of the pressure gradients. As analysed in Chapter 2, ice sliding is one important component of ice sheet motion. It plays an important role in both the dynamical regime and the thermal regime of an ice sheet. Sliding increases the overall velocity of ice flow. Friction between ice and bedrock generates heat that further warms up the basal ice. Basal motion seems to account for nearly all the flow of the ice streams that drain most of the ice from West Antarctica [Paterson, 1994]. Thus an understanding of basal processes is the key to such problems as explaining the rapid decay of the ice-age ice sheets that began some 18,000 ^{14}C years ago or predicting whether global warming will lead to the disintegration of the West Antarctic Ice Sheet. Moreover, until we understand basal motion, the mechanisms of glacier surges and of glacier erosion and deposition will remain obscure.

The relationships between basal velocity, shear stress, water pressure and the characteristics of the glacier bed comprise one of the basal boundary conditions in the analysis of glacier flow with basal ice at the pressure melting point. This relationship is often referred to as a sliding law. Its correct formulation is essential for predicting the overall motion of an ice sheet and predicting how an ice sheet will react to changes in mass balance. The sliding law, however, is one of the major current puzzles in glacier physics, for the mechanism of basal sliding is still unclear and direct observations under an ice sheet are still technically difficult. Huybrechts

[1992] suggests an expression that integrates the ice sliding parameter, f_s, into basal mass diffusion, D^s,

$$D^s = f_s H^{n+1} (\rho_{ice} g)^n \left\{ \left[\frac{d(H+h)}{dx} \right]^2 + \left[\frac{d(H+h)}{dy} \right]^2 \right\}. \qquad (3.16)$$

Equation (3.16) models basal sliding as a linear function of a sliding parameter and reflects the non-linearity by the flow law exponent n. Huybrechts [1992] has obtained reasonably satisfactory results by modelling basal sliding of the Antarctic Ice Sheet this way. The ice sheet model developed in this research therefore follows this approach.

Equation (3.16) is applicable if we assume that basal sliding only occurs when the basal ice is at the pressure melting point. Weertman's [1957, 1972] sliding law allows basal sliding and enhances basal creep when the basal pressure-melting condition does not apply. However, Weertman's approach creates a further thermodynamic coupling and this dramatically increases the numerical difficulty and introduces further factors, resulting in unstable numerical behaviour. When applying equation (3.16) as the sliding law, basal sliding is actually controlled by the sliding parameter f_s, which is an arbitrary value used to produce modelling results that match observational results. This simple empirical simulation is a practical solution until we have a better understanding of the mechanism of basal sliding.

3.3.2 Ice-atmosphere interface

An isolated system exchanges mass and energy with the external world through its boundaries. The upper boundary of the Antarctic Ice Sheet system we defined in this research is the ice-atmosphere interface. The surface temperatures of the ice sheet determine the energy exchange between the ice sheet and the atmosphere above; the mass balance at the ice surface represents the mass exchange. In the ice sheet model developed in this research, these two upper boundary conditions of the ice sheet

system reflect climatic change. Other factors like thermal radiation are merged into these two parameters.

- **Ice surface temperature**

Since ice sheet behaviour responds to large-scale long-term thermodynamic processes, it is justified to assume that ice surface temperatures are equivalent to surface annual mean temperatures. Huybrechts [1993] estimates the temperatures at the surface of the East Antarctic Ice Sheet by an empirical linear function of ice surface topography and latitude (*lat*):

$$T_{sur}|_{z=H+h} = 34.46 - 0.00914\times(H+h) - 0.68775\times lat + 273.16 \qquad (3.17)$$

Applying equation (3.17), the ice sheet model developed in this research satisfactorily calculates the surface temperature distributions of the present-day Antarctic Ice Sheet (See Figures 5.1 and 5.2).

- **Surface mass balance**

The ice sheet systems defined in this modelling research gain mass through surface accumulation. Surface accumulation also contributes to the vertical component of ice flow velocity. In the ice sheet model developed in this research, the mass balance pattern on the surface of an ice sheet is varied from experiment to experiment.

When testing the effectiveness of thermal controls of the model in the idealised two-dimensional ice sheet system, we set the surface mass balance, a in m/yr, as a function of geographic position, as suggested by the EISMINT benchmark research [Huybrechts *et al.*, 1996].

$$a(x,y) = \min\left[a_{\max}, s_a\left(R_{el} - \sqrt{(x-\hat{x})^2 + (y-\hat{y})^2}\right)\right] \qquad (3.18)$$

where (x,y) is the coordinate in km of a sub-grid, with $(\hat{x},\hat{y})$ the centre of the ice sheet; $a_{\max}$, the maximum accumulation rate; s_a, the gradient of the rate of change of mass balance with horizontal distance; and R_{el}, the distance from the centre of the ice sheet to the equilibrium line where ablation balances accumulation. We can set the mass balance rate as zero if we want to test other parameters without the influence of mass balance.

Equation (3.18) results in negative values at positions outside the equilibrium line. This modelling approach provides a modelled ice sheet system with a mechanism for losing mass, and leads to a stabilised ice sheet at some stage. In the Antarctic Ice Sheet system, however, the ice sheet loses mass predominantly through its marine margin and surface ablation is insignificant. In such a case, the surface accumulation rate used for model calibration (§4.3) and experiments (Chapter 5) in the three-dimensional Antarctic Ice Sheet system is set as an empirical exponential function of the surface temperature over the Antarctic continent, as suggested by Huybrechts and Oerlemans [1988]:

$$a = c_3 2^{(T_{sur}-273.16)/10} \tag{3.19}$$

where c_3 is a tuning coefficient. Equation (3.19) implies that the surface accumulation rate over the Antarctic Ice Sheet is a function of the surface temperature. This is a reasonable assumption because the precipitation capability of the atmosphere over the Antarctic continent is dominated by air temperature [Huybrechts and Oerlemans, 1988].

3.3.3 Ice-shelf/seawater interface

Ice melting beneath ice shelves accounts for mass loss that is compatible to that lost by iceberg calving [Denton *et al.*, 1993]. Near the ice shelf front of the Ross Ice Shelf and Ronne-Filchner Ice Shelf, bottom melting is known to be significant and the melting rates can reach as high as 10 m/yr [Doake, 1985; Robin, 1979]. In the ice

sheet model developed in this research, the ice shelf bottom-melting rate is set as a function inversely proportional to latitude,

$$H_{yr+1}^{floating} = H_{yr}^{floating} - M_{shelf-melt} / lat, \tag{3.20}$$

where $M_{shelf\text{-}melt}$ is the ice shelf basal melting rate parameter. Simulated by equation (3.20), the ice shelf basal melting increases towards lower latitudes where seawater tends to be warmer. This simple relationship is a preliminary modelling attempt. More field observation and modelling work is needed to estimate ice shelf basal melting rates more precisely.

3.3.4 Ice sheet marine margin

In the ice sheet model developed in this research, a marine margin of the Antarctic Ice Sheet is modelled by the use of a cell with the following conditions. Firstly, ice thickness is greater than zero (meaning there is some ice); secondly, ice thickness in at least one of the adjacent cells is zero (meaning no ice); and thirdly, the altitude of the bedrock is below sea level. With lower sea level, more of the ice sheet will become grounded and the marine restraints for ice sheet expansion will be reduced.

Iceberg calving from the marine margin of the ice sheet is the main mechanism of mass loss from the Antarctic Ice Sheet system. It dominates the process of ice shelf ablation and may account for several hundreds of metres of ice lost annually from the marine margin of the Antarctic Ice Sheet. From initial functionality tests to sophisticated running experiments, this research has tried to model different aspects of the iceberg calving process including the effects of water depth, ice thickness and latitude. The overall iceberg calving rate is the combined effect of these calving mechanisms. Switches are provided in the model in order to carry out experiments with different combinations of iceberg calving mechanisms.

In the numerical regime of the ice sheet model developed in this research, iceberg calving provides a potential mechanism for the ice sheet to retreat when the iceberg

calving rate exceeds the supply of ice. In cases where the amount of ice supplied to a cell exposed to the sea is less than the iceberg calving rate, ice in the cells will all be lost. Moreover, the cells adjacent to the margin cells could also lose mass. The result is that the modelled ice sheet will retreat toward the continent.

- **Fixed calving rate**

The simplest simulation of the iceberg calving process is to assume that a fixed percentage of ice, r, is lost from the edge of the ice shelf each year,

$$H_{yr+1}^{edge} = H_{yr}^{edge}(1-r). \tag{3.21}$$

In this case, r is an adjustable parameter that is specified for a model run. Equation (3.21) is used for the initial functionality test of iceberg calving in the model.

In Antarctica, since the iceberg calving rate changes seasonally, the seasonal oscillation of the marine boundary of the ice sheet moves faster than typical ice flow. Although we are interested in the annually averaged calving rate, this phenomenon suggests that the iceberg calving rate is a function of spatial and temporal factors. A more sophisticated modelling approach is therefore needed to estimate the iceberg calving rate more precisely.

- **Iceberg calving against latitude**

Latitude is used as a "seaward exposure" factor in the Antarctic Ice Sheet model. The iceberg calving is essentially a mechanical process. As an ice shelf grows towards lower latitudes, where air and seawater temperatures tend to be warmer and solar radiation is stronger, the ice will become brittle. Also, the ice shelves receive less support from the continental ice sheet at lower latitudes and the iceberg calving rate increases. It is therefore more reasonable to set the iceberg calving rate as a function of latitude than as a simple constant, such that

$$H_{yr+1}^{edge} = H_{yr}^{edge}\left[1-\left(r + r_{lat} \cdot lat\right)\right] \tag{3.22}$$

where r_{lat} is ice calving gradient against latitude.

- **Ice loss against water depth**

When ice reaches deeper water, ice melting intensifies. The thickness at the front of an ice shelf is typically 250 metres with some 30 metres above sea level [Paterson, 1994; Huybrechts, 1992]. These figures suggest that an ice front normally cannot extend into water more than about 200 metres deep. Mass loss of ice shelves is thus a function of water depth H_{water}.

$$H_{yr+1} = H_{yr}(1-r_{wd}H_{water}) \tag{3.23}$$

where r_{wd} is mass loss gradient of an ice shelf against *w*ater *d*epth. Along the ice shelf margin, all ice is calved away if it reaches 200 metres below sea level.

$$H^{edge} = 0 \qquad \text{if } H_{water} \geq 200 \text{ m} \tag{3.24}$$

The threshold of water depth is read into the ice sheet model during a run. This makes it easy to test various thresholds or even switch the function off.

- **Segmented linear iceberg calving**

The calving routines relating the loss of ice mass to ice thickness work well when the loss of mass by iceberg calving is only part of the process of ablation at the ice front. Problems arise when the ice shelf is thin because of a mismatch between the temporal and spatial scales of the process and its representation in the model. If the modelled calving rates remove a disproportionate amount of mass during any one time step in the model, it may be impossible in the model for the ice shelf to escape the confines of the cell at the marine margin.

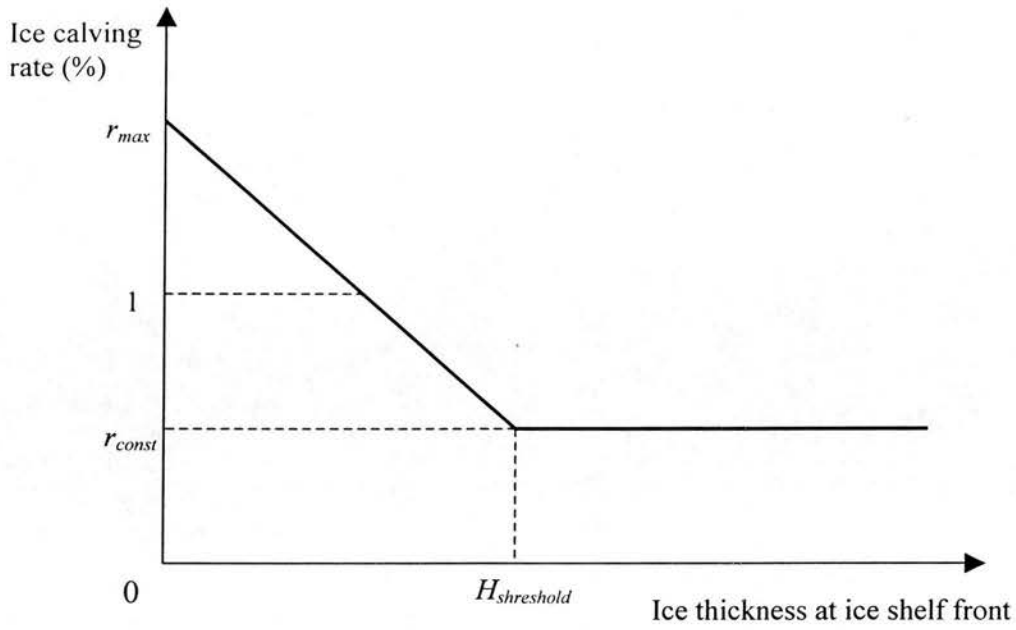

Figure 3.4 Segmented linear iceberg calving. When the ice thickness at the ice shelf front is thicker than a threshold, a constant iceberg calving rate, r_{const}, applies; otherwise, a linear calving rate that is inversely proportional to the *in situ* ice thickness applies. When the calving rate is higher than 100 percent, the surplus ice will be calved from the sub-front computing cells.

In order to tackle the above problem, the ice sheet model developed in this research adopts a new approach to model iceberg calving. Figure 3.4 shows a segmented iceberg calving function. First of all, the iceberg calving routine identifies those computing cells that are at the marine margin. If the ice thickness at an ice shelf front cell is thicker than a threshold, a constant iceberg calving rate, r_{const}, applies; otherwise, a linear calving rate that is inversely proportional to the *in situ* ice thickness applies:

$$\begin{cases} r = r_{const} & H_{margin} > H_{threshold} \\ r = r_{\max} - \dfrac{r_{\max} - r_{const}}{H_{threshold}} \cdot H_{margin} & H_{margin} < H_{threshold} \end{cases} \tag{3.25}$$

where r_{const}, r_{max} and $H_{threshold}$ are set by the model during run time.

In order to make the modelled ice sheet retreat, r_{max} must be set larger than 1, which means the amount of ice calved from the marine margin is more than the amount in the front cell when

$$H_{margin} < \frac{r_{\max} - 1}{r_{\max} - r_{const}} \cdot H_{threshold} \cdot \tag{3.26}$$

In this case, the surplus ice will be calved by equal amounts from each of those computing cells that are adjacent to the marginal cell. In other words, if the defined ice thickness for the ice shelf at this point is very thin, then all of this ice can be lost and calving is thus applied to the next upstream landward computing cell. If the allocation of calved ice in an adjacent cell is larger than the amount of ice in that cell, then all the ice in that cell will also be calved.

In view of the lack of good observational data, it is reasonable to define a linear iceberg calving function for the time being. More detailed field research, monitoring the ice front of the Ross Ice Shelf and Ronne-Filchner Ice Shelf by remote sensing for example, will help to model iceberg calving more precisely. A non-linear iceberg calving function and more complicated marine margin treatment may be needed to reflect the behaviour of the marine limit of the Antarctic Ice Sheet in more detail. More sophisticated models will nevertheless utilise a relationship that defines iceberg calving rate as a function of the thickness of the ice shelf.

3.3.5 Isostasy

As outlined in Chapter 2, the bedrock under the continental-scale Antarctic Ice Sheet tends to subside when the overlying ice load increases and rebounds when this ice load decreases, just as water does with an object floating on it. Given a sufficiently long time for the bedrock to sense the change in ice load, the isostatic process satisfies Archimedes' principle.

The deflection of bedrock, h_{bed} in equation (3.2), follows local hydrostatic equilibrium. When the basal topography is above sea level, all the ice mass loads onto the bedrock. When the ice sheet is grounded below sea level, according to the Archimedes' principle, the loading on bedrock is still equivalent to the ice mass as the buoyancy effect of the seawater does not exist, and the effective seawater load is ignored (Figure 3.5). The deflection is:

$$h_{bed} = \frac{\rho_{ice}}{\rho_{bed}} H \tag{3.27}$$

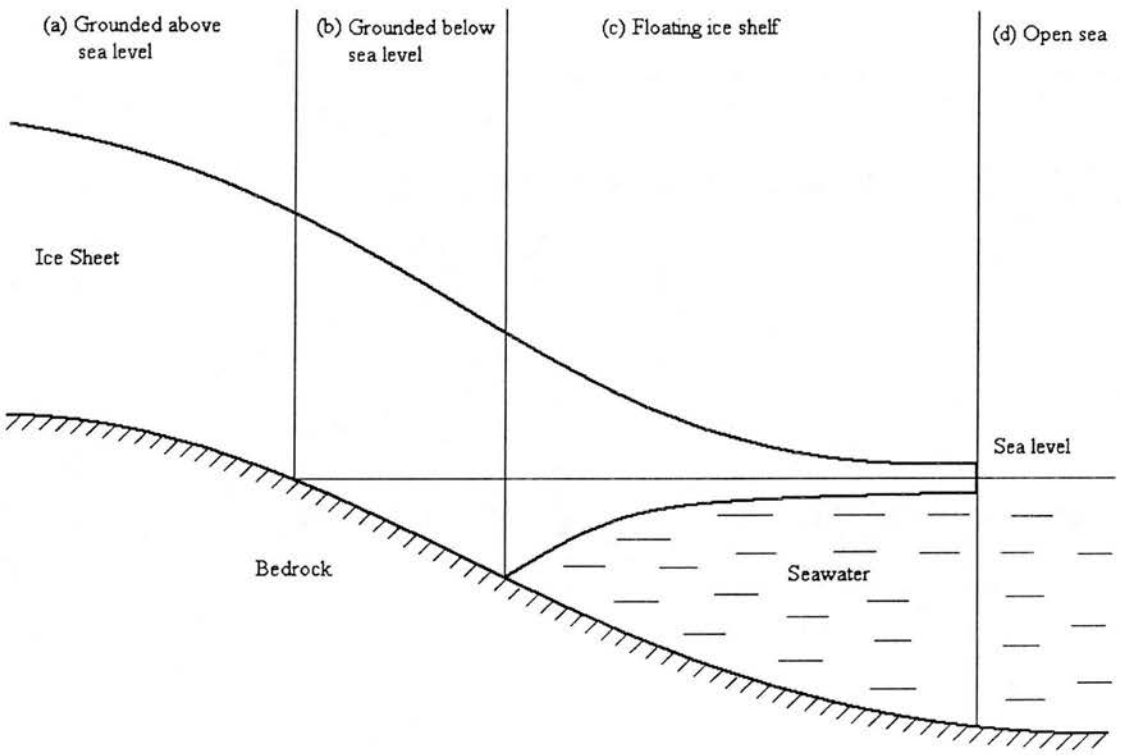

Figure 3.5 Isostatic effect of an ice sheet in respect with its landing status. For (a) and (b), equation (3.34) applies; for (c) and (d), equation (3.35) applies.

When the ice floats on seawater, an ice shelf forms. In this case, the loading on the bedrock is equivalent to the overlying water mass, as if the ice shelf does not exist according the Archimedes' principle,

$$w_{bed} = \frac{\rho_{water}}{\rho_{bed}} H_{water} . \tag{3.28}$$

In equations (3.27) and (3.28), ρ_{ice}, ρ_{water} and ρ_{bed} denote the densities of ice, seawater and the Earth's crust respectively; H represents ice thickness; and d water depth. The unloaded basal topography, h^0, can thus be obtained by calculating the equilibrium condition that would occur should all of the present ice load overlying the Antarctic continent be removed. In effect, this involves elevating the bedrock by an amount equal to the overlying ice thickness multiplied by the rock/water density ratio and taking into account the ingress and loading of seawater into areas presently grounded below sea level.

If all of the ice overlying the Antarctic continent today were removed, the present-day basal topography would rebound from its current elevations. Based on the above analysis, we reconstruct this scenario according to the ice surface topography and the basal topography of the present-day Antarctic Ice Sheet, which are obtained from the Antarctic map folio [Drewry, 1983]. If the thickness of the present-day Antarctic Ice Sheet (H^p), which represents the ice load, is derived from the difference between the present-day ice surface topography and basal topography (h^p) of the ice sheet, the rebounded ice-free topography of the Antarctic continent can then be reconstructed as

$$h^0 = h^p + \frac{\rho_{ice}}{\rho_{bed}} H^p \tag{3.29}$$

Equation (3.29) assumes that all the ice loading on the present-day basal topography has been removed and a sufficiently long time has permitted the unloaded Antarctic topography to reach a new equilibrium. Diagrams for the present-day Antarctic surface topography, basal topography and the rebounded ice-free topography are given in Chapter 4 for easy referencing.

The value of the diffusion coefficient of the asthenosphere D_a is the main source of uncertainty in resolving equation (3.2). A range of values, from a magnitude of 10^6 m²/yr to 10^8 m²/yr, has been tested in this research and a value of 10^7 m²/yr is found to be optimistic.

3.3.6 Restriction effect of a bay to an ice shelf

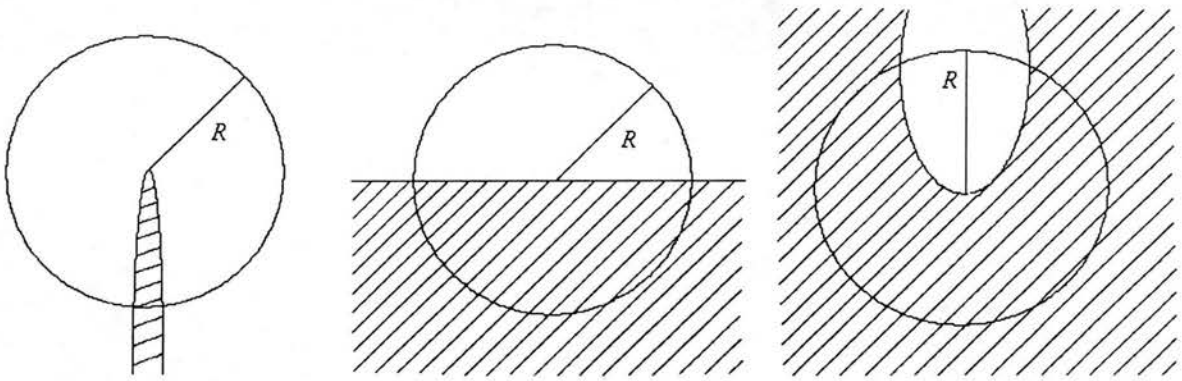

Figure 3.6 Embayment factor. The shaded area represents land and the open area represents sea. A circle with a radius large enough to cover the bay area is drawn. The embayment factor is then determined by the ratio of the land area in the circle to the whole circle area.

Because the mass loss of the Antarctic Ice Sheet is dominantly from the ice front through iceberg calving, the shorter the ice front facing the open sea, the less ice mass will be lost. When the ice sheet grows into a bay and forms an ice shelf, mass loss from the ice front reduces dramatically due to the geometry of the enclosed coastline. In order to measure this embayment effect on the marine part of the ice sheet system, an enclosure factor φ is introduced. By drawing a circle on the bay area with a sufficiently large radius r to cover the whole bay, φ is defined as the portion of the land area to the whole circle area. As illustrated in Figure 3.6, a straight coastline is represented by a value of φ approximate to 0.5, a more enclosed bay

corresponds to a value of φ closer to 1 and a peninsula corresponds to a value of φ closer to 0. In a numerical model, the embayment factor is calculated as the proportion of the grids occupied by land in the circle, equation (3.30). According to our experiments, we find that a circle with the radius of 20,000 metres gives satisfactory results.

$$\varphi = \frac{\text{Number of grids occupied by land in the circle}}{\text{Number of grids in the circle}} \tag{3.30}$$

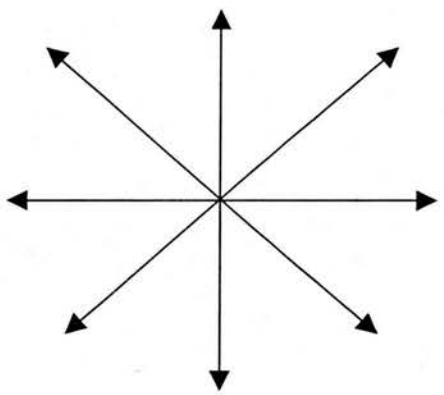

Figure 3.7 Eight cardinal points go from a computing grid point toward the model edges. A score of ⅛ is counted for each direction that encounters land. The total score counts the embayment factor.

Another way to define the embayment factor is illustrated in Figure 3.7. Eight cardinal points go from a computing grid point toward the model edges. If there is land encountered in any direction, it scores ⅛. The embayment factor is then defined as the sum of the total scores. This approach to calculating the embayment factor reduces the computing load, although it may not be as accurate as the approach defined by equation (3.30). The ice sheet model developed in this research applies equation (3.30) to determine the embayment factors of the ice shelves in Antarctica.

3.3.7 Climate forcing

In the ice sheet model developed in this research, long term climatic factors are reflected by eustatic sea level changes and annual mean temperature changes on the ice surface. The sea level and climatic conditions for a model's running period are read in from a forcing file. In order to test the response of the Antarctic Ice Sheet to a glacial maximum, sea level was dropped by 120 metres and the annual mean temperature on the ice surface was lowered by 6°C. This climatic situation is generally believed to represent the Last Glacial Maximum *c.* 22,000 years ago [Lowe and Walker, 1997]. In the ice sheet model developed in this research, we assume the glacial maximum conditions form an equilibrium climate in order to impose a consistent forcing to the numerical regime.

3.4 Initial Conditions

An ice sheet can in principle grow from an ice-free topography. An existing ice sheet can expand or retreat from its original ice dimensions. The existing ice sheet can be either the present-day Antarctic Ice Sheet or an ice sheet generated by a previous model run. An ice sheet model should permit the modelled ice sheet start to evolve from all these possible situations. The initial conditions of an ice sheet model indicate this starting point based on which the modelled ice sheet begins to evolve. The initial data required by the ice sheet model developed in this research are ice thickness, bedrock elevation and temperature distribution in the existing ice sheet. The HOTSTART parameter in the runtime parameters and switches file tells the model the files that should be read in as initial condition data (Table 3.1). The rebounded ice-free Antarctic topography, which is reconstructed by equation (3.29), is required both as a reference in the isostatic calculations and as an initial condition.

3.5 Numerical Scheme

High non-linearity of the governing partial differential equations (3.1) ~ (3.3) and the boundary conditions gives the modeller little choice but to apply numerical methods to reach solutions. This requires discretization of the originally continuous partial differential equations into approximated discrete algebraic equations on a proper mesh grid. Huybrechts [1986] first applies the Alternating-Direction-Implicit (ADI) scheme to discretize and integrate the governing equations for ice sheets. This is a two-step numerical method involving the solution of the equation set along lines parallel to the x-axis as the first step and to the y-axis as the second step. This scheme evaluates the diffusion coefficients that form a tridiagonal linear matrix from the old time step and calculates the ADI coefficients for the new time step through Gaussian elimination. The ADI scheme is able to deal with changing boundaries of the dynamic ice sheet margin and is time-efficient for computing. The ice sheet model developed in this research follows the ADI scheme. The key points of the derivations of the mathematical equations and numerical techniques are outlined below.

3.5.1 Mesh grid

The horizontal mesh grid applied in this Antarctic Ice Sheet model is a 141 × 141 grid point matrix centred at the South Pole. The resolution of each grid cell is 40 km × 40 km. A 61 × 61 mesh grid with a resolution of 20 km × 20 km, which dramatically reduces the computing load, is applied in the sensitivity tests to the idealised two-dimensional ice sheet system. The vertical coordinate is normalised as discussed in the next section and divided into 11 layers with N_ζ=1 representing the ice-bedrock boundary and N_ζ=11 representing the ice surface.

The model can take a denser 281 × 281 mesh grid over Antarctica. It doubles the resolution (20 km × 20 km) but takes much more computing time.

3.5.2 Vertical normalisation

When modelling ice sheets, researchers are more interested in layers of ice because the characteristics of an ice sheet within one layer as a function of the relative depth are more significant than the characteristics relating to the absolute depth. Thus, it is more convenient to normalise the vertical coordinate and calculate the parameters by layers. Let ζ denote the vertical axis and normalise the ice thickness such that $\zeta = 0$ at the ice surface and $\zeta = 1$ at the bottom for the whole ice sheet,

$$\zeta = \frac{H + h - z}{H}. \tag{3.31}$$

The features of an ice sheet stratify along the relative depth of an ice sheet, ζ. The normalisation equation (3.31) transforms an absolute coordinate into a dimensionless relative community-ordinate. It normalises the parameters of the ice sheet in the same layer but possibly at different absolute depths. This approach makes the analysis more efficient and more logical.

3.5.3 Alternating-Direction-Implicit scheme

A two-step Alternating Direction Implicit (ADI) scheme divides the computed area into a grid with N_x columns and N_y rows (61 × 61, 141 × 141 or 281 × 281 in the model runs discussed in this thesis) denoted by i and j respectively. It involves the solution of sets of equations along lines parallel to the x and y-axes as the first step and second step respectively. It is constructed with the Peaceman-Rachford formula [Mitchell and Griffiths, 1980], employing a staggered grid in space, so that mean mass fluxes are calculated between grid points. Smoothing in this way keeps the integration stable. Due to the non-linearity of the flow law, equation (2.20), and the coupling between the thermal regime and the dynamical regime of the ice sheet system, the reiterating time steps are restricted to less than 10 model years in order to keep the integration processes stable.

Considering a rectangular domain in the x-y space, where i and j denote the index numbers of a grid point with N_x and N_y the total number along the respective axes, the ADI scheme discretizes the ice mass continuity equation (3.1) as:

$$H_{ij,t+\frac{1}{2}} + \frac{\Delta t}{2\Delta x}\left(F_{i+\frac{1}{2},j,t+\frac{1}{2}} - F_{i-\frac{1}{2},j,t+\frac{1}{2}}\right) = H_{ijt} - \frac{\Delta t}{2\Delta y}\left(F_{i,j+\frac{1}{2},t} - F_{i,j-\frac{1}{2},t}\right) + \frac{\Delta t}{2}\left(b_{ijt} - m_{ijt}\right)$$

$$i = 2, \ldots, N_x - 1 \text{ for } j = 2, \ldots, N_y - 1 \qquad (3.32)$$

along the columns of constant j for the first step of reiteration, where the mass fluxes across adjacent computing cells, Fs, are

$$\begin{aligned}
F_{i+\frac{1}{2},j,t+\frac{1}{2}} &= \frac{\left(D_{ijt} + D_{i+1,jt}\right)\left(H_{i+1,j,t+\frac{1}{2}} - H_{ij,t+\frac{1}{2}} + h_{i+1,jt} - h_{ijt}\right)}{2\Delta x} \\
F_{i-\frac{1}{2},j,t+\frac{1}{2}} &= \frac{\left(D_{i-1,jt} + D_{ijt}\right)\left(H_{ij,t+\frac{1}{2}} - H_{i-1,j,t+\frac{1}{2}} + h_{ijt} - h_{i-1,jt}\right)}{2\Delta x} \\
F_{i,j+\frac{1}{2},t} &= \frac{\left(D_{ij,t-\frac{1}{2}} + D_{i,j+1,t-\frac{1}{2}}\right)\left(H_{i,j+1,t} - H_{ijt} + h_{i,j+1,t-\frac{1}{2}} - h_{ij,t-\frac{1}{2}}\right)}{2\Delta y} \\
F_{i,j-\frac{1}{2},t} &= \frac{\left(D_{i-1,j,t-\frac{1}{2}} + D_{ij,t-\frac{1}{2}}\right)\left(H_{ijt} - H_{i,j-1,t} + h_{ij,t-\frac{1}{2}} - h_{i,j-1,t-\frac{1}{2}}\right)}{2\Delta y}
\end{aligned} \qquad (3.33)$$

There are similar set of equations along the rows of constant i for the second step:

$$H_{ij,t+1} + \frac{\Delta t}{2\Delta y}\left(F_{i,j+\frac{1}{2},t+1} - F_{i,j-\frac{1}{2},t+1}\right) = H_{ij,t+\frac{1}{2}} - \frac{\Delta t}{2\Delta x}\left(F_{i+\frac{1}{2},j,t+\frac{1}{2}} - F_{i-\frac{1}{2},j,t+\frac{1}{2}}\right) + \frac{\Delta t}{2}\left(b_{ij,t+\frac{1}{2}} - m_{ij,t+\frac{1}{2}}\right)$$

$$j = 2, \ldots, N_y - 1 \quad \text{for} \quad i = 2, \ldots, N_x - 1 \qquad (3.34)$$

where

$$\begin{aligned}
F_{i,j+\frac{1}{2},t+1} &= \frac{\left(D_{ij,t+\frac{1}{2}} + D_{i,j+1,t+\frac{1}{2}}\right)\left(H_{i,j+1,t+1} - H_{ij,t+1} + h_{i,j+1,t+\frac{1}{2}} - h_{ij,t+\frac{1}{2}}\right)}{2\Delta y} \\
F_{i,j-\frac{1}{2},t+1} &= \frac{\left(D_{i,j-1,t+\frac{1}{2}} + D_{ij,t+\frac{1}{2}}\right)\left(H_{ij,t+1} - H_{i,j-1,t+1} + h_{ij,t+\frac{1}{2}} - h_{i,j-1,t+\frac{1}{2}}\right)}{2\Delta y} \\
F_{i+\frac{1}{2},j,t+\frac{1}{2}} &= \frac{\left(D_{ijt} + D_{i+1,jt}\right)\left(H_{i+1,j,t+\frac{1}{2}} - H_{ij,t+\frac{1}{2}} + h_{i+1,jt} - h_{ijt}\right)}{2\Delta x} \\
F_{i-\frac{1}{2},j,t+\frac{1}{2}} &= \frac{\left(D_{i-1,jt} + D_{ijt}\right)\left(H_{ij,t+\frac{1}{2}} - H_{i-1,j,t+\frac{1}{2}} + h_{ijt} - h_{i-1,jt}\right)}{2\Delta x}
\end{aligned} \qquad (3.35)$$

The relative relations of those mass fluxes across adjacent computing cells with different subscripts are shown in Figure 3.8.

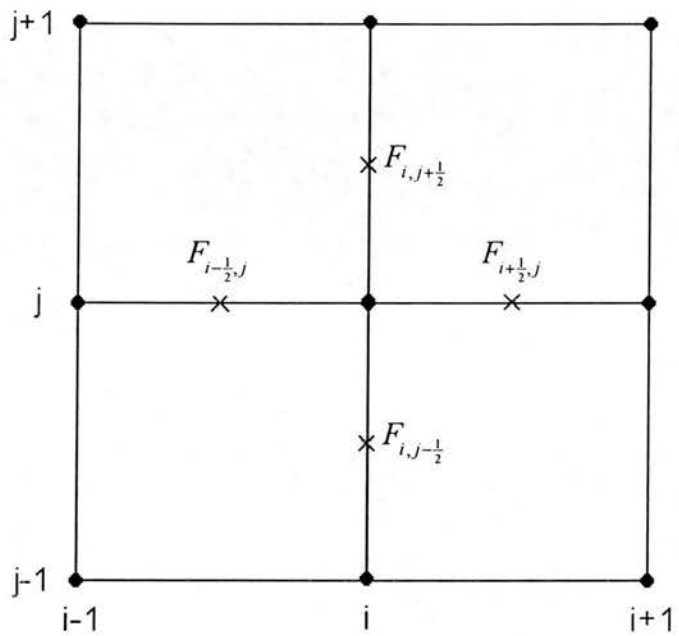

Figure 3.8 Relative spatial relations of mass fluxes across adjacent computing cells (adopted from Huybrechts [1992]).

Like the diffusion coefficient of the asthenosphere, D_a, in the isostatic equation (3.2), Ds in the discretized equations (3.32) ~ (3.35) derived from the ice mass continuity equation (3.1) reflect the diffusivity of ice. The diffusion coefficient is vertically integrated and contains a deformational term evaluated at layers of constant ζ, D^l, and a contribution from basal sliding, D^s:

$$D = H\int_0^1 D^l(\zeta)d\zeta + D^s\,, \tag{3.36}$$

where D^s has been discussed in §3.3.1 – Basal sliding.

Since the vertical ice deformation is caused by the huge weight of above ice load, the ice in the upper layer of an ice sheet is free from vertical deformation. In a vertically normalised computing grid defined in §3.5.2, given the free surface boundary condition

$$D^l_{ijN_\zeta t} = 0\,, \tag{3.37}$$

the vertically integrated diffusion coefficient at each sub-grid can then be expressed as

$$D_{ijt} = H_{ijt} \sum_{k=2}^{N_\zeta} \frac{\left(D^l_{ijkt} + D^l_{ij,k-1,t}\right)\left(\zeta_k - \zeta_{k-1}\right)}{2} + D^s_{ijt} \tag{3.38}$$

where D^ls can be obtained by back substitution:

$$D^l_{ijkt} = \left(\rho_{ice} g \frac{\zeta_{k+1} + \zeta_k}{2}\right)^n \left(\zeta_{k+1} + \zeta_k\right)\left[A\left(T^*_{ij,k+1,t}\right) + A\left(T^*_{ijkt}\right)\right] H^{n+1}_{ijt} \sqrt{\left(G_x^2 + G_y^2\right)^{n-1}} + D^l_{ij,k+1,t}$$

$$k = N_\zeta\text{–}1,\ldots,1 \tag{3.39}$$

with

$$\begin{aligned} G_x &= \frac{H_{i+1,jt} - H_{i-1,jt} + h_{i+1,jt} - h_{i-1,jt}}{2\Delta x} \\ G_y &= \frac{H_{i,j+1,t} - H_{i,j-1,t} + h_{i,j+1,t} - h_{i,j-1,t}}{2\Delta y}\,, \end{aligned} \tag{3.40}$$

and n the flow law exponent that normally adopts the value 3 in ice sheet calculations and $A(T^*)$ the temperature dependent flow law coefficient defined by equation (2.1). D^ss adopt different values at different conditions.

Equation (3.32) can formally be rearranged as a linear set of equations:

$$-\alpha_{ijt}H_{i-1,j,t+\frac{1}{2}}+\beta_{ijt}H_{ij,t+\frac{1}{2}}-\gamma_{ijt}H_{i+1,j,t+\frac{1}{2}}=\delta_{ijt}$$

$$i=2,\ldots,N_x-1 \text{ for } j=2,\ldots,N_y-1 \qquad (3.41)$$

or more clearly as a matrix equation set of tridiagonal type for row j:

$$\begin{pmatrix} -\alpha_{2jt} & \beta_{2jt} & -\gamma_{2jt} & & & \\ & -\alpha_{3jt} & \beta_{3jt} & -\gamma_{3jt} & & \\ & & \ddots & & & \\ & & & -\alpha_{Nx-1,jt} & \beta_{Nx-1,jt} & -\gamma_{Nx-1,jt} \end{pmatrix} \begin{pmatrix} H_{1,j,t+\frac{1}{2}} \\ H_{2,j,t+\frac{1}{2}} \\ \vdots \\ H_{Nx,j,t+\frac{1}{2}} \end{pmatrix} = \begin{pmatrix} \delta_{2jt} \\ \delta_{3jt} \\ \vdots \\ \delta_{Nx-1,jt} \end{pmatrix}$$

$$i=2,\ldots,N_x-1 \text{ for } j=2,\ldots,N_y-1 \qquad (3.42)$$

The ice sheet system fulfils additional conditions to the relations among the ADI coefficients α, β and γ [Huybrechts, 1992], which are

$$\begin{cases} \alpha_{ijt},\beta_{ijt},\gamma_{ijt}\neq 0 \\ \beta_{ijt}\geq\alpha_{ijt}+\gamma_{ijt} \end{cases}. \qquad (3.43)$$

By defining

$$w_{2jt}=\frac{\gamma_{2jt}}{\beta_{2jt}} \qquad g_{2jt}=\frac{\delta_{2jt}+\alpha_{2jt}H_{1j}}{\beta_{2,jt}}$$

$$w_{ijt}=\frac{\gamma_{ijt}}{\beta_{ijt}-\alpha_{ijt}w_{i-1,jt}} \qquad g_{ijt}=\frac{\delta_{ijt}+\alpha_{ijt}g_{i-1,jt}}{\beta_{ijt}-\alpha_{ijt}w_{i-1,jt}} \qquad i=3,\ldots,N_x-1 \quad (3.44)$$

and with an obvious condition that ice thickness cannot be negative,

$$H_{ij,t+\frac{1}{2}}\geq 0, \qquad (3.45)$$

the new ice thickness at the intermediate time step in equation (3.41) can thus be obtained by back substitution:

$$H_{N_{x-1},j,t+\frac{1}{2}} = w_{N_{x-1},jt} H_{N_x,j} + g_{N_{x-1},jt}$$
$$H_{ij,t+\frac{1}{2}} = w_{ijt} H_{i+1,j,t+\frac{1}{2}} + g_{ijt} \qquad i = N_x\text{–}2,\ldots,2 \quad (3.46)$$

The above numerical procedure involves firstly the solutions of N_y–2 tridiagonal sets of N_x equations with N_x–2 unknowns along columns of constant j. And then the whole procedure is repeated along rows of constant i to complete the integration forward in time. Temperature and bedrock elevation are updated every half time step. All the ADI coefficients are time dependent and thus need continuous re-evaluation.

The ADI coefficients, α, β, γ and δ, have different expressions depending on the problem the model tackles. For ice thickness calculations:

$$\alpha_{ijt} = -\frac{\Delta t}{4(\Delta x)^2}\left(D_{i-1,jt} + D_{ijt}\right)$$
$$\beta_{ijt} = 1 - \frac{\Delta t}{4(\Delta x)^2}\left(D_{i-1,jt} + 2D_{ijt} + D_{i+1,jt}\right)$$
$$\gamma_{ijt} = -\frac{\Delta t}{4(\Delta x)^2}\left(D_{ijt} + D_{i+1,jt}\right)$$
$$\delta_{ijt} = H_{ijt} - \frac{\Delta t}{2\Delta y}\left(F_{i,j+\frac{1}{2},t} - F_{i,j-\frac{1}{2},t}\right) + \frac{\Delta t}{2}\left(b_{ijt} - m_{ijt}\right) + \gamma_{ijt} h_{i+1,jt} - \left(\beta_{ijt} - 1\right) h_{ijt} + \alpha_{ijt} h_{i-1,jt}$$

(3.47)

Similarly, the isostatic equation (3.2) can be discretized as

$$\begin{pmatrix} -\alpha_{2jt} & \beta_{2jt} & -\gamma_{2jt} & & & \\ & -\alpha_{3jt} & \beta_{3jt} & -\gamma_{3jt} & & \\ & & \ddots & & & \\ & & & -\alpha_{Nx-1,jt} & \beta_{Nx-1,jt} & -\gamma_{Nx-1,jt} \end{pmatrix} \begin{pmatrix} h_{1,j,t+\frac{1}{2}} \\ h_{2,j,t+\frac{1}{2}} \\ \vdots \\ h_{Nx,j,t+\frac{1}{2}} \end{pmatrix} = \begin{pmatrix} \delta_{2jt} \\ \delta_{3jt} \\ \vdots \\ \delta_{Nx-1,jt} \end{pmatrix}$$

$$i = 2,\ldots,N_x\text{–}1 \text{ for } j = 2,\ldots,N_y\text{–}1 \qquad (3.48)$$

where the corresponding ADI coefficients are:

$$\alpha = \gamma = \frac{D_a \cdot \Delta t}{2(\Delta x)^2}$$

$$\beta = 1 + \frac{D_a \cdot \Delta t}{(\Delta x)^2}$$

$$\delta_{ijt} = h_{ijt} + \frac{D_a \cdot \Delta t}{2(\Delta x)^2}\left[\frac{\rho_{ice}}{\rho_{mantle}}\left(H_{i+1,j,t+\frac{1}{2}} - 2H_{ij,t+\frac{1}{2}} + H_{i-1,j,t+\frac{1}{2}}\right) - h^0_{i+1,j} + 2h^0_{ij} - h^0_{i-1,j}\right]$$

$$+ \frac{D_a \cdot \Delta t}{2(\Delta y)^2}\left[h_{i,j+1,t} - 2h_{ijt} + h_{i,j-1,t} + \frac{\rho_{ice}}{\rho_{mantle}}\left(H_{i,j+1,t+\frac{1}{2}} - 2H_{ij,t+\frac{1}{2}} + H_{i,j-1,t+\frac{1}{2}}\right) - h^0_{i,j+1} + 2h^0_{ij} - h^0_{i,j-1}\right] \tag{3.49}$$

For the first time step, the bedrock topography, h_{ij}, is based on the initial basal topography file, while those for the subsequent time steps are from the previous time step. Equation (3.49) shows that the ADI coefficients α, β, and γ are independent of time in isostatic calculations. They can therefore be regarded as constants in any single run.

The energy conservation equation (3.3) involves a three-dimensional temperature distribution. Besides the horizontal mesh grid defined for the above two-step ADI scheme, the vertical scale is normalised as equation (3.31) and divided into N_ζ layers (11 in this model) denoted by k, with $k = 1$ at the bottom layer and $k = N_\zeta$ at ice surface. Equation (3.3) can then be expressed as

$$\frac{\partial T}{\partial t} = \frac{k_{ice}}{\rho_{ice} c_{p\_ice} H^2}\frac{\partial^2 T}{\partial \zeta^2} - u\left.\frac{\partial T}{\partial x}\right|_\zeta - v\left.\frac{\partial T}{\partial y}\right|_\zeta$$

$$-\frac{1}{H}\frac{\partial T}{\partial \zeta}\left[\frac{\partial (H+h)}{\partial t} + \vec{v}\cdot\nabla(H+h) - \zeta\left(\frac{\partial H}{\partial t} + \vec{v}\cdot\nabla H\right) - w\right] + \frac{g}{c_{p\_ice}}\zeta\frac{\partial \vec{v}}{\partial \zeta}\cdot\nabla(H+h) \tag{3.50}$$

The normalised energy conservation equation (3.50) can be discretized as

$$-\alpha_{ijkt}T_{ij,k-1,t+1}+\beta_{ijkt}T_{ijk,t+1}-\gamma_{ijkt}T_{ij,k+1,t+1}=\delta_{ijkt}$$

$$i=2,\ldots,N_x-1;\ j=2,\ldots,N_y-1;\ k=2,\ldots,N_\zeta-1 \quad (3.51)$$

where the corresponding ADI coefficients are:

$$\alpha_{ijkt}=\frac{2k_{ice}\Delta t}{\rho_{ice}c_{p\_ice}H_{ij}^2(\zeta_{k+1}-\zeta_{k-1})(\zeta_k-\zeta_{k-1})}+\frac{\Delta t}{H_{ij}(\zeta_{k+1}-\zeta_{k-1})}\cdot$$
$$\left[u_{ijk}\frac{(1-\zeta_k)(H_{i+1,j}-H_{i-1,j})+h_{i+1,j}-h_{i-1,j}}{2\Delta x}+v_{ijk}\frac{(1-\zeta_k)(H_{i,j+1}-H_{i,j-1})+h_{i,j+1}-h_{i,j-1}}{2\Delta y}\right.$$
$$\left.+\frac{(1-\zeta_k)(H_{ij,t+1}-H_{ijt})+h_{ij,t+1}-h_{ijt}}{\Delta t}-w_{ijk}\right]$$

$$\beta_{ijkt}=1+\frac{2k_{ice}\Delta t}{\rho_{ice}c_{p\_ice}H_{ij}^2(\zeta_{k+1}-\zeta_k)(\zeta_k-\zeta_{k-1})}$$

$$\gamma_{ijkt}=\frac{2k_{ice}\Delta t}{\rho_{ice}c_{p\_ice}H_{ij}^2(\zeta_{k+1}-\zeta_{k-1})(\zeta_{k+1}-\zeta_k)}-\frac{\Delta t}{H_{ij}(\zeta_{k+1}-\zeta_{k-1})}\cdot$$
$$\left[u_{ijk}\frac{(1-\zeta_k)(H_{i+1,j}-H_{i-1,j})+h_{i+1,j}-h_{i-1,j}}{2\Delta x}+v_{ijk}\frac{(1-\zeta_k)(H_{i,j+1}-H_{i,j-1})+h_{i,j+1}-h_{i,j-1}}{2\Delta y}\right.$$
$$\left.+\frac{(1-\zeta_k)(H_{ij,t+1}-H_{ijt})+h_{ij,t+1}-h_{ijt}}{\Delta t}-w_{ijk}\right]$$

$$\delta_{ijkt}=T_{ijkt}-\Delta t(A_x+A_y)+\frac{g\zeta_k\Delta t}{2c_{p\_ice}(\zeta_{k+1}-\zeta_{k-1})}\cdot$$
$$\left[\frac{(u_{ij,k+1}-u_{ij,k-1})(H_{i+1,j}+h_{i+1,j}-H_{i-1,j}-h_{i-1,j})}{\Delta x}+\frac{(v_{ij,k+1}-v_{ij,k-1})(H_{i,j+1}+h_{i,j+1}-H_{i,j-1}-h_{i,j-1})}{\Delta y}\right] \quad (3.52)$$

with

$$A_x=\begin{cases}u_{ijk}\dfrac{T_{ijk}-T_{i-1,jk}}{\Delta x} & v_{ijk}>0\\ u_{ijk}\dfrac{T_{i+1,jk}-T_{ijk}}{\Delta x} & v_{ijk}<0\end{cases}$$
$$A_y=\begin{cases}v_{ijk}\dfrac{T_{ijk}-T_{i-1,jk}}{\Delta y} & u_{ijk}>0\\ v_{ijk}\dfrac{T_{i+1,jk}-T_{ijk}}{\Delta y} & u_{ijk}<0\end{cases} \quad (3.53)$$

The term $\frac{2k_{ice}\Delta t}{\rho_{ice}c_{p\_ice}H_{ij}^2(\zeta_{k+1}-\zeta_k)(\zeta_k-\zeta_{k-1})}$ in α_{ijkt}, β_{ijkt} and γ_{ijkt} in equation (3.52) represents the vertical advection of heat transfer in the ice sheet system; the second term in δ_{ijkt}, $-\Delta t(A_x+A_y)$, represents the horizontal advection; and the last term in δ_{ijkt} represents the strain heating within ice.

According to principles of mass continuity, the three-dimensional ice flow velocity components can now be expressed as

$$u_{ijkt}=\frac{\left(H_{ijt}D^l_{ijkt}+H_{i+1,jt}D^l_{i+1,jkt}+D^s_{ijt}+D^s_{i+1,jt}\right)\left(H_{i+1,jt}-H_{ijt}+h_{i+1,jt}-h_{ijt}\right)}{\Delta x\left(H_{ijt}+H_{i+1,jt}\right)}$$
$$+\frac{\left(H_{i-1,jt}D^l_{i-1,jkt}+H_{ijt}D^l_{ijkt}+D^s_{i-1,jt}+D^s_{ijt}\right)\left(H_{ijt}-H_{i-1,jt}+h_{ijt}-h_{i-1,jt}\right)}{\Delta x\left(H_{i-1,jt}+H_{ijt}\right)}$$
$$v_{ijkt}=\frac{\left(H_{ijt}D^l_{ijkt}+H_{i,j+1,t}D^l_{i,j+1,kt}+D^s_{ijt}+D^s_{i,j+1,t}\right)\left(H_{i,j+1,t}-H_{ijt}+h_{i,j+1,t}-h_{ijt}\right)}{\Delta y\left(H_{ijt}+H_{i,j+1,t}\right)}$$
$$+\frac{\left(H_{i,j-1,t}D^l_{i,j-1,kt}+H_{ijt}D^l_{ijkt}+D^s_{i,j-1,t}+D^s_{ijt}\right)\left(H_{ijt}-H_{i,j-1,t}+h_{ijt}-h_{i,j-1,t}\right)}{\Delta y\left(H_{i,j-1,t}+H_{ijt}\right)}$$
$$w_{ijkt}=\left[\begin{array}{l}\dfrac{H_{i-1,jt}+2H_{ijt}+H_{i+1,jt}}{4}\cdot\dfrac{u_{i+\frac{1}{2},jkt}-u_{i-\frac{1}{2},jkt}+u_{i+\frac{1}{2},j,k+1,t}-u_{i-\frac{1}{2},j,k+1,t}}{2\Delta x}\\ +\dfrac{H_{i,j-1,t}+2H_{ijt}+H_{i,j+1,t}}{4}\cdot\dfrac{v_{i,j+\frac{1}{2},kt}-v_{i,j-\frac{1}{2},kt}+v_{i,j+\frac{1}{2},k+1,t}-v_{i,j-\frac{1}{2},k+1,t}}{2\Delta y}\\ +\dfrac{u_{ijkt}-u_{ij,k+1,t}}{\zeta_k-\zeta_{k+1}}\cdot\dfrac{(1-\zeta_k)\left(H_{i+1,jt}-H_{i-1,jt}\right)+h_{i+1,jt}-h_{i-1,jt}}{2\Delta x}\\ +\dfrac{v_{ijkt}-v_{ij,k+1,t}}{\zeta_k-\zeta_{k+1}}\cdot\dfrac{(1-\zeta_k)\left(H_{i,j+1,t}-H_{i,j-1,t}\right)+h_{i,j+1,t}-h_{i,j-1,t}}{2\Delta y}\end{array}\right]\cdot(\zeta_k-\zeta_{k+1})$$

$$k=N_\zeta-1,\ldots,1 \qquad (3.54)$$

3.6 Model Structure

The numerical ice sheet model developed in this research consists of three parts: input data, computing routines and output data (Figure 3.9).

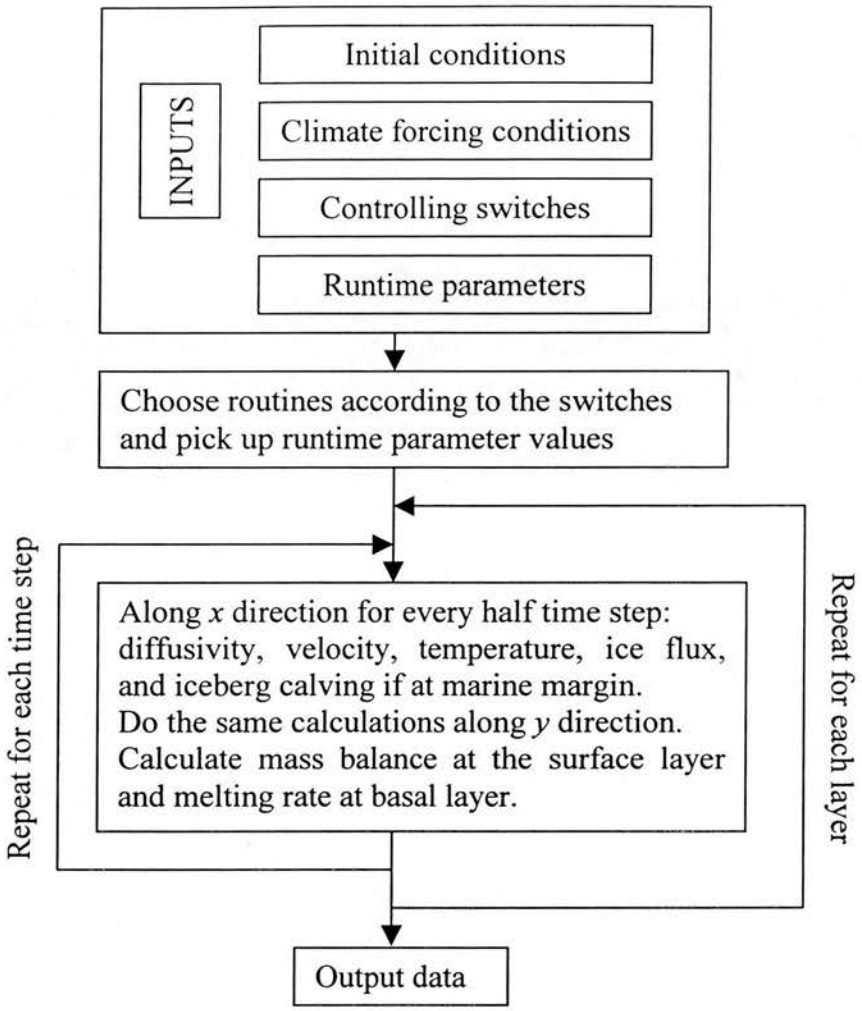

Figure 3.9 Model Structure

3.6.1 Model inputs

The ice sheet model developed in this research needs three kinds of input data files: initial conditions, climate forcing, and runtime parameters and controls. The initial conditions are the initial ice-surface topography, initial bedrock topography, ice-free bedrock topography and, if performing fully thermodynamic calculation, initial temperature distribution in the entire ice body. The initial ice-surface topography and bedrock topography can come either from the field survey (*e.g.* Figure 4.21) or from the results of previous model runs. The ice-free bedrock topography is obtained according to equation (3.29) and serves as a calculation reference, *e.g.* in equation

(3.2). The climate-forcing file contains the changes of eustatic sea level and ice surface temperature with time that reflect the climatic changes.

The most important and dynamic data inputs are in the runtime parameter and control file. While the thermophysical properties are hard-coded in the ice sheet model, all the runtime values for the ice sheet parameters are supplied through this file. Table 3.1 contains the key runtime input parameters and the corresponding sample values.

There are also some controlling switches in the runtime parameter and control file for choosing different routines in the model representing different assumptions and scenarios concerning the ice sheet system. Table 3.2 contains some key controlling switches and their functions. New runtime parameters and control switches can easily be added into or taken off from this file during model development.

Table 3.1 Key parameters in the runtime input file

Input runtime parameters	Sample values
Ice sheet sliding parameter	5×10^{-13}, 1×10^{-12}
Computing mesh grid	(141×141×11), (282×282×11)
Computing grid resolution	40000 m, 20000 m
Arrhenius constant	1×10^{-16}, 5×10^{-16}
Horizontal advection, Vertical advection, Strain heating	0 (advection not considered), 1.0, 1.5, 2.0, –1(reverse direction)
Time of simulation	100,000 model years, 200,000 model years
Time step	1 year, 5 years, 10 years
Initial condition files	Bedrock elevation, ice thickness, ice temperature
Iceberg calving rate	25%, 50% per year
Ice shelf spreading rate	5%, 15% per year
Ice shelf basal melting rate	1 m per year
Maximum depth of ice shelf	–200 m (– means below sea level)
Diffusion of asthenosphere	1×10^{7} m²/year
Geothermal heat flux	42.0 mW/m², 54.6 mW/m²
Mass balance multiplier	1, 1.5

Table 3.2 Key control switches and their functions

Runtime control switches	Explanations
Ice sheet system switch	Choose the ice sheet system the model is going to be running, the two-dimensional system or the Antarctic
Ice sheet sliding	On: calculate the effect with the sliding parameter Off: ice sliding not considered
Marine margin	Choose different approaches to simulating iceberg calving processes
Isothermal	On: ignore vertical differences in the ice sheet Off: fully thermodynamic calculations
Velocity	On: calculate three-dimensional ice flow velocity Off: speed up model runs by not calculating velocity
Temperature	On: calculate ice temperature in every computing cell Off: speed up model runs by not calculating temperature
Thermo-dynamical coupling	On: dynamical regime coupled with thermal regime Off: calculate ice flow with a constant Arrhenius factor
Isostasy	On: bedrock elevation changes with the ice load Off: fixed bedrock elevation

Table 3.3 Possible output data files

Bedrock elevation
Difference in bedrock elevation from last iteration
Ice thickness
Difference in ice thickness from last iteration
Ice sliding diffusivity
Ice temperature
x component of the ice flow velocity
y component of the ice flow velocity
z component of the ice flow velocity
Ice flow diffusivity
Ice sheet grounding status
Ice surface mass balance
Ice surface temperature
Basal temperature
Iceberg calving rate

3.6.2 Model outputs

Depending on which parameters the user is interested in, there are a variety of output choices. Table 3.3 lists the possible output data files that the model can produce. These choices are also made in the runtime parameter and control file.

The output data can be either in binary format (as the imported files of the AVS/Express Visualization package) or in ASCII format (for Microsoft Excel) depending on what visualisation package is used. The output format is also chosen in the runtime parameter and control file. In this research, all visualisations to the output data are carried out in AVS/Express Visualization, with the exception of the analyses of ice volume, ice covered area and ice thickness (Figures 4.25 and 5.7).

3.7 How the Ice Sheet Model Works

The model is coded in FORTRAN 90. It consists of three main parts as shown in Figure 3.7: input data files, source code files and output data files. There are two kinds of source code files: parameter-defining files and numerical computing routines. The data-defining files define and initiate variables, read in runtime parameters and switches, load in the initial conditions of the modelled ice sheet and make those global variables visible by necessary routines. The numerical computing routines form the kernel of the ice sheet model. One routine normally simulates one representation of the thermodynamical processes of the ice sheet system. Which representation to choose is controlled by those switches read in from the runtime parameter and control file. Once the source code files are successfully compiled and linked together, an executable file will be generated and the ice sheet model is ready for use.

It is the user's responsibility to set the values for those parameters, to set the switches to choose different scenarios, and to decide the ice sheet conditions from which the ice sheet model starts to evolve. If the ice sheet is assumed to be isothermal during its

evolution, only the initial bedrock topography and the initial ice thickness files are needed because temperatures will not be calculated; otherwise, the initial temperature distribution file for the entire ice body are needed as one of the input files. The rebounded ice-free Antarctic topography is always needed as a reference. Before a model run, the user should also design a climatic scenario under which the ice sheet will evolve. In this research, the ice sheet model is driven by a stepped change in ice surface temperatures and eustatic sea level.

Chapter 4 Sensitivity and Calibration of the Ice Sheet Model

The purpose of this modelling research is to help understand the evolution of the Antarctic Ice Sheet in the past and to predict its future under different climatic changes caused by human activities and natural processes. Therefore robustness in the working assumptions and boundary conditions is essential in interpreting the results of the model. Before it can be applied to the research objective, the ice sheet model must be tested against related parameters under idealised conditions and calibrated against observed data. Sensitivity analysis is also crucial in identifying the role of each individual variable in the working of the model.

All numerical methods have potential problems of stability and convergence. Besides improper numerical algorithms, poor modelling of the real world can also cause instability and divergence in computing. Coarse grids and long time steps, for example, can hide the necessary details of the modelled natural processes. Poor boundary conditions and unrealistic parameter inputs can pass wrong signals into the modelled system. Deviations may accumulate throughout the model run and may eventually lead to unreasonable modelling results or the divergence of numerical processes and crash the model run. This chapter aims to test the sensitivities of the ice sheet variables to related parameters through the use of a range of values and by calibration against best fit solutions.

As analysed in Chapter 2, different factors affect the thermodynamical processes in the ice sheet system to a varying degree. For example, because the horizontal scale of the Antarctic Ice Sheet is three orders of magnitude larger than its vertical scale, the vertical temperature gradient in the ice sheet is far greater than the horizontal temperature gradient [Paterson, 1994]. Thermal conduction in the Antarctic Ice Sheet is primarily a one-dimensional (vertical) process. For similar reasons, thermal advection in the Antarctic Ice Sheet is primarily a two-dimensional process. It

follows that we can use idealised systems of different dimensions to highlight different thermal and dynamical processes in the ice sheet. In this chapter, working from the simple to the complex, we analyse the thermal and dynamical processes characterised in each idealised ice sheet system.

- One-dimensional ice sheet system — Thermal conduction only.
  In such a system with one vertical axis, heat transfer is dominated by thermal conduction. In this simplest ice sheet system without thermal advection, internal strain heating and ice sliding gives us a clear view of the fundamental heat processes related to thermal conduction.

- Two-dimensional ice sheet system — Thermal advection and internal strain heating introduced.
  Thermal advection and internal strain heating are caused by ice flow. Without basal topography and isostasy, the two horizontal dimensions are identical. Therefore these two thermal processes are best illustrated in a two-dimensional ice sheet system with one vertical axis and one horizontal axis.

- Three-dimensional ice sheet system — Isostasy introduced.
  Under the effect of basal topography, the thermal and dynamical processes in an ice sheet are three-dimensional. The isostatic effect is more significant. The modelled ice sheet is allowed to evolve from the rebounded Antarctic ice-free topography and calibrated against the present-day Antarctic Ice Sheet.

Working from the one-dimensional idealised ice sheet system to the three-dimensional Antarctic Ice Sheet system, factors affecting the thermal and dynamical regimes in the ice sheet are gradually introduced and tested and combined together. This modelling procedure identifies the function of each individual factor in the ice sheet system. The systematic procedure also makes it easier for the modeller to identify problems in the model and to adjust the parameters accordingly.

4.1 One-dimensional Idealised Ice Sheet System — an Equilibrium System

As analysed earlier, heat transfer in ice sheets is a three-dimensional process including three-dimensional thermal advection, internal strain heating, heating related to ice sliding and thermal conduction. These three-dimensional sub-processes are introduced into the ice sheet system by ice flow except for heat conduction, which is an intrinsic attribute of materials. Ice flow intensifies heat transfer in the ice sheet system by means of advection. It also causes internal stresses in the ice that lead to strain heating. Warm-based ice sheets slide over bedrock. Ice sheet sliding produces heat by friction and accelerates the entire ice sheet flow. All these thermal effects due to ice flow change with ice sheet evolution and can be linearly integrated with the thermal processes related to the intrinsic attributes of materials. When investigating thermal conduction in the ice sheet system, we can temporarily put aside those thermal processes caused by the three-dimensional ice flow. In an ice sheet of a continental scale, heat flux due to horizontal thermal conduction is negligible compared to that due to vertical thermal conduction [Paterson, 1994]. Given the reasonable assumption that the ice in an ice sheet is an isotropic material, a one-dimensional system is therefore sufficient in telling us the contribution of thermal conduction to the thermal regime of the ice sheet.

In an ice sheet system, ice flow, or the potential of ice flow, is driven by the gravitational gradient. In the idealised one-dimensional ice sheet system illustrated in Figure 4.1, there is neither surface slope nor basal gradient. Ice in such a system bears no gravitational gradient. Bearing in mind that thermal conduction is an intrinsic attribute of materials, we can simplify the system by not considering surface accumulation over time. Under the above assumptions, ice cannot flow. Hence the three components of ice flow velocity, u, v, w in equation (3.3), and the basal sliding velocity, $\vec{v}_b$ in equation (3.4), are all zero. As a consequence, heat advection, internal strain heating and frictional heating due to sliding do not occur, *i.e.* the internal heating term $\dot{q}$ in equation (3.3) is zero. The only thermal process left in such an idealised ice sheet system is thermal conduction driven by vertical temperature

gradients. If we assume air temperature above the ice sheet is colder than the ice, which is true on the Antarctic continent, the thermal process in the vertical dimension is simplified as that heat is transferred from one heat source to one heat sink solely by thermal conduction. The heat source is the geothermal heat flux across the ice-bedrock interface and the heat sink is at the ice-atmosphere interface. With a further assumption of infinite ice extent, which is reasonable for the continental-scale ice sheets in Antarctica, the ice centre problem is eliminated and thermal conduction can be considered as one-dimensional. This simplification is similar to the "shallow ice approximation", which is widely employed in large-scale ice sheet modelling [Nye, 1957].

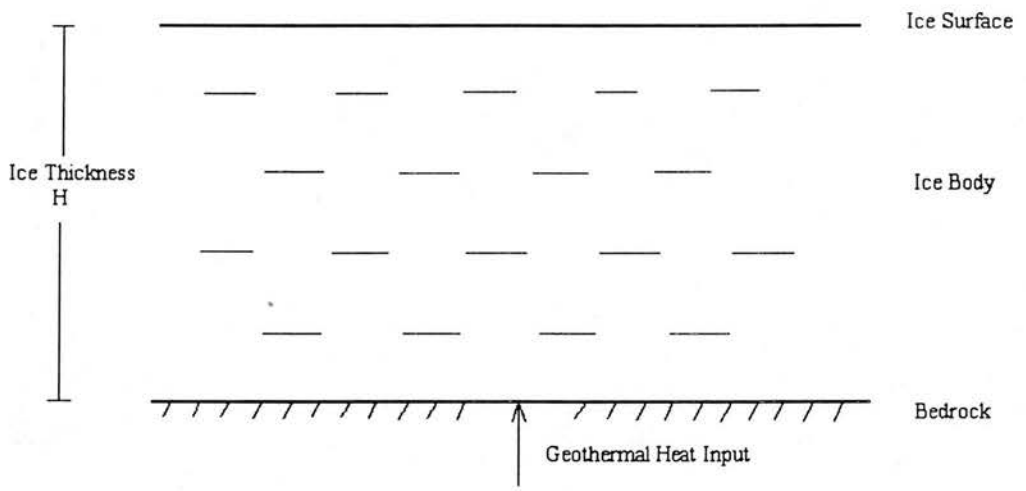

Figure 4.1 One-dimensional idealised ice sheet system. The system has an infinite horizontal extent; there are no surface and basal gradients; constant geothermal heat flux enters the ice sheet system across the ice-bedrock interface and heat leaves the system from the ice-atmosphere interface; the ice body is formed by pure isotropic rigid crystal material.

In the idealised one-dimensional ice sheet system defined in Figure 4.1, heat transfer occurs only in the vertical direction. If both ice and bedrock are treated as rigid bodies, the energy equation (3.3) can be simplified as:

$$\frac{\partial T}{\partial t} - \alpha_{ice} \frac{\partial^2 T}{\partial z^2} = 0 \tag{4.1}$$

where $\alpha_{ice} = \dfrac{k_{ice}}{\rho_{ice} c_{p\_ice}}$, the thermal diffusivity of ice, is a function of temperature. Equation (4.1) is a thermal diffusion equation. It governs the process of heat transfer in a continuous media without an inner heat source, in this case, the ice sheet.

If initially the ice sheet is in an equilibrium state with a uniform temperature T_{ini},

$$T(z,0) = T_{ini}, \tag{4.2}$$

the general solution of equation (4.1) gives the time-dependent temperature distribution in the idealised one-dimensional ice sheet system [Incropera and Dewitt, 1996]:

$$T(z,t) = \frac{T_{ini}}{2\sqrt{\pi \alpha_{ice} t}} \int_0^H \exp\left[-\frac{(z-\xi)^2}{4\alpha_{ice} t} \right] d\xi \ . \tag{4.3}$$

Further assumptions and boundary conditions to the Antarctic Ice Sheet system are required to integrate equation (4.3) for the final expression of the time-dependent temperature distribution.

4.1.1 Semi-infinite assumption

Patankar [1980] gives the solutions of the integral in equation (4.3) under two important boundary conditions — constant surface temperature and constant heat flux across a surface, both of which are very much like the situations in the centre of the Antarctic Ice Sheet. If climate does not change, the annual mean temperature at the ice surface is constant and geothermal heat flux across the ice-bedrock interface is assumed to be constant. These two standard boundary conditions therefore can reasonably be applied in the ice sheet system.

The integral solutions under both of the above boundary conditions need an additional assumption — that of a semi-infinite continuous medium. In the case of an ice sheet, this assumption means that when one surface of the ice sheet system, either the ice-atmosphere interface or the ice-bedrock interface, is defined, the other surface can be regarded as at an infinitely far distance away from the defined one. The conditions of the undefined surface will therefore not be affected by changes on the defined surface and so remain at its initial conditions. This assumption is reasonable for the Antarctic Ice Sheet when analysing transient heat conduction in the system. The average thickness of the Antarctic Ice Sheet is about 2300 m. The maximum difference of the annual mean temperature on the surface of the southeast Norwegian Sea during the last glacial-interglacial cycle was about 10°C [Lowe and Walker, 1997]. The annual mean temperature change due to long term climatic change over the Antarctic continent is of similar scale. In addition, because ice is a bad heat conductor, the heat flux in the Antarctic Ice Sheet is very low. A thermal signal on one surface of the ice sheet, which could reflect climatic change, may last shorter than the response time scale of the other surface. During the characteristic time span of the thermal signal, thermal conditions of the other surface can safely be regarded as unchanged.

Besides the semi-infinite assumption, the time-dependent temperature distributions in the one-dimensional ice sheet system discussed in the following two sections require another assumption — that the whole body of Antarctic ice is a rigid solid. With this assumption, thermal conductivity of the entire ice body is constant and neither thermal advection nor internal strain can occur. This rigid solid assumption is not accurate for an ice sheet, especially near the bottom. Since thermal advection and strain heating will be added into the two-dimensional system and, as will be seen in later analysis, thermal conduction plays a minor role in a large-scale ice sheet system, this assumption is nevertheless reasonable when analysing the thermal processes in the idealised one-dimensional ice sheet system.

4.1.2 Constant ice surface temperature — a transient state

Ice surface temperature serves as the upper boundary condition of the ice sheet system. Because large-scale ice sheet evolution is a long-term process, seasonal surface temperature oscillations cannot affect the thermal regime. As a matter of fact, this oscillation fades out within about 10 metres from the surface of an ice sheet [Loewe, 1970]. Bearing in mind that the average thickness of the Antarctic Ice Sheet is about 2300 metres, this fading means the ice sheet, more importantly the base of the ice sheet, cannot feel the oscillation. Therefore, the annual mean surface temperature over the ice sheet can be employed as the upper boundary condition of the system.

Based on the analysis at the beginning of §4.1, if the z-axis is set vertically with $z = 0$ at the ice surface, the transient thermal conduction process in this semi-infinite rigid system is depicted by equation (4.1). Suppose that the ice sheet has an initial uniform temperature T_{ini} (initial condition equation (4.2)) and the annual mean surface temperature increases by ΔT due to a long-term climate warming,

$$T(0,t) = T_{sur} = T_{ini} + \Delta T_{sur}. \tag{4.4}$$

Under the above conditions, this temperature disturbance will be conducted towards the bottom of the ice sheet. Following Incropera and Dewitt [1996], the time-dependent temperature distribution in such a system is:

$$T(z,t) = T_{ini} + \Delta T_{sur}\left[1 - erf\left(\frac{z}{2\sqrt{\alpha_{ice}t}}\right)\right] \tag{4.5}$$

where α_{ice} is thermal diffusivity of ice and $erf(\omega)$ is the Gaussian error function. Following the Compiling Group [1979], the Gaussian error function is defined as

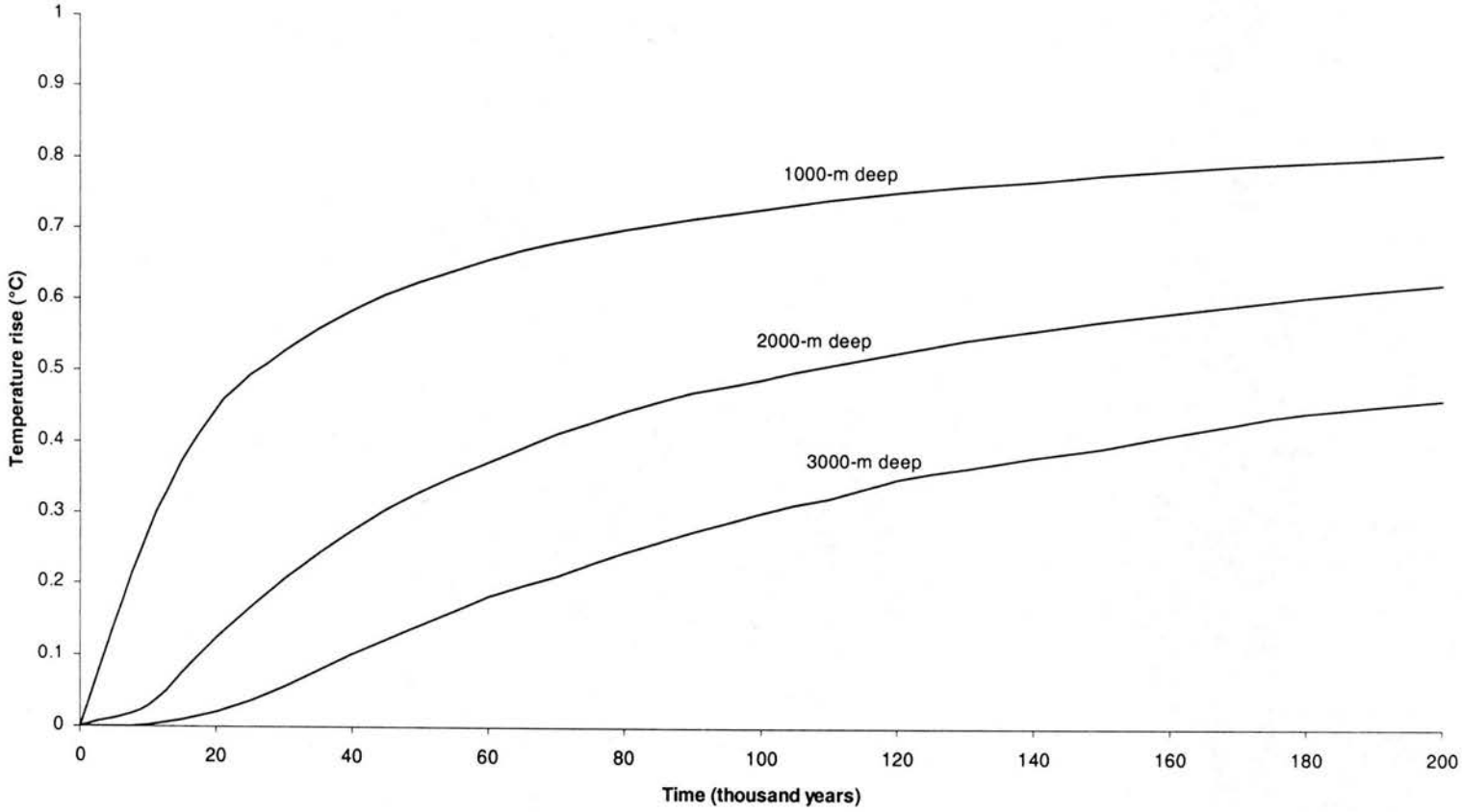

Figure 4.2 The contribution of thermal conduction to the temperature field in the idealised one-dimensional ice sheet system. This chart shows the temperature rise with time at three depths in the ice sheet if the ice sheet has an initial uniform temperature of –30°C and if its surface temperature goes up by 1°C and remains unchanged. After 100,000 years, the intensity of temperature change at all depths becomes stable and the process of thermal conduction in the ice sheet is approaching a quasi-equilibrium state.

$$erf(\omega) \equiv \frac{2}{\sqrt{\pi}} \int_0^{\omega} e^{-\xi^2} d\xi$$
$$= \frac{2}{\sqrt{\pi}} e^{-\omega^2} \sum_{k=0}^{\infty} \frac{2^k \omega^{2k+1}}{(2k+1)!} \qquad |\omega| < \infty . \qquad (4.6)$$

In equation (4.5), expression $\frac{z}{2\sqrt{\alpha_{ice} t}}$ substitutes ω in the definition equation (4.6). Since the thermal diffusivity of ice and ice sheet evolution time are both greater than zero, this expression always satisfies the finite condition of equation (4.6). ξ is an integral variable.

Equation (4.5) gives the contribution of ice surface temperature change through thermal conduction to the thermal regime of an ice sheet system. It serves as one component of the time-dependent temperature distribution in an ice sheet and will be linearly integrated with the contributions by other thermal processes like geothermal heating, strain heating and advection later. Changing ΔT_{sur} in equation (4.5) gives the sensitivity of the temperature evolution in an ice sheet to the surface temperature change through thermal conduction.

Since the thermal conductivity and specific heat capacity of ice are constants in the temperature range involved, the initial temperature field of the ice sheet does not affect the process of thermal conduction when the surface temperature changes. Applying equation (4.5), we can investigate the response of the temperature field of an ice sheet to the surface temperature change. Let us assume the ice sheet has a uniform initial temperature of –30°C (T_{ini} = –30°C). The thermal diffusivity of ice at this temperature is 1.33×10^{-6} m²/s ($\alpha_{ice}|_{T=-30°C} = 1.33\times10^{-6}$ m²/s) [Paterson, 1994]. If ice surface temperature goes up by 1°C (ΔT_{sur} = 1°C) and remains unchanged, the temperature rises over time. Figure 4.2 indicates the amplitude and rate of change at three different depths in the ice sheet, 1000 metres, 2000 metres and 3000 metres. With the propagation of this thermal signal, the temperature gradients in the ice sheet become weaker and weaker. As a consequence, the speed of temperature rise in the ice sheet becomes slower and slower. After 100,000 model years, the intensity of

temperature change at all depths becomes stable, which indicates the process of thermal conduction in the ice sheet system is approaching a quasi-equilibrium state.

4.1.3 Constant geothermal heat flux — a transient state

Beneath a real ice sheet, continuous geothermal heat from the lithosphere enters the ice sheet via the ice-bedrock interface. As indicated in the last section, the seasonal temperature fluctuation of the air above the ice sheet normally cannot penetrate the 10-metre depth layer. This phenomenon can help to simplify the ice sheet system and set up the boundary conditions. Since ice temperatures below the 10-metre depth layer will not be affected by the seasonal ice surface temperature fluctuation, the ice temperature at the 10-metre depth layer can be regarded as a constant if the climate does not change. Compared to the average thickness of the Antarctic Ice Sheet, the depth of 10 metres is very shallow. Ice temperatures at the 10-metre depth layer can therefore be approximated by the annual mean temperature at the ice surface,

$$T(\infty,t) = T_{ini}. \tag{4.7}$$

As a consequence, there is no heat exchange across the 10-metre depth layer. This is equivalent to a situation in which the ice surface is infinitely far away from the ice-bedrock interface. The ice sheet system is thus simplified as a semi-infinite system and condition (4.7) serves as the semi-infinite boundary with reference to the ice-bedrock interface. The ice material in this simplified ice sheet system is still regarded as a rigid solid.

For convenience, the z-axis here is set as vertically upwards with $z = 0$ at the ice-bedrock interface. The transient thermal conduction process in this semi-infinite rigid system is still depicted by equation (4.1). If the geothermal heat flux across the ice-bedrock interface is evenly distributed over the entire base, the basal boundary condition of the idealised one-dimensional ice sheet system, equation (3.4), is consequently simplified as:

$$-k_{ice}\left.\frac{\partial T}{\partial z}\right|_{z=0} = \dot{q}_{geoth}\,. \tag{4.8}$$

This uniform geothermal heat flux assumption is widely employed by Antarctic Ice Sheet modellers due to the lack of direct field measurement [Näslund, 1998]. Under the initial condition (4.2) and the boundary conditions (4.7) and (4.8), the time-dependent temperature distribution in the one-dimensional semi-infinite rigid ice sheet system can be derived following Incropera and Dewitt [1996]:

$$T(z,t) = \frac{2\dot{q}_{geoth}\sqrt{\alpha_{ice}t/\pi}}{k_{ice}}\exp\left(-\frac{z^2}{4\alpha_{ice}t}\right) - \frac{\dot{q}_{geoth}z}{k_{ice}}erfc\left(\frac{z}{2\sqrt{\alpha_{ice}t}}\right) + T_{ini} \tag{4.9}$$

where $erfc(\omega)$ is the supplementary error function, which is defined as

$$erfc(\omega) \equiv 1 - erf(\omega)\,. \tag{4.10}$$

Expression (4.9) gives the geothermal contribution to the temperature evolution in an ice sheet. It forms another part of the final time-dependent temperature distribution in an ice sheet. The direction of the z-axis should be rearranged when adding the contribution by geothermal heating (expression (4.9)) to that of ice surface temperature change through thermal conduction (expression (4.5)).

4.1.4 Between two equilibrium states

When modelling the evolution of the Antarctic Ice Sheet, either from an ice-free Antarctic topography or from an existing ice sheet topography, we normally assume the ice sheet starts to evolve from an equilibrium condition. When the boundary conditions of an equilibrium ice sheet change, ice surface temperature and sea level for example, the original equilibrium is broken. If the disturbance persists for a sufficiently long time, the ice sheet will eventually reach a new equilibrium state. Although a new equilibrium state may never be reached in the real world, the

difference of a certain ice sheet variable between two equilibrium states reveals the sensitivity of the variable to that disturbance.

When examining differences between two equilibrium states, we are not interested in the changes over time. Introducing the steady state condition,

$$\frac{\partial T}{\partial t} = 0 \tag{4.11}$$

in mathematical language, the thermal diffusion equation (4.1) is further simplified as

$$\frac{d^2T}{dz^2} = 0 \ . \tag{4.12}$$

The integral of equation (4.12) gives

$$T(z,0) = c_1 z + c_2 \tag{4.13}$$

where c_1 and c_2 are two integral constants that can be confined by the basal boundary condition (4.8) and surface boundary condition. If we assume the ice surface temperature does not change with time,

$$T(H,t) = T_{sur} \ , \tag{4.14}$$

and geothermal heat flux is steady over the entire continent, then

$$\begin{cases} c_1 = -\dfrac{\dot{q}_{geoh}}{k_{ice}} \\ c_2 = T_{sur} + \dfrac{\dot{q}_{geoth}}{k_{ice}} \end{cases} . \tag{4.15}$$

Hence the vertical temperature distribution in a steady state ice sheet system is

$$T(z) = -\frac{\dot{q}_{geoth}}{k_{ice}} z + \frac{\dot{q}_{geoth}}{k_{ice}} H + T_{sur} \qquad (0 \le z \le H) . \qquad (4.16)$$

The assumption of a steady ice surface temperature, equation (4.14), is reasonable if the smallest time step is one year. In this case, seasonal temperature oscillations are suppressed.

Expression (4.16) gives the final temperature distribution in an idealised one-dimensional ice sheet system if a new steady ice surface temperature and/or a new steady geothermal heat flux are unchanged for a sufficiently long time for the ice sheet system to reach a new equilibrium state. As mentioned above, such a state may never be reached in a real ice sheet system. However this distribution is nevertheless worth discussing, for it indicates the evolutionary trend of ice temperatures due to thermal conduction under certain climatic conditions. Figure 4.3 shows the temperature distributions given a series of ice surface temperatures in a one-dimensional equilibrium ice sheet system. On the Antarctic plateau, the annual mean surface temperature is –50°C [Rubin and Weyant, 1965]. For an ice sheet under such an upper boundary condition, thermal conduction alone can allow the ice to reach its local pressure melting point at a depth of about 2500 metres. However, in the case of a real ice sheet, the actual melting zone under the Antarctic Ice Sheet is a combined result of many other factors like thermal convection, strain heating and ice sliding, *etc.*

Temperature expressions (4.9) or (4.16) could result in a temperature figure higher than the local pressure melting point (*pmp*) of ice at a certain depth,

$$T(z)|_{calculated} > T_{pmp} . \qquad (4.17)$$

Since this obviously cannot happen, such a result simply means the ice at that spot is at the local pressure melting point and is melting. In the ice sheet model, we force the ice temperature at that point to be at the pressure melting point,

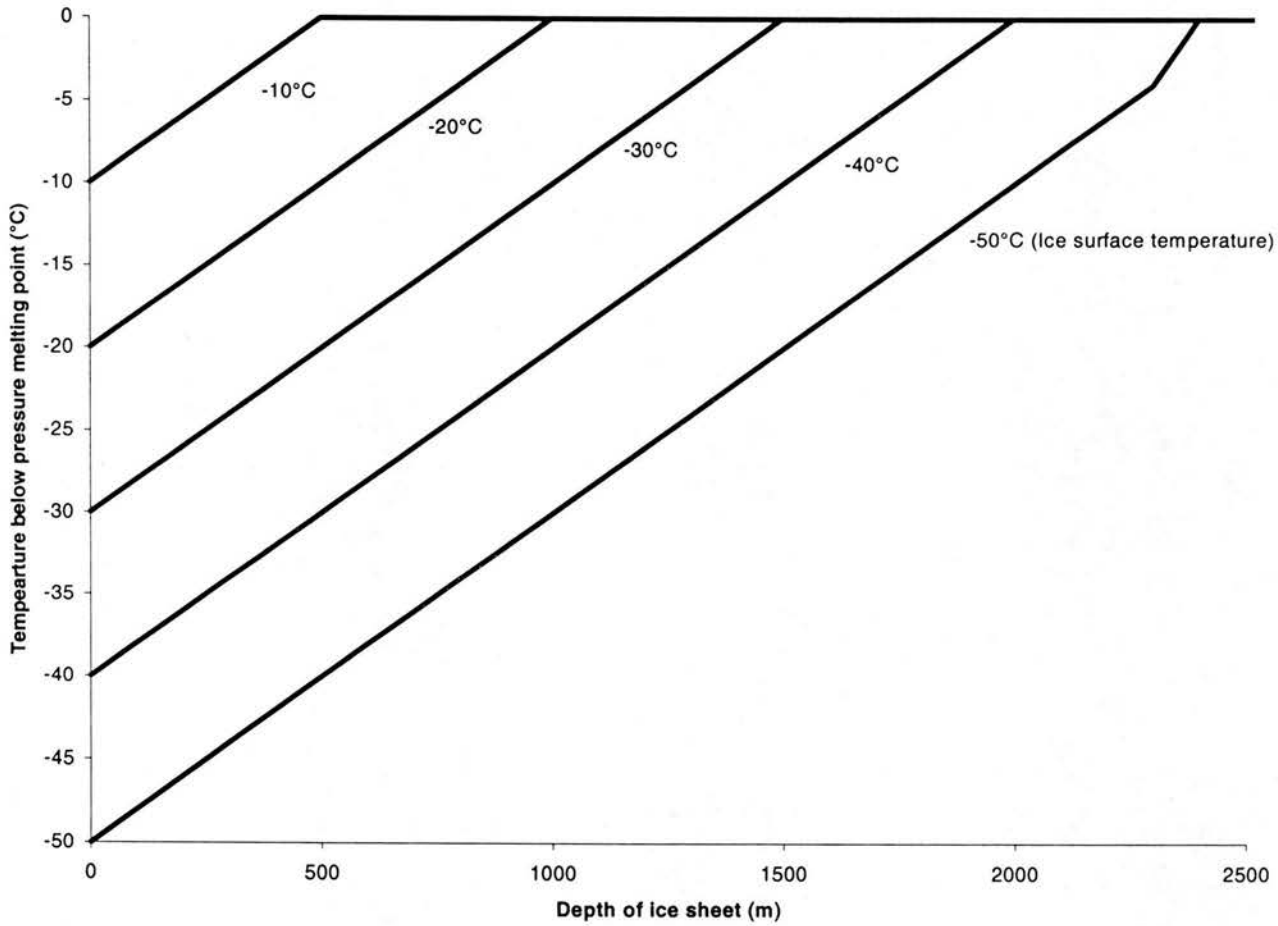

Figure 4.3 Equilibrium temperature distributions due to thermal conduction in an idealised one-dimensional ice sheet system at different ice surface temperatures. It indicates the evolutionary trend of ice temperatures due to thermal conduction under a certain climatic condition.

$$T(z) = T_{pmp} \,. \tag{4.18}$$

The surplus heat, which would have raised the temperatures of the "virtual ice" beyond its local pressure melting point by $T(z)|_{calculated} - T_{pmp}$ if there were no phase change, is absorbed by the ice as the latent heat of fusion. To calculate the amount of this surplus heat, we must first find out the depth at which the ice reaches its local pressure melting point due to thermal conduction. It can be easily obtained from the temperature distribution expression (4.16) by setting $T(z)$ as T_{pmp}:

$$z_{pmp} = \frac{k_{ice}}{\dot{q}_{geoth}}\left(T_{sur} - T_{pmp}\right) + H \,. \tag{4.19}$$

The local pressure melting point of ice, T_{pmp}, is obtained by the empirical formula (3.14) [Paterson, 1996]. Substituting formula (3.14) into expression (4.19) gives

$$z_{pmp} = \frac{\frac{k_{ice}}{\dot{q}_{geoh}}\left[T_{sur} - T^0 + T_{cc}(H+h)\right] + H}{1 + \frac{k_{ice}}{\dot{q}_{geoth}} T_{cc}} \,, \tag{4.20}$$

where $T^0 = 273.16$ K is the triple-point temperature of water; and $T_{cc} = 8.7\times10^{-4}$ K/m is the Clausius-Clapeyron gradient. T_{cc} designates the change of ice melting point with ice depth, which reflects the effect of high pressure.

If the thermal process does not involve phase change, the amount of heat required to raise the temperature of a column of ice with a differential element height dz and a unit area by ΔT is:

$$dQ_{surplus} = c_{p\_ice} \Delta T \rho_{ice} dz \,, \tag{4.21}$$

where c_{p_ice} is the specific heat capacity of ice at the pressure melting point; and ρ_{ice} is the density of ice. The definite integral of this differential equation (4.21) from the bottom of the ice sheet to z_{pmp} gives the total amount of heat that melts basal ice,

$$Q_{melt} = \rho_{ice} c_{p\_ice} \int_0^{z_{pmp}} [T(z) - T_{pmp}]\,dz = \frac{\dot{q}_{geoth}}{2\alpha_{ice}} z_{pmp}^2 , \qquad (4.22)$$

This amount of heat must serve as the latent heat of fusion of ice and melts the basal ice. The thickness of basal ice that is melted by the surplus heat is

$$M_b = \frac{Q_{melt}}{L_{ice}\rho_{ice}} , \qquad (4.23)$$

where L_{ice} = 335 kJ/kg, is the specific latent heat of fusion of ice.

The above analysis helps to address one of the hot debates about the stability of the Antarctic Ice Sheet under global climatic change. The present-day air temperatures over the Antarctic continent are so cold that climate warming of a few degrees is not enough to form an ablation zone and cause surface melting [Huybrechts and Oerlemans, 1990; Huybrechts, 1993]. The extent to which climate must warm to contribute to the basal melting under the ice sheet is helpful to an understanding of the basal thermal regime. Figure 4.4 shows the contribution of climate warming by 1°C to basal ice melting solely through thermal conduction in idealised ice sheets of 2000 m, 3000 m and 4000 m depth. For instance, for a typical 2000-m-deep ice sheet, a 1°C temperature rise on the ice surface can result in more than 5 metres of basal ice eventually being melted. Since the pressure melting point of ice is in inverse proportion to pressure, hence ice thickness, more ice will be melted under thicker ice sheets. Under a 4000-m-deep ice sheet, 30 metres of ice can eventually be melted by a 1°C temperature rise on the ice surface.

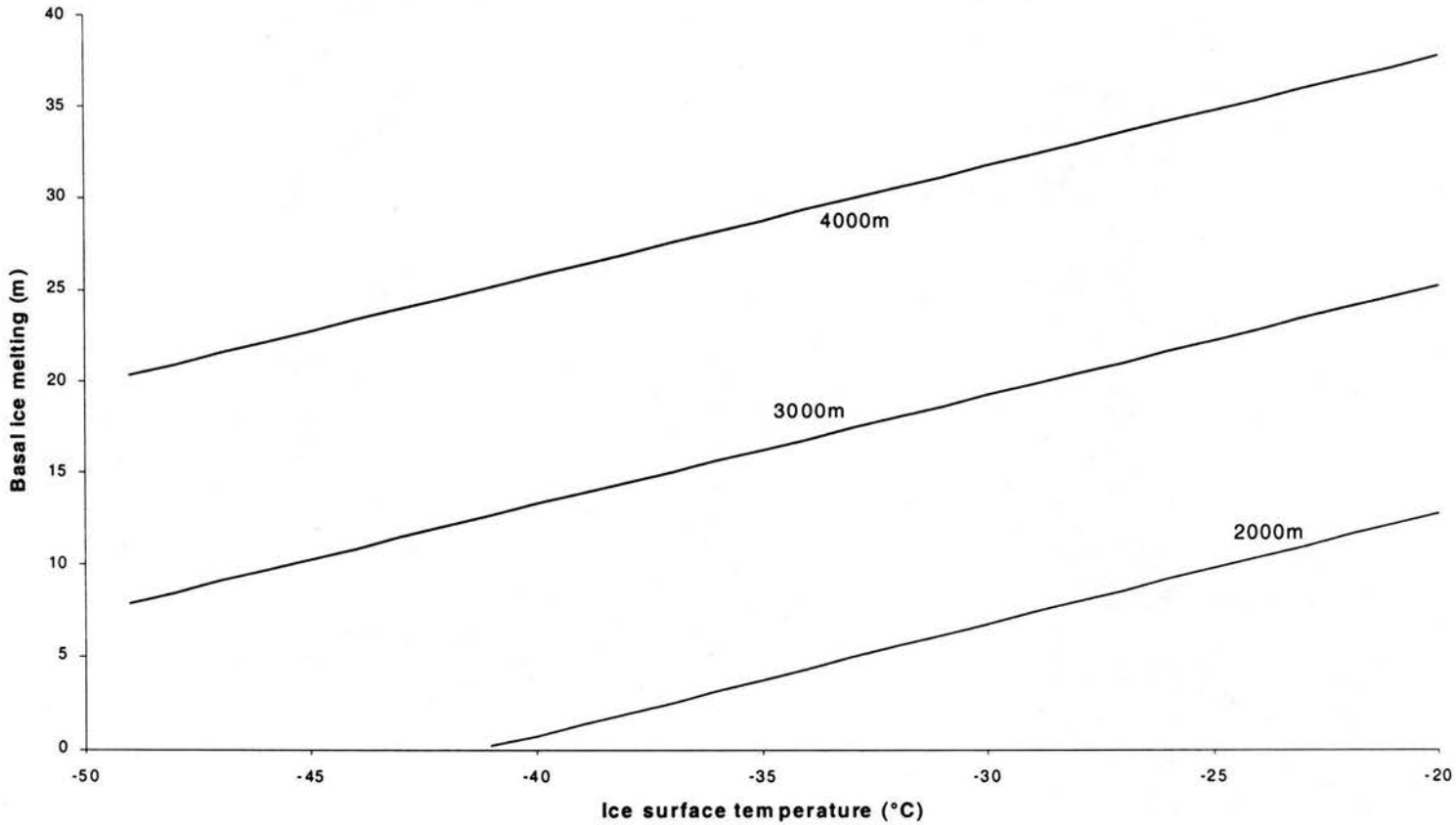

Figure 4.4 The amount of basal ice melting that could occur given a 1°C warming on the ice sheet surface. The ice sheet is assumed to be 2000 m, 3000 m and 4000 m deep. The graphs assume that the ice sheet reaches a new equilibrium.

4.2 Ice Sheet Evolution in a Two-dimensional Idealised System

All analyses in the previous section are based on an idealised one-dimensional ice sheet system with a rigid ice body (Figure 4.1). In the real world, however, because ice under a deep ice sheet can no longer be treated as a rigid body due to very high pressure, the ice will deform and flow, and thus strain heating occurs. Also because an ice sheet cannot be infinitely large and is constrained by irregular topography, thermal advection exits. Heat and mass transfers in such a system are therefore three-dimensional processes. With three-dimensional ice flow, thermal advection and strain heating will dominate the thermal regime under the ice sheet. This section will test the sensitivity of thermal advection and strain heating by analysing the thermal regime of a radial-symmetric two-dimensional ice sheet system.

Suppose that an ice sheet starts to grow on an infinite flat topography that is parallel to the geoid and is free from interaction with the sea. Three-dimensional thermal processes like advection and strain heating and dynamical processes like ice flow and deformation exist in such an ice sheet system. If the geothermal heat flux is constant over the entire base and the ice surface mass balance has radial symmetry, because there are no geometrical constraints from the bed and surface, the radially idealised ice sheet will be radially symmetric as well. Because the x dimension and y dimension of a radially symmetric system are identical, this ice sheet system can be treated as a two-dimensional system if we consider the vertical profile passing through the centre. Figure 4.5 shows such a profile.

Compared to the one-dimensional ice sheet system shown in Figure 4.1, this two-dimensional idealised ice sheet system has two additional features. One is that the ice sheet has a limited extent and a characteristic surface topography that provides the driving potential of ice flow. The other is that the ice is now treated as a visco-elastic material and thus incorporates ice deformation and hence strain heating.

As analysed in Chapter 2, ice surface mass balance, ice surface temperature, geothermal heat flux and the Arrhenius constant for ice are important factors directly affecting thermal processes in an ice sheet system. When modelling ice sheets, modellers are interested in the extent to which the changes in these factors influence the temperature distribution in the system. This knowledge can help modellers adjust parameters in a sensible way when calibrating the model and simulating climatic changes. It is also helpful in understanding the role of these factors in the fundamental thermal regime of an ice sheet.

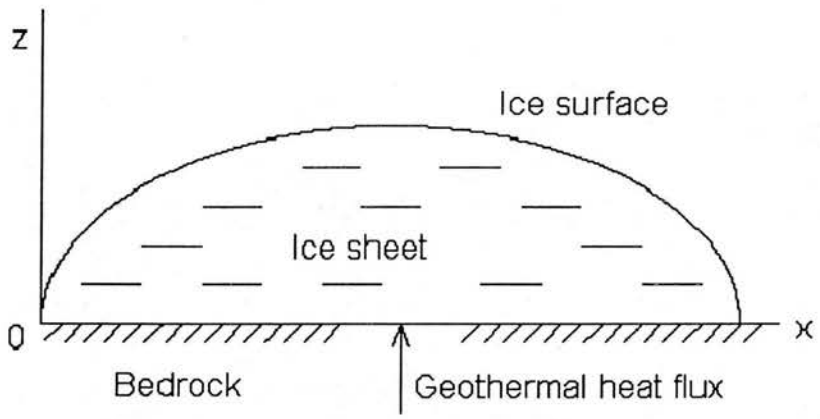

Figure 4.5 Two-dimensional idealised ice sheet system. The ice is a visco-elastic material and has surface gradients. Since the bedrock is still a rigid material and has an infinite extent, isostatic effect is not included.

The following experiments in this section are designed to test the sensitivities of the thermodynamic regime of an ice sheet to thermal advection and strain heating. From an ice-free flat surface, an ice sheet starts to grow. In these experiments, the values for certain parameters are based on the modelling experiments of the European Ice Sheet Modelling Initiative and some present-day conditions of the Antarctic Ice Sheet (Table 4.1). Before running the experiments, a standard run is made with these reference values. When one parameter is tested, a range of values of this parameter is

substituted into the ice sheet model while all other parameters are kept at their reference values.

Table 4.1 Reference values for the testing variables

Symbol	Value	Description
T_{centre}	–35°C	Ice surface temperature at the centre
M_{centre}	0.1 m/yr	Surface mass balance
$\dot{q}_{geoth}$	42.0 mW/m²	Geothermal heat flux
A	1.0×10^{-16} kPa^{-3}s^{-1}	Arrhenius constant for ice

In such sensitivity tests we are interested in the correlation between a certain variable and the thermodynamic regime of the ice sheet system, rather than whether or not the system reaches a new equilibrium. Figure 4.2 indicates that all the changes invoked by a disturbance to the ice sheet system happen within the first 50,000 model years and the evolutionary trends are hardly changed after then. 50,000 model years of a model run is therefore sufficiently long to reveal the sensitivity of a variable in the thermodynamic regime of an ice sheet system.

Unlike the plank shaped ice sheet with fixed thickness in the one-dimensional system, the ice sheet in the two-dimensional system is dynamical. It is crucial to run the ice sheet model at a time step that is short enough to keep the numerical process stable. Optimal iteration times depend on the computing resolution of the model and the precision of the boundary conditions. With a flat basal boundary condition and a linear upper boundary condition, a five-year time step proves to be an optimal choice for the experiments in the idealised two-dimensional ice sheet system. As we will see in the next section, this time step is not precise enough for the three-dimensional Antarctic Ice Sheet system, when a one-year time step, which represents a natural seasonal cycle, should be employed.

When testing the function of a particular factor in an ice sheet system, the experiment should try to avoid the influence of other interrelated factors. Accordingly, the

thermal regime of the ice sheet system should be decoupled from its dynamical regime in the sensitivity tests. The decoupled mode gives a clearer picture of the sensitivity of the modelled ice sheet system to the specific factor tested.

4.2.1 Ice surface temperatures

Surface temperature, T_{sur}, for each grid cell is set as a linear function of radial distance from the central grid [Huybrechts *et al.*, 1996],

$$T_{sur} = T_{centre} + s_T \sqrt{(x - \hat{x})^2 + (y - \hat{y})^2} \tag{4.24}$$

where s_T is an empirical factor for surface temperature change with latitude, $(\hat{x}, \hat{y})$ are the coordinates of the ice sheet centre and T_{centre} is the ice surface temperature at the central part of the grids. Here s_T is set at 1.67×10^{-2} K/km. For the test runs, the temperature at the centre was varied and ranged from –25°C to –45°C with a 5°C interval. All these temperatures are within the range of annual mean air temperatures found at different locations over the Antarctic Ice Sheet (Figure 5.2).

From an ice-free flat surface, an idealised ice sheet starts to grow using the values listed in Table 4.1. Keeping the surface mass balance, geothermal heat flux and Arrhenius constant as reference values, we substitute the above range of ice surface temperatures individually into the two-dimensional system to build up a series of idealised ice sheets, which are pie-shaped. At this stage of the experiments, thermal advection and strain heating are still not considered due to the decoupling of the thermal regime from the dynamical regime. The controlling dynamical process is positive mass balance in the centre of the idealised ice sheet and negative mass balance at the margins (as will be shown in next section). The controlling thermal process is geothermal heating with a fixed heat flux entering the ice sheet system from the bed and being transferred towards a heat sink with different temperatures at the ice surface.

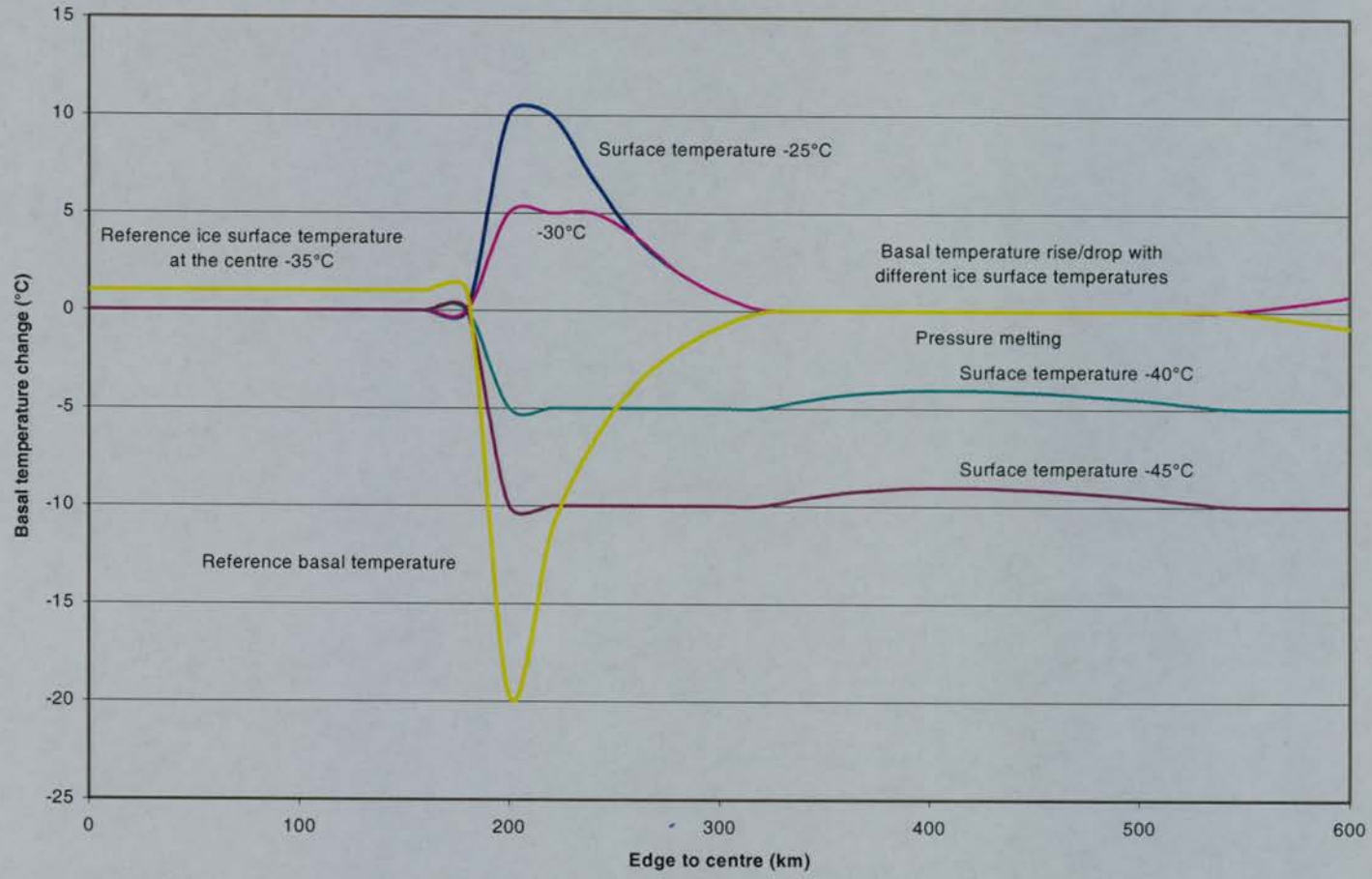

Figure 4.6 The sensitivity of basal temperature distribution to ice surface temperatures. This chart shows the reference basal temperatures assuming the surface temperature at the centre of the idealised two-dimensional ice sheet is –35°C. It gives the differences in basal temperature from the reference values when the surface temperature at the centre is varied from –25°C to –45°C with a 5°C interval. A pressure melting zone exists when the surface temperature is at or higher than the reference values.

In this section, we are interested in the influence of ice surface temperature to the basal temperature distribution. Figure 4.6 shows the reference basal temperatures of the idealised two-dimensional ice sheet when the surface temperature at the ice sheet centre is at –35°C, and the basal temperature deviations from the reference line when ice surface temperature changes. A pressure melting zone exists at the bottom of the idealised ice sheet if the surface temperature at the ice sheet centre is at or higher than the reference value of –35°C. This zone becomes wider with a warmer ice surface. When the ice surface temperature drops below the reference value, the idealised ice sheet becomes cold based. These experiments indicate that temperature changes at the ice sheet surface indeed influence the basal thermal regime, although it may not be of the same magnitude as shown in Figure 4.6 because of the idealisation in these experiments.

4.2.2 Surface mass balance

Mass balance on the ice sheet surface is the net ice equivalent of mass gain from precipitation and mass loss by ablation. In an ice sheet system, there are normally positive mass balances in the interior area and negative mass balances at the margin area. Ice flows from the interior of the ice sheet towards the margin. In the following experiments, the mass balance on the surface of the idealised two-dimensional ice sheet, a in m/yr, is set as a function of the radial distance from the centre of the ice sheet to reflect its spatial distribution [Huybrechts *et al.*, 1996]:

$$a = \min\left\{a_{centre}, s_a\left(R_{el} - \sqrt{(x-\hat{x})^2 + (y-\hat{y})^2}\right)\right\} \tag{4.23}$$

where a_{centre} is the surface mass balance at the central grid, s_a is an empirical gradient of the change of ice surface mass balance with latitude, and R_{el} is the radius of the equilibrium line where ice surface ablation equals the accumulation and $(\hat{x}, \hat{y})$ are the coordinates of the ice sheet centre. Modellers participating in the European Ice Sheet Modelling Initiative used a value of 0.002 m/yr·km for s_a and 450 km for R_{el} [Huybrechts *et al.*, 1996]. These values are also employed in this work for easy

comparison with the previous work. Figure 4.7 shows the reference values of ice surface mass balance and their pattern over the idealised two-dimensional ice sheet.

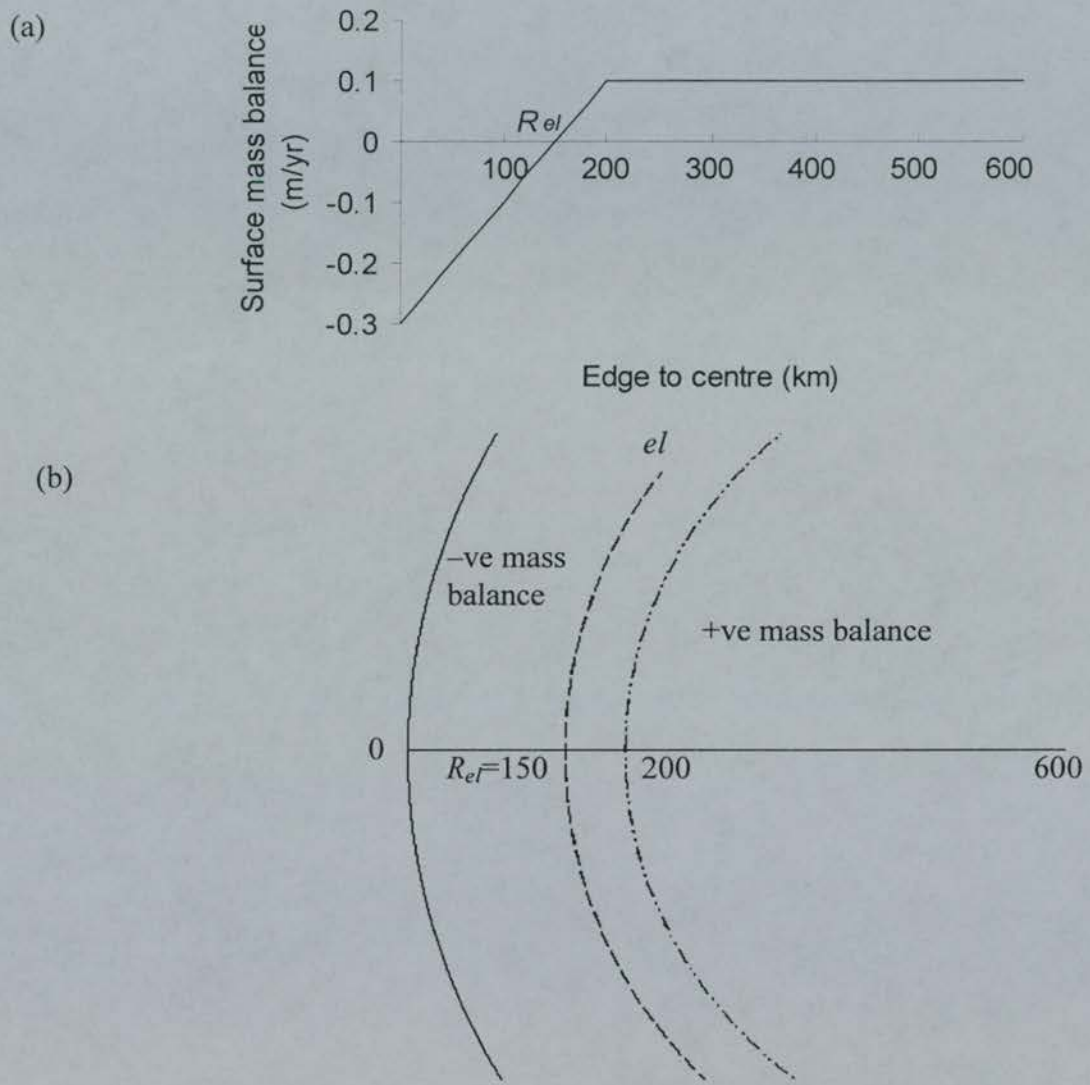

Figure 4.7 The settings of ice surface mass balance for the sensitivity tests in the idealised two-dimensional ice sheet system. (a) Side view of the vertical section passing through the centre of the ice sheet. (b) Vertical view from above the ice sheet. The ice surface mass balance is a positive constant within a radius of 400 km from the centre. It reduces beyond this radius and reaches the equilibrium line at the radius of 450 km. Beyond this radius, the ice surface mass balance becomes negative.

Separate values ranging from 5 cm/yr to 15 cm/yr with a 1-cm/yr interval are tested for the surface mass balance at the centre of the ice sheet. This range of values covers the present-day annual mean accumulation rates in the interior of the Antarctic plateau [van der Veen, 1987]. The sensitivities of basal temperature and ice thickness to the mass balance on ice surface are analysed using this range of a_{centre} values. All of the computing results are compared to the reference results derived by the reference value of 10 cm/yr for a_{centre}.

Figure 4.8 shows the thickness of the idealised two-dimensional ice sheet when the surface mass balance at the centre of the ice sheet is 10cm/yr and the deviations of ice thickness from this reference line in response to the changes in surface mass balance. Higher mass balance means more ice will accumulate on the ice sheet surface. As expected, the idealised ice sheet becomes thicker with an increase of ice surface mass balance.

Figure 4.9 shows the reference basal temperature distribution of the idealised two-dimensional ice sheet and deviations from this reference line when different values of mass balance are applied. From Figure 4.9 we can see that basal temperatures increase with mass balance. According to Fouries' law, thermal conduction is a function of the thickness of the medium. As indicated by Figure 4.8, higher surface mass balance results in a thicker ice sheet. Given a certain surface temperature, the temperature gradient in the ice sheet decreases. As a consequence, less geothermal heat is transferred away from the bottom of the ice sheet. A pressure-melting zone exists at the bottom of the idealised two-dimensional ice sheet when the surface mass balance at the centre is higher than 8 cm/yr. This pressure-melting zone becomes wider and the basal temperature becomes warmer with an increase in ice surface mass balance.

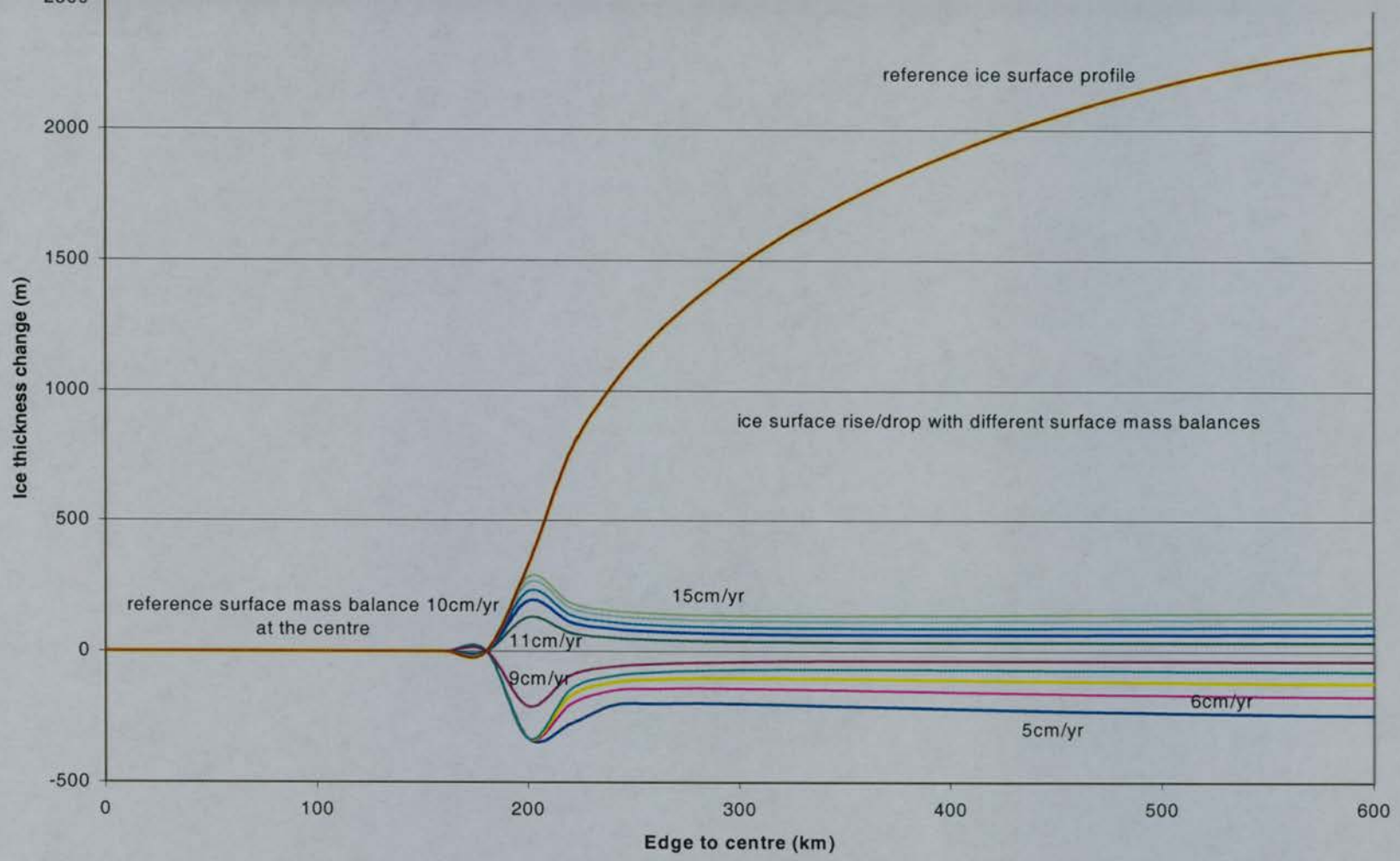

Figure 4.8 The sensitivity of ice thickness to changes in surface mass balance. This chart shows the ice thickness when a_{centre}=10cm/yr and the deviations of ice thicknesses from this reference line under other a_{centre} values. The idealised ice sheet becomes thicker with the increase of surface mass balance.

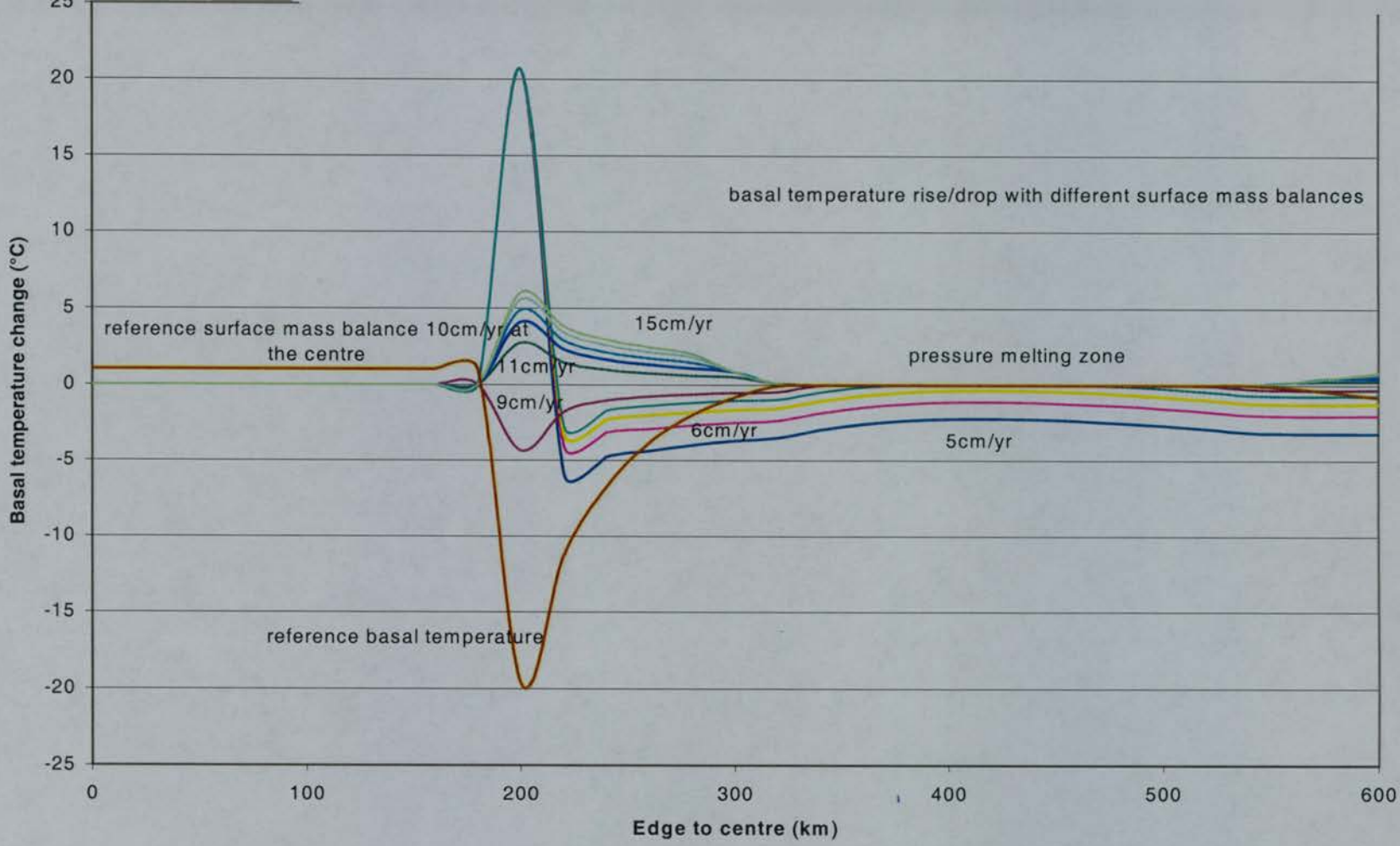

Figure 4.9 The sensitivity of basal temperatures to surface mass balance (a_{centre}). This chart shows the basal temperature distribution when surface mass balance at the centre of the ice sheet is 10 cm/yr and the deviations of basal temperatures from this reference line when the surface mass balance changes. A pressure melting zone exists when $a_{centre} \geq 8$ cm/yr. This pressure-melting zone becomes wider and basal temperature becomes warmer as a whole with an increase in surface mass balance.

4.2.3 Geothermal heat flux

Due to the physical difficulty of reaching the ice-bedrock interface beneath ice sheets, the value of geothermal heat flux is one of the major uncertainties when modelling the Antarctic Ice Sheet. Values applied by modellers are normally estimated from the correlation between heat flux and major geological features [Lee and Uyeda, 1965]. Many modellers apply 42.0 mW/m^2 as a reference geothermal heat flux value, especially when testing their ice sheet models [Huybrechts and Payne, 1996]. This value is derived from Precambrian shields in general [Lee and Uyeda, 1965] and could therefore be applicable to the East Antarctic Ice Sheet [Näslund *et al.*, 1998].

The sensitivity tests in this research also apply 42.0 mW/m^2 as the reference value. In order to test the modelled ice sheet's sensitivity of basal temperature to the changes in geothermal heat flux, geothermal heat flux was increased and decreased by 10 to 50 percent from the reference value. Figure 4.10 shows the basal temperature distribution of the idealised two-dimensional ice sheet when geothermal heat flux is at the reference value, and the deviations of basal temperatures from this reference line when other values of geothermal heat flux are used. As expected, geothermal heat strongly influences the basal temperature. This experiment shows that a change of the value of geothermal heat flux by 10 percent can correspond to about 2°C to 3°C of basal temperature change in the same direction. Figure 4.10 indicates that a pressure-melting zone at the bottom of the idealised two-dimensional ice sheet exists if geothermal heat flux is higher then the reference value. This zone becomes wider with increasing geothermal heat flux. The idealised ice sheet is cold based if geothermal heat flux is lower than the reference value. In all the tests in the idealised two-dimensional ice sheet system, it is assumed that geothermal heat flux is constant across the entire ice-bedrock interface.

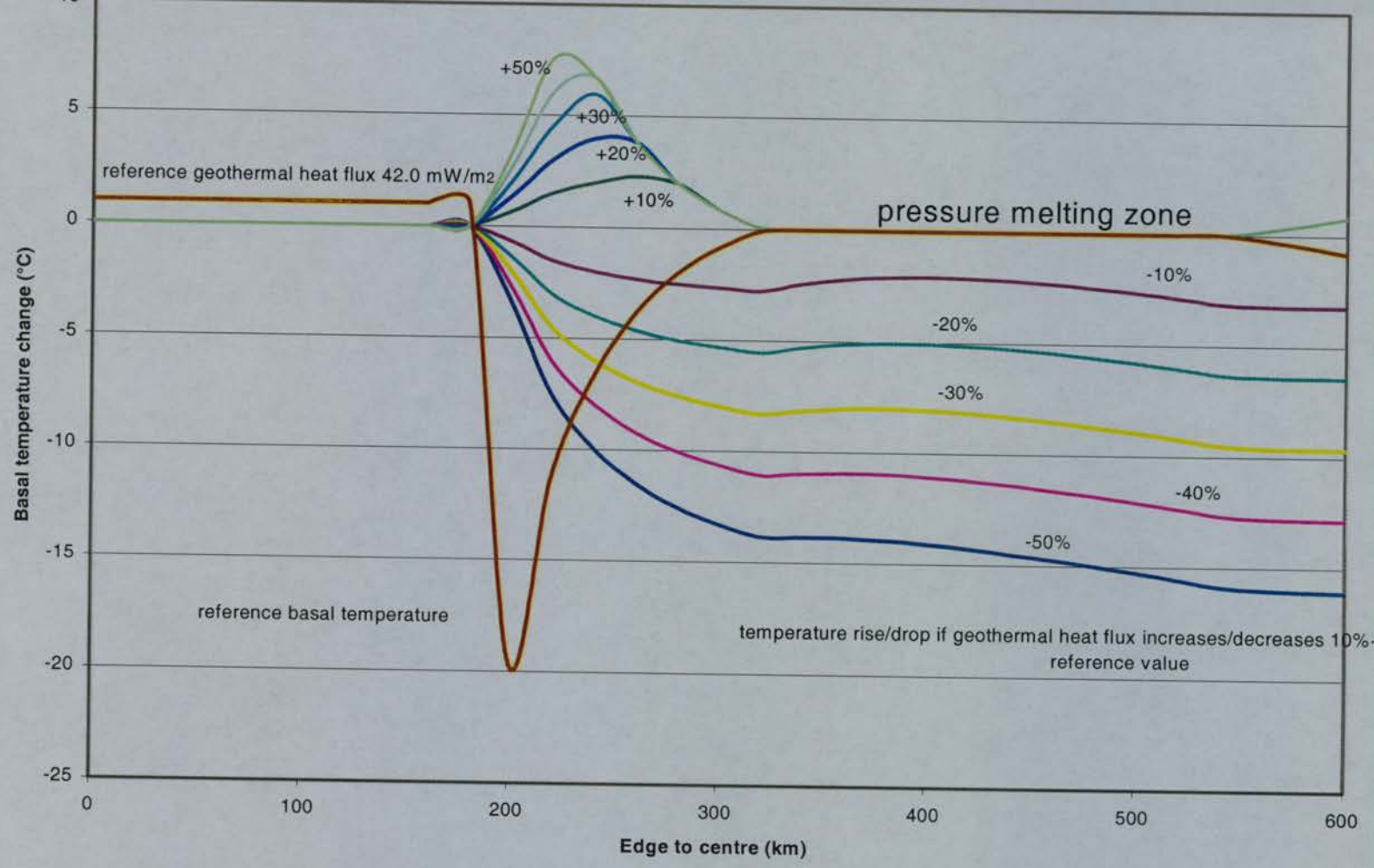

Figure 4.10 The sensitivity of basal temperature to changing geothermal heat flux. This chart shows the basal temperatures when the geothermal heat flux is 42.0 mW/m² and the basal temperature deviations from this reference line when the geothermal heat flux deviates from the reference value. A pressure-melting zone exists when the geothermal heat flux is at or higher than the reference value. The two-dimensional ice sheet is cold based if geothermal heat flux is reduced below the reference value.

4.2.4 Arrhenius factor for ice

Ice deforms and creeps under high pressure. The Arrhenius factor of ice, also called the flow law coefficient of ice, reflects the rigidity of ice. It describes the sensitivity of the stress-strain relationship (equation (2.1)). The stress-strain relationship is pressure dependent, and thus a function of depth in an ice sheet. The Arrhenius parameter is temperature dependent (equation (2.2)). Since we are interested in the sensitivity of the thermodynamic processes in an ice sheet to the Arrhenius factor of ice, we decouple the thermal regime from the dynamical regime and assume a constant Arrhenius parameter throughout the ice sheet.

Paterson [1994] recommends a range of values of the Arrhenius parameter for ice at temperatures from 0°C to –50°C, Table 2.1. The value at between –20°C and –25°C, 1.0×10^{-16} $kPa^{-3}s^{-1}$, is used as the reference value because this temperature range is roughly in the middle of the temperature spectrum of polar ice sheets and ice caps in their accumulation areas [Paterson, 1994]. The sensitivities of basal temperature and ice thickness in the idealised two-dimensional ice sheet system to the Arrhenius parameter for ice are tested by increasing and decreasing this reference value by 5 and 10 times. These values of the Arrhenius parameter for ice represent a temperature range from –5°C to –40°C.

Figure 4.11 shows the reference basal temperature distribution of the idealised two-dimensional ice sheet when the Arrhenius constant for ice is uniformly at the reference value of 1.0×10^{-16} $kPa^{-3}s^{-1}$, and the basal temperature deviations from the reference line when the Arrhenius constant for ice is varied uniformly. A pressure-melting zone exists in the two-dimensional ice sheet when the ice is softer than the reference status, *i.e.* the Arrhenius constant is larger than 1.0×10^{-16} $kPa^{-3}s^{-1}$. This pressure-melting zone becomes wider with softer ice. The idealised ice sheet is cold based if the ice is harder than the reference status. These results correspond with ice core and borehole studies in Antarctica. Ice temperatures at Law Dome [Budd *et al.*, 1976], Mirny [Bogoslovski, 1958], and Ice Stream B [Engelhardt, *et al.*, 1990], Antarctica, are at or above the range of –20°C and –25°C that gives the reference

value for the Arrhenius parameter for ice. Basal ice under these ice sheets is all at the pressure melting point [Peterson, 1994]. The temperatures of the upper half of the ice sheet at Vostok, East Antarctica, are below the reference temperature range and the ice temperature there is below –35°C to a depth of 2000 metres, far below the pressure melting point. The basal ice at Vostok is at the pressure melting point though, where the ice thickness at Vostok is 3700 metres and there is a subglacial lake [Peterson, 1994]. At Byrd Station, Antarctica, the upper ice (shallower than 1500 metres) is at –25°C to –30°C, slightly below the reference temperature range. The temperature of the deeper ice increases quickly and the ice becomes softer. Eventually, the ice reaches its pressure melting point at the base at about 2300 metres deep [Gow *et al.*, 1968]. This experiment indicates that the thermal regime of an ice sheet is sensitive to the Arrhenius factor of ice. Since the Arrhenius factor of ice is temperature dependent, we should couple it with the ice temperatures in the three-dimensional experiments. In this way, the stress-strain relationship at different depths in the ice sheet can be modelled using appropriate Arrhenius parameters.

Figure 4.12 shows how ice thickness varies with changes in the Arrhenius constant. Again, the results show that the thickness of an idealised two-dimensional ice sheet is sensitive to the Arrhenius parameter.

The experiments from §4.2.1 to §4.2.4 indicate that the four tested parameters, ice surface temperature, surface mass balance, geothermal heat flux and the Arrhenius factor of ice, play important roles in ice sheet evolution. The thermal and dynamical regimes of an ice sheet are sensitive to the changes of these parameters.

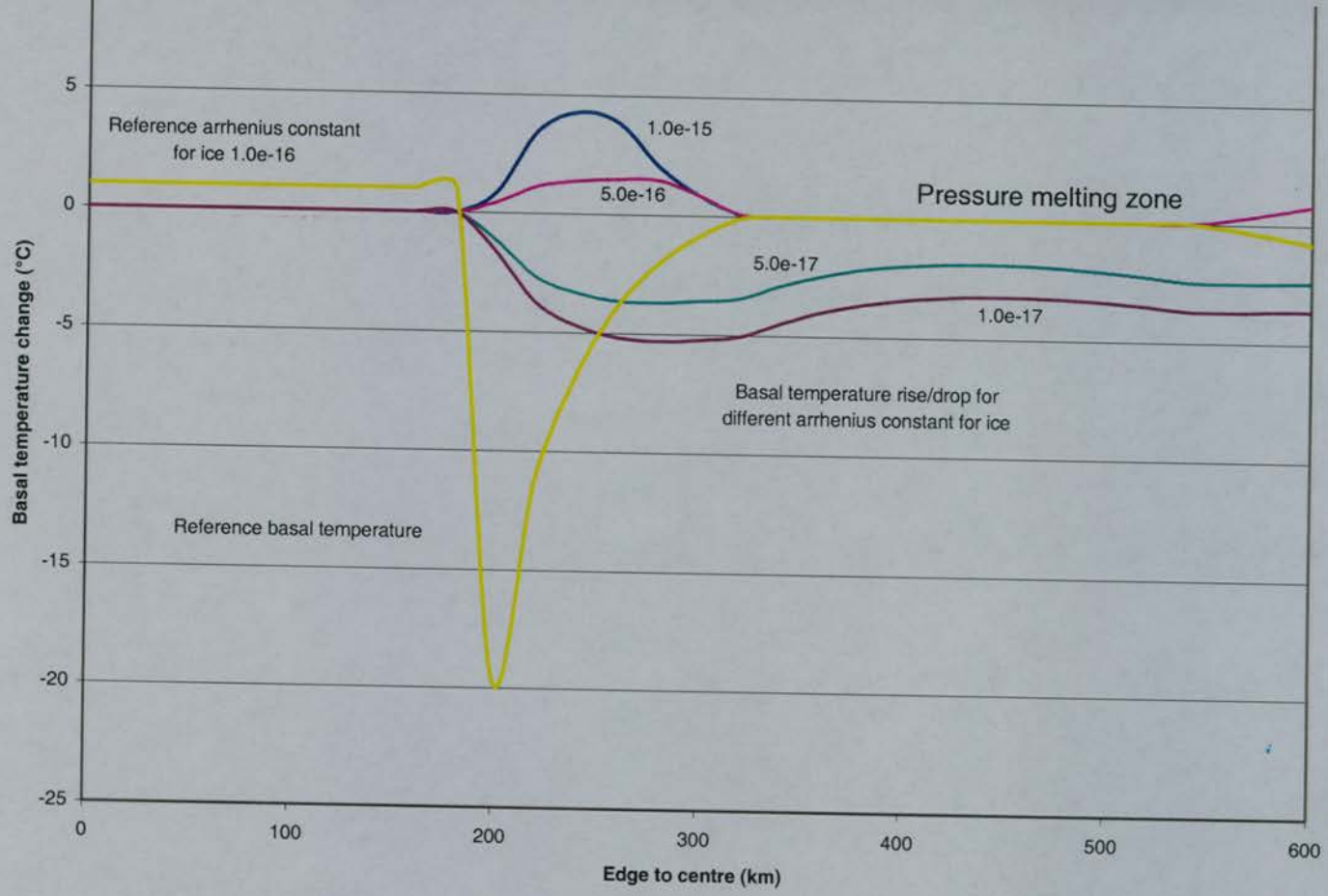

Figure 4.11 The sensitivity of basal temperature to changes in the Arrhenius constant of ice. This chart shows the basal temperature distribution when the Arrhenius constant for ice is 1.0×10^{-16} $kPa^{-3}s^{-1}$ and the basal temperature deviations from this reference line when the Arrhenius constant for ice deviates from the reference value. A pressure melting zone exists when the Arrhenius constant for ice is at or softer than the reference value.

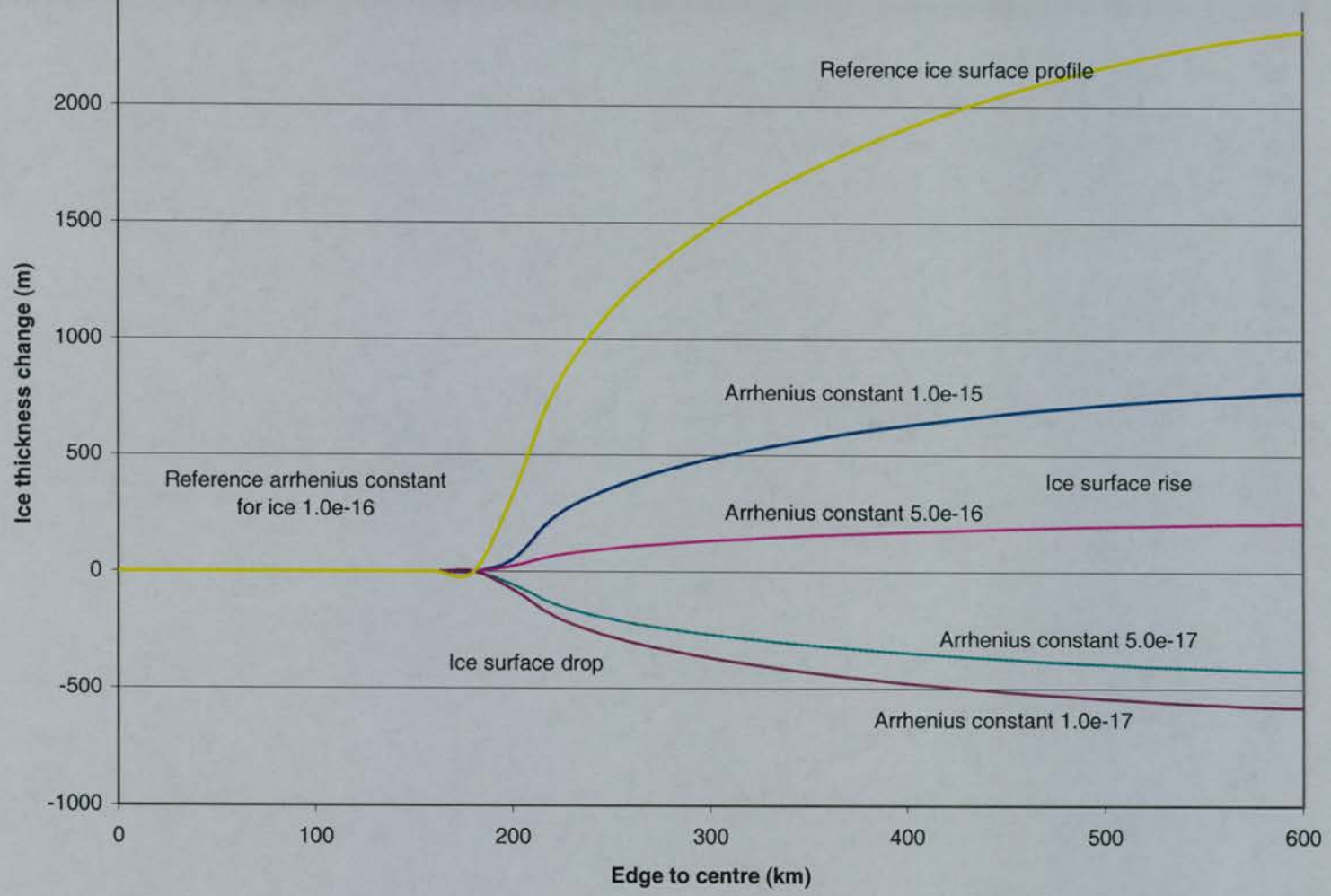

Figure 4.12 Ice thickness under the reference Arrhenius constant for ice (1.0×10^{-16} $kPa^{-3}s^{-1}$) and the deviations from the reference thickness when the Arrhenius constants deviate from the reference value.

4.2.5 Advection and strain heating

In the previous sections, in order to highlight the effects incurred solely by four selected parameters, thermal advection and strain heating within the ice were not considered. Horizontal and vertical advection plays an important role in heat transfer. Also, strain heating within the ice body is a significant heat source (See equation (3.3)). They affect the ice sheet in different ways. Strain heating, for instance, is strongest near the bottom of an ice sheet where stress is largest, whereas the advection effect is strong where ice flows faster. Knowledge of their functions, their relative importance in heat transfer and their main effects on the ice sheet system, is helpful in understanding the mechanism of heat transfer in an ice sheet. The following experiments are designed to test the individual role of horizontal advection, vertical advection and strain heating in the idealised two-dimensional ice sheet system.

We first set up a reference model run by including vertical advection, horizontal advection and strain heating. In order to test the effectiveness of the thermal advection and heating mechanisms, we then artificially switch off or double these mechanisms one by one, whilst allowing the mechanical development to continue. Since thermo-mechanical coupling is not considered in these experiments, the thermal processes are linearly independent within the idealised two-dimensional ice sheet system. Therefore, switching off or doubling one thermal mechanism will not affect the functionality of other thermal mechanisms.

Figure 4.13 shows the standard run with horizontal advection, vertical advection and strain heating included. In order to aid visualisation, the vertical coordinate is exaggerated 50 times when compared to the horizontal axis. Figure 4.13(a) shows the temperature distribution in a vertical section through the centre of the idealised two-dimensional ice sheet. Ice is the coldest in the centre and the cold ice extends to the bottom of the ice sheet. At the bottom of the ice sheet, Figure 4.13(b), basal ice becomes warmer towards the edge and then the temperature goes down at the edge. These are what we would expect. Cold ice accumulates on the ice surface and travels

down to the bottom by advection. At the same time, geothermal heating and strain heating warm up the bottom ice. At the edge of the ice sheet, the ice thins sufficiently for surface conditions to cool the bottom ice once more.

If horizontal advection is switched off (Figure 4.14), the cold accumulated on the ice surface cannot be transferred horizontally by thermal advection, whereas vertical advection and strain heating is still as strong as in the reference run. Figure 4.14(a) clearly shows that the cold area is narrower than that in Figure 4.13(a) and the idealised ice sheet as a whole is warmer. Vertical advection nevertheless transfers the cold from the surface to the bottom of the ice sheet but cannot propagate it laterally along the base. As a consequence, the cold signal is constrained within an upside-down conical column at the centre of the idealised two-dimensional ice sheet. Since strain heating is strongest near the bottom and geothermal heat enters the ice sheet system from the bottom as well, more heat will accumulate at the bottom and raise the basal temperature significantly. Figure 4.14(b) shows the distribution of the warmer basal temperatures and their higher values compared to the reference run (Figure 4.13(b)).

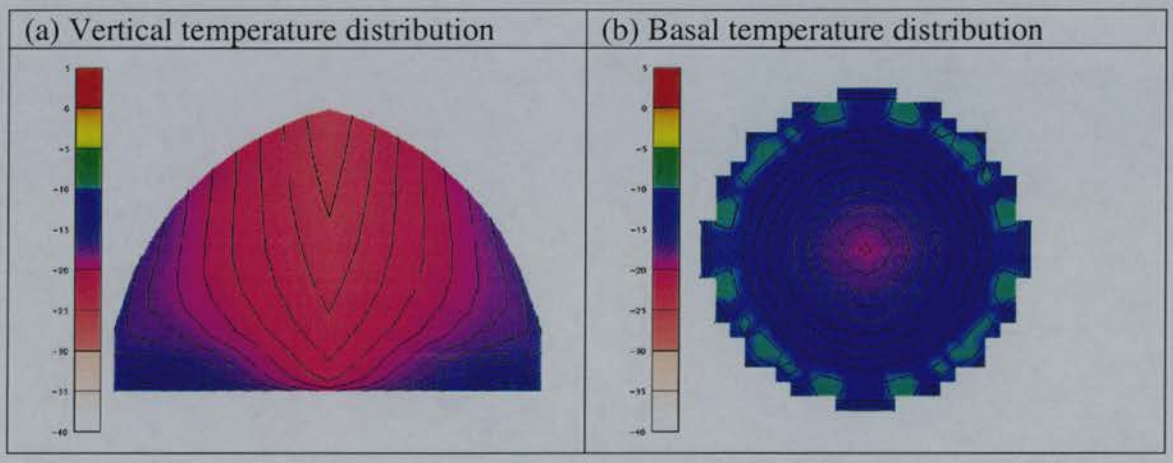

Figure 4.13 Effects of advection and strain heating on ice temperature distribution (°C, 2°C contours) in the idealised two-dimensional ice sheet system. Reference run with vertical advection, horizontal advection and strain heating on.

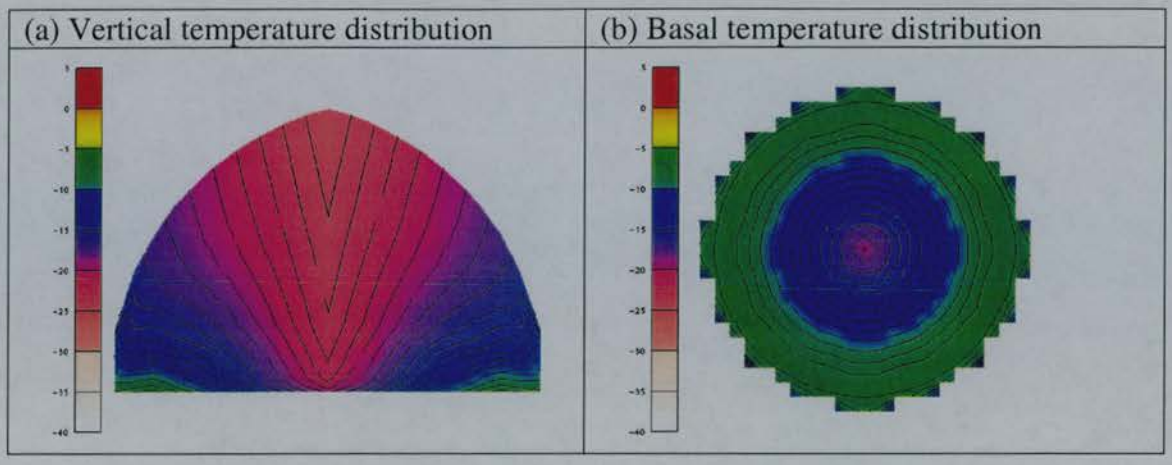

Figure 4.14 Temperature distribution (°C, 2°C contours) in the idealised two-dimensional ice sheet system with horizontal advection switched off. Compared to the reference run, Figure 4.13, the ice sheet, as a whole, is warmer. Cold area is narrower, (a), and basal temperatures rise significantly, (b).

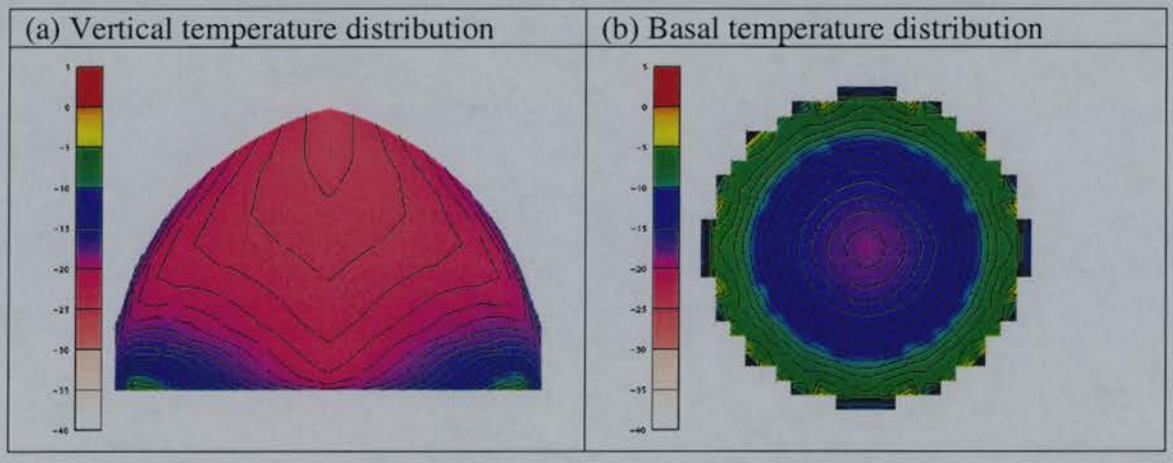

Figure 4.15 Temperature distribution (°C, 2°C contours) in the idealised two-dimensional ice sheet system with vertical advection switched off. Temperatures in the ice body as a whole are lower than from the reference run, Figure 4.13(a). Basal temperatures are higher than those in Figure 4.13(b), but the scope of temperature rise is not as large as the experiment without horizontal advection (Figure 4.14(b)).

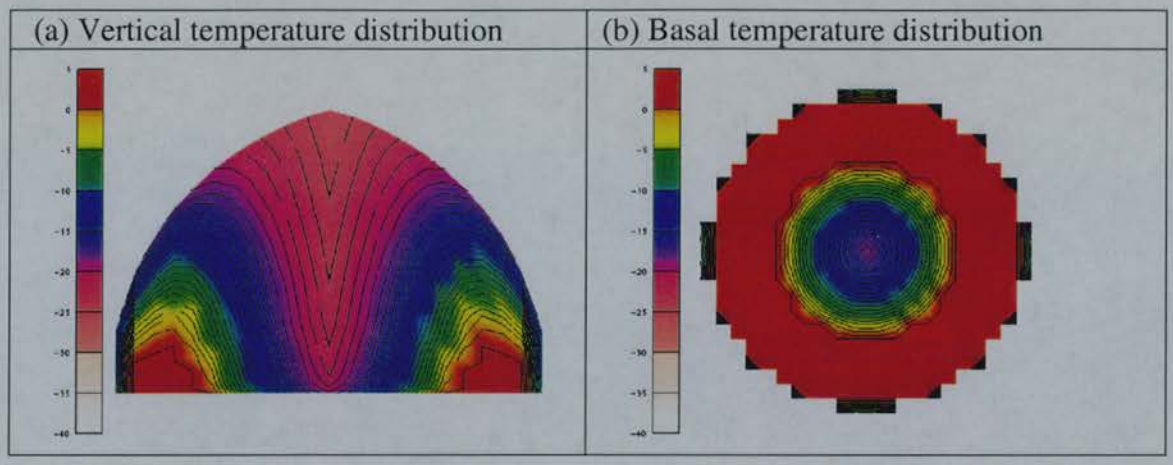

Figure 4.16 Temperature distribution (°C, 2°C contours) in the idealised two-dimensional ice sheet system with both horizontal advection and vertical advection switched off. Ice in the red areas is at the pressure melting point. There is no means except thermal conduction for heat transfer in the system. Heat is accumulated at the bottom of the ice sheet and melts the bottom ice; whereas coldness is restricted to the centre of the ice sheet.

The vertical advection effect is much stronger in the body of the ice sheet than at the bottom. Figure 4.15(a) shows that temperatures in the ice body are much colder if vertical advection is switched off while horizontal advection remains switched on. The basal layer is the dominant heat source of the ice sheet. Without vertical advection, heat from the bottom of the ice sheet is not transferred upwards, whereas horizontal advection spreads the surface cold in the ice body and makes the ice sheet as a whole colder. The heat accumulated at the bottom of the ice sheet raises the basal temperatures, as shown by a comparison of Figure 4.15(b) with Figure 4.13(b). With horizontal advection, the basal warming effect is stronger because horizontal advection transfers some heat away.

Temperatures in the idealised two-dimensional ice sheet system rise dramatically if both horizontal advection and vertical advection are switched off, as shown in Figure 4.16. The ice in the red areas is at the pressure melting point. Without thermal advection, heat accumulates at the bottom of the ice sheet; it either raises the basal temperature or melts the basal ice, whereas cold ice is restricted to the centre of the ice sheet. Overall, the idealised two-dimensional ice sheet develops stronger

temperature gradients along its vertical dimension than along its horizontal dimensions.

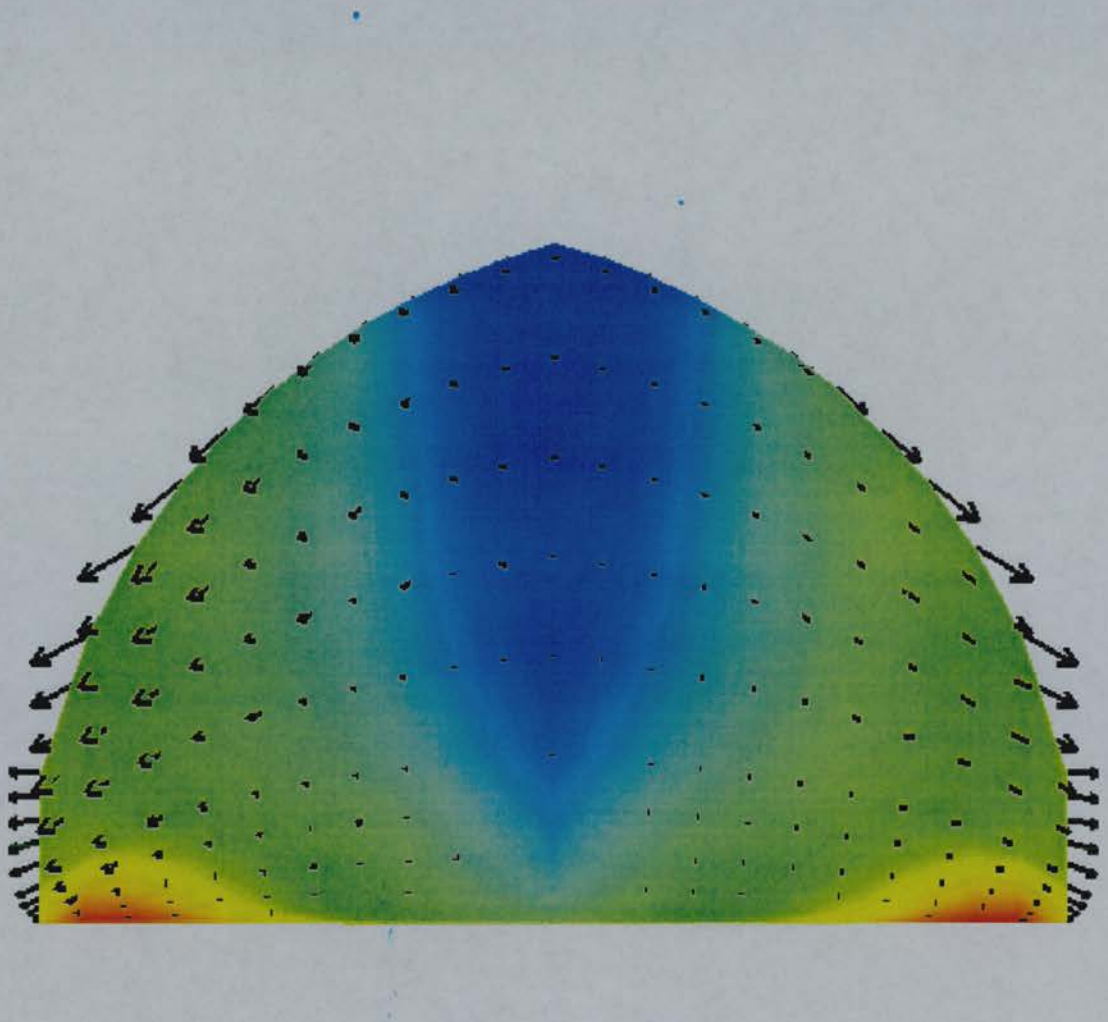

Figure 4.17 Ice flow velocity field and temperature distribution in the idealised two-dimensional ice sheet system (reference run). The arrows point to ice flow direction; the relative length of the arrows reflects the relative ice flow velocity. The background colour shows the ice temperature distribution, using the same colour codes as in Figures 4.13 – 4.16.

Ice flow causes advection; the faster the ice flows, the stronger the advection effect. Figure 4.17 shows the ice flow velocity distribution in the reference run of the idealised two-dimensional ice sheet. It is clearly seen that the ice flows from the centre to the edge of the ice sheet. At the basal layer of the ice sheet, the horizontal components of the flow velocity, u and v in equation (3.1), of the ice close to the edge of the ice sheet are higher than those close to the centre. Strain heating is therefore stronger near the edge. This explains why basal temperatures near the edge are higher than the temperatures near the centre of the ice sheet (Figures 4.13(b), 4.14(b) and 4.15(b)). Cold ice from the upper layers of the ice sheet moves downwards to replace the ice in the lower layers flowing towards the edge. The vertical component of the ice flow velocity, w in equation (3.1), is thus higher in the upper layers than that in the basal layer. Vertical advection is therefore more significant in the upper layers of the ice sheet (Figure 4.15(a)).

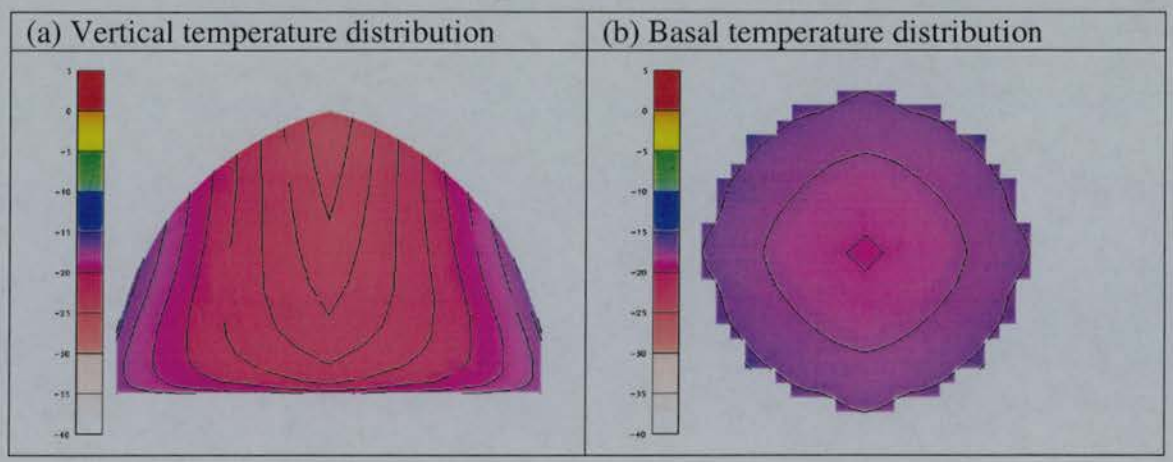

Figure 4.18 Temperature distribution (°C, 2°C contours) in the idealised two-dimensional ice sheet system with strain heating switched off. The ice sheet becomes significantly colder as a whole due to the absence of its main heat source.

Strain heating is the major means of transforming mechanical energy into heat. If strain heating is switched off in the modelled ice sheet, the whole ice sheet system will cool down, especially near the bottom where strain heating is strongest due to ice deformation. In the experiment shown by Figure 4.18, strain heating is switched

off while other factors are kept unchanged. Without strain heating, temperatures in the whole ice sheet drop dramatically. This result indicates that strain heating plays a significant role in the thermal regime of the ice sheet system.

Strain between ice crystals increases the temperature gradient between the upper cold layers and the lower warm layers of the ice sheet. Thermal advection has the contrary effect; it transfers heat in the direction that tends to reduce the temperature gradient. In the experiment shown in Figure 4.19, strain heating and all forms of thermal advection are switched off. Thermal conduction is the only mechanism of heat transfer in this system, which is similar to the idealised one-dimensional ice sheet system analysed in §4.1 except that its horizontal extension is limited and the ice thickness is not uniform. Thermal conduction in such a system is two-dimensional. The resulting temperature distribution in the idealised ice sheet is slightly colder than that of the reference run (Figure 4.13), while the structure is similar. This results from the countervailing effects of strain heating and thermal advection. It indicates that thermal advection is comparable to strain heating in the ice sheet energy system, but slightly stronger.

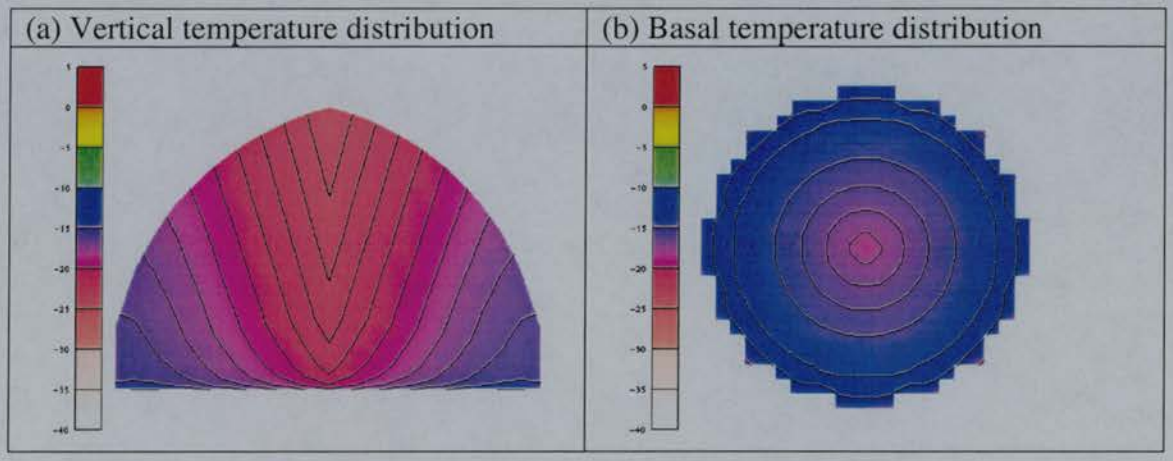

Figure 4.19 Temperature distribution (°C, 2°C contours) in the idealised two-dimensional ice sheet system with strain heating and all forms of thermal advection switched off. Because of the countervailing effects of strain heating and thermal advection, the result is similar to that in the reference run, Figure 4.13.

The significance of strain heating is one of the main uncertainties in ice sheet modelling. Knowledge about the sensitivity of the thermal regime of an ice sheet to strain heating can give us an idea about how to tune it when calibrating the ice sheet model with real-world topography. The experiment shown in Figure 4.20 is designed to test the response of the temperature distribution to a doubled strain heating rate, whilst horizontal advection and vertical advection are kept unchanged. Comparing the result with the reference run shown in Figure 4.13, it is seen that the temperatures in the upper layers of the idealised two-dimensional ice sheet are not influenced much by strain heating even if the rate is doubled (Figure 4.20(a)). At the bottom of the ice sheet, however, the effect of the doubled strain heating is remarkable, especially in regions that are close to the ice edge (Figure 4.20(b)). This result strengthens the theoretical analysis above that strain heating is most significant in the basal layer, especially near the edge of the ice sheet.

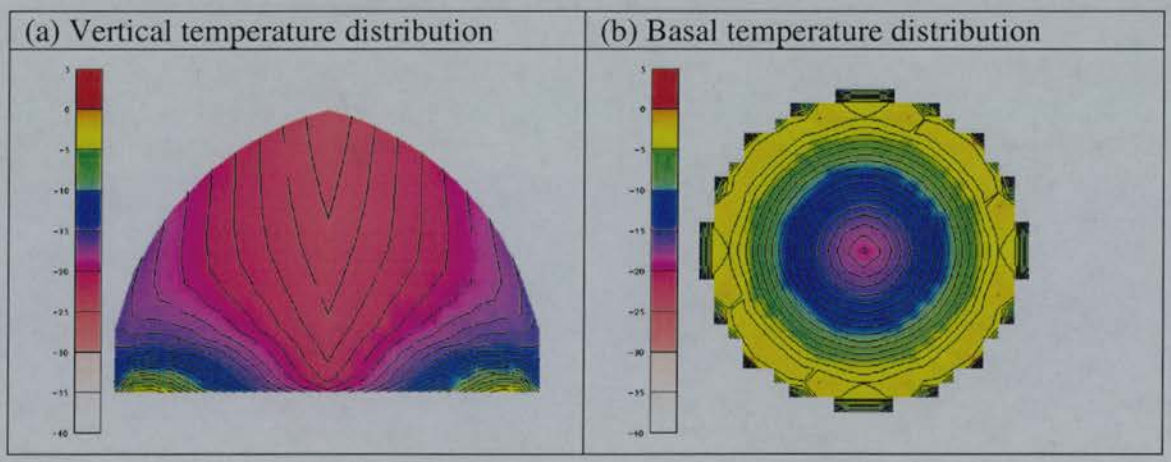

Figure 4.20 Temperature distribution (°C, 2°C contours) in the idealised two-dimensional ice sheet system with doubled strain heating rates whilst thermal advection is kept unchanged. Basal temperatures, especially those near the edge of the ice sheet rise remarkably (Compare the reference run Figure 4.13(b)). Temperature increases in the upper layers are less significant (Compare reference run Figure 4.13(a)).

4.3 Model Calibration

Both of the idealised one-dimensional and two-dimensional ice sheet systems are based on a flat and level topography with infinite extent. This implies that the bedrock has no isostatic effect in response to the ice load and ice does not slide on the bedrock. However, basal topography exists under real ice sheets. Isostatic effects and basal sliding influence heat and mass transfer in a real ice sheet system, which is a three-dimensional system. As analysed in §2.1, the Arrhenius factor for ice, which depicts the sensitivity of the stress-strain relationship, is temperature dependent. Due to the complexity of temperature distribution in a real ice sheet, it is no longer precise enough to decouple the dynamical regime of the ice sheet system from its thermal regime. This thermo-mechanical coupling introduces additional feedback complexity into the ice sheet model. In this section, we introduce the three-dimensional Antarctic Ice Sheet model. This system employs present-day Antarctic basal topography. Isostasy, basal sliding and heating due to sliding will also be considered in the final calibration of the Antarctic application of the ice sheet model.

4.3.1 Experimental framework

Unlike the infinite extension of the bed in the two simplified ice sheet systems, the Antarctic continent has a limited extent. Under the solid crust lies the semi-liquid mantle. The equilibrium that exists between parts of the Earth's crust, which behaves as if it consists of blocks floating on the underlying mantle, is referred to as isostasy. In this research, the elevation of the crust responding to the ice load is simply modelled by Archimedes' principle: rising if material is removed and sinking if material is deposited, equation (3.27). If the Antarctic continent were free of ice, Antarctic topography would rebound from the currently depressed elevation (Figure 4.21(b)). Substituting the present-day ice thickness into equation (3.27) gives the corresponding bedrock depression due to the ice load if we assume present-day Antarctic isostasy is in an equilibrium state. This depression represents the maximum displacement the bedrock could rebound should the Antarctic Ice Sheet completely

disappear. Figure 4.22 shows a rebounded ice-free Antarctic topography if the Antarctic isostasy is assumed to reach the new equilibrium.

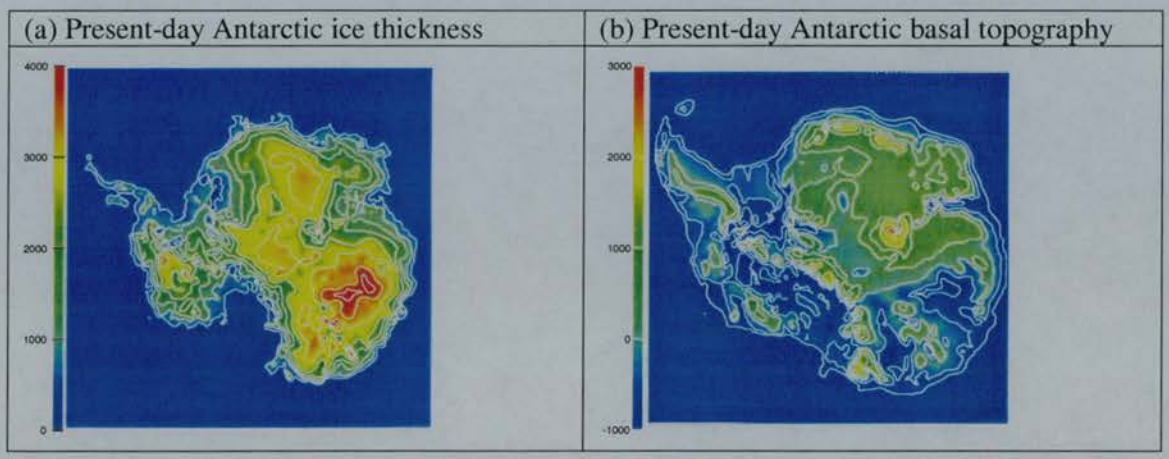

Figure 4.21 Present-day Antarctic Ice Sheet (m, with 500-m contours) [Drewry, 1983].

A convenient comparison when calibrating the Antarctic version of the ice sheet model is the present-day status of the Antarctic Ice Sheet (Figure 4.21). If the model can reconstruct the evolution of the Antarctic Ice Sheet to its present status, we shall then gain confidence in our ability to predict the response of the Antarctic Ice Sheet to climatic changes. When calibrating the ice sheet model under the Antarctic conditions, we run it for a sufficiently long time from an ice-free Antarctic topography in order to reconstruct the present-day Antarctic Ice Sheet. There is an assumption that the present-day Antarctic Ice Sheet is at an equilibrium state. The ice-free Antarctic topography, shown in Figure 4.22, is obtained by completely removing the present-day Antarctic Ice Sheet whilst assuming sea level keeps unchanged. A sufficiently long time is given to allow the depressed elevations to respond isostatically. The calibrating experiments are normally run for 200,000 model years, long enough for the modelled ice sheet to reach a quasi-equilibrium state.

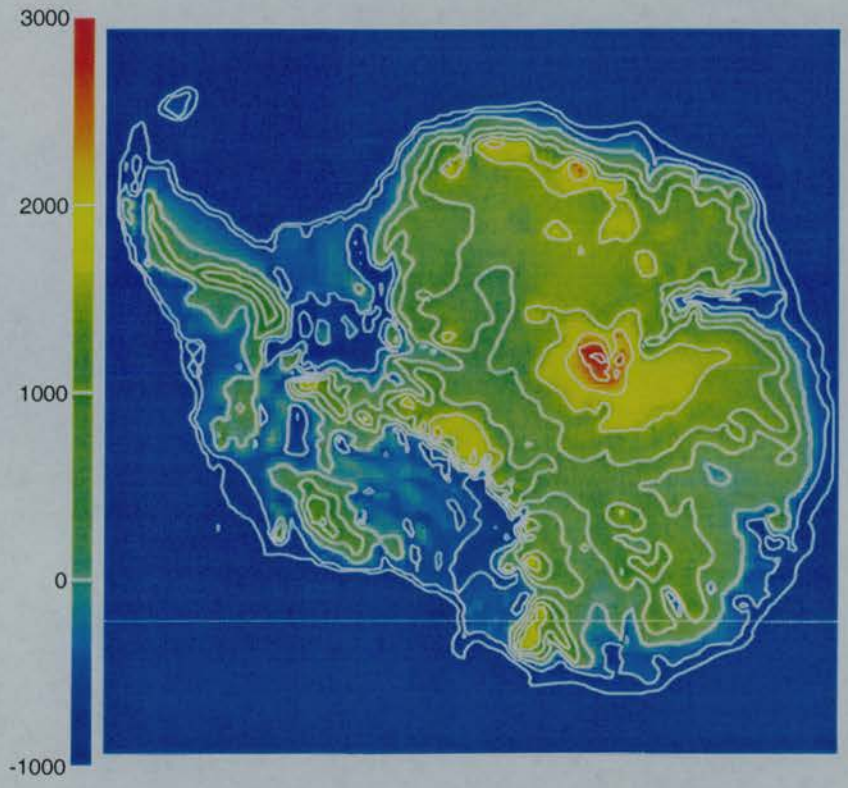

Figure 4.22 Rebounded ice-free Antarctic topography (m, 500-m contours) if the present-day Antarctic Ice Sheet were completely removed and a sufficiently long time is allowed for the ice-free bedrock to rebound to a quasi-equilibrium state. It is assumed that the present-day sea level is unchanged.

4.3.2 Calibrating experiments

The initial set of parameter values being calibrated is selected on the basis of other modelling work [Huybrechts *et al.*, 1996] and theoretical analyses [Paterson, 1994; Näslund, 1998]. These values are adjusted against conditions associated with the present-day Antarctic Ice Sheet. When the modelled ice sheet is reasonably compatible with the present-day status, that set of parameters are then used as the reference modelling parameters. The reference values are listed in Table 4.2. The reference value of the ice sliding parameter is an empirical dimensionless figure. Its purpose is to scale the computed ice flow velocities in order to represent the real flow velocities of the Antarctic Ice Sheet. It does not have a clear physical meaning. This is one point in the ice sheet model that could be improved in the future.

Table 4.2 Reference settings for model calibration

Factor	Value or status
Ice sliding parameter	2.0×10^{-13}
Thermal and dynamical regime coupling	Coupled
Computing time step	1 year
Ice calving pattern	At the edge of ice shelves only
Ice calving rate	50% of ice thickness per year
Ice shelf strain rate	5% per year
Ice shelf melting rate	1 m/yr
Maximum ice thickness below sea level	200 m
Mean geothermal heat flux	42.0 mW/m^2
Starting status	Rebounded ice-free Antarctic topography
Sea level	Current sea level
Ice surface temperatures	Current ice surface temperatures

Figure 4.23 shows the reconstruction based on the reference settings in Table 4.2 after the ice sheet has evolved for 100,000 model years. The ice sheet expands rapidly during the first 50,000 model years of the integration. After 100,000 model years, it is approaching stability. 200,000 model years proves long enough for the modelled Antarctic Ice Sheet to reach a quasi-equilibrium state.

Comparing the ice thickness of the modelled Antarctic Ice Sheet (Figure 4.23(a)) with the present-day situation (Figure 4.21(a)), we find that the ice distribution of the modelled Antarctic Ice Sheet matches the present-day ice distribution well except that the modelled ice sheet is thicker. This discrepancy may come either from the numerical model or from the real ice sheet or both, although we assume the real values are correct when doing modelling. From the point of view of numerical modelling, the inappropriateness of system parameters may be responsible for the unrealistic result. The modelled surface ice accumulation rate may be overestimated; the iceberg calving rate from the edge of the ice shelves or the basal melting rate under the ice shelves may be too small; or ice may actually slide faster than the velocities defined by the sliding parameter. Perhaps the discrepancy partly relates to our view of the present ice sheet. The Antarctic Ice Sheet may not be in equilibrium state and could be still expanding in response to Holocene warming [Sugden, 1996].

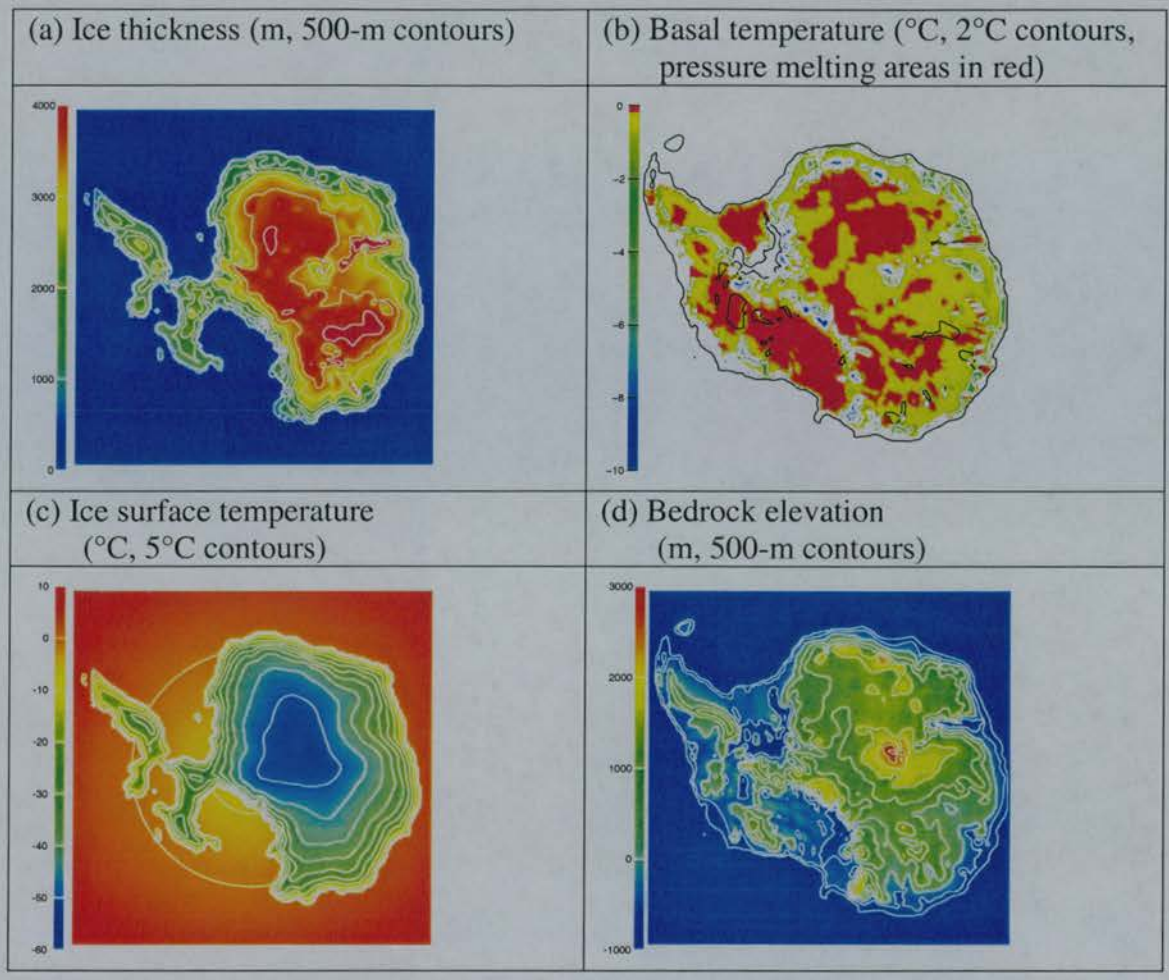

Figure 4.23 Modelled characteristics of the Antarctic Ice Sheet after 100,000 model years. The model started from a rebounded ice-free Antarctic topography. The modelled Antarctic Ice Sheet is approaching stability after 100,000 model years. Compared to the present-day Antarctic Ice Sheet (Figure 4.21), the settings for this experiment need calibrating.

To test the first hypothesis, we reduce the net mass balance for the modelled ice sheet system. This can be achieved by reducing the ice surface accumulation rate that represents the mass input to the system and increasing the iceberg calving rate and ice shelf melting rate that represent the mass output from the system. Figure 4.24 shows the results of the experiment when the mass accumulation rate on the ice surface was reduced to 66 percent of the starting run and the iceberg calving rate was reduced to 25 percent per year of the ice edge thickness. With these modifications, the modelled Antarctic Ice Sheet is fairly satisfactory when compared to the present-

day situation. Compared to Figure 4.23(a), the modelled ice thickness shown in Figure 4.24(a) is closer to the present-day situation shown in Figure 4.21(a).

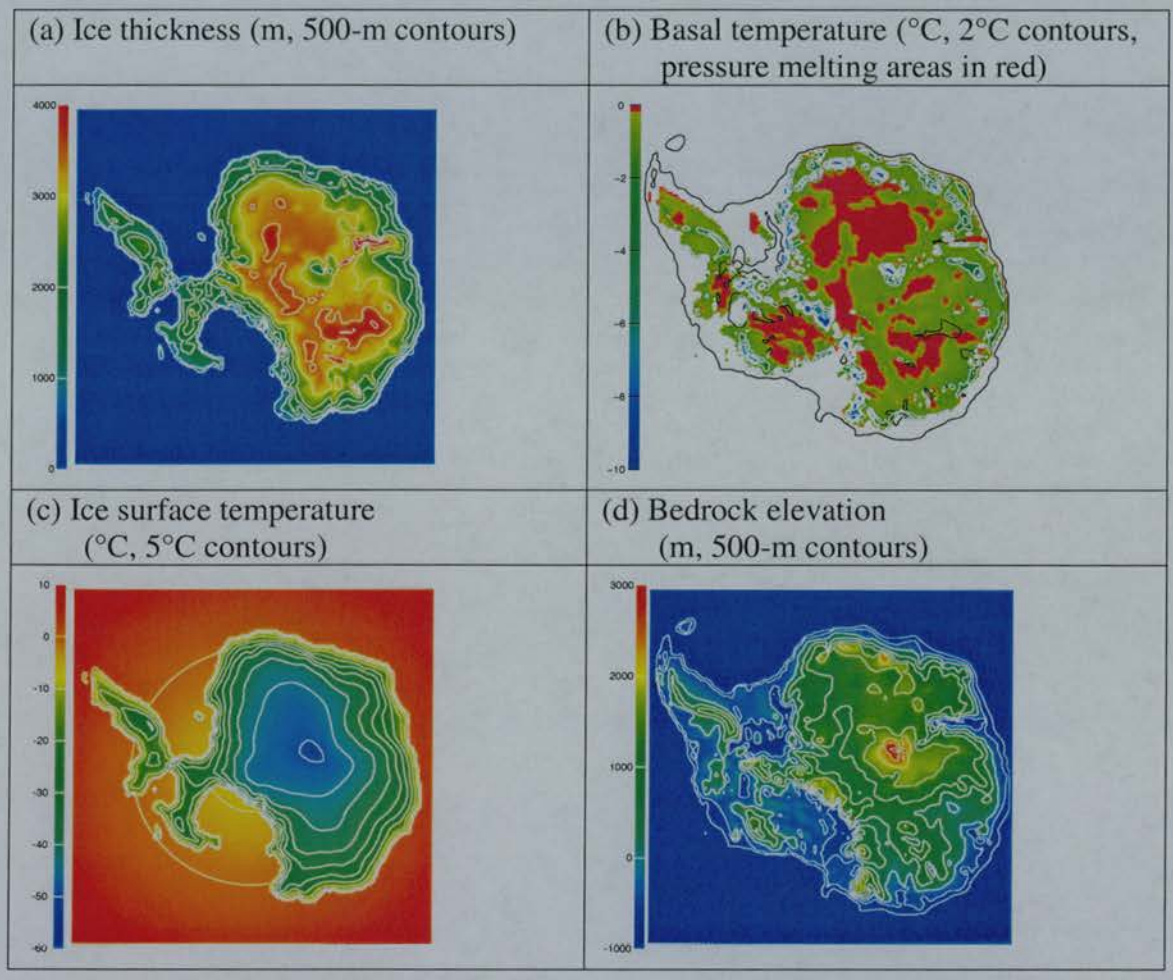

Figure 4.24 Model calibration by reducing the mass accumulation rate on the ice surface to 66 percent of the starting run (Figure 4.23), and the iceberg calving rate to 25 percent per year of ice edge thickness. Integrating from the rebounded ice-free Antarctic topography for 100,000 model years. Comparing with Figure 4.23(a), the ice thickness (a) is closer to the present-day situation (Figure 4.21(a)).

The distribution of the modelled East Antarctic Ice Sheet matches the present-day ice distribution very well whilst the modelled ice distribution in West Antarctica is thicker. This discrepancy may come from the treatment of marine factors that influence different parts of Antarctica to different extents. The ice sheet model

developed in this research treats the marine influence equally everywhere. Equal treatment cannot reflect the diversities of different regions of the Antarctic Ice Sheet and may lead to inappropriate model parameters in certain regions. In future, the coupling of the ice sheet model to a climatic model may help cope with this problem [Purves and Hulton, 2000a, 2000b].

Modelling work cannot demonstrate whether the current Antarctic Ice Sheet is in equilibrium or not. What it can do is to suggest a possibility. If the modelled ice sheet conforms to the real ice sheet but the modelled one is slightly thicker, it may suggest that the real ice sheet could still be at an evolving stage and has yet to become stabilised. So the present-day Antarctic Ice Sheet could still be growing under the current climatic situation if the ice sheet parameters are represented effectively. As long as the discrepancy between the modelling results and the real situation of the Antarctic Ice Sheet can be explained, we can conclude that the modelling results shown by Figures 4.23 and 4.24 indicate a reasonable working numerical model for the Antarctic Ice Sheet.

4.3.3 Quasi-equilibrium state

The following experiment is designed to justify the assumption that the modelled Antarctic Ice Sheet reaches a quasi-equilibrium state after 100,000 years of evolution under stepped climatic forcing. Starting from the modelled ice sheet shown in Figure 4.24 and applying the same parameter settings, the ice sheet model runs for further 100,000 model years (Figure 4.25). The similarity of these two sets of figures shows that the modelled Antarctic Ice Sheet approaches a stable state after 100,000 years. Figure 4.26 gives an alternative illustration of ice sheet evolution showing its rate of growth, ice volume (Figure 4.26(a)) and average ice thickness (Figure 4.26(b)). Starting with a rebounded ice-free Antarctic topography, the modelled ice sheet builds up rapidly during the first 50,000 model years. The rate of growth of the modelled ice sheet becomes slower during the second 50,000 model years. After 100,000 model years, the ice volume and average ice thickness approach an equilibrium state.

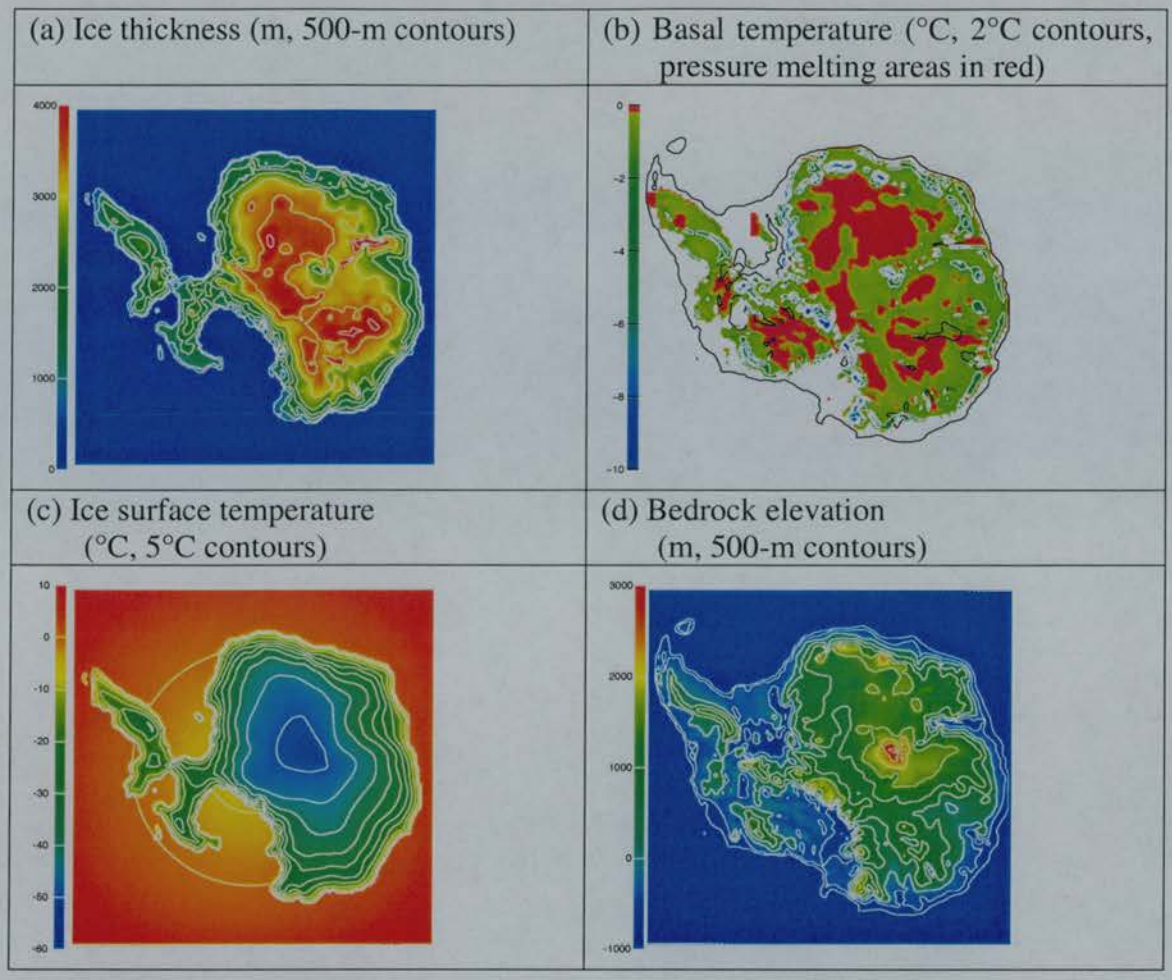

Figure 4.25 Integrating for 200,000 model years with the same set of parameter values as those in Figure 4.24. The modelled Antarctic Ice Sheet now reaches a stable equilibrium. The modelled ice sheet at this stage does not have significant differences from that in Figure 4.24. This indicates that the modelled ice sheet has reached a quasi-equilibrium state after 100,000 model years of integrating.

This stable result indicates two points: from the numerical point of view, the numerical algorithms employed in the ice sheet model developed in this research are convergent; from the modelling point of view, it takes 100,000 model years for the modelled Antarctic Ice Sheet to evolve from one equilibrium state to a new quasi-equilibrium state. This time scale also corresponds with the time scale needed for the conduction of temperature signals (Figure 4.2).

(a)

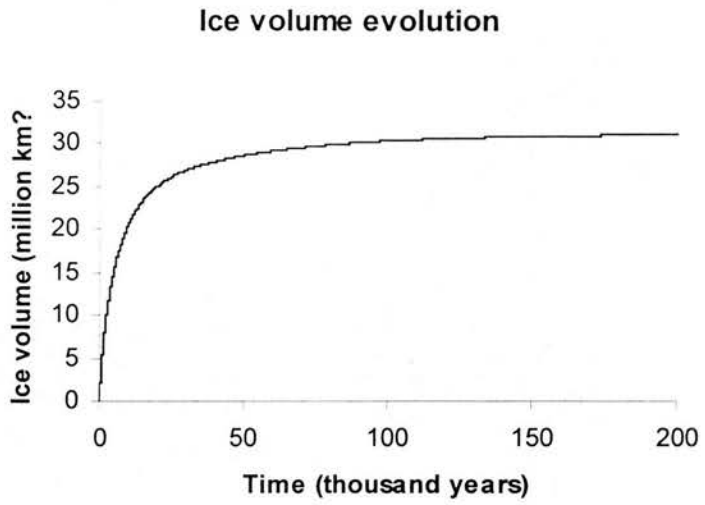

(b)

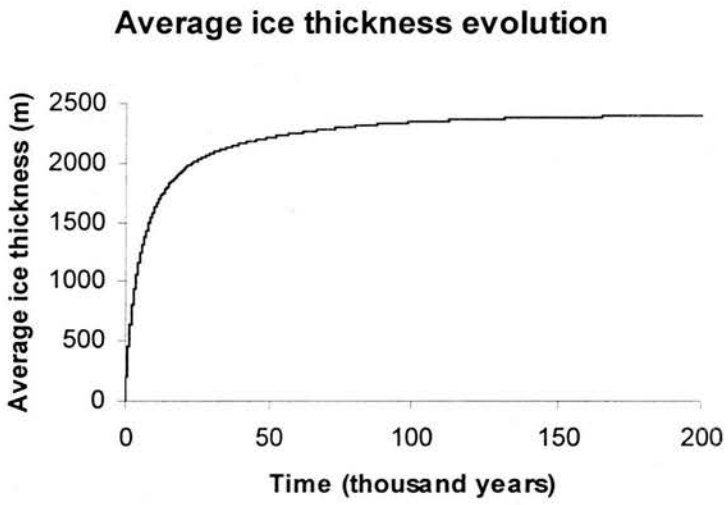

Figure 4.26 Evolution of ice volume (a) and average ice thickness (b) of the modelled Antarctic Ice Sheet. Both ice volume and the average ice thickness increases rapidly during the first 50,000 model years. Their rate of growth slows down during the second 50,000 model years. After 100,000 model years, they approach an equilibrium state.

Although the climatic cycles during the Quaternary are not constant, they nevertheless have rhythm. Ruddiman *et al.* [1986] pointed out that the climatic cycles shifted from a periodicity of around 41,000 years to around 100,000 years over the course of the last 700,000 to 800,000 years. Based on the isotope and CO_2 concentration analyses in a 2,083-metre long ice core recovered at Vostok, East

Antarctica, Jouzel, *et al.* [1987] and Barnola *et al.* [1987] conclude that, over the past million years, a *c.* 100,000-year rhythm of temperature oscillation dominates the climatic record. The paleo-climatic information recorded in the Vostok ice core fully covers the last glacial-interglacial cycle. Therefore, even though a new equilibrium state can never be fully reached, the 100,000-year simulation is nevertheless sufficiently long for modelling analysis.

4.3.4 Comparison with the Antarctic sub-glacial lake record

Based on the air-borne radio-echo sounding (RES), Dowdeswell and Siegert [1999] identify about 70 subglacial lakes under the Antarctic Ice Sheet (Figure 4.27). Areas of Antarctica covered by the RES flights are shown in the lower left corner in Figure 4.27. These subglacial lakes are distributed widely in the flight-covered area. It is inferred that many areas of the Antarctic Ice Sheet are warm-based and the meltwater drains to favourable topographic sites to form sub-glacial lakes. The basal temperature distribution shows that several patches of the modelled ice-sheet/bedrock interface are at the pressure melting point (Figure 4.24(b)). These pressure-melting areas match the lake groups plotted in Figure 4.27 well. For example, the RES flights plot out a group of subglacial lakes near Vostok in East Antarctica (Figure 4.27) and the modelled basal temperatures indicate a corresponding pressure melting area (Figure 4.24(b)). The temperature over a subglacial lake is no doubt at the pressure melting point. The basal ice surrounding and between the subglacial lakes may also be melting and the meltwater drains into these lakes. So it is reasonable to infer that the entire area with subglacial lake clusters in Figure 2.7 is at the pressure melting point. Other subglacial lake clusters are found under the Dome C, Ridge B, South Pole and Hercules Dome. All the areas of subglacial lake clusters match areas modelled as being at the pressure melting point at the base. The good match is an independent and effective way of demonstrating that the ice sheet model developed in this research works effectively. We will discuss the thermal regime of the Antarctic Ice Sheet in more detail in the next Chapter.

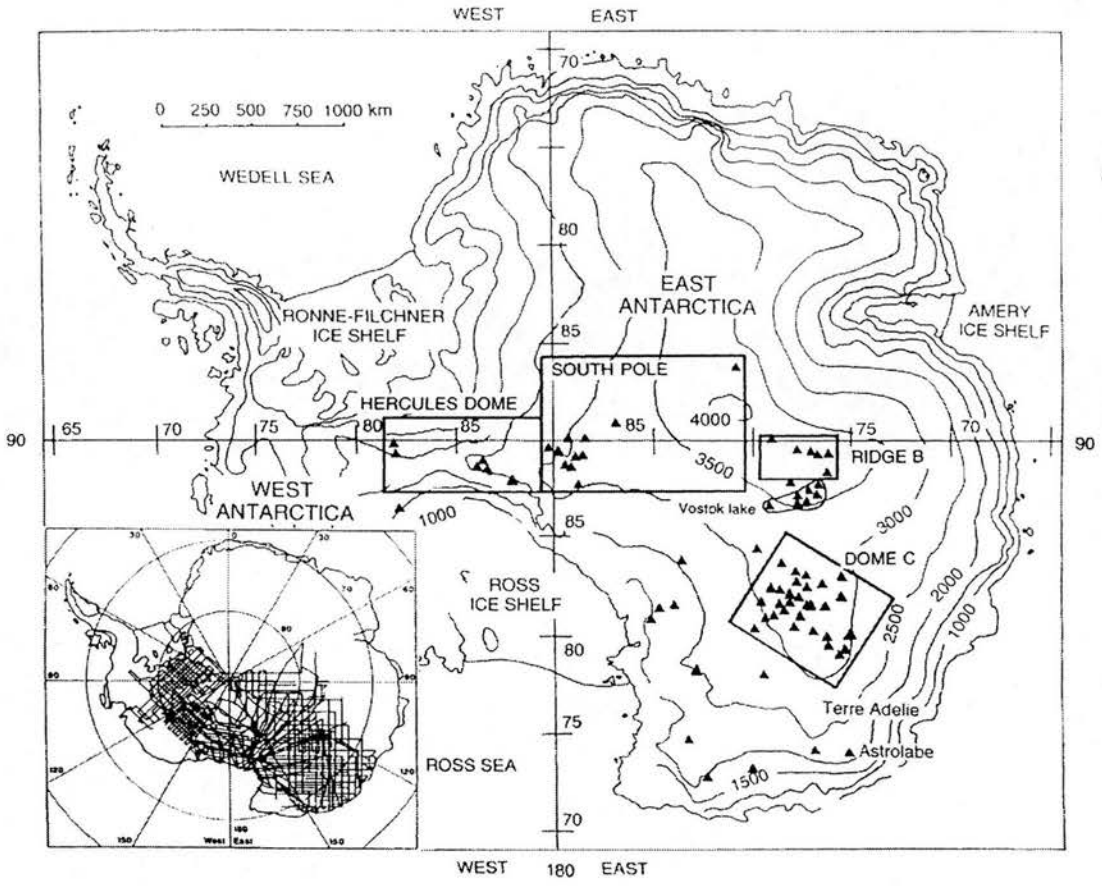

Figure 4.27 Locations of lakes beneath the Antarctic Ice Sheet (marked by triangles), identified from 60 MHz airborne radio-echo sounding records. Ice-sheet surface elevation is contoured at 500 metre intervals. Four regions are located within the ice sheet (Dome C, Ridge B, South Pole, and Hercules Dome). Inset is the network of radio-echo sounding flight lines from the collaborative SPRI-NSF-TUD programmes [Robin *et al.*, 1977], which forms a data set of about 400,000 km from which subglacial lake locations are identified (from Dowdeswell and Siegert, 1999).

Chapter 5 Dynamical and Thermal Regimes of the Antarctic Ice Sheet under the Present-day and Glacial Maximum Conditions

This chapter firstly aims to analyse the development of the thermal and dynamic regimes of the Antarctic Ice Sheet by reconstructing ice sheet growth from its early stage to a quasi-equilibrium state. Secondly, it aims to examine the changes of the thermal and dynamic regimes that accompany ice sheet growth to its full maximum extent. By examining the detail of the behaviour of the Antarctic Ice Sheet under changing climates, we can gain insight into the mechanisms controlling the long-term evolution of the ice sheet.

5.1 Time Scale and Climate Conditions

The duration of the ice sheet model run and the time step of numerical iteration are required as control data before the model starts running. Climatic conditions serve as the boundary conditions of the numerical regime and must be set by the model user.

5.1.1 Time of iteration and time step

In order to set up a reasonable time scale for the ice sheet model to reflect the real world, we should firstly look at what has happened on the Earth. The Quaternary is the most recent major subdivision of the geological record. It extends from 2.6 million years **b**efore **p**resent (BP) up to, and including, the present day. One of the most distinctive features of the Quaternary has been the build-up of major continental ice sheets and the expansion of mountain glaciers in many parts of the world [Lowe and Walker, 1997]. The last interglacial-glacial cycle in the Quaternary dates from *c.*130,000 years BP to *c.*10,000 years BP [Lowe and Walker, 1997]. This

time span of ~100,000 years is typical of climatic cycles in the last 800,000 years. Secondly, from the numerical point of view, the results from Chapter 4 suggest that the simulated thermal and dynamical regimes of the Antarctic Ice Sheet approach a quasi-equilibrium state after 100,000 model years of integration. 100,000 model years is therefore a good choice for the time scale of the modelling experiments.

When choosing the time step of numerical iteration, we similarly consider these two respects: the real world and the numerical regime. The climatic change we are concerned with is the average effect of the seasonal temperature and precipitation oscillations over a comparatively long period of time. So calculating the parameters of the ice sheet at a time step of one year is frequent enough for our research. Longer time steps, although speeding up the model runs, may sometimes affect the stability of the numerical regime and the reliability of the modelling results. Therefore a one-year time step is chosen in the following experiments.

5.1.2 Climate Conditions over the Present-day Antarctic Ice Sheet

Climate forcing is a fundamental issue since it represents the environment under which the Antarctic Ice Sheet system develops. In the ice sheet model, climatic conditions are represented by ice surface temperatures and sea level in a climate-forcing file. As discussed in Chapter 3, surface temperatures over the present-day Antarctic Ice Sheet are modelled as an empirical function of the local latitude and altitude of the ice surface (equation (3.17)). The ice surface temperatures are then used to model ice surface mass balance. Sea level information is used to identify the marine margin of the modelled Antarctic Ice Sheet.

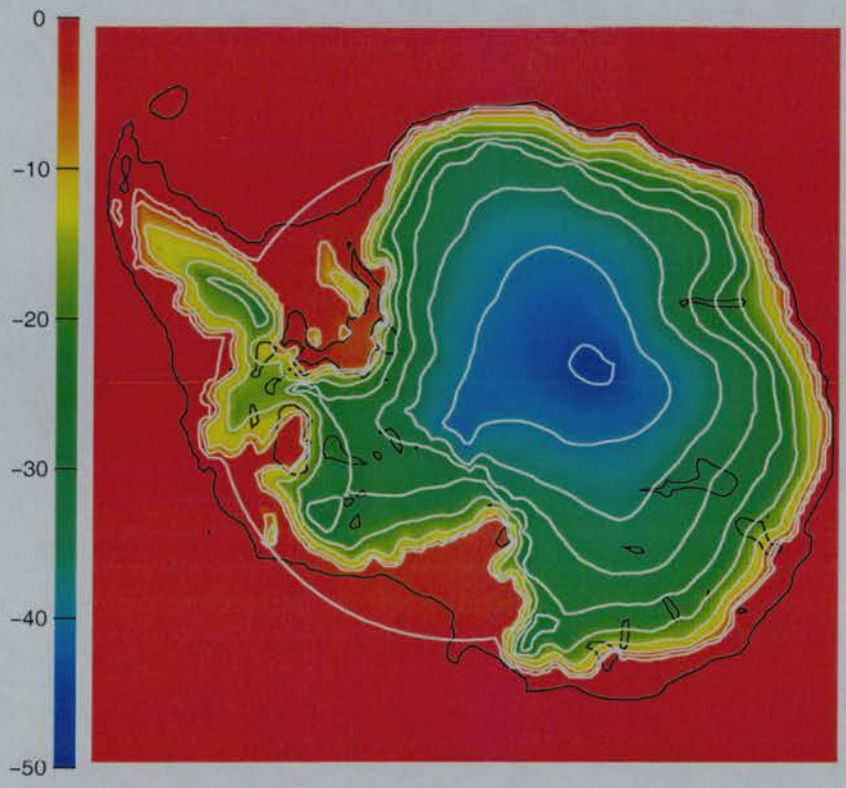

Figure 5.1 Modelled surface temperature distribution over the present-day Antarctic Ice Sheet (°C, with 5°C contours in white). The outermost contour represents 0°C, within which the ice sheet can develop.

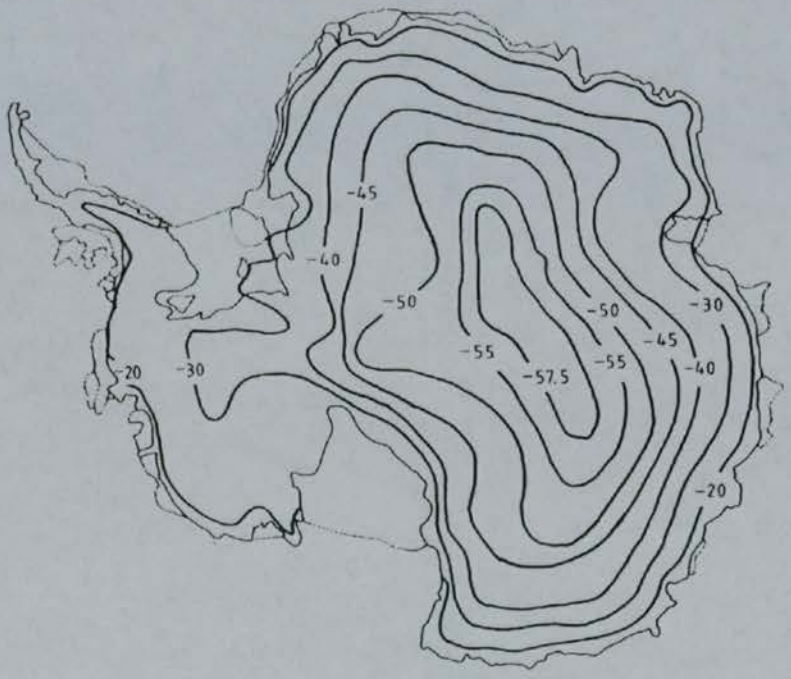

Figure 5.2 Present-day annual mean temperature (°C) distribution of the Antarctic Ice Sheet surface [from van der Veen, 1987].

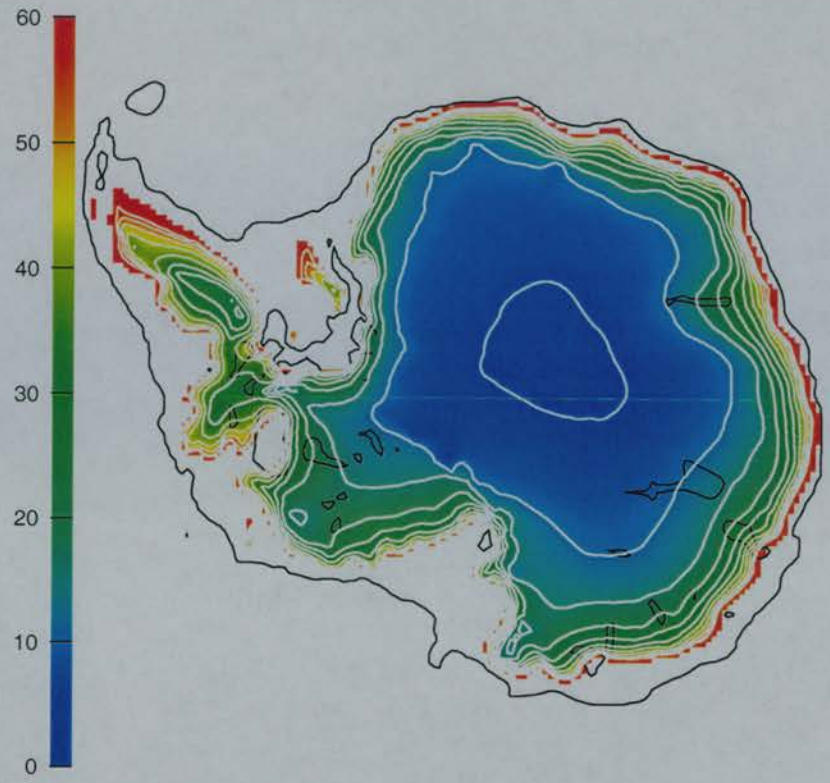

Figure 5.3 Modelled surface accumulation rate over the Antarctic Ice Sheet under the present-day sea level and annual mean surface temperatures (cm/yr, with 5 cm/yr contours in white).

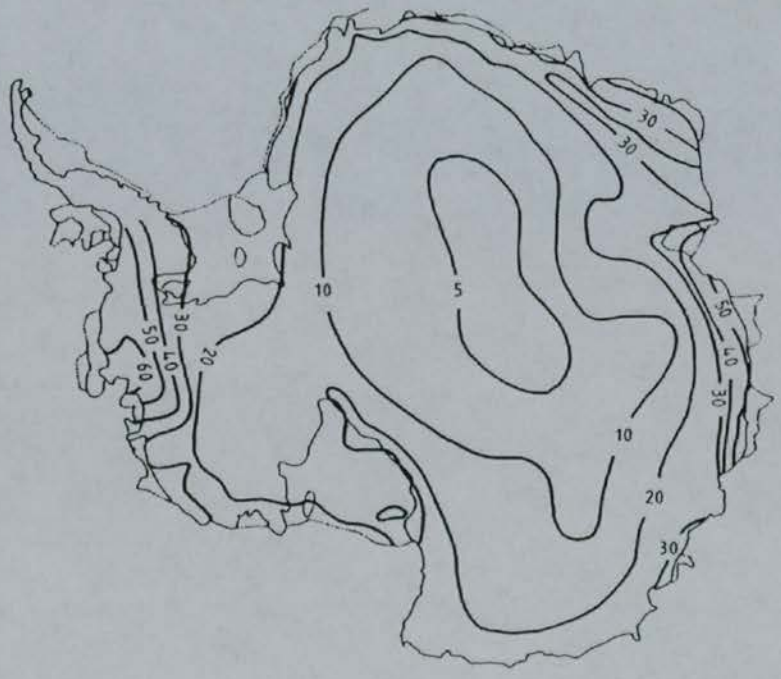

Figure 5.4 Present-day surface accumulation rate (cm/yr) distribution of the Antarctic Ice Sheet [from van der Veen, 1987].

Figure 5.1 shows the surface temperatures over the modelled Antarctic Ice Sheet after 100,000 model years of iteration from an ice-free Antarctic topography. Assuming that the Antarctic Ice Sheet is in a quasi-equilibrium state, we can regard this surface temperature distribution as the present-day situation. This is a reasonable assumption if we compare Figure 5.1 with the field records of the annual mean surface temperatures over the Antarctic Ice Sheet in Figure 5.2. The outermost contour in Figure 5.1 (and later in Figure 5.5) represents 0°C. It defines the area within which the ice sheet can develop. Over the sea the 0°C line is of a circular pattern reflecting latitude.

Based on the satisfactory modelling of ice surface temperatures, we can calculate the surface accumulation rates over the Antarctic Ice Sheet with the empirical temperature-accumulation relation, equation (3.19). The modelled surface accumulation is shown in Figure 5.3. Again there is a good match with present day field records of the surface accumulation rates over the Antarctic Ice Sheet (Figure 5.4). This agreement gives us confidence that the modelling results represent the real world effectively. The credibility of the following experiments and analyses of the response of the Antarctic Ice Sheet to glacial maximum conditions is hence enhanced.

5.1.3 Climate forcing conditions during a glacial maximum

The data for the present-day Antarctic Ice Sheet are more abundant, more precise and probably more accurate than data from the past. So the ice sheet model employs the present-day climatic conditions described in last section as a reference. The climatic conditions during a glacial maximum are modelled as the differences in ice surface temperature and sea level from their present-day conditions. These differences are read into the ice sheet model as a stepped climatic change.

The experiments in this chapter are designed to simulate the thermal and dynamical regimes of the Antarctic Ice Sheet under glacial maximum conditions. So before carrying out the experiments, we should first find out the proper values of the

differences from the present-day conditions in surface temperature and sea level during a glacial maximum climate.

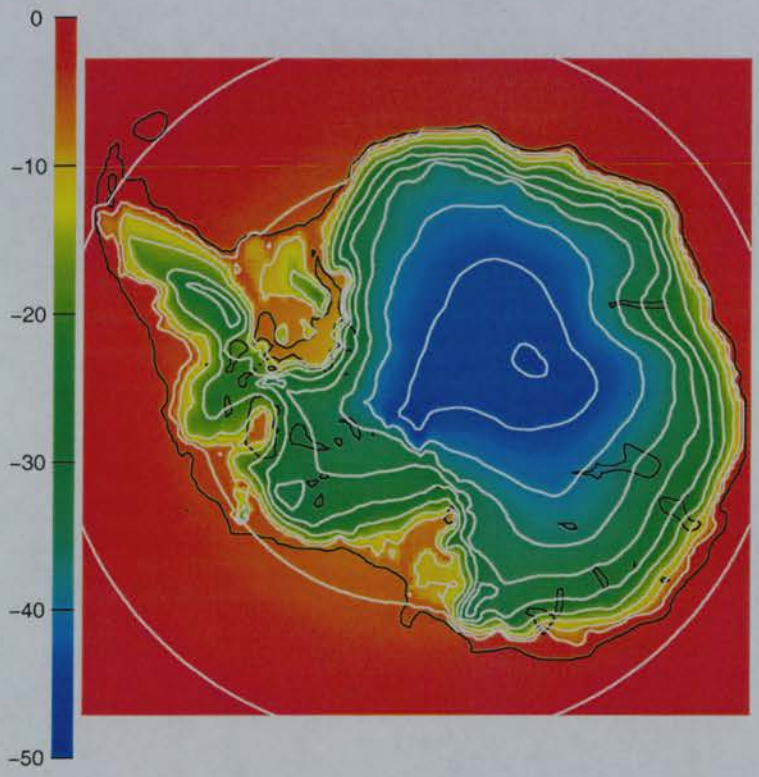

Figure 5.5 Modelled surface temperature distribution over the Antarctic Ice Sheet under the climate forcing conditions during a glacial maximum (°C, with 5°C contours). The 0°C contour expands well into the sea, providing a larger area for the Antarctic Ice Sheet to develop.

The Last Glacial Maximum (LGM) during the Quaternary is the most recent glacial maximum. Field evidence for this period is comparatively abundant and precise. Thus sea level and temperature situations during the LGM are a good choice for modelling a glacial maximum climate. Quaternary scientists commonly believe that during the LGM the sea level was 120 metres lower than the current sea level and the global annual mean temperature was 6°C lower than the present day [Jouzel *et al.* 1987; Robin, 1988; Robert *et al.*, 1992; Jouzel *et al.*, 1993; Marchant *et al.*, 1993;

Lowe and Walker, 1997; Petit *et al.*, 1997; Bentley, 1999]. These conditions are employed as the climate forcing in this research to initiate a glacial maximum starting from a quasi-equilibrium Antarctic Ice Sheet developed under the present-day climate conditions. Figure 5.5 shows the modelled surface temperature distribution over the Antarctic Ice Sheet under the above climate forcing conditions during the glacial maximum. Compared to the corresponding result under the present-day climate conditions, shown in Figure 5.1, the 0°C isotherm at the modelled glacial maximum climate expands well into the sea.

5.2 Evolution of the Antarctic Ice Sheet under the Present-day Climatic conditions

Now we have modelled the climate forcing conditions for a glacial maximum, the next step is to find out the quasi-equilibrium condition of the Antarctic Ice Sheet from which the glacial maximum climate forcing is initiated. In order to get this initial ice sheet condition for the glacial maximum experiment, we build up the Antarctic Ice Sheet from the rebounded ice-free Antarctic topography (Figure 4.22) under present-day climatic conditions to a quasi-equilibrium state. This experiment is also useful for investigating the early stages of the development of the Antarctic Ice Sheet.

5.2.1 Evolution of the dynamic regime

The parameters of the dynamic regime of the Antarctic Ice Sheet concerned in this modelling research are ice thickness, ice surface topography and ice flow. In this section we analyse the modelled results of these parameters.

- **Ice thickness evolution**

Figure 5.6 shows the evolution of ice thickness of the modelled Antarctic Ice Sheet. We can see that the ice sheet grows quickly during the early stage of development.

Its initial outline has formed after 1000 model years. At an early stage, when the ice front has not yet reached the sea, there is no mechanism for the ice sheet system to lose mass. As a consequence, net ice accumulation builds up the ice sheet rapidly (Figures 5.6(a) to 5.6(g)). After 20,000 model years, the overall outline of the modelled Antarctic Ice Sheet has formed (Figure 5.6(g)). As more and more ice front reaches the sea, mass loss from the ice sheet system increases and the speed of ice sheet growth decreases. After 100,000 model years, the modelled Antarctic Ice Sheet becomes stable (Figure 5.6(h)). The stability is more obvious after 200,000 model years (Figure 5.6(i)). During the first 100,000 model years, from an ice-free topography, the majority portion of the East Antarctic Ice Sheet grows to over 2000 metres thick and over 3000 metres thick on the interior plateau (Figure 5.6(h)). During the same modelling period, the West Antarctic Ice Sheet grows to less than 1000 metres thick near the coast and over 2000 metres thick inland. The modelled ice sheet matches the present-day situation of the Antarctic Ice Sheet. Compared to this rapid growth, the ice sheet growth speed dramatically slows down during the second 100,000 model years. The distribution of ice thickness after 200,000 model years (Figure 5.6(i)) does not have significant changes compared to the result after 100,000 model years (Figure 5.6(h)). The main change in ice thickness after 100,000 model years is the flattening of ice thickness gradients. The ice thickness contours after 200,000 model years (Figure (5.6(i)) are denser than the result after 100,000 model years (Figure 5.6(h)). Denser ice thickness contours indicate smoother surface gradients because ice thickness must be complementary to the rough Antarctic basal topography in order to flatten the surface topography. Smoother gradients of ice thickness indicate that the modelled ice sheet becomes less dynamic and approaches a quasi-equilibrium state.

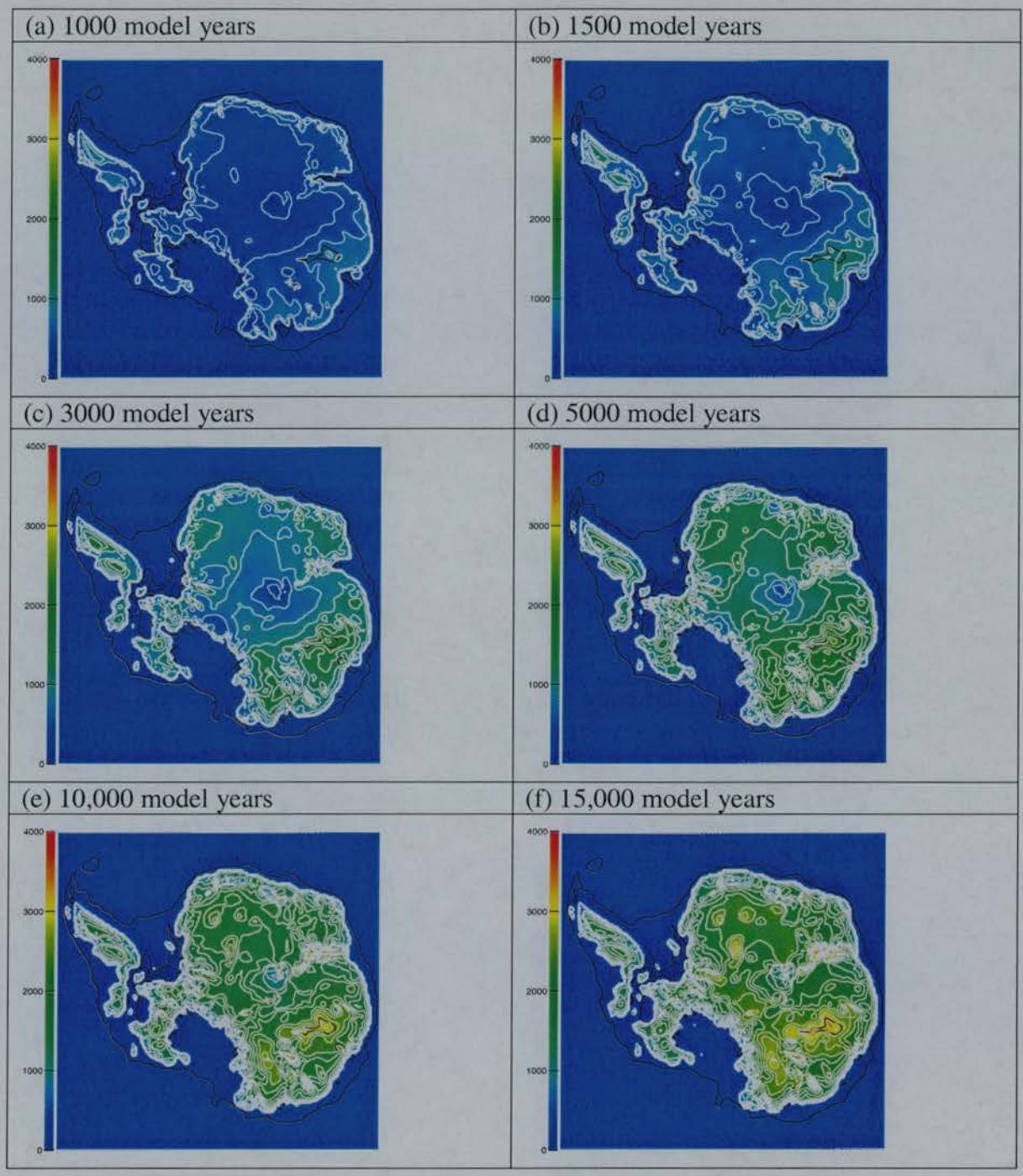

Figure 5.6 Evolution of the ice thickness (m, with 200-m contours) of the modelled Antarctic Ice Sheet under present-day climatic conditions from an ice-free Antarctic topography. After 100,000 model years, (h), the modelled ice sheet approaches a quasi-equilibrium state. The black contour is the –1000-m continental shelf contour.

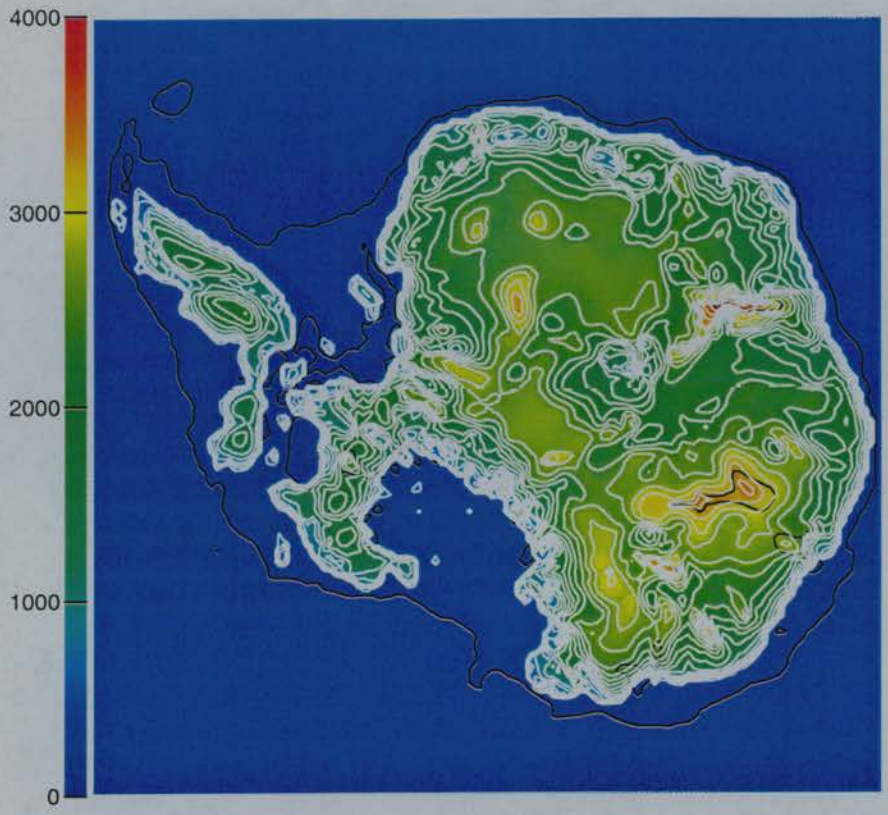

(g) 20,000 years

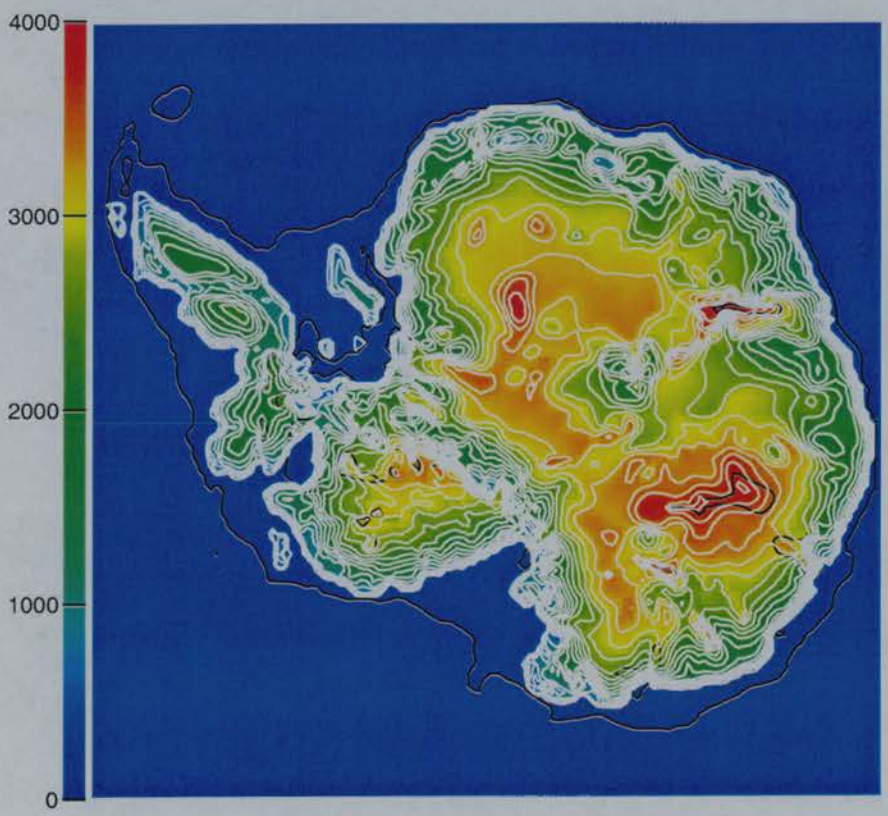

(h) 100,000 years

Figure 5.6 (Continue) Ice thickness evolution under present-day climatic conditions.

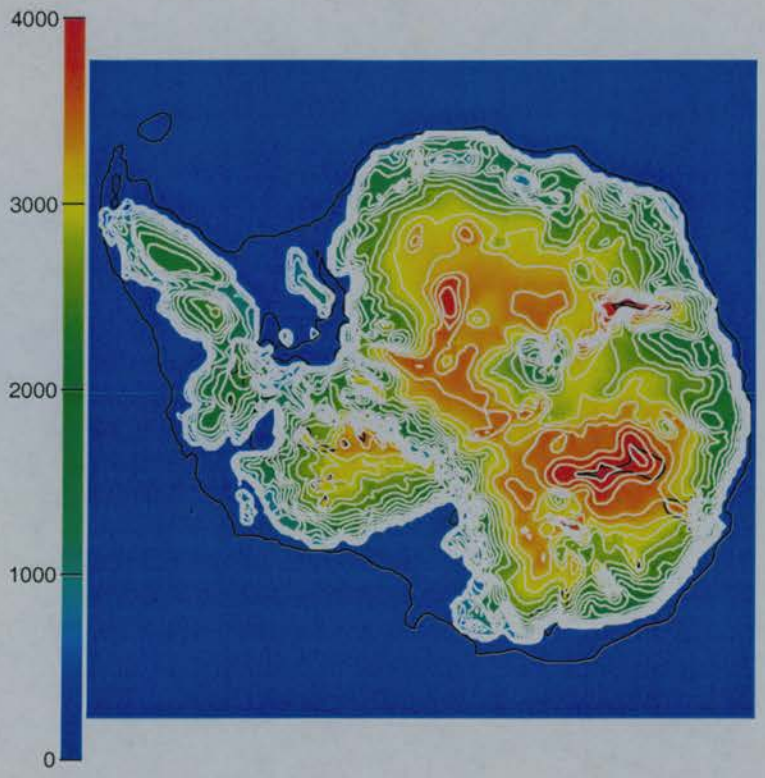

(i) 200,000 years

Figure 5.6 (Continue) Ice thickness evolution under present-day climatic conditions. Ice thickness contours now are denser than the result after 100,000 model years (h). This indicates smoother ice surface gradients.

- **Ice surface topography**

Ice surface topography illustrates the development of the ice sheet in a straightforward way. Combining the modelled ice thickness with the Antarctic basal topography under the ice sheet, we have the surface topography of the modelled Antarctic Ice Sheet (Figure 5.7). After 100,000 model years, the modelled ice sheets in East Antarctica and West Antarctica are well established (Figure 5.7(h)). In the interior of the modelled East Antarctic Ice Sheet, the surface altitudes are over 4000 metres above sea level. In West Antarctica, however, since the majority of the West Antarctic Ice Sheet is grounded below sea level, its surface altitudes are about 2000 metres above sea level. This result matches the present-day situation in Antarctica.

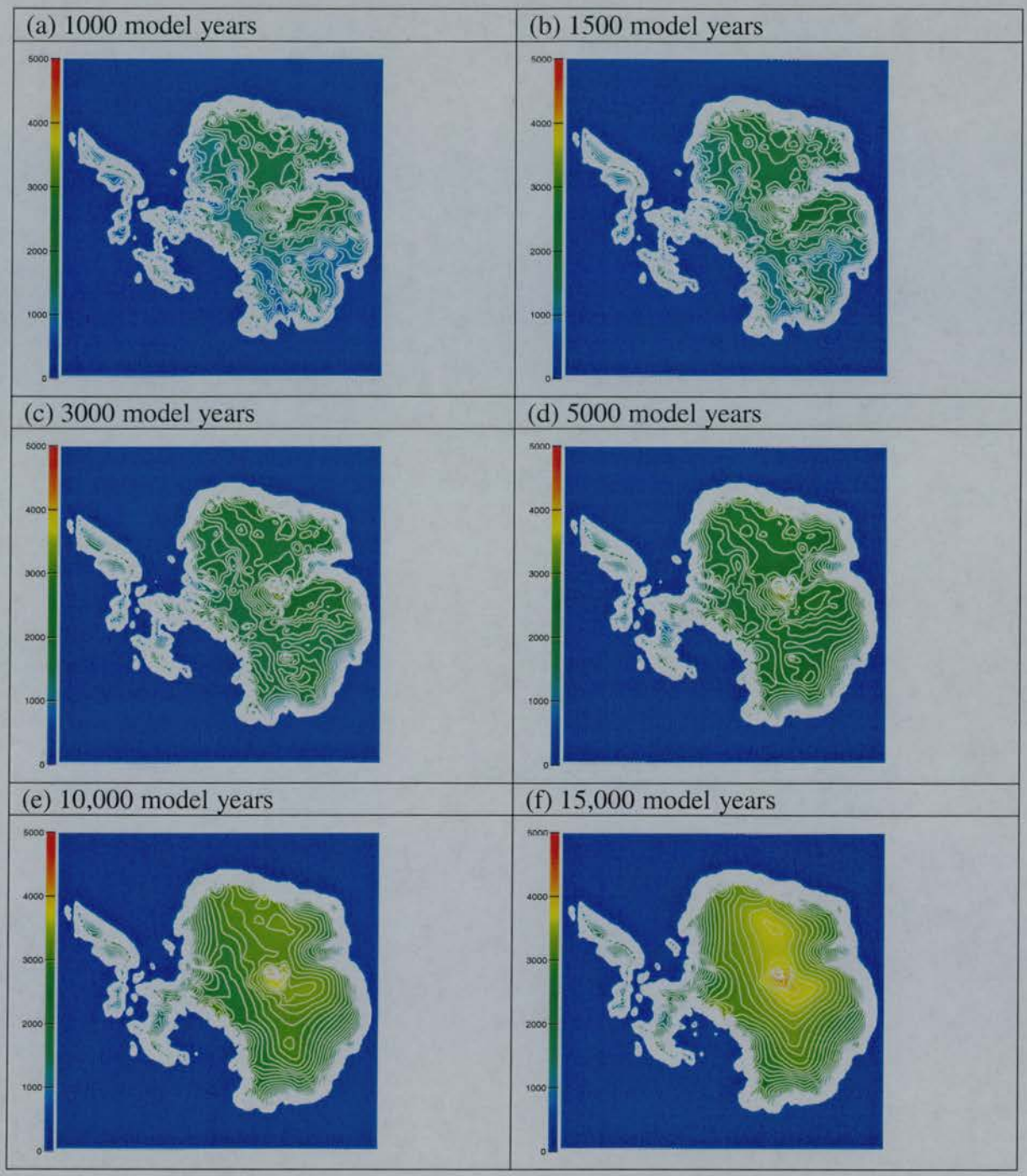

Figure 5.7 Evolution of ice surface altitude (m, with 100-m contours) of the modelled Antarctic Ice Sheet under the present-day climate conditions from an ice-free Antarctic topography. After 100,000 model years, (h), the ice sheet approaches a quasi-equilibrium state.

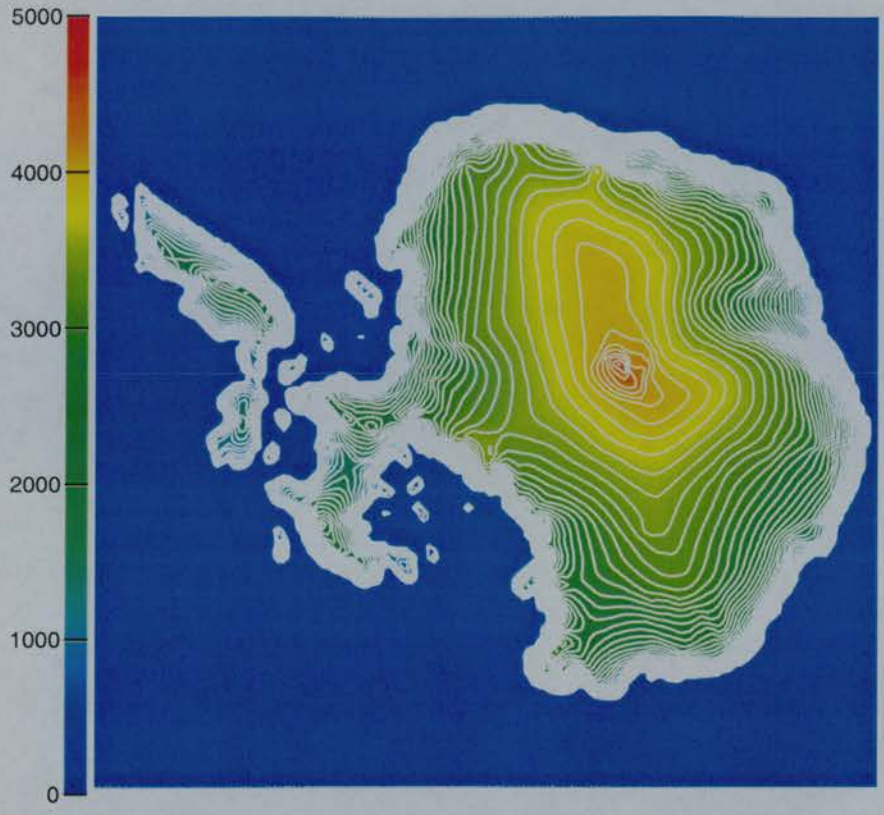

(g) 20,000 years

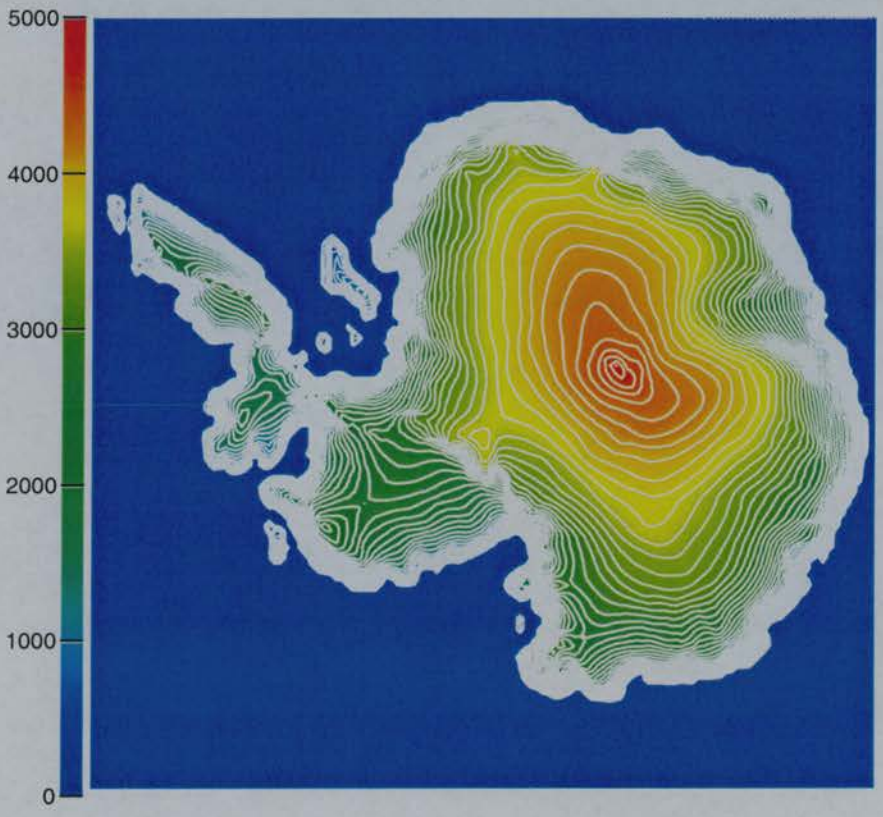

(h) 100,000 years

Figure 5.7 (Continue) Ice surface topography.

- **Ice flow**

Figure 5.8 shows the ice flow lines on the surface of the modelled Antarctic Ice Sheet at different stages of its development. The ice flow lines clearly indicate the overall direction of ice flow: from the interior of the Antarctic continent towards the sea. Once the ice reaches its marine margin, the ice flow velocities are high as the ice is calved away into the sea. The pattern of ice flow velocity corresponds with the theoretical analysis that surface ice at the periphery of the continent flows faster than that in the interior because the surface gradient toward the periphery is steeper. Comparing ice flow velocities with ice thickness (Figure 5.6) and basal temperature distribution discussed later (Figure 5.9), we find that surface ice above thicker and warmer areas flows faster. It reflects the effect of basal sliding. Some ice streams like the Lambert Glacier are clearly shown in the flow-line pictures. The ice flow field stabilises after 100,000 model years. The amount of ice calved away from the marine margin and melted way from the seawater/ice-shelf interface now compensates for the amount of ice flowing from the ice accumulation area towards the ice shelves. At the early stage of the ice sheet development, since the ice sheet is thin, it is cold-based. The grey shading in Figure 5.8 indicates ice diffusivity, which is a function of ice temperature and ice thickness. The light grey in Figures 5.8(a) and 5.8(b) indicates stiff ice. Ice flow is thus not significant. When approaching a quasi-equilibrium, due to the thickening of the ice sheet and flattening of the ice surface gradients, many parts of the ice sheet become warm-based. Ice near the bottom of the ice sheet becomes softer. The dark grey in Figure 5.8(h) indicates the ice's stronger tendency to flow. In the interior of the modelled Antarctic Ice Sheet, ice flows 10 to 20 metres a year towards the ice sheet margin. At the periphery of the ice sheet, ice flow velocities increase to 50 to 100 metres a year. In some areas of the ice sheet margin where fast flowing ice streams exist, ice flow velocities can reach nearly as high as 200 metres a year.

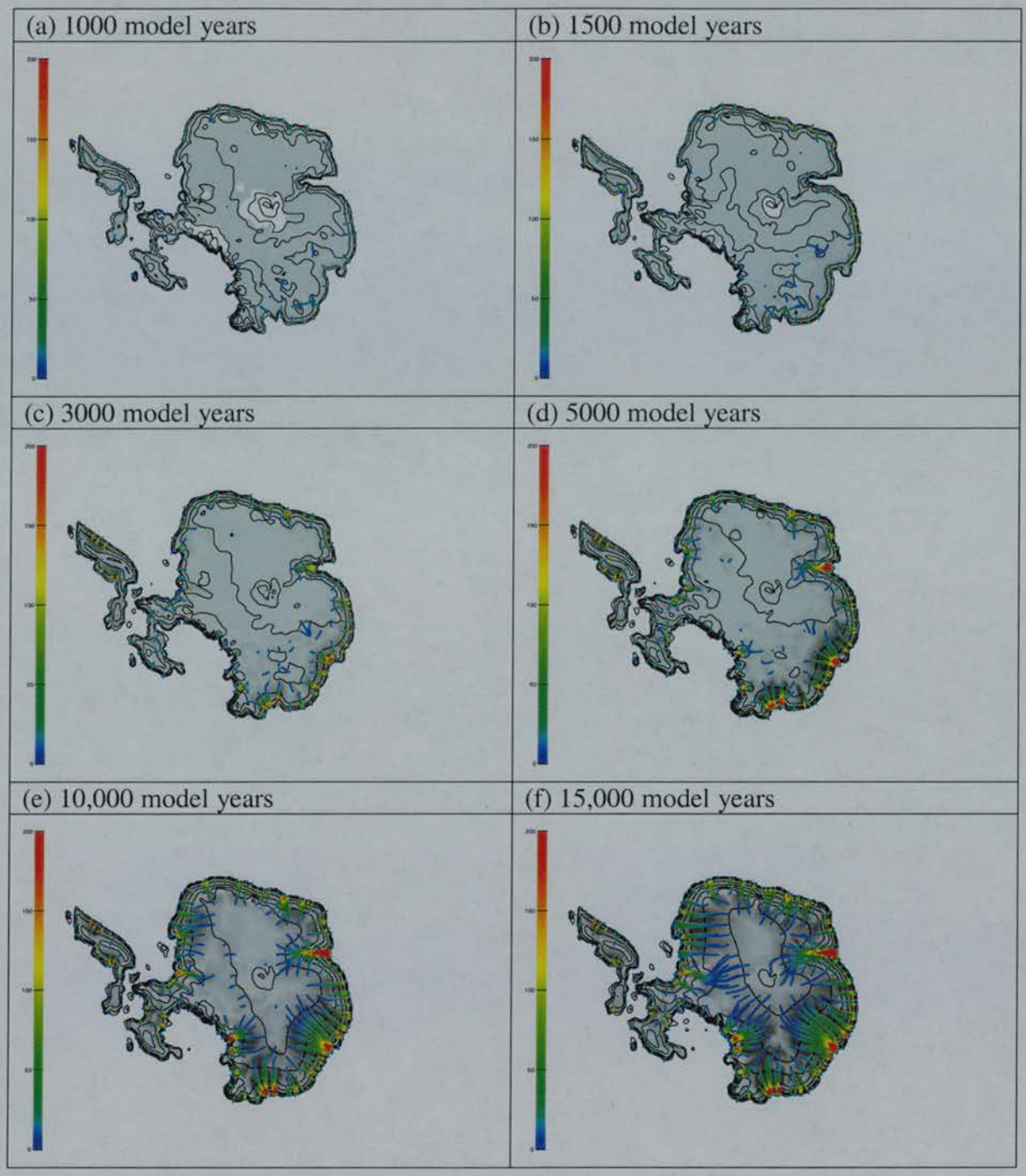

Figure 5.8 Evolution of surface ice flow (m/yr) of the modelled Antarctic Ice Sheet under the present-day climatic conditions. The coloured lines are ice flow lines, which indicate the direction and speed of ice flow. From light grey to dark grey, the diffusivity of the modelled ice sheet, which indicates the potential for ice flow, increases. The contours (500-m) are ice surface altitude.

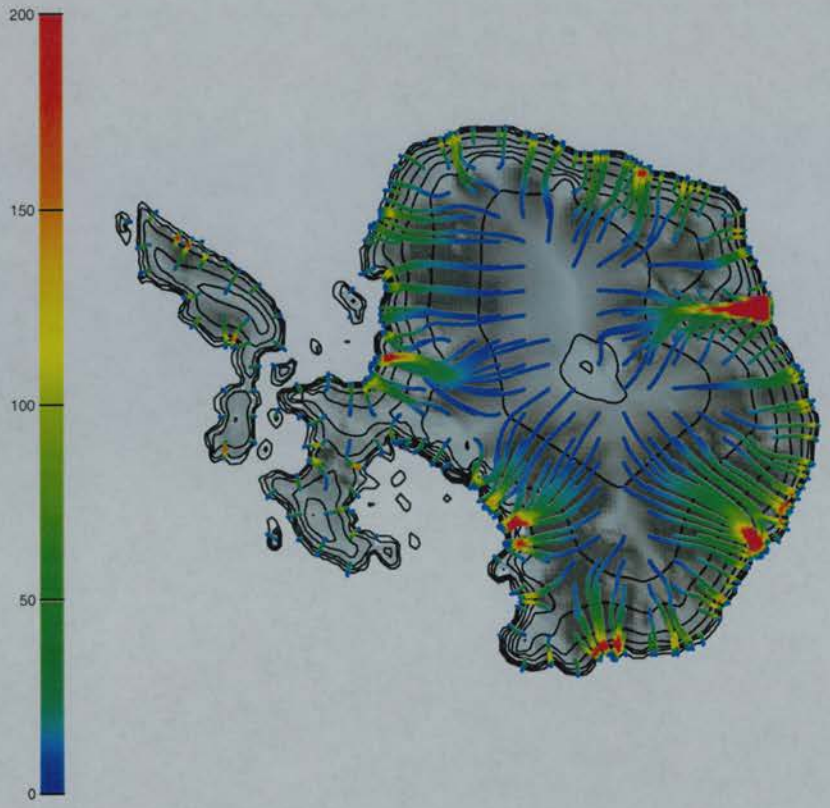

(g) 20,000 years

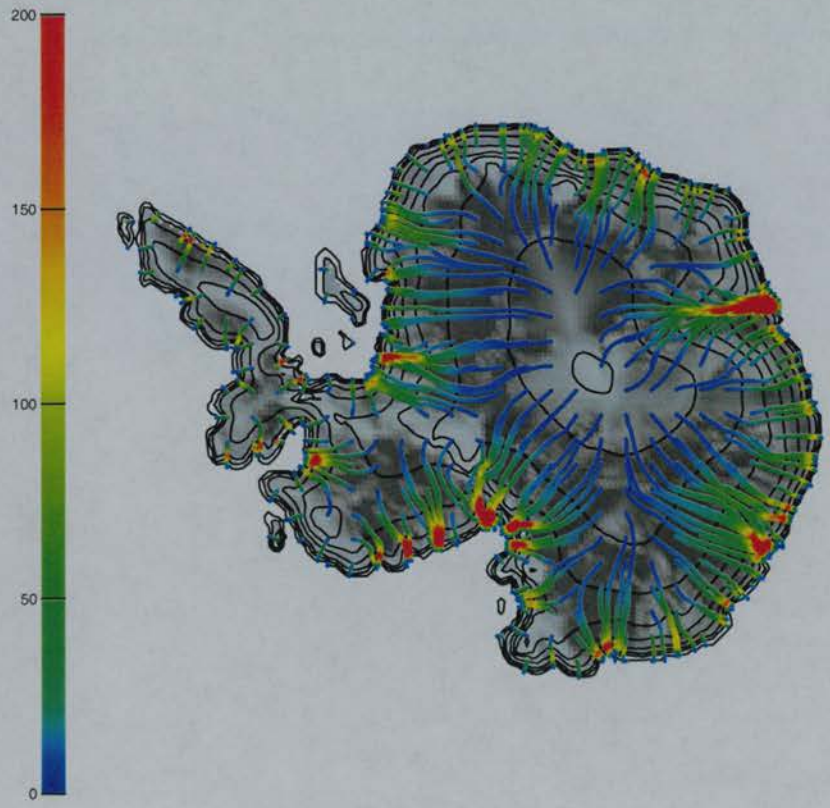

(h) 100,000 years

Figure 5.8 (Continue) Ice flow evolution

5.2.2 Evolution of the thermal regime

The thermal regime of the Antarctic Ice Sheet is the main concern of this research. It directly determines the basal melting rate and hence the stability of the Antarctic Ice Sheet. The thermal regime is coupled with the dynamical regime in an ice sheet, since the Arrhenius factor for ice, which determines the stiffness of ice, is a function of ice temperature (equation (2.2)). On the other hand, the pressure-melting point of ice is a positive function of ice thickness (equation (3.14)), and basal frictional heating is a function of ice flow (equation (2.6)) and surface gradient (equation (2.7)). Knowledge of the thermal regime helps us understand the dynamic mechanism of the Antarctic Ice Sheet system as a whole.

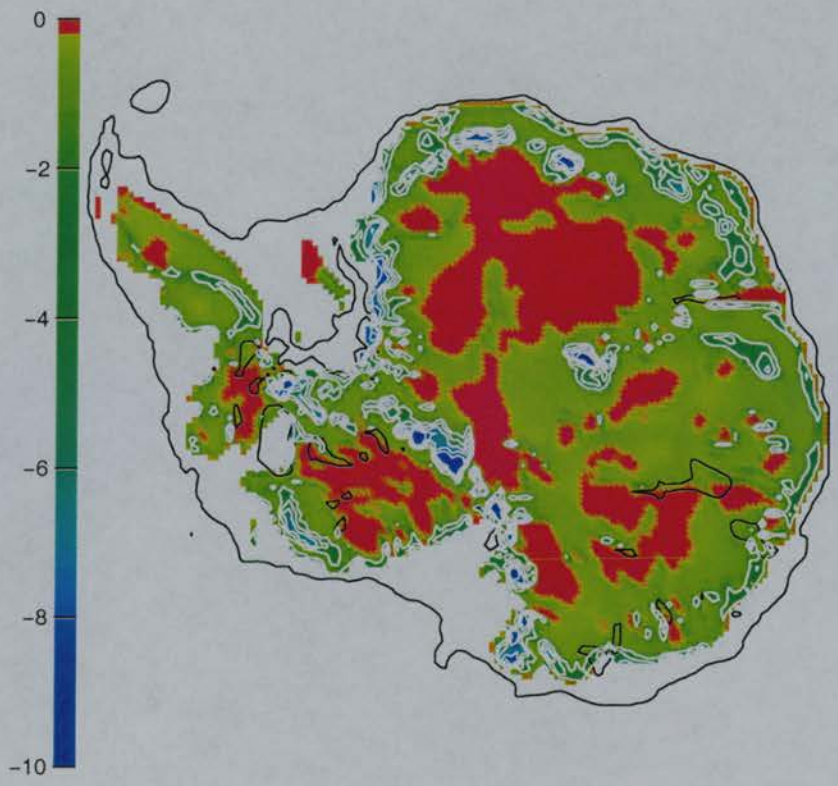

Figure 5.9 Basal temperature distribution (°C, with 2°C contours) of the modelled Antarctic Ice Sheet system developed under the present-day climate conditions for 100,000 model years from an ice-free Antarctic continent. Red areas are at pressure melting point.

Figure 5.9 shows the basal temperature distribution of the modelled Antarctic Ice Sheet system developed under present-day climatic conditions for 100,000 model years from an ice-free Antarctic topography. Direct field measurements of basal temperatures under the Antarctic Ice Sheet are very rare. The credibility of the modelled basal thermal regime can nevertheless be inferred from the comparison with ice thickness (Figure 5.6(h)); the modelled basal temperature distribution satisfactorily reflects the basal temperature – ice thickness relationship. The majority of pressure-melting areas in Figure 5.9 are beneath thick ice in East Antarctica. Some small pressure-melting patches in West Antarctica and the periphery of East Antarctica are associated with dynamic ice streams, such as under the Lambert Glacier in East Antarctica. This reflects the fact that fast flowing ice generates more heat through friction. As shown in Chapter 4, the modelled basal temperature distribution under the Antarctic Ice Sheet can also be justified by the comparison with the distribution of subglacial lakes in Antarctica obtained through the air-borne radio echo sounding research [Dowdeswell and Siegert, 1999]. The interface between the subglacial lakes and the overlying ice must be at pressure-melting point. The subglacial lake clusters shown in Figure 4.27 coincide with areas at the pressure-melting point shown in Figure 5.9. For example, the Vostok area, holding the biggest subglacial lake identified in Antarctica so far, is picked out in Figure 5.9.

In the next section, we are going to investigate the response of the modelled Antarctic Ice Sheet system to a glacial maximum climate. The modelling results of ice thickness, bedrock topography and ice temperatures of the Antarctic Ice Sheet after 100,000 model years of integration from an ice-free Antarctic continent are used as the initial conditions of the ice sheet from which the glacial maximum climatic conditions are applied.

5.3 Glacial Maximum experiments

A lower sea level and lower ice surface temperatures, as occurred during a glacial maximum, affect ice sheet evolution in different ways. As sea level drops, more ice

will be grounded and the marine limit of the Antarctic Ice Sheet will also retreat to lower latitudes. As a consequence, less ice will be calved away from the marine edges of the Antarctic Ice Sheet and less ice will be melted from the ice-water interface under the ice shelves. The Antarctic Ice Sheet will tend to expand. On the other hand, the saturated water vapour pressure in the air decreases with lower temperature. Lowered surface temperatures over the Antarctic Ice Sheet will decrease the water-holding capacity of the overlying atmosphere, hence precipitation rates will reduce, especially in the interior of the Antarctic plateau where both latitude and altitude are high. Less precipitation causes less surface accumulation on the continental ice sheet. The decreased mass input into the Antarctic Ice Sheet system will undermine the ice sheet's ability to expand. This temperature-accumulation relationship is reflected in this ice sheet model by the empirical exponential function (equation (3.19)). How are these contrasting effects reflected in ice sheet behaviour?

The experiment is this section employs the quasi-equilibrium conditions of the modelled Antarctic Ice Sheet under the present-day climate as the initial condition and the climatic conditions of the glacial maximum obtained in §5.1.3 as the forcing boundary conditions. It is designed to simulate the responses of the thermal and dynamical regimes of the present-day Antarctic Ice Sheet to a glacial maximum climate.

5.3.1 Dynamic regime of the Antarctic Ice Sheet under the climate forcing of the glacial maximum

The overall effect of the glacial maximum forcing should be to let the area of the Antarctic Ice Sheet expand further into the sea, whereas the thickening in the interior of the ice sheet should not be dramatic. Starting from the stabilised conditions of the modelled Antarctic Ice Sheet system under the present-day climate, the ice sheet model ran under the glacial maximum climate forcing conditions for 100,000 model years to approach a new quasi-equilibrium state. Figure 5.10 shows the evolution of the ice thickness of the modelled Antarctic Ice Sheet system in different stages.

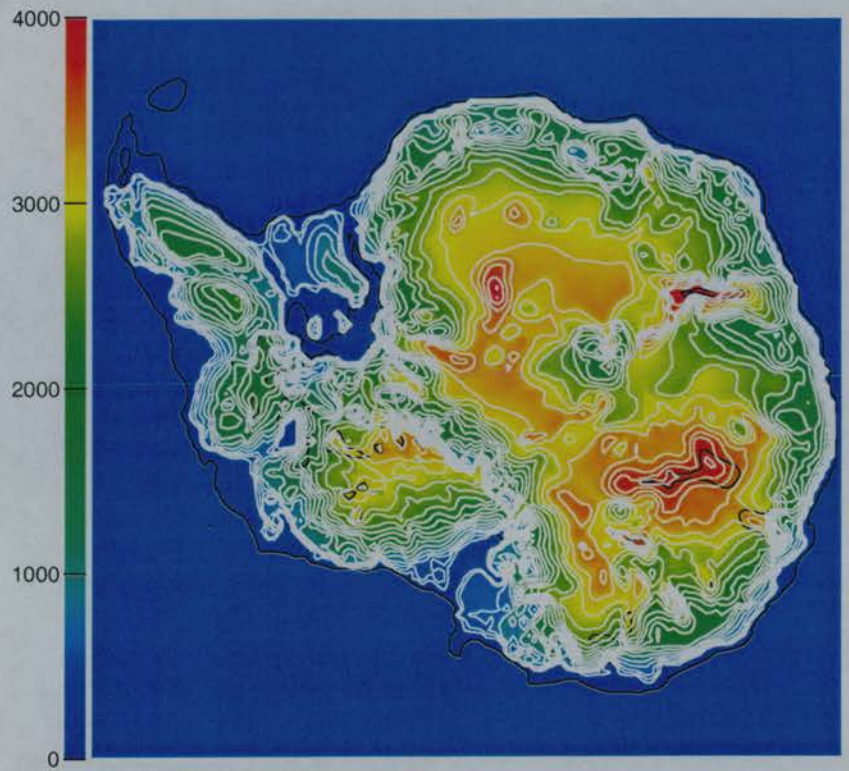

(a) 1000 years

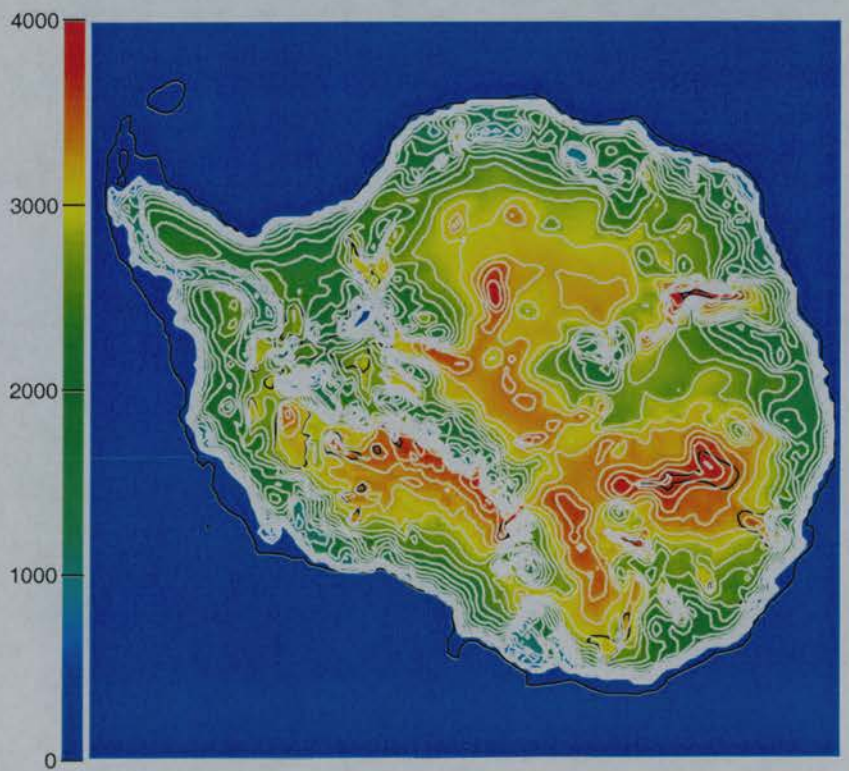

(b) 20,000 years

Figure 5.10 Evolution of ice thickness under glacial maximum climate forcing conditions (To be continued).

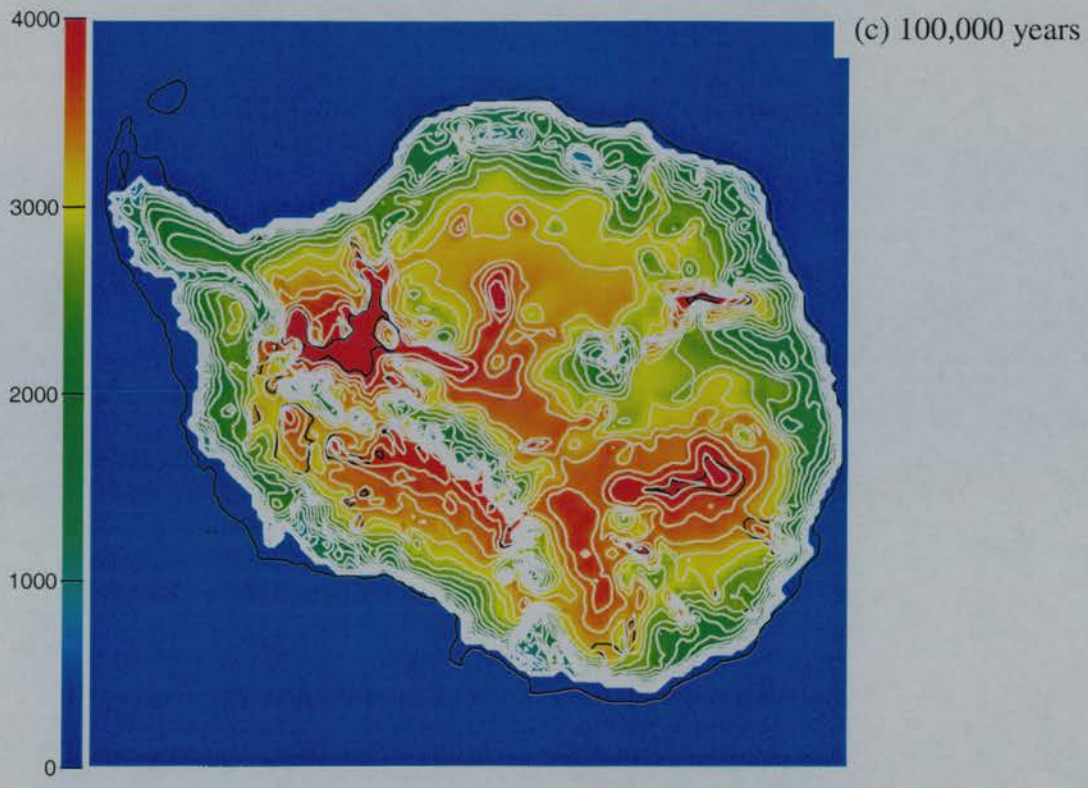

Figure 5.10 Evolution of ice thickness (m, with 500-m contours) of the modelled Antarctic Ice Sheet under glacial maximum climate forcing conditions. (a) Ice shelves begin to form in bay areas. (b) After 20,000 model years, the ice sheet has nearly reached its maximum limit. Now most of the Ross Sea and the Weddell Sea are covered by ice. (c) The modelled Antarctic Ice sheet system as a whole approaches a new quasi-equilibrium state after 100,000 model years of full maximum climatic conditions.

The modelled Antarctic Ice Sheet system responds quickly after the enforcement of the glacial maximum climatic conditions. Due to the lowering of sea level, more land emerges and ice can quickly build up. Under present-day climatic conditions, only the continental ice sheet can expand itself into the sea and form ice shelves (Figure 5.8), whereas after only 1000 model years of the enforcement of glacial maximum climatic conditions, the small ice cap on Berkner Island (Figure 5.6) is expanding into the Weddell Sea to form the Ronne-Filchner Ice shelf (Figure 5.10(a)). The map of surface ice flow lines at the same time clearly shows the significant increase in ice flow (Figure 5.11(a)). The modelled Antarctic Ice Sheet system is most dynamic

during the first 1000 model years of enforcement of the glacial maximum climate conditions. By 20,000 model years, most of the Ross Sea and Weddell Sea has been covered by ice (Figure 5.10(b)). After 100,000 model years, the modelled Antarctic Ice Sheet system as a whole again reaches a new quasi-equilibrium state (Figures 5.10(c) and 5.11(b)). Comparing the marine margin of the ice sheet in Figure 5.10(b) with that in Figure 5.10(c), we find that the modelled Antarctic Ice Sheet almost reaches its maximum ice limit after 20,000 model years of evolution under glacial maximum climatic conditions and remains quasi-stable subsequently.

These modelling results reflect natural processes in the real world. A lower sea level grounds more ice shelves. As a consequence, less ice is melted from the ice-shelf/water interface and calved away from the ice front. More land also emerges from the sea, which provides the ice sheet with more room to develop. The embayment effect is important in the case of the Ross Sea and Weddell Sea, where it encourages the Ross Ice Shelf and the Ronne-Filchner Ice Shelf to expand even faster. Both ice shelves reach almost half their extent during the first 1000 model years (Figure 5.10(a)), and are well developed after 20,000 model years (Figure 5.10(b)).

It is worth noticing that the shape of the modelled ice sheet on the East Antarctic continent does not change significantly after the application of the glacial maximum climatic conditions as can be seen by a comparison of Figure 5.10(c) with Figure 5.6(i). This suggests that the East Antarctic Ice Sheet is stable under changing climatic conditions. This modelling result supports the argument that the East Antarctic Ice Sheet remains robust throughout Pliocene-Pleistocene time [Denton *et al.*, 1993; Sugden, 1996]. It also agrees with the conclusion from marine sediments research that the East Antarctic Ice Sheet is almost as large now as it was during the Last Glacial Maximum [Anderson, 1999]. The stable dynamic regime of the East Antarctic Ice Sheet also implies a stable thermal regime.

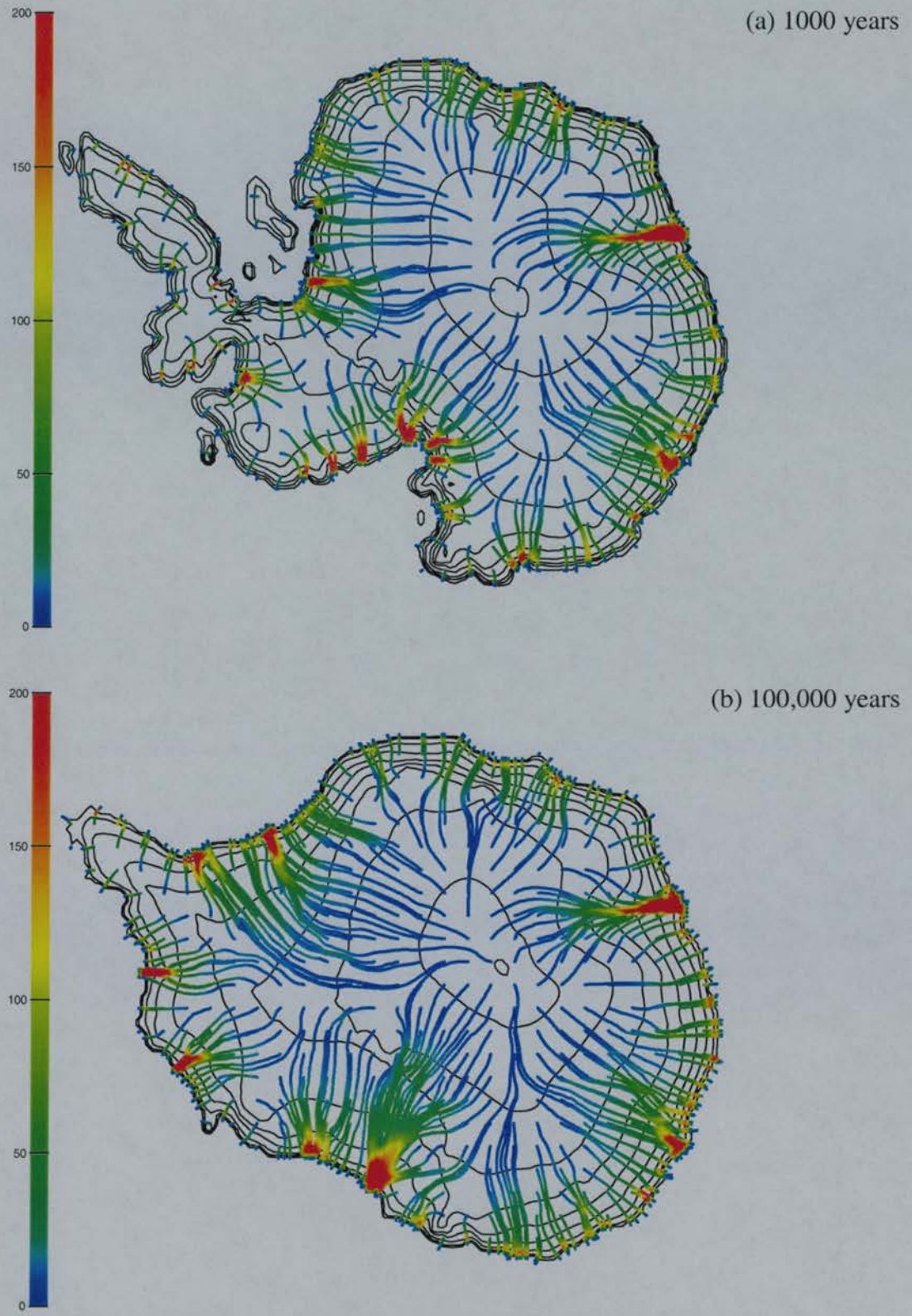

Figure 5.11 Flow lines of surface ice of the modelled Antarctic Ice Sheet after the enforcement of glacial maximum climate forcing conditions. (a) Ice expands fast into the Ross Sea and the Weddell Sea not only from the continent but also from offshore islands. (b) The dynamical regime of the ice sheet reaches a new quasi-equilibrium state.

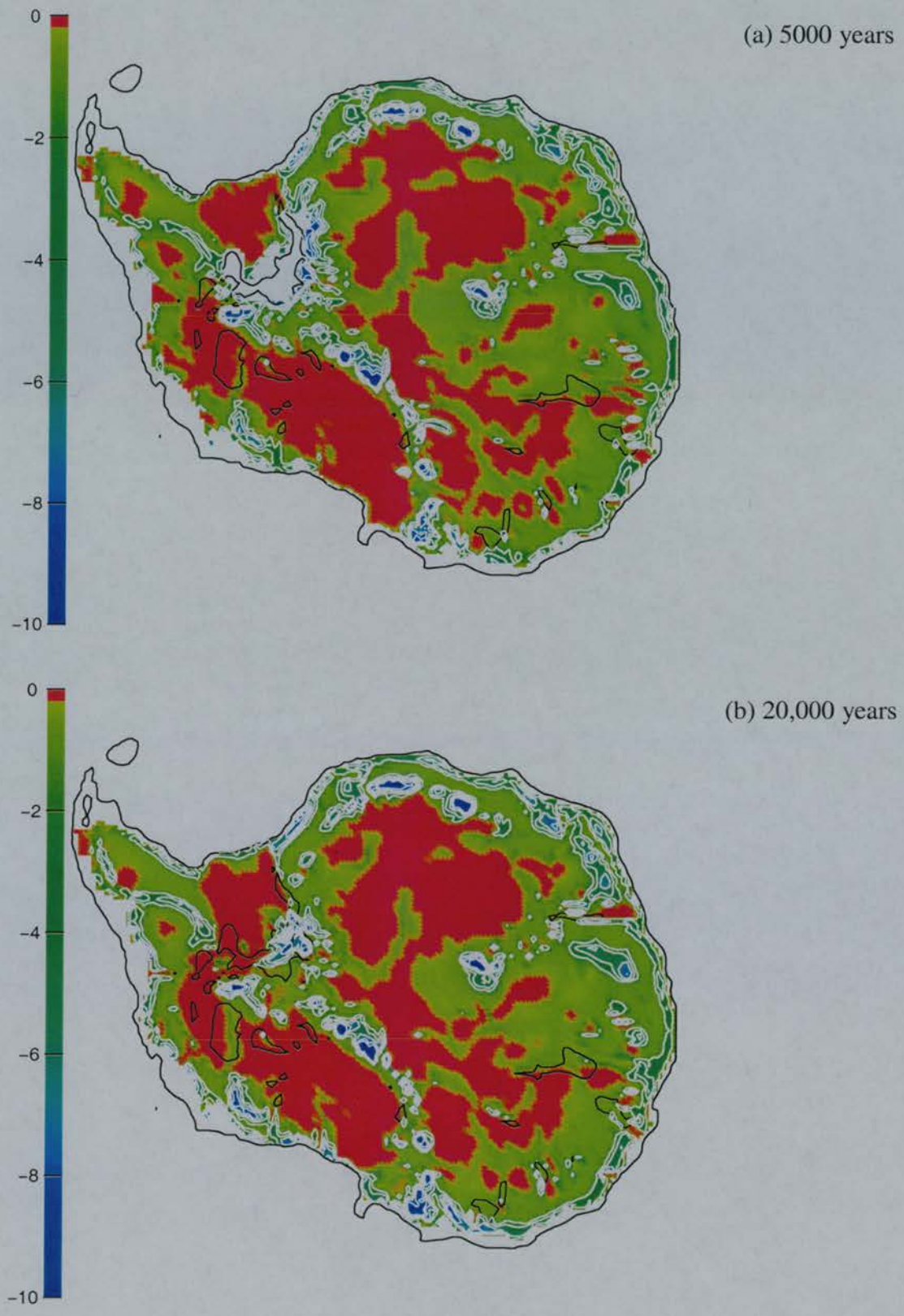

Figure 5.12 Basal temperature distribution of the modelled Antarctic Ice Sheet after the enforcement of glacial maximum climatic conditions. The East Antarctic Ice Sheet is more stable than its western counterpart because larger portion of the East Antarctic Ice Sheet is cold based.

5.3.2 Thermal regime of the Antarctic Ice Sheet under the climate forcing of the glacial maximum

It is widely believed that global surface temperatures during the Last Glacial Maximum were 6°C colder than at present. However, because ice is a poor heat conductor (Figure 4.2), basal temperature under thick ice sheets is more a function of ice thickness and ice flow velocities than of ice surface temperatures. The thermal regime of the Antarctic Ice Sheet, especially its basal temperatures, is therefore controlled primarily by its dynamic conditions.

As expressed in equation (3.14), the local pressure-melting temperatures at the bottom of an ice sheet are a function of ice thickness above that point. If the distribution of ice thickness of the East Antarctic Ice Sheet is resistant to a temperature change of a few degrees, so will be the distribution of basal temperatures. The modelling results of basal temperatures of the Antarctic Ice Sheet under the glacial maximum climatic conditions are as expected (Figure 5.12).

When the dynamical regime of the modelled Antarctic Ice Sheet system reaches a quasi-equilibrium state after 100,000 model years as discussed in the previous section, how is its thermal regime? Figure 5.13 shows the basal temperature distribution after the modelled Antarctic Ice Sheet system has developed for further 100,000 model years. Comparing Figure 5.13 with the corresponding result after the first 100,000 model years (Figure 5.9), we can see that the shape and distribution of those pressure-melting areas barely change. The absolute differences between the basal temperatures of the modelled Antarctic Ice Sheet system after 100,000 model years of evolution starting from an ice-free Antarctic topography and those after 200,000 model years are shown in Figure 5.14. The small differences demonstrate the stability of the thermal regime of the modelled Antarctic Ice Sheet system. After the second 100,000 model years, basal temperatures across most areas under the modelled Antarctic Ice Sheet are hardly changed. Those areas with significant changes are mostly located in those comparatively more dynamic parts of the ice

sheet under a strong marine influence such as the Antarctic Peninsula, West Antarctica and along the coast.

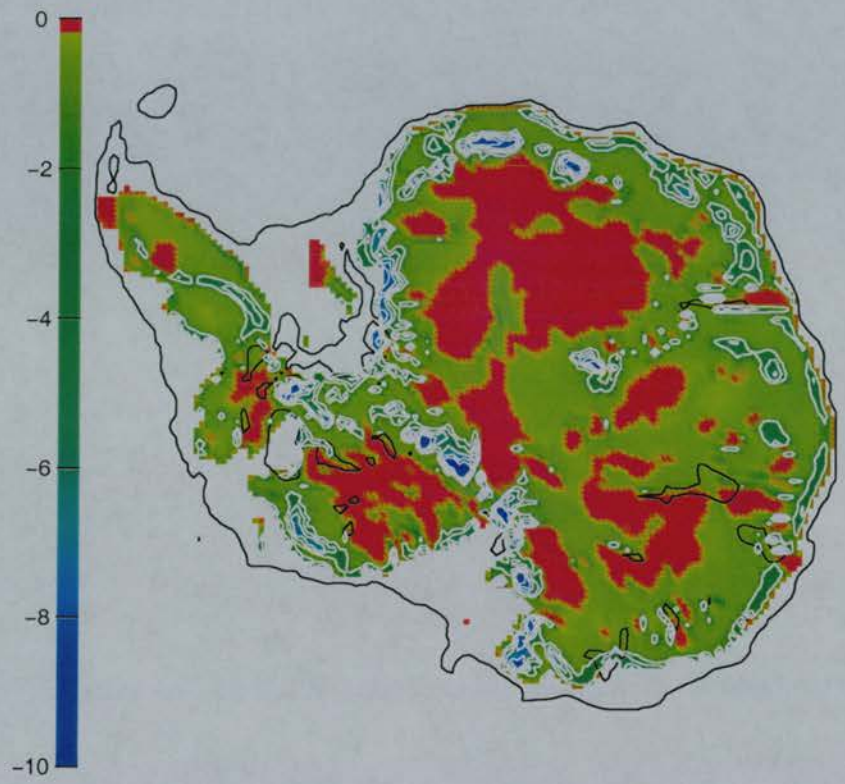

Figure 5.13 Basal temperature distribution (°C, with 2°C contours) of the modelled Antarctic Ice Sheet system developed under the present-day climatic conditions for 200,000 model years from the ice-free Antarctic continent. Red areas are at the pressure melting point.

Based on the stability of the modelled Antarctic Ice Sheet system, we can conclude with confidence that after 100,000 model years of evolution starting from an ice-free Antarctic topography under present-day climatic conditions, both the modelled dynamical and thermal regimes of the resulting Antarctic Ice Sheet approach a quasi-equilibrium state. Bearing in mind that the real present-day Antarctic Ice Sheet may not be at a full equilibrium state itself [Sugden, 1992, 1996], these quasi-static changes in ice sheet parameters after the first 100,000 model years are reasonable.

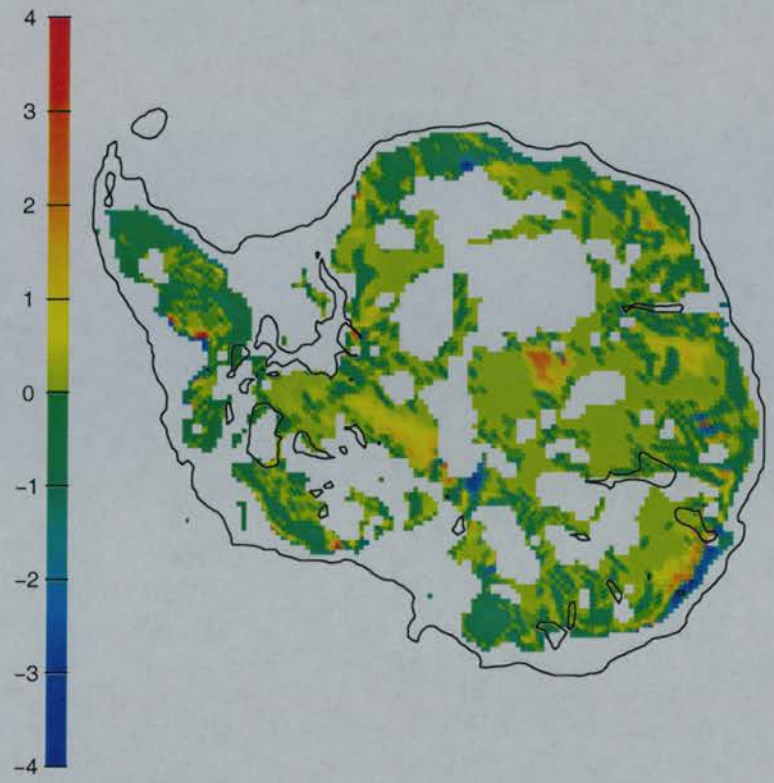

Figure 5.14 Absolute basal temperature changes from 100,000 model years of evolution of the modelled Antarctic Ice Sheet to 200,000 model years of evolution. The small temperature changes indicate a quasi-equilibrium thermal regime. The white areas are at the pressure-melting areas in both modelling stages.

There is an interesting contrast in the changing patterns of basal thermal regime between East and West Antarctica as the ice grows to maximum glacial conditions. The basal temperature distribution of the East Antarctic Ice Sheet on the interior plateau does not change significantly with the climatic change after 100,000 model years of glacial maximum conditions, as can be seen by comparing Figure 5.12 with Figure 5.9. The climate of the interior of East Antarctica is affected mainly by cooling on the surface of the ice sheet and a consequent reduction in snowfall. Since ice thickness in the interior of East Antarctica is greater than 3000 metres (Figure 5.10), it takes 100,000 years for 30 percent of the cold signal from the ice surface to penetrate 3000 metres of ice (Figure 4.2). So the low thermal conductivity of ice and

the counteracting effects of temperature and snowfall explain the stability of the East Antarctic Ice Sheet.

Basal temperatures beneath the periphery of the East Antarctic Ice Sheet are much colder under glacial maximum climatic conditions than under present-day climatic conditions. Under present-day climatic conditions, a warm-based zone encircles the East Antarctic Ice Sheet due to the strong strain heating and marine influence (Figure 5.13). Under glacial maximum climatic conditions (Figure 5.12), this warm-based zone disappears except beneath a few dynamic glaciers (the Lambert Glacier and Law Dome for example). It is easier for the cold temperature signal of the glacial maximum climate to penetrate the relatively thin ice to the base at the periphery of the ice sheet and thus decrease basal temperatures.

The West Antarctic Ice Sheet has an interesting different and story. Under present-day climatic conditions, the ice at the Siple Coast is mostly cold-based (Figure 5.13); Under glacial maximum climatic conditions, it becomes warm-based (Figure 5.12). Why does an ice age, which results in lower basal temperatures along the coast of East Antarctica, result in higher basal temperatures near the coast of West Antarctica? The West Antarctic Ice Sheet is also referred to as a marine ice sheet for it is strongly influenced by sea level changes. Maximum glaciation dramatically thickens the ice sheet in West Antarctica (Figure 5.10(c) compared to the present ice thickness Figure 5.6(i)). Also ice along the Siple Coast flows faster at the maximum glaciation (Figure 5.11(b) compared to the present ice flow lines Figure 5.8(h)). Based on the analysis of marine sediment on the West Antarctic continental shelf, Anderson [1999] concludes that the West Antarctic Ice Sheet may have a history of sporadic, and possibly very rapid, growth and collapse and is currently loosing mass. The modelling results from this research support this view of a dynamic West Antarctic Ice Sheet.

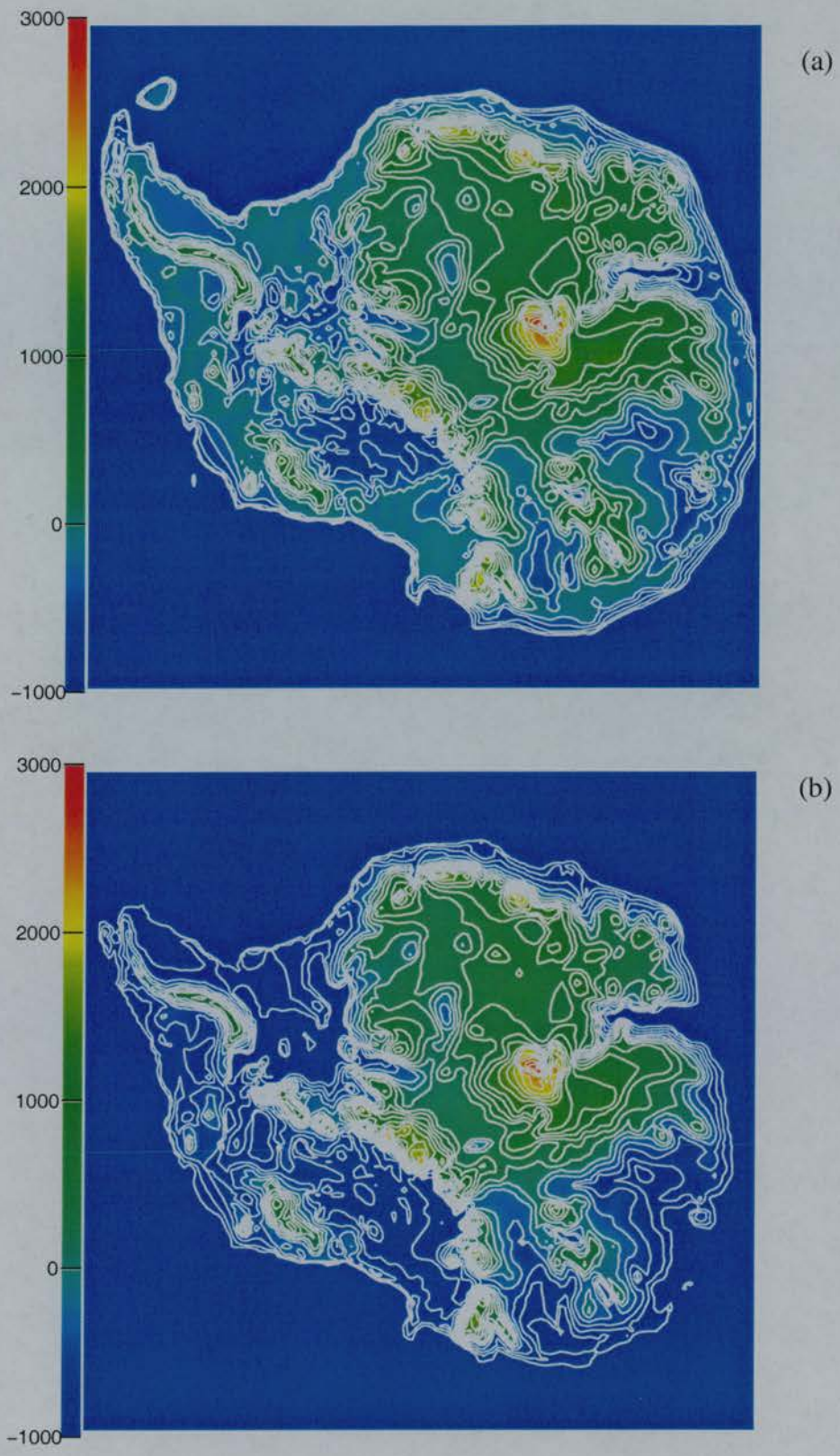

Figure 5.15 Modelled Antarctic bedrock topographies (m, with 200-m contours) under the present-day (a) and the glacial maximum (b) climatic conditions. During the glaciation, the bedrock in West Antarctica is weighed down relatively more than its eastern counterpart.

Isostasy also plays an important role in the stability of the East and West Antarctic Ice Sheets. Figure 5.15 shows the modelled Antarctic bedrock topographies (a) at present and (b) at the glacial maximum climatic conditions. The effect of sea-level lowering makes the West Antarctic Ice Sheet expand much more rapidly than its eastern counterpart under glacial maximum climatic conditions, as illustrated by comparing Figure 5.10(c) with Figure 5.6(i). As a consequence, the West Antarctic topography is depressed relatively more than in East Antarctica (Figure 5.15(b)). As the bedrock beneath the ice sheet is lowered, the ice sheet becomes increasingly unstable, responding even more rapidly to rising and falling sea level. This positive feedback causes the West Antarctic Ice Sheet to become increasingly sensitive to global climatic changes. Although the West Antarctic Ice Sheet is comparatively sensitive to climatic changes, the Antarctic Ice Sheet as a whole is nevertheless stable because the stable East Antarctic Ice Sheet is much larger than its western counterpart.

Figure 5.16 illustrates the response of the modelled Antarctic Ice Sheet to climatic changes by means of the evolution of its ice volume and area. Figure 5.16(a) indicates that the modelled Antarctic Ice Sheet builds up quickly during the first 50,000 model years. Under present-day climatic conditions, the volume of the ice sheet stabilises after 100,000 model years (blue line in Figure 5.16(a)). After 100,000 model years of glacial maximum climatic conditions, the ice volume is again approaching a stable state (Figure 5.16(a)).

The area of the modelled Antarctic Ice Sheet responds to climatic changes much more quickly than the ice volume. Figure 5.16(b) shows that the modelled Antarctic Ice Sheet has nearly completed its expansion within the first 10,000 model years. This result implies that the ice margin of the Antarctic Ice Sheet is very sensitive to climatic changes, and especially sea level change. The ice front may take only a hundred years to advance significantly after new climatic conditions come into force. Referring to the ice sheet evolution map (Figure 5.10), the quick expansion of the ice shelves in the Ross Sea and the Weddell Sea may account for much of the increase in

ice area. So this result of a dynamic ice margin does not undermine the conclusion of a stable East Antarctic Ice Sheet.

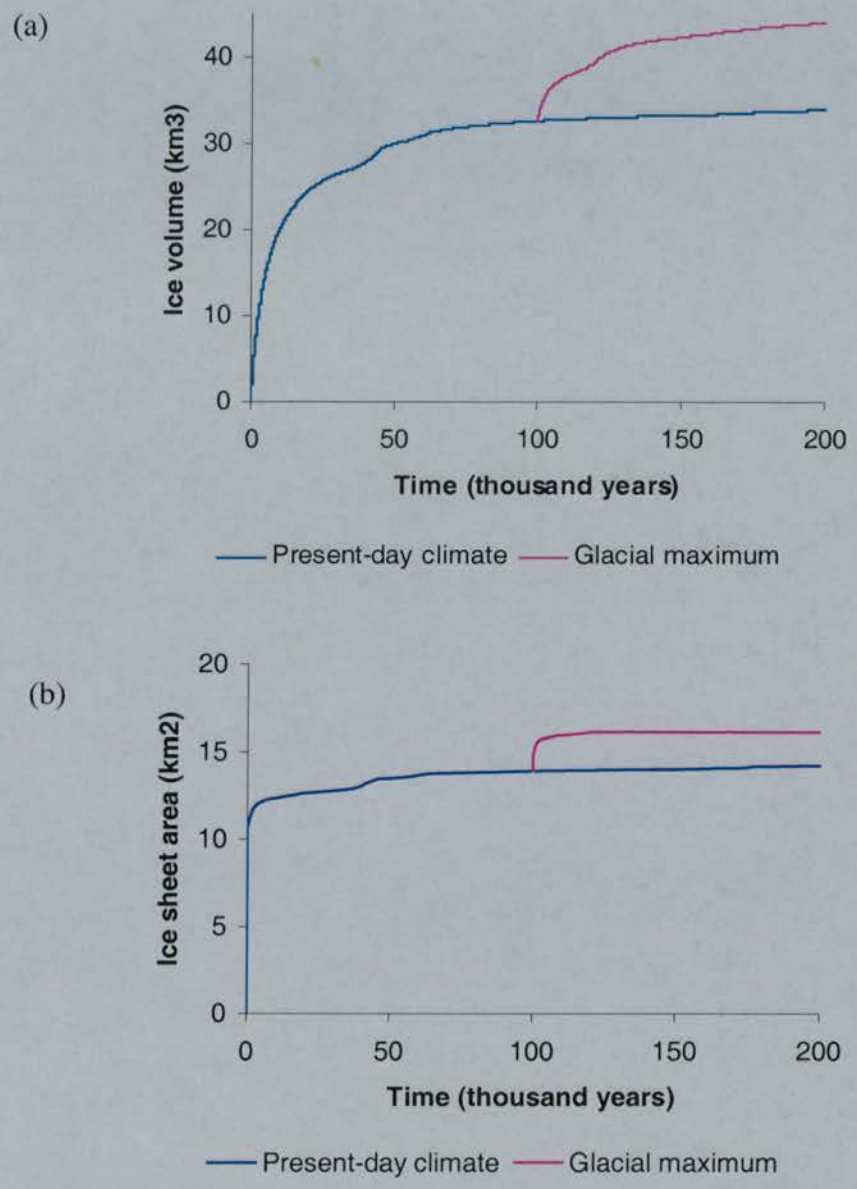

Figure 5.16 Evolution of (a) ice volume and (b) the area of the modelled Antarctic Ice Sheet. The ice area responds to climatic changes much more quickly than the ice volume. It implies a dynamic ice margin under changing climates. The ice sheet as a whole becomes stable after 100,000 model years.

It is worth pointing out that during the Last Glacial Maximum, the Antarctic Ice Sheet did not get offshore to the edge of the continental shelf, except perhaps in West Antarctica. The full ice sheet maximum may have been 14 million years ago, since this is its age when the Transantarctic Mountains were last overridden by thicker ice flowing towards the outer shelf [Sugden *et al.* 1993; Sugden 1996]. Thus what the modelling results of this research suggests is an indication of general trends.

5.4 Geomorphology — Landscape in the Dry Valleys, southern Victoria Land, East Antarctica

Modelling results can help to explain geomorphological evidence found in field studies. In particular they can provide insight into the glaciological processes and contexts that may be responsible for certain landforms.

Let us first focus our attention on ice thickness and the corresponding basal temperatures along the Transantarctic Mountains, especially in southern Victoria Land, East Antarctica. Under present-day climatic conditions, thick ice is restricted to the inland side of the Transantarctic Mountains (Figure 5.6(h)). Nowadays, the seaward side of the Transantarctic Mountains in southern Victoria Land has an ice-free topography, such as the Dry Valleys or local glaciers (Figure 5.17). During the ice maximum, the East Antarctic Ice Sheet expanded across the Transantarctic Mountains towards the sea and Victoria Land was totally covered by ice (Figures 5.10). Due to the high altitudes of the mountain topography, the part of the ice sheet over the Transantarctic Mountains was thin except at the site of a few transverse valleys across the mountains. The consequence is that the ice sheet was warm-based on both sides of the Transantarctic Mountains while cold-based along most ranges of the mountains. This is clearly illustrated in Figures 5.12(a) and 5.12(b).

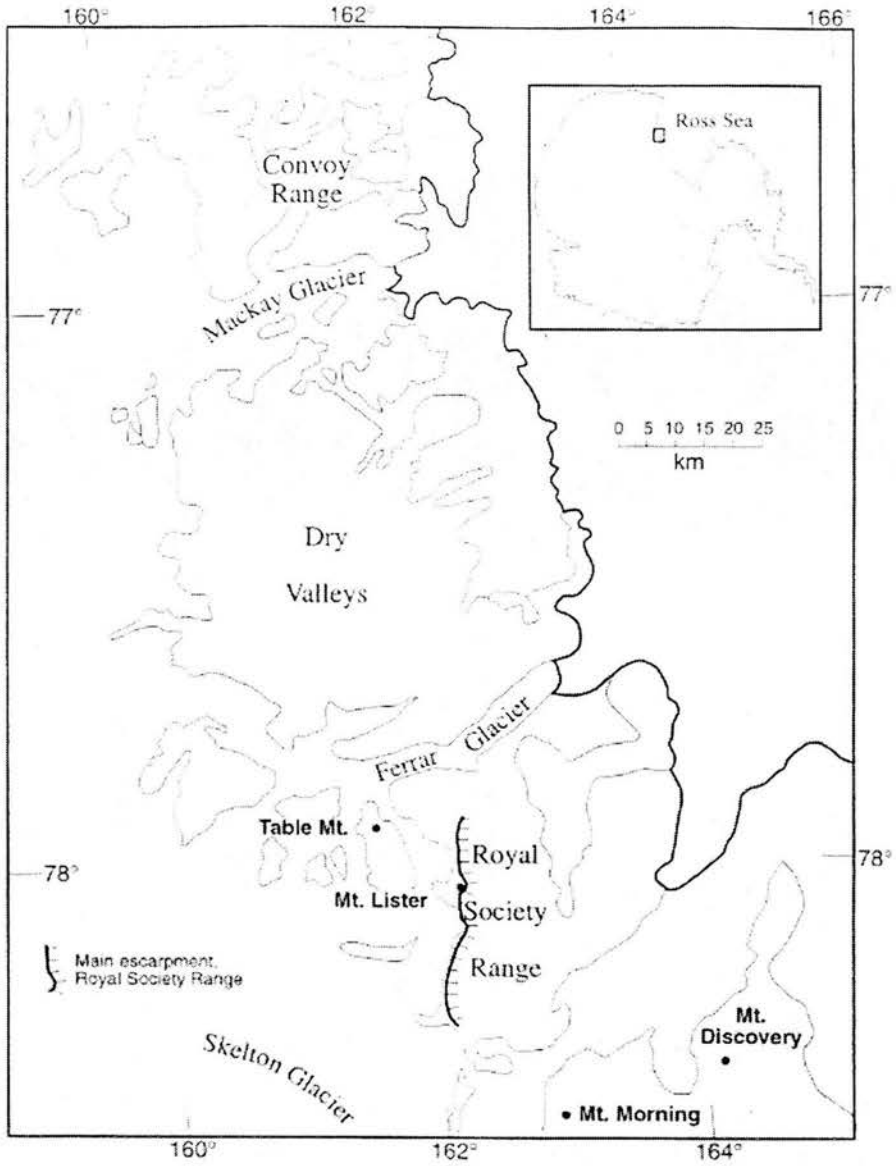

Figure 5.17 Locations of the Dry Valleys and the Royal Society Range, southern Victoria Land, East Antarctica. (from Sugden *et al.*, 1999)

The formation of the Labyrinth landscape (Figure 1.2) and the meltwater channel and pothole system (Figure 1.3) requires a warm-based ice sheet in the vicinity of the Transantarctic Mountains in order to provide enough meltwater. The modelling results from this research strongly support the argument of Sugden *et al.* [1995] regarding the geomorphological history of the landscape of the main valleys along the Transantarctic Mountains. The landscape had undergone development under pre-

existing fluvial conditions, and the subsequent glacial modification, even over the long term, has been selective and limited to the straightening of certain troughs and partial scouring of pre-existing surfaces. Old river landscapes have survived, presumably because they were covered by cold-based ice. Warm-based ice extended to 2000 metres up the Ross Sea flank of the Transantarctic Mountains to create the areal scouring landscapes visible today [Sugden *et al.*, 1999]. The modelled evolution of the thermal regime of the Antarctic Ice Sheet simulates the thermal conditions required by these scenarios and thus agrees with these hypotheses.

Field research by Sugden *et al.* [1991] and Denton *et al.* [1993] on the meltwater channels that traverse the Transantarctic Mountains suggests that outflows of subglacial lakes may have extended across the Transantarctic Mountains in places. The modelled basal thermal regime of the Antarctic Ice Sheet successfully simulates warm-based ice leading from areas of significant subglacial melting in the interior and the modelled dynamic regime of the ice sheet clearly shows ice flowing in the same direction as suggested by the field research. Thus the modelling corroborates the conclusions from the above field research.

Field studies suggest that the East Antarctic Ice Sheet has remained stable for about 14 million years [Denton *et al.*, 1993; Sugden *et al.*, 1995]. Figure 5.16 indicates that after 200,000 model years, if there are no abrupt climatic changes, the modelled volume and area of the Antarctic Ice Sheet approach equilibrium. The result of stable thermal and dynamical regimes derived from this modelling research also suggest a stable Antarctic Ice Sheet system, especially in East Antarctica (Figures 5.6 and 5.14). The modelling supports the hypothesis of a stable East Antarctic Ice Sheet.

Chapter 6 Conclusions and Discussions

This thesis develops a three-dimensional time-dependent ice sheet numerical model that simulates energy and mass movement in the Antarctic Ice Sheet. The model focuses on the internal system dynamics that affect the ways in which the ice sheet responds to global climatic change. By reconstructing the evolution of the Antarctic Ice Sheet under glacial maximum conditions, the model provides insight into the behaviour of the Antarctic Ice Sheet in the past. In particular, the model experiments help demonstrate the evolution of the distribution of basal temperatures, ice thickness, basal topography and surface ice flow.

6.1 Model Achievements

This model is an improvement to an ice sheet model that has been continuously developed in the Department of Geography, University of Edinburgh [Payne, 1988; Hulton *et al.*, 1994; Hulton and Sugden, 1995, 1997; Purves and Hulton, 2000a, 2000b; Mineter and Hulton 2001]. The existing Edinburgh model has been successful when applied to the cases of Europe and Patagonia, South America [Hulton and Sugden, 1994, 1995 and 1997]. The main improvements are as follows:

- By considering potential energy release when ice flows from the Antarctic plateau towards the sea, the model reflects the thermal regime of the real ice sheet more comprehensively than previously. The potential energy is a source of heat to the base of a grounded ice sheet.
- When the ice thickness at the marine margin is thinner than a specified threshold, the ice calving rate is modelled as a segmented linear function of ice thickness (Figure 3.4). This is more realistic than the previous use of a constant iceberg calving rate since a thinner ice shelf is more susceptible to iceberg calving than a thicker one.

- The ice sheet model includes more parameters influencing iceberg calving. The iceberg calving rate is a function of water depth, ice shelf exposure to the open sea and grounding at the ice front.
- Representation of iceberg calving is improved to provide the ice sheet model with a more effective mechanism of retreat. Previously, ice could only be calved from the ice margin. With the new algorithm, if ice mass at the ice margin is less than the iceberg calving rate, additional ice will be calved from ice inland of the ice front.
- Isostatic effects have been considered in the ice sheet model. For an ice sheet with an average thickness of more than 2000 m and more than 4000 km in diameter, isostasy is crucial in influencing ice sheet evolution.
- Basal melting of the ice shelves, together with iceberg calving, is added into the ice sheet model as a mechanism of mass loss in the ice sheet system. Inclusion of this parameter improves the portrayal of ice shelves.
- A mechanism that localises geothermal heat flux is introduced into the ice sheet model. Due to the lack of observed data under the Antarctic Ice Sheet and geological evidence, the geothermal heat flux into the ice sheet system is set as a function of crustal thickness.
- Some non-dimensional coefficients are introduced to make the ice sheet model more adjustable. Although some of them may not have explicit physical meaning, such as the mass balance multiplier and the ice rheology multiplier, their existence allows modellers to adjust parameters in the modelled ice sheet system. This facility is particularly useful when testing the functionality and sensitivity of parameters in the model.

6.2 Model Limitations

The grounding line of a marine ice sheet is one of the most dynamic parts of the ice sheet (Figure 3.5). How to simulate the ground line behaviour of a marine ice sheet is a big problem in ice sheet modelling for the thermodynamic processes of grounding line vibrations are still not clear. Since the aim of this research is at the ice sheet

behaviour in the continental scale, the model does not take grounding line physics into consideration. This simplification satisfies the required resolution of this research; it nevertheless limits the application of this model. Even if a finer mesh grid that represents the spatial displacement of the grounding line vibration is applied in a model experiment, the modelled results cannot reflect the thermodynamic processes at the grounding line region of a marine ice sheet.

The subglacial topography in the Dronning Maud Land region of East Antarctica is currently poorly known. The basal topography of this area shown in Figure 4.21(b) is largely an artefact of interpolation in data free areas. Therefore, the modelled results for this area can only be of artefacts as well due to the unreliable input data.

6.3 Ice Sheet Behaviour

The ice sheet model simulates the present-day dynamics and thermal processes of the Antarctic Ice Sheet effectively. The modelled pressure-melting areas match the regions of the subglacial lakes identified by the RES research as shown in a comparison of Figure 4.25(b) and Figure 4.27. Starting from this baseline, the modelled ice sheet is grown to its maximum extent in order to illustrate the changing dynamics and thermal processes.

We can draw the following key conclusions from the model experiments under the simulated climatic scenarios:

- The modelled Antarctic Ice Sheet at its maximum is sensitive to sea level lowering. The marine margin will quickly reach ice maximum limits within 20,000 model years (Figure 5.10(b)).
- The thermal regime in the interior of the East Antarctic Ice Sheet is not sensitive to the surface temperature lowering on a 100,000-year time scale. This is demonstrated by the modest changes in basal temperature and ice thickness after dropping ice surface temperatures by 6°C from their present-day values. Thus

temperature changes at the ice surface are not strong enough to lead to an unstable Antarctic Ice Sheet. The East Antarctic Ice Sheet can sustain climate warming of at least 6°C and remain stable.

- The East Antarctic Ice Sheet responds to glacial maximum conditions differently from the West Antarctic Ice Sheet. The ice sheet on the Siple Coast in West Antarctica becomes warm-based during glacial maximum conditions, whilst the warm-based zone encircling East Antarctica disappears (Figure 5.12 and Figure 5.13). This implies that the East Antarctic Ice Sheet is immune to climatic changes, whereas the West Antarctic Ice Sheet will respond actively.
- Geothermal heat flux plays a significant role in the basal thermal regime of the Antarctic Ice Sheet. A consistent value of 54.6 mW/m^2 over the entire Antarctic Continent gave the best-fit results.
- The sensitivity experiment shown in Figure 4.19 indicates that the effect of thermal advection is comparable to that of strain heating in the ice sheet energy system.
- It takes 100,000 model years for the modelled Antarctic Ice Sheet to reach a new quasi-equilibrium state after a stepped climatic change (Figure 5.11). This is true of both the initial growth from an ice-free Antarctic topography and a change from the present to glacial maximum conditions.
- At its maximum, the Antarctic Ice Sheet expands across the Transantarctic Mountains. Some areas on the flanks of the Transantarctic Mountains are at pressure melting point (Figure 5.15). These modelling results support the arguments of Sugden *et al.* [1995] that (a) the landscape of the Transantarctic Mountains is relict and has survived beneath cold-based ice, and that (b) glacial erosion is restricted to the flanks affected by ice at the pressure melting point.
- Subglacial lakes are likely to be widespread in central East Antarctica, including the Dronning Maud Land sector where there are as yet no radio-echo sounding records (Figure 4.27).

6.4 Wider Implications

The sensitivity of the Antarctic Ice Sheet to global temperature change is a question that is critical to the welfare of human beings and is still puzzling scientists. This study helps to answer this question by analysing the mechanisms of energy and mass movement in the Antarctic Ice Sheet.

The stability of an ice sheet is basically controlled by its thermal regime. Ice temperature has a positive feedback effect on ice flow. The change from a cold-based regime to a warm-based regime causes basal sliding and this in turn produces more basal heating. The result is more basal melting which further aids basal sliding. The experiments in this study indicate that basal temperatures under the main Antarctic Ice Sheet on the continent are relatively insensitive to temperature changes of 6°C on the ice surface. From the aspect of the evolution of the basal regime, the result of these experiments corresponds with the conclusion of Huybrechts [1993] that the East Antarctic Ice Sheet appears to be very robust in the face of climate warming. On the Antarctic continent at present, the mean annual temperatures vary from *c.* –60°C on the ice sheet summit to *c.* –10°C around much of the coast [Sugden, 1982]. The present-day surface temperatures in the interior of the Antarctic Ice Sheet are so low that even a 10°C climate warming is still far from forming significant surface melting, which is the only realistic mechanism able to lead to a smaller ice sheet [Huybrechts, 1993]. In addition, because ice is a bad heat conductor, climate warming at this scale could barely been sensed by the ice base under thick ice for as long as 100,000 years (Figure 4.2).

An additional factor is the increase in snowfall that would accompany climate warming. Air at warmer temperatures can hold more moisture. The increase in snowfall increases ice thickness unless there is additional ablation. This explains the modelled scenario that, instead of causing the Antarctic Ice Sheet to retreat, a climate warming of 5°C would lead to an even thicker ice sheet than the present-day. Modelling research by Huybrechts [1993] draws a similar conclusion. Furthermore, it is backed up by evidence of thicker ice bodies in the Dry Valleys during the warm

period of the Pliocene [Denton *et al.*, 1993].

Experiments in this research indicate that basal ice is sensitive to geothermal heat flux. Unfortunately, the values of geothermal heat flux applied by most modellers, including those in this research, are based on little field evidence from Antarctica. This research attempts to make geothermal heat flux a function of the thickness of the Earth's crust. This attempt, although plausible, nevertheless lacks justification from field measurements. More research, both theoretical and in the field, waits to be done.

Iceberg calving from the marine margin dominates the mass loss of the Antarctic Ice Sheet system. In the model developed in this research, iceberg calving approaches a maximum percentage of ice loss when the ice shelf is thin. This maximum percentage could be greater than 100 percent, in which case it implies that the surplus amount of ice is calved from ice inland of the ice front. Numerically, this provides a mechanism for the modelled ice sheet to retreat toward the continent. We can also set ice shelf basal melting to contribute to mass loss of the Antarctic Ice Sheet system. We simply set the basal melting rate of ice shelf as a linear function of latitude. In the real world, however, iceberg calving and ice shelf melting are much more complicated than the linear simulations employed here. The settings of these parameters, such as the maximum and constant iceberg calving rates, the threshold to apply the linear iceberg-calving function and the basal melting rate of ice shelf with latitude, are rather arbitrary. Again, more modelling and field measurement will help improve our understanding of iceberg calving and thereby our ability to model the Antarctic Ice Sheet effectively.

References:

Allen, J R L, 1971, A theoretical and experimental study of climbing-ripple cross-lamination, with a field application to the Uppsala esker, *Geografiska Annaler* **53A** (3-4) 157–87

Alley, R B, D D Blankenship, S T Rooney and Bentley, 1989, Sedimentation beneath ice shelves – the view from Ice Stream B, *Marine Geology* **85** 101–20

Anderson, J B, 1999, *Antarctic Marine Geology*, Cambridge University Press

Anderson, M G and T P Burt, 1985, Modelling strategies, *Hydrological Forecasting*, ed M G Anderson and T P Burt, John Wiley & Sons Ltd., 1–13

Andrews, J T, 1975, *Glacier Systems*, Duxbury, Massachusetts

Bamber, J L and P Huybrechts, 1996, Geometric boundary conditions for modelling the velocity field of the Antarctic ice sheet, *Annals of Glaciology* **23** 364–73

Bard, E, B Hamelin, M Arnold, L Monaggioni, G Cabioch, G Faure and F Rougerie, 1996, Deglacial sea-level record from Tahiti corals and the timing of global meltwater discharge, *Nature* **382** 241–4

Barnola, J M, D Raynaud, Y S Korotkevich and C Lorius, 1987, Vostok ice core provides 160,000-year record of atmospheric CO_2, *Nature* **329** 408–14

Barrett, P J, C J Adams, W C McIntosh, C C Swisher III and G S Wilson, 1992, Geochronological evidence supporting Antarctic deglaciation three million years ago, *Nature* **359** 816–8

Barry, R G and R J Chorley, 1992, *Atmosphere, Weather and Climate* 6th ed, Methuen, London

Bentley, C R, 1996, Water kept liquid by warmth from within, *Nature* **381** 645

Bentley, C R and M B Giovinetto, 1991, Mass balance of Antarctica and sea level change, *Role of Polar Regions in Global Change*, ed G Weller, J Wilson and B Severin, Geophysical Institute and Center for Global Change and Arctic System Research, University of Alaska, Fairbanks, 489–94

Bentley, M J, 1999, Volume of Antarctic Ice at the Last Glacial Maximum, and its impact on global sea level change, *Quaternary Science Reviews* **18** 1569–95

Birchfield, G E, 1977, A study of the stability of a model continental ice sheet subject to periodic variations in heat input, *Journal of Geophysical Research* **82** 4909–13

Birchfield, G E, J Weertman and A T Lunde, 1981, A paleoclimate model of Northern Hemisphere ice sheets, *Quaternary Research* **15** 126–42

Blanchon, P and J Shaw, 1995, Reef drowning during the last deglaciation: Evidence for catastrophic sea-level rise and ice-sheet collapse, *Geology* **23** (1) 4–8

Blatter, H, G K C Clarke and J Colinge, 1998, Stress and velocity fields in glaciers: Part II. Sliding and basal stress distribution, *Journal of Glaciology* **44** (148) 457–66

Bogoslovski, V N, 1958, The temperature conditions (regime) and movement of the Antarctic glacial shield, *IASH* **47** 287–305

Boulton, G S and A Payne, 1992, Simulation of the European ice sheet through the last glacial cycle and prediction of future glaciation, *SKB Technical Report 93-14*, University of Edinburgh

Briffa, K R, P D Jones, F H Schweingruber and T J Osborn, 1998, Influence of volcanic eruptions on Northern Hemisphere summer temperature over the past 600 years, *Nature* **393** (6684) 450–5

Budd, W F, D Jenssen and U Radok, 1971, Meteorology Department, University of Melbourne, Publication No.18

Budd, W F and D Jenssen, 1975, Numerical modelling of glacier systems, *IAHS Publication* **104** 257–91

Budd, W F and D Jenssen, 1989, The dynamics of the Antarctic ice sheet, *Annals of Glaciology* **12** 16–22

Budd, W F, D Jenssen and I N Smith, 1984, A three-dimensional time-dependent model of the West Antarctic Ice Sheet, *Annals of Glaciology* **5** 29–36

Budd, W F and T H Jacka, 1989, A review of ice rheology for ice-sheet modelling, *Cold Regions Science and Technology* **16** 107–44

Budd, W F and N W Young and C R Austin, 1976, Measured and computed temperature distributions in the Law Dome ice cap, Antarctica, *Journal of Glaciology* **16** 99–110

Bull, C B B, B C MacKelvey and P-N Webb, 1962, Quaternary glaciations in southern Victoria Land, Antarctica, *Journal of Glaciology* **4** 63–78

Calkin, P E, 1974, Processes in the ice-free valleys of southern Victoria Land, Antarctica, *Research in Polar and Alpine Geomorphology*, ed B D Fahey and R D Thompson, University of Guelph, Ontario, 167–86

Carslaw, H S and J C Jaeger, 1959, *Conduction of Heat in Solids* 2nd ed, Clarendon Press, Oxford
Clapperton, C M, D E Sugden, J Birnie and M J Wilson, 1989, Late-glacial and Holocene glacier fluctuations and environmental change on South Georgia, Southern Ocean, *Quaternary Research* **31** 210–28
Colinge, J and H Blatter, 1998, Stress and velocity fields in glaciers: Part I. Finite-difference schemes for higher-order glacier models, *Journal of Glaciology* **44** (148) 448–56
Compiling group, 1979, *Mathematics Handbook*, People's Education Press, Beijing
Crank, J, 1975, *The Mathematics of Diffusion* 2nd ed, Clarendon Press, Oxford
Cutler, P M, 1998, Modelling the evolution of subglacial tunnels due to varying water input, *Journal of Glaciology* **44** (148) 485–97
David, T W E and R E Priestley, 1914, Glaciology, physiography, stratigraphy and tectonic geology of south Victoria Land, *British Antarctic Expedition 1907-09, Reports on the Scientific Investigations* **1**, *Geology*, Heinemann, London
Denton, G H, R L Armstrong and M Stuiverm, 1971, The Late Cenozoic glacial history of Antarctica, *The Late Cenozoic Glacial Ages*, ed K K Turekian, Yale University Press, New Haven, 267–306
Denton, G H, M L Prentice, D E Kellogg and T B Kellogg, 1984, Late Tertiary history of the Antarctic ice sheet: evidence from the Dry Valleys, *Geology* **12** 263–7
Denton, G H, D E Sugden, D R Marchant, B L Hall and T I Wilch, 1993, East Antarctic Ice Sheet sensitivity to pliocene climatic change from a Dry Valleys perspective, *Geografiska Annaler* **75A** (4) 155–204
Doake, C S M, 1985, Antarctic mass balance: glaciological evidence from Antarctic Peninsula and Weddell Sea sector, *Glaciers, Ice Sheets, and Sea Level: Effect of a CO_2-induced climatic change*, United States Department of Energy, Washington DC, 197–209, 317–30
Doake, C S M, 1987, Antarctic ice and rocks, *Antarctic Science*, ed D W H Walton, Cambridge University Press, Cambridge, 140–92
Dowdeswell, J A and M J Siegert, 1999, The dimensions and topographic setting of Antarctic subglacial lakes and implications for large-scale water storage beneath continental ice sheets, *Geological Society of America Bulletin* **111** (2) 254–63
Drewry, D J, 1982, Ice flow, bedrock and geothermal studies from radio echo sounding inland of McMurdo Sound, Antarctica, *Antarctic Geoscience*, ed C Craddock, University of Wisconsin Press, 977–83
Drewry, D J, 1983, *Antarctica: Glaciological and geophysical folio*, Scott Polar Research Institute, University of Cambridge
Drewry, D J, 1991, The response of the Antarctic ice sheet to climatic change, *Antarctica and Global Climatic Change*, ed C M Harris and B Stonehouse, Belhaven Press, London, 90–106
Duval, P, 1977, The role of water content on the creep rate of polycrystalline ice, IUGG General Assembly of Grenoble, 1975, *IAHS Publication* **118** 29–33
Engelhardt, H, N Humphrey, B Kamb and M Fahnestock, 1990, Physical conditions at the base of a fast moving Antarctic ice stream, *Science* **248** 57–9
Fairbanks, R G, 1989, A 17,000-year glacio-eustatic sea level record: Influence of glacial melting rates on the Younger Dryas event and deep-ocean circulation, *Nature* **342** 637–42
Fastook, J L and J E Chapman, 1989, A map-plane finite-element model: three modeling experiments, *Journal of Glaciology* **35** (119) 48–52
Ferrar, H T, 1907, *Report on the Field Geology of the Region Explored During the "Discovery" Antarctic Expedition, 1904-4, National Antarctic Expedition 1901-4, Natural History, vol.1, Geology*, British Museum, London
Fisher, D A and R M Koerner, 1986, On the special rheological properties of ancient microparticle-laden Northern hemisphere ice as derived from borehole and core measurements, *Journal of Glaciology* **32** 501–10
Fortuin, J P F and J Oerlemans, 1990, Parameterisation of the annual surface temperature and mass balance of Antarctica, *Annals of Glaciology* **14** 78–84
Gamble, C, 1994, Time for Boxgrove man, *Nature* **369** 275–6
Genthon, C, J M Barnola, D Raynaud, C Lorius, J Jouzel, N I Barkov, Y S Korotkevich and V M Kotlyakov, 1987, Vostok ice core: climatic response to CO_2 and orbital forcing changes over the last climatic cycle, *Nature* **329** 414–8
Giovinetto, M B and C R Bentley, 1985, Surface balance in ice drainage systems of Antarctica, *Antarctic Journal of the United States* **20** 6–13

Glen, J W, 1955, The creep of polycristalline ice, *Proceedings of the Royal Society* **A 228** 519–38
Gow, A J, H T Ueda and D E Garfield, 1968, Antarctic ice sheet: preliminary results of first core hole to bedrock, *Science* **161** 1011–3
Gröber, H, S Erk and U Grigull, 1961, *Fundamentals of Heat Transfer* 3rd ed, McGraw-Hill Book Company, Inc.
Hansen, I and R Greve, 1996, Polythermal modelling of steady states of the Antarctic ice sheet in comparison with the real world, *Annals of Glaciology* **23** 382–7
Hansen, J and S Lebedeff, 1987, Global trends of measured surface air temperature, *Journal of Geophysical Research* **92** 13345–72
Hansen, J E, M Sato, A Lacis, R Ruedy, I Gegen and E Matthews, 1998, Climate forcings in the industrial era, *Proceedings of the National Academy of Sciences* **95** (12) 12753–8
Hansom, J D and J D Gordon, 1998, *Antarctic Environments and Resources*, Addison Wesley Longman, New York
Harwood, D M, 1986, *Diatom biostratigraaphy and paleoecology and a Cenozoic history of Antarctic ice sheets*, PhD dissertation, Ohio State University, Columbus, Ohio
Herterich, K, 1988, A three-dimensional model of the Antarctic ice sheet, *Annals of Glaciology* **11** 32–5
Hindmarsh, R C A, 1990, Time-scales and degrees of freedom operating in the evolution of continental ice-sheets, *Transactions of the Royal Society of Edinburgh: Earth Sciences* **81** 371–84
Hindmarsh, R C A, 1993, Modelling the dynamics of ice sheets, *Progress in Physical Geography* **17** (4) 391–412
Hindmarsh, R C A, G S Boulton and K Hutter, 1989, Modes of operation of thermo-mechanically coupled ice-sheets, *Annals of Glaciology* **12** 57–69
Hindmarsh, R C A and A J Payne, 1996, Time-step limits for stable solutions of the ice-sheet equation, *Annals of Glaciology* **23** 74–85
Holmlund, P and J-O Näslund, 1994, The glacially sculptured landscape in Dronning Maud Land, Antarctica, formed by wet-based mountain glaciation and not by the present ice sheet, *Boreas* **23** 139–48
Hubbard, A L, 1996, *High Resolution Modelling of Glacier Flow*, PhD thesis, University of Edinburgh
Hubbard, A L, 1997, Modelling climate, topography and palaeoglacier fluctuations in the Chilean Andes, *Earth Surface Processes and Landforms* **22** 79–92
Hughes, T J, 1981, Numerical reconstruction of paleo-ice sheets, *The Last Great Ice Sheets*, ed G H Denton and T J Hughes, John Wiley & Sons, New York, 221–61
Hulton, N, D Sugden, A Payne and C Clapperton, 1994, Glacier modeling and the climate of Patagonia during the last glacial maximum, *Quaternary Research* **42** 1–19
Hulton, N R J and D E Sugden, 1995, Modelling mass balance on former maritime ice caps: a Patagonian example, *Annals of Glaciology* **21** 304–10
Hulton, N and D Sugden, 1997, Dynamics of mountain ice caps during glacial cycles: the case of Patagonia, *Annals of Glaciology* **24** 81–9
Hulton, N R J and M J Mineter, 2000, Modelling self-organisation in ice streams, *Annals of Glaciology* **30** 127–36
Hutter, K, 1983, *Theoretical Glaciology*, D Reidel Publishing Company, Dordrecht
Hutter, K, S Yakowitz and F Szidarovszky, 1986, A numerical study of plane ice sheet flow, *Journal of Glaciology* **32** 139–60
Huybrechts, P, 1986, A three-dimensional time-dependent numerical model for polar ice sheets: some basic testing with a stable and efficient finite difference scheme, Geografisch Instituut, Vrije Universiteit Brussel, Report 86-1
Huybrechts, P, 1990a, A 3-D model for the Antarctic ice sheet: a sensitivity study on the glacial-interglacial contrast, *Climate Dynamics* **5** 79–92
Huybrechts, P, 1990b, The Antarctic ice sheet during the last glacial-interglacial cycle: a three-dimensional experiment, *Annals of Glaciology* **14** 115–9
Huybrechts, P, 1992, The Antarctic ice sheet and environmental change: a three-dimensional modelling study, *Reports on Polar Research*, Alfred-Wegener-Institut für Polar- und Meeresforschung, 99
Huybrechts, P, 1993, Glaciological modelling of the late Cenozoic East Antarctic Ice Sheet: stability or dynamism?, *Geografiska Annaler* **75A** (4) 221–38

Huybrechts, P, 1996, Basal temperature conditions of the Greenland ice sheet during the glacial cycles, *Annals of Glaciology* **23** 226–36
Huybrechts, P and J Oerlemans, 1988, Evolution of the East Antarctic ice sheet: a numerical study of thermo-mechanical response patterns with changing climate, *Annals of Glaciology* **11** 52–9
Huybrechts, P and J Oerlemans, 1990, Response of the Antarctic Ice Sheet to future greenhouse warming, *Climate Dynamics* **5** 93–102
Huybrechts, P, T Payne and the EISMINT Intercomparison Group, 1996, The EISMINT benchmarks for testing ice-sheet models, *Annals of Glaciology* **23** 1–12
Incropera, F P and D P Dewitt, 1996, *Fundamentals of Heat and Mass Transfer* 4th ed, John Wiley & Sons, New York
Jacka, T H, 1984, The time and strain required for development of minimum strain rates in ice, *Cold Region Science and Technology* **8** 261–8
Jacka, T H and W F Budd, 1991, The use of tertiary creep rates in ice at high strains in compression and shear, *Ice-Structure Interaction: IUTAM-IAHR Symposium*, ed S Jones, RG McKenna, J Tillotson and I Jordaan, St. John's, Newfoundland, Springer-Verlag, Berlin, 21–35
Jacka, T H and M Maccagnan, 1984, Ice crystallographic and strain rate changes with strain in compression and extension, *Cold Region Science and Technology* **8** 269–86
Jacobs, S S, 1992, Is the Antarctic ice sheet growing?, *Nature* **360** 29–33
Jacobs, S S, D R MacAyeal and J L Ardai, Jr, 1986, The recent advance of the Ross Ice Shelf, Antarctica, *Journal of Glaciology* **32** 464–74
Jóhannesson, T, C Raymond and E Waddington, 1989, Time scale for adjustment of glaciers to changes in mass balance, *Journal of Glaciology* **35** 355–69
Jones, P D and K R Briffa, 1992, Global surface air temperature variations during the 20th century: Part 1 - spatial, temporal and seasonal details, *Holocene* **1** 165–79
Jones, P D, K R Briffa, T P Barnett and S F B Tett, 1998, High-resolution paleoclimatic records for the last millennium: interpretation, integration and comparison with General Circulation Model control-run temperatures, *Holocene* **8** (4) 455–471
Jones, P D, T J Osborn and K R Briffa, 1997, Estimating sampling errors in large-scale temperature averages, *Journal of Climate*, **10** (10), 2548–68
Jouzel, J, C Lorius, J R Petit, C Genthon, N I Barkov, V M Kotlyakov and V M Petrov, 1987, Vostok ice core: a continuous isotope temperature record over the last climatic cycle (160.000 years), *Nature* **329** 403–8
Jouzel, J, N I Barkov, J M Barnola, M Bender, J Chappellaz, C Genthon, V M Kotlyakov, V Lipenkov, C Lorius, J R Petit, D Raynaud, G Raisbeck, C Ritz, T Sowers, M Stievenard, F Yiou and P Yiou, 1993, Extending the Vostok ice-core record of paleoclimate to the penultimate glacial period, *Nature* **364** 407–12
Kapitsa, A, J K Ridley, G de Q Robin, M J Siegert and I Zotikov, 1996, Large deep freshwater lake beneath the ice of central East Antarctica, *Nature* **381** 684–6
Keeling, C D and T P Whort, 1998, Atmospheric CO_2 records from sites in the SIO air sampling network, *Trends: A Compendium of Data on Global Change*, Carbon Dioxide Information Analysis Center, Oak Ridge National Laboratory, Oak Ridge, Tennessee
Kennett, J P, 1982, *Marine Geology*, Englewood Cliffs, Prentice-Hall
Kellogg, D E and T B Kellogg, 1996, Diatoms in South Pole ice: Implications for eolian contamination of Sirius group deposits, *Geology* **24** (1) 115–8
Kerr, A, D E Sugden and M A Summerfield, 2000, Linking tectonics and landscape development in a passive margin setting: the Transantarctic Mountains, *Geomorphology and Global Tectonics*, ed M A Summerfield, John Wiley & Sons Ltd., 303–19
Lamb, H H, 1972, *Climate: Present, Past and Future, Volume 1, Fundamentals and Climate Now*, Methuen & Co Ltd, London
Lamb, H H, 1977, *Climate: Present, Past and Future, Volume2, Climate History and the Future*, Methuen & Co Ltd, London
Lambeck, K, 1991, A model for Devensian and Flandrian glacial rebound and relative sea-level change in Scotland, *Glacial Isostasy, Sea Level and Mantle Rheology* ed R Sabadini, K Lambeck and E Boschi, Kluwer, Dordrecht, 33–62
Ledley, T S, E T Sundquist, S E Schwartz, D K Hall, J D Fellows T L and Killeen, 1999, Climate change and greenhouse gases, *Eos: Transactions, American Geophysical Union* **80** (39) 453
Lee, H K and S Uyeda, 1965, Review of heat flow data, Terrestrial heat flow, *Geophysical Monograph*, American Geophysical Union, **8** 87–190

Le Meur, E, 1996, A comparison of different ways of dealing with isostasy: examples from modelling the Antarctic ice sheet during the last glacial cycle, *Annals of Glaciology* **23** 309–17
Loewe, F, 1970, Screen temperatures and 10 m temperatures, *Journal of Glaciology* **9** (56) 263–8
Lowe, J J and M J C Walker, 1997, *Reconstructing Quaternary Environments* 2nd ed, Longman
Mahaffey, M A W, 1976, A three-dimensional numerical model of ice sheets: tests on the Barnes Ice Cap, Northwest Territories, *Journal of Geophysical Research* **81** 1059–66
Mann, M E, R S Bradley and M K Hughes, 1998 Global-scale temperature patterns and climate forcing over the past six centuries, *Nature* **392** (6678) 779–87
Mann, M E, R S Bradley and M K Hughes, 1999, Northern hemisphere temperatures during the past millennium: inferences, uncertainties, and limitations, *Geophysical Research Letters* **26** 759–62
Marchant, D R, C C Swisher III, D R Lux, D P West and G H Denton, 1993, Pliocene paleoclimate and East Antarctic Ice-Sheet history from surficial ash deposits, *Science* **260** 667–70
Marchant, D R and D E Denton, 1996, Miocene and Pliocene palaeoclimate of the Dry Valleys region, southern Victoria Land: a geomorphological approach, *Marine Micropaleontology* **27** (1–4) 269–71
McInnes, B J and W F Budd, 1984, A cross-sectional model for West Antarctica, *Annals of Glaciology* **5** 95–9
Mercer, J H, 1978, West Antarctic ice sheet and CO_2 greenhouse effect: a threat of disaster, *Nature* **271** 321–5
Mineter, M J and N R J Hulton, 2001, Parallel Processing for finite difference modelling of ice sheets, *Computers and Geosciences* **27** (7) 829–38
Mitchell, A R and D F Griffiths, 1980, *The Finite Difference Method in Partial Differential Equations*, John Wiley
Morland, L W, 1984, Thermo-mechanical balances for ice sheets, *Geophysical and Astrophysical Fluid Dynamics* **29** 237–66
Näslund, J-O, 1997, Subglacial preservation of valley morphology at Amundsenisen, western Dronning Maud Land, Antarctica, *Earth Surface Processes and Landforms* **22** 441–55
Näslund, J-O, 1998, Numerical modelling of the ice sheet in western Dronning Maud Land, East Antarctica - impacts of present, past, and future climates, *Ice Sheet, Climate, and Landscape Interactions in Dronning Maud Land, Antarctica*, Doctoral Dissertation, Naturgeografiska Institutionen, Stockholms Universitet
NERC, 1989, *Antarctica 2000 NERC Strategy for Antarctic Research*, Natural Environment Research Council, Swindon
Nichols, R L, 1971, Glacial geology of the Wright Valley, McMourdo Sound, *Research in the Antarctic*, ed L O Quam, American Association for the Advancement of Science, Washington DC, 293–340
Nicholls, N, G V Gruza, J Jouzel, T R Karl, L A Ogallo and D E Parker, 1996, Observed climate variability and change, *Climate Change 1995: The Science of Climate Change*, ed J T Houghton, L G M Filho, B A Callander, N Harris, A Kattenberg and K Maskell, Intergovernmental Panel on Climate Change, Cambridge University Press, Cambridge, 133–92
Nye, J F, 1952, The mechanics of glacier flow, *Journal of Glaciology* **2** 82–93
Nye, J F, 1957, The distribution of stress and velocity in glaciers and ice sheets, *Proceedings of the Royal Society of London, Serial A* **239** 113–33
Nye, J F, 1960, The response of glaciers and ice-sheets to seasonal and climatic changes, *Proceedings of the Royal Society of London, Serial A* **256** 559–84
Nye, J F and F C Frank, 1969, The hydrology of the intergranular veins in a temperate glacier, *Symposium on the hydrology of glaciers*, Union Géodésique et géophysique Internationale, Association Internationale d'Hydrologie Scientifique, Commission de Neiges et Glaces, Cambridge
Oerlemans, J, 1981, Some basic experiments with a vertically integrated ice-sheet model, *Tellus* **33** 1–11
Oerlemans, J, 1989, A projection of future sea level, *Climate Change* **15** 151–74
Oerlemans, J and C J van der Veen, 1984, *Ice Sheets and Climate*, D Reidel Publishing Company
Oke, T R, 1978, *Boundary Layer Climates*, University Paperbacks, Methuen
Oswald, G K A and G de Q Robin, 1973, Lakes beneath the Antarctic ice sheet, *Nature* **245** 251–4
Overpeck, J, K Hughen, D Hardy, R Bradley, R Case, M Douglas, B Finney, K Gajewski, G Facoby, A Jennings, S Lamoureaus, A Lasca, G MacDonald, J Moore, M Retelle, S Smith, A Wolfe

and G Zielinski, 1997, Arctic environmental change of the last four centuries, *Science* **278** 1251–6

Patankar, S V, 1980, *Numerical Heat Transfer and Fluid Flow*, Hemisphere Publishing Co.

Paterson, W.S.B., 1994, *The Physics of Glaciers* 3rd ed, Pergamon

Paterson, W S B and W F Budd, 1982, Flow parameters for ice sheet modelling, *Cold Regions Science and Technology* **6** 175–7

Payne, A, 1988, *Modelling former ice sheets*, PhD thesis, University of Edinburgh

Payne, A J, 1999, A thermomechanical model of ice flow in West Antarctica, *Climate Dynamics* **15** 115–25

Petit, J R, I Basile, A Leruyuet, D Raynaud, C Lorius and J Jouzel, 1997, Four climate cycles in Vostok ice core, *Nature* **387** 359–60

Petrenko, V F and R W Whitworth, 1999, *Physics of Ice*, Oxford University Press

Phillpot, H R, 1985, Physical geography – climate, *Key Environments: Antarctica*, ed W N Bonner and D W H Walton, Pergamon, Oxford, 23–38

Prather, M, R Kerwent, D Ehhalt, P Fraser, E Sanhueza, X Zhou, Radiative forcing of climate change, 1996, *Climate Change 1995: The Science of Climate Change*, ed J T Houghton, L G Meira Filho, B A Callander, N Harris, A Kattenberg and K Maskell, Cambridge University Press, Cambridge, 86–103

Press, W H, B P Flannery, S A Teukolsky and W T Vetterling, 1996, *Numerical Recipes in Fortran 90: the art of parallel scientific computing*, Cambridge University Press, Cambridge

Priestley, R E, 1909, Scientific results of the western journey, *The heart of the Antarctic* **2**, ed E H Shackleton, Heinemann, London, 315–33

Purves, R S and N R J Hulton, 2000a, Experiments in linking regional climate, ice-sheet models and topography, *Journal of Quaternary Science* **15** (4) 369–75

Purves, R S and N R J Hulton, 2000b, A climatic-scale precipitation model compared with the UKCIP baseline climate, *International Journal of Climatology* **20** 1809–21

Robert, C and H Chamley, 1992, Late Eocene-early Oligocene evolution of climate and marine circulation: deep-see clay mineral evidence, *The Antarctic Paleoenvironment: A Perspective on Global Change, 1, Antarctic Research Series* **56** 97–117

Roberts, M B, C B Stinger and S A Parfitt, 1994, A hominid tibia from Middle Pleistocene sediments at Boxgrove, UK, *Nature* **369** 311–3

Robin, G de Q, 1955, Ice movement and temperature distribution in glaciers and ice sheets, *Journal of Glaciology* **2** (18) 523–32

Robin, G de Q, 1979, Formation, flow, and disintegration of ice shelves, *Journal of Glaciology* **24** 259–71

Robin, G de Q, 1988, The Antarctic ice sheet, its history and response to sea level and climatic changes over the past 100 million years, *Palaeogeography, Palaeoclimatology, alaeoeclgy* **67** 31–50

Robin, G de Q, K J Drewry and K T Meldrum, 1977, International studies of ice sheet and bedrock, *Philosophical Transactions of the Royal Society*, London, serial A **279** 185–96

Röthlisberger, H, 1972, Water pressure in intra- and subglacial channels, *Journal of Glaciology* **11** (62) 177–202

Rubin, M J and W S Weyant, 1965, Antarctic meteorology, *Antarctica*, ed T Hatherton, Methuen, London, 375–401

Ruddiman, W F, A F McIntyre and M E Raymo, 1986, Matuyama 41,000-year cycle: North Atlantic Ocear and northern hemisphere ice sheets, *Earth and Planetary Science Letters* **80** 117–29

Schimel, D, D Alves, I Enting, M Heimann, F Joos, D Raynaud, T Wigley, M Prather, R Derwent, D Ehhalt, P Fraser, E Sauhueza, Zhou X, P Jonas, R Charlson, H Rodhe, S Sadasivan, K P Shine, Y Fouquart, V Ramaswamy, S Solomon, J Srinivasan, D Albritton, R Derwent I Isaksen, M Lal and D Wuebbles, 1996, Radiative forcing of climate change, *Climate Change 1995: The Science of Climate Change*, ed J T Houghton, L G M Filho, B A Callander, N Harris, A Kattenberg and K Maskell, Cambridge University Press, Cambridge

Schneider, P J, 1955, *Conduction Heat Transfer*, Addison-Wesley Publishing Company, Inc., Cambridge, Massachusetts

Sclater, J G, C Jaupart and D Galson, 1980, The heat flow through oceanic and continental crust and the heat loss of the earth, *Reviews of Geophysics and Space Physics*, **18** 289–311

Selby, M J and A T Wilson, 1971, Possible Tertiary age for some Antarctic cirques, *Nature* **229** 623–4

Shaw, J, 1996, A meltwater model for Laurentide sub-glacial landscapes, *Geomorphology sans Frontieres*, ed S B McCann and D C Ford, Wiley, London, 181–236
Sharp, M, K Richards, I Willis, N Arnold, P Nienow, W Lawson and J-L Tison, 1993, Geometry, bed topography and drainage system structure of the Haut Glacier D'Arolla, Switzerland, *Earth Surface Processes and Landforms* **18** 557–71
Shreve, R L, 1972, Movement of water in Glaciers, *Journal of Glaciology* **11** (62) 205–14
Siegert, M J and J A Dowdeswell, 1996, Spatial variations in heat at the base of the Antarctic ice sheet from analysis of the thermal regime above sub-glacial lakes, *Journal of Glaciology* **42** 501–9
Siegert, M J, J A Dowdeswell, M R Gorman and N F McIntyre, 1996, An inventory of Antarctic sub-glacial lakes, *Antarctic Science* **8** (3) 281–6
Siegert, M J and J K Ridley, 1998, Determining basal ice sheet conditions in the Dome C region of East Antarctica using satellite radar altimetry and airborne radio-echo sounding, *Journal of Glaciology* **44** (146) 1–8
Smith, G D, 1985, *Numerical Solution of Partial Differential Equations: Finite Difference Methods* 3rd ed, Clarendon Press, Oxford
Sugden, D E, 1977, Reconstruction of the morphology, dynamics, and thermal characteristics of the Laurentide Ice Sheet at its maximum, *Arctic and Alpine Research* **9** (1) 21–47
Sugden, D E, 1982, *Arctic and Antarctic*, Barnes & Noble Books, Totowa, New Jersey
Sugden, D, 1992, Antarctic ice sheets at risk? *Nature* **359** 775–6
Sugden, D E, 1996, The East Antarctic Ice Sheet: unstable ice or unstable ideas?, *Transactions of the Institute of British Geographers* **21** 443–54
Sugden, D E and B S John, 1976, *Glaciers and Landscape*, Arnold, London
Sugden, D E, G H Denton and D R Marchant, 1991, Subglacial meltwater channel systems and ice sheet overriding, Asgard Range, Antarctica, *Geografiska Annaler* **73A** (2) 109–21
Sugden, D E, D R Marchant and G H Denton, 1993, The case for a stable East Antarctic Ice Sheet: the background, *Geografiska Annaler* **75A** (4) 151–4
Sugden, D E, G H Denton and D R Marchant, 1995, Landscape evolution of the Dry Valleys, Transantarctic Mountains: tectonic implications, *Journal of Geophysics Research* **100** 9949–67
Sugden, D E, M A Summerfield, D H Denton, T I Wilch, W C McIntosh, D R Marchant and R H Rutford, 1999, Landscape development in the Royal Society Range, southern Victoria Land, Antarctica: stability since the mid-Miocene, *Geomorphology* **28** 181–200
Swithinbank, C W M, 1988, Glaciers of the world: Antarctica, *US Geological Survey Professional Paper* 1386-B
Swithinbank, C W M and J H Zumberge, 1965, The ice shelves, *Antarctica*, ed T Hatherton, Methuen, London, 199–220
Taylor, G, 1922, *The Physiography of McMurdo Sound and Granite Harbour Region, British Antarctic (Terra Nova) Expedition 1910-13*, Harrison, London
UNEP, 1992, *Glaciers and the Environment*, Nairobi
van der Veen, C J, 1987 The West Antarctic Ice Sheet: the need to understand its dynamics, *Dynamics of the West Antarctic Ice Sheet*, ed C J van der Veen and J Oerlemans, D Reidel Publishing Company, Dordrecht, Holland, 1–16
van der Veen, C J and I M Whillans, 1989, Force budget: I. Theory and numerical methods, *Journal of Glaciology* **35** (119) 53–60
van der Wateren, F M and A L L M Verbers, 1990, Cenozoic glaciation of the Rennick Glacier area, the Everest Range and Yule Bay area, North Victoria Land, Antarctica, *Polarforschung* **60** 73–7
van der Wateren, R and R Hindmarsh, 1995, East Antarctic Ice sheet: stabilists strike again, *Nature* **376** 389–91
Vaughan, D G and C S M Doake, 1996, Recent atmospheric warming and retreat of ice shelves on the Antarctic Peninsula, *Nature* **379** 328–31
Verbers, A L L M and F M van der Wateren, 1992, A glacio-geological reconnaissance of the southern Prince Albert Mountains, Victoria Land, Antarctica, *Recent Progress in Antarctic Earth Science – Proceedings of the sixth International Symposium on Antarctic Earth Science*, ed Yoshida Y, Kaminuma K and Shiraishi K, Terrapub, Tokyo, 715–9
Warrick, R and J Oerlemans, 1990, Sea level rise, *Climate Change – The IPCC Scientific Assessment*, ed J T Houghton, G J Jenkins and J J Ephraums, Cambridge University Press, Cambridge, 257–81

Webb, P-N, 1994, Paleo-drainage systems of East Antarctica and sediment supply to West Antarctic rift system basins, *Terra Antarctica* **1** 457–61
Webb, P-N, D M Harwood, B C McKelvey, J H Mercer and L D Stott, 1984, Cenozoic marine sedimentation and ice volume variation on the East Antarctic craton, *Geology* **12** 287–91
Weertman, J, 1957, On the sliding of glaciers, *Journal of Glaciology* **3** 33–8
Weertman, J, 1961, Stability of ice-age ice sheets, *Journal of Geophysical Research* **66** 3783–92
Weertman, J, 1968, Comparison between measured and theoretical temperature profiles of the Camp Century, Greenland, borehole, *Journal of Geophysical Research* **73** 2691–700
Weertman, J, 1972, The theory of glacier sliding, *Glaciers and Glacial Erosion*, ed C Embleton, Macmillan, London, 244–68
Yen Y C, 1981, Review of thermal properties of snow, ice, and sea ice, *US Army Corps of Engineers Cold Regions Research and Engineering Laboratory Report* 81-10
Yen Y C, Cheng K C and Fukusako S, 1991, Review of intrinsic thermophysical properties of snow, ice, sea ice, and frost, *Third International Symposium on Cold Regions heat Transfer*, ed J P Zarling and S L Faussett, 187–218, University of Alaska, Fairbanks, Alaska
Yuan X, M A Cane and D G Martinson, 1996, Cycling around the South Pole, *Nature* **380** 673–4